Aus dem Walther-Straub-Institut für Pharmakologie und Toxikologie

Institut der Ludwig-Maximilians-Universität München

Pharmacodynamics of carfentanil and its neutralization by antagonists and antibodies in HEK293-μOR cells

Dissertation

zum Erwerb des Doktorgrades der Humanbiologie

an der Medizinischen Fakultät

der Ludwig-Maximilians-Universität München

vorgelegt von

Franziska Clara Endt

aus

Freistett, Rheinau

Jahr

2025

Mit Genehmigung der Medizinischen Fakultät der Ludwig-Maximilians-Universität München

Erstes Gutachten:	Prof. Dr. med. Thomas Gudermann
Zweites Gutachten:	Prof. Dr. Dirk Steinritz
Drittes Gutachten:	Prof. Dr. Oliver Scherf-Clavel

Dekan:	Prof. Dr. med. Thomas Gudermann

Tag der mündlichen Prüfung: 06.11.2025

Table of Contents

1. Abstract

Highly potent synthetic opioids, such as carfentanil (CAR), pose significant challenges to the healthcare system due to their misuse as drugs and potential application as chemical weapons. The interactions between CAR and the μ-opioid receptor (μOR) remain poorly understood and current treatments with μOR antagonists, such as naloxone, are often insufficient. This study aims to elucidate the pharmacodynamics of CAR at μOR, assess its impact on antagonist effectiveness and evaluate anti-fentanyl antibodies for their potential to neutralize CAR´s μOR binding and activation.

Binding assays using HEK293 cells stably expressing the μOR and [^{3}H]-naloxone as a tracer were performed to determine the binding affinities of CAR, fentanyl (FEN), remifentanil (REMI), morphine (MOR) and endomorphin-1 (ENDO). In combination with functional characterization through forskolin-stimulated cyclic adenosine monophosphate (cAMP) assays and Western Blot analysis of extracellular signal-regulated kinases 1 and 2 (ERK1/2) phosphorylation, this analyses demonstrated that CAR acts as a high-affinity ligand with exceptionally strong cAMP inhibition, yet induces comparatively weak ERK1/2 phosphorylation. μOR phosphorylation patterns, analyzed by ELISA at saturated opioid concentrations, showed that CAR promotes significantly increased phosphorylation at residues T370 and T379, distinguishing it from other tested opioids. A phospho-kinase array was used to screen for opioid-induced phosphorylation profile of cellular proteins; however, CAR exhibited phosphorylation patterns largely comparable to those of the other opioids tested. Antagonist potency against opioid concentrations of equal affinity was assessed in cAMP assays, revealing that both naloxone and nalmefene were significantly less effective at reversing CAR-induced μOR activation.

The potential of anti-fentanyl antibodies to interfere with opioid binding and signaling was evaluated through additional binding and cAMP assays. Of nine antibodies tested, three selectively blocked FEN binding, four inhibited both FEN and CAR and one uniquely targeted CAR, with no cross-reactivity toward REMI, MOR or ENDO. Selected antibodies also attenuated CAR- and FEN-induced cAMP signaling, although inhibition was generally more potent for FEN.

The pharmadynamic analysis revealed a unique μOR conformation stabilized by CAR that elicits selectively ultra-active cAMP inhibition and increased μOR phosphorylation, while showing reduced sensitivity to antagonists. Neutralizing CAR with specific antibodies could inhibit μOR binding independently of its conformation. This study underscores the need for alternative countermeasures, highlighting the potential of antibodies in treating or preventing FEN and CAR intoxications.

2. Zusammenfassung

Abgesehen von ihren medizinischen Vorteilen stellen hochpotente synthetische Opioide wie Carfentanil (CAR) das Gesundheitssystem vor Herausforderungen, da sie missbräuchlich als Drogen oder potenzielle chemische Waffen verwendet werden können. Die Interaktionen zwischen CAR und μ-Opioidrezeptoren (μOR) sind nicht ausreichend verstanden und die aktuelle Standardtherapie mit μOR-Antagonisten (z. B. Naloxon) ist oft unzureichend. Alternative Gegenmaßnahmen sind dringend erforderlich. Diese Studie zielt darauf ab, die Pharmakodynamik von CAR am μOR zu untersuchen, um Mechanismen zu identifizieren, die CAR´s hoher Toxizität zugrunde liegen könnten. Darüber hinaus untersucht sie die Effektivität der Antagonisten Naloxon und Nalmefen gegen CAR und analysiert spezifische Anti-Fentanyl-Antikörper hinsichtlich ihrer neutralisierenden Wirkung auf die μOR-Bindung und -Aktivierung sowie hinsichtlich der Kreuzreaktivität zu anderen Opioiden *in vitro*.

Liganden-Bindungsassays mit stabil μOR-exprimierenden HEK293-Zellen und [^{3}H]-Naloxon als Tracer dienten der Bestimmung der Bindungsaffinitäten von CAR, Fentanyl (FEN), Remifentanil (REMI), Morphin (MOR) und Endomorphin-1 (ENDO). Ergänzend dazu zeigten forskolin-stimulierte Assays zur Messung von zyklischem Adenosinmonophosphat (cAMP) sowie Western-Blot-Analysen der Phosphorylierung der extrazellulären signalregulierten Kinasen 1 und 2 (ERK1/2), dass CAR ein hochaffiner Ligand mit außergewöhnlich starker Aktivierung des cAMP-Signalwegs ist, jedoch nur eine vergleichsweise geringe ERK1/2-Phosphorylierung induziert. Die Untersuchung der μOR-Phosphorylierung mittels ELISA bei gesättigten Opioidkonzentrationen ergab, dass CAR eine deutlich stärkere Phosphorylierung an den Aminosäuren T370 und T379 bewirkt als andere getestete Opioide. Ein Phospho-kinase Array zur Analyse opioid-induzierter Phosphorylierungsmuster zellulärer Proteine zeigte, dass CAR weitgehend ähnliche Muster wie die anderen Opioide hervorrief. Die Wirksamkeit der Antagonisten Naloxon und Nalmefen gegen die Opioide wurde anhand von cAMP-Assays unter Berücksichtigung gleicher Rezeptorbelegung überprüft; dabei zeigte sich, dass beide Antagonisten deutlich weniger effektiv waren, die CAR-induzierte μOR-Aktivierung zu blockieren.

Das Potenzial von Anti-Fentanyl-Antikörpern, die Bindung und Signaltransduktion von Opioiden zu hemmen, wurde in weiteren Bindungs- und cAMP-Assays untersucht. Von neun getesteten Antikörpern blockierten drei selektiv die FEN-Bindung, vier hemmten sowohl FEN als auch CAR und ein Antikörper erkannte spezifisch CAR, ohne Kreuzreaktionen mit REMI, MOR oder ENDO zu zeigen. Zudem konnten ausgewählte Antikörper die cAMP-Inhibition durch CAR und FEN abschwächen - wobei die Potenz gegen FEN insgesamt stärker ausfiel.

Die Ergebnisse deuten darauf hin, dass CAR eine einzigartige μOR-Konformation stabilisiert, die durch eine außergewöhnlich hohe Effektivität im cAMP-Signalweg, verstärkte Rezeptor-Phosphorylierung und eine verminderte Empfindlichkeit gegenüber Antagonisten gekennzeichnet ist. Die Neutralisierung von CAR durch spezifische Antikörper könnte die μOR-Bindung unabhängig von seiner Konformation unterbinden. Damit verdeutlicht diese Arbeit die dringende Notwendigkeit alternativer therapeutischer Ansätze und unterstreicht das Potenzial spezifischer Antikörper bei der Behandlung oder Prävention von FEN- und CAR-Vergiftungen.

3. Introduction

3.1. Opioids - general information and relevance

Opioids are a class of analgesic agents that are indispensable in modern clinical practice. Their broad range of applications includes acute and chronic pain treatment, anesthesia and palliative care [1-5]. However, the clinical utility of opioids is often limited by a complex landscape of challenges, primarily severe side effects, but also the potential for misuse, dependence and overdose [6].

The term opioid describes substances that bind to opioid receptors (OR) and can be classified based on their activity at these receptors [7,8]. Opioids are categorized as agonists, partial agonists or antagonists. Agonists activate OR to produce a maximal physiological response. In contrast, antagonists bind to receptors without eliciting a functional response while simultaneously preventing agonists from activating the receptor. Partial agonists occupy a middle ground, producing only a limited response upon receptor binding [9,10].

Opioid agonists can further be divided into two primary categories: endogenous and exogenous [11,12]. Endogenous opioids are naturally occurring peptides, that play critical roles in the body's pain modulation system and other physiological processes [13]. Exogenous opioids, on the other hand, include substances introduced to the body and are classified into three subgroups: natural opioids - sometimes referred to as opiates - derived from plants, semi-synthetic opioids produced through chemical modifications of natural precursors (e.g. Diacetylmorphine = heroin [14,15]) and fully synthetic opioids, such as fentanyl (FEN) derviatives, methadone, tramadol and U-compounds [16,17]. Due to structural modifications, synthetic opioids like the FEN analog carfentanil (CAR) can exhibit exceptionally high potency, which correlates with increased toxicity [18].

3.1.1. Properties and therapeutic use

The poppy plant (*Papaver somniferum*) was domesticated for more than 8000 years [19,20]. Ancient cultures of Egypt, Persia or Mesopotamia used it primarily for the pain relieving and calming properties of the opium (dried latex) it contains [16,21]. Opium´s most important pharmacologically active compound, namely

Morphine (MOR), was first isolated in the early 1800s by the german pharmacist Friedrich Sertürner and named after the greek god of dreams: Morpheus [22-24].

MOR has a well established role in clinical practice and research and is often used as a reference for estimating the *in vivo* potency of other opioids [25]. Natural (plant-derived) opioids are ever since, together with newer synthetic derivatives, the most widely used narcotics worldwide [26]. Their therapeutic efficacy in attenuating acute and chronic pain, combined with their sedative properties, has made them indispensable in medical practice, ranging from postoperative care and anesthesia to palliative treatment for terminal illnesses [27]. In clinical practice, opioids are most commonly administered orally or intravenously. However, depending on the clinical context, alternative routes such as subcutaneous, transdermal, intramuscular, sublingual, intrathecal, epidural and intra-articular delivery are also frequently utilized [9].

Pain regulation through opioids is mediated by the activation of the descending pain modulation circuit (antinociceptive system), which refers to the body's physiological mechanisms for reducing pain. This system involves a complex interplay of neurotransmitters, receptors and neuronal pathways, such as the projections from the periaqueductal gray to the rostral ventromedial medulla. These projections regulate incoming nociceptive signals at the spinal cord level, inhibit their processing in central structures like the thalamus and cortex and thereby induce analgesia [28-31]. Specifically, opioids exert their effects by acting as full or partial agonists at OR expressed on pain-transmitting neurons in both the central and peripheral nervous systems [32]. This agonism generally reduces neuronal excitability through multiple mechanisms, which will be discussed in detail in section 3.2 [33].

In addition to analgesia and sedation, which are the primary effects utilized in clinical practice, opioids exhibit various other central and peripheral physiological effects, including euphoria, cough suppression, constipation, nausea, urinary retention, and respiratory depression [34]. The latter is the most dangerous and in case of an overdose the lethal side effect. By this manifestation of toxicity, the medical-clinical use of opioids is not only impaired, but when used improperly and without supervision, opioids also carry significant health risks. Despite the risks

and side effects associated with opioids they remain indispensable in modern medicine and essential for the treatment of severe pain conditions [35].

3.1.2. The fentanyl group – highly potent synthetic opioids

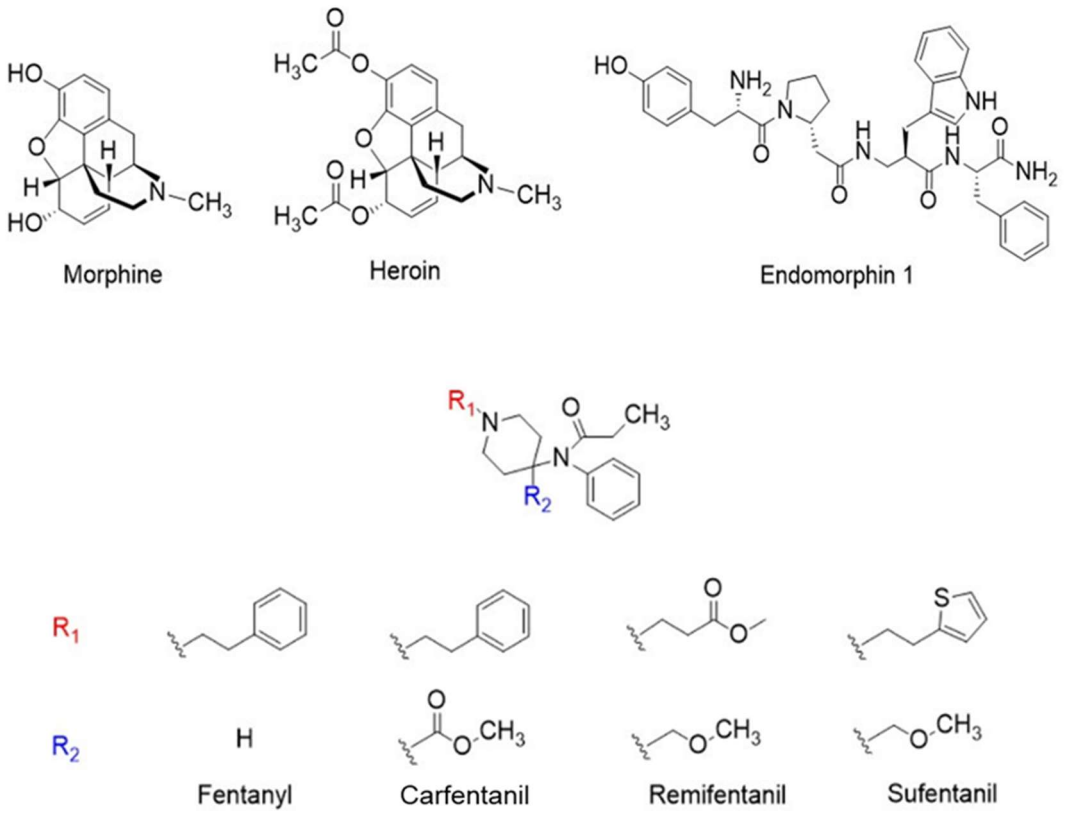

Figure 1: Chemical structure of OR agonists

In 1960, Dr. Paul Janssen developed FEN along with several derivatives, all of which are fully synthetic μ-opioid receptor (μOR) agonists [36,37]. Shortly later FEN was approved for human use as an anesthetic for intravenous administration [38]. FEN is approximately 100 times more potent than MOR; for instance, a dose of just 100 μg provides analgesia equivalent to 10 mg of MOR [39]. In clinical settings, typical intravenous doses for analgesia range from 2-5 mg of MOR every 2-4 hours as needed, whereas FEN is administered in doses of 0.025-0.1 μg/kg every 30-60 minutes, depending on the indication and patient condition [40]. Consequently, since its introduction, FEN has become indispensable in the management of severe pain and in anesthesia [41]. As the leading substance among FEN-like opioids, it is included on the World Health Organization's (WHO) List of Essential Medicines, emphasizing its critical importance in global healthcare [42,43].

While MOR and other natural opioids derived from the poppy plant (e.g. Codeine) belong to the family of benzylisoquinoline alkaloids with a morphinan scaffold, FEN-type opioids (commonly referred to as "fentanyls") are structurally distinct. They are characterized by a 4-anilidopiperidine core, consisting of a piperidine ring and a N-phenyl-propanamide group (Figure 1: Chemical structure of OR agonists) [44]. Structural differences among fentanyls are primarily due to variations in substituents attached to the nitrogen atom of the piperidine ring (R1) and at the 4-position of the piperidine ring (R2) [45].

Remifentanil (REMI) and Sufentanil are widely used FEN derivatives in clinical practice. Sufentanil is among the most potent opioids approved for human use, with an estimated potency 500 to 1,000 times greater than MOR [46]. REMI, on the other hand, exhibits similar potency as FEN [47], with typical intravenous doses ranging from 0.5-1 µg/kg for anesthesia induction [48]. It features an ester functional group making it prone to non-specific esterases present in blood and tissues [49]. This results in its fast hydroxylation and short half life of only 3-5 minutes [50]. These properties allow for easy titration and make REMI especially suitable for use in anesthesiology, such as for the induction of anesthesia [51].

Carfentanil (CAR) represents another modification of FEN itself, with an additional carbomethoxy group on the fourth position of the FEN piperidine ring (Figure 1: Chemical structure of OR agonists) [52]. This chemical structure gives it the alternate name of (4-methoxycarbonyl)fentanyl [53]. It was synthesized in 1974 and introduced to the market in 1984 as Wildnil® for the tranquillization of large animals [36,54,55]. Notably, CAR exhibits extraordinary potency, as demonstrated in animal studies [56]. Its relative analgesic potency is approximately 10,000 times that of MOR and 100 times that of FEN in rats [57,58].

Despite its extraordinary potency, CAR has not been extensively studied in terms of pharmacological or toxicological properties, as it was - due to its severe toxicity - never intended for human clinical use [18,59]. Though the exact lethal dose of CAR in humans is not yet known, based on relative potency estimates, as little as 20 µg is believed to be fatal [60]. Post-mortem analyses of plasma concentrations following human exposure revealed CAR levels approximately

8,000 times lower than those of MOR, with values of 0.5 ng/mL for CAR compared to 2,300 ng/mL for MOR [61,62]. These findings suggest that the estimated 10,000-fold potency difference observed in animal studies may also approximate potency relations in humans.

The *in vivo* potency and, more importantly, the toxicity of opioid agonists can be influenced by both their pharmacodynamics and pharmacokinetics. The latter includes factors such as absorption, distribution, half-life and elimination, all of which can be significantly impacted by chemical modifications. This is particularly true for newly synthesized opioids, where structural adaptions can lead to drastic alterations in pharmacokinetics and, consequently, their physiological effects [45]. For instance, MOR, the standard opioid, crosses the blood-brain barrier (BBB) relatively slowly due to its low lipid solubility, resulting in a delayed onset of action [63]. In contrast, fentanyls are characterized by high lipophilicity and small molecular size, enabling rapid absorption into the bloodstream, quick passage through the BBB and subsequent distribution within the central nervous system (CNS) [64]. These properties lead to a fast onset of effects, including analgesia and euphoria, thereby also increasing the risk of psychological dependence. Furthermore, some FEN analogs are characterized by a long duration of action; for instance, CAR has a relatively long half-life of approximately 6 hours [65]. Cases of renarcotization - the re-emergence of opioid toxicity up to 72 hours after initial recovery - have been observed in large animals sedated with the drug [66]. This phenomenon is likely due to CAR´s high lipophilicity, which facilitates distribution into adipose tissue [67], combined with strong plasma protein binding that results in prolonged release back into circulation [68]. Similarly, renarcotization has been reported in humans following high doses of FEN [69], indicating that the prolonged and rebound effects observed with FEN also occur in humans exposed to CAR.

Even though pharmacokinetics play a significant role in a substance's toxicity, its pharmacodynamics - particularly interactions at the receptor level - likely also contribute to its toxic effects [70]. As summarized in Table 1, μOR binding affinities of opioids have been extensively studied and reported in the literature, with results varying depending on the methodology. These differences arise from parameters such as the choice of cell line, receptor preparation, radiolabeled

tracer and assay buffer. It is well established that FEN derivatives exhibit a higher affinity for μORs, enabling them to induce cellular responses at lower concentrations [71].

Source	**μOR binding affinity [nM]**					**Cell line**	**Assay buffer**
	CAR	FEN	REMI	MOR	ENDO		
[72]				8.91		COS-μOR	TRIS
[73]	0.08			1.40		Human brain	TRIS + 0.5 mM Sodium
[74]		14.0		20.0		CHO-K-μOR	TRIS
[75]	0.15	0.39				SH-SY5Y	TEMD
[76]		1.40				Chem-5-μOR	HEPES
[71]		0.14				CHO-μOR	TRIS
[77]					9.50	Rat brain	TRIS
[78]					2.60	HEK293-μOR	HEPES
[79]			0.60			Rat brain	TRIS
[80]	0.42	3.30				Rat brain	TRIS
[81]	0.024	1.20				Guinea pig	TRIS
[82]		520		445		Frog brain	TRIS + 100 mM Sodium
[83]		98.7		95.9		SH-SY5Y	HEPES + 143 mM Sodium
[84]				1.20		Rat brain	TRIS
[85]		1.60		4.20		Rat brain	TRIS
[86]				8.40		CHO-μOR	Not specified
[87]		1.60				CHO-μOR	TRIS

Table 1: Summary of opioid μOR binding affinities, including experimental conditions (cell lines and buffers)

CAR exhibits the highest μOR binding affinity among the opioid agonists shown. However, the affinity difference compared to MOR ranges from just 18-fold (within the same study) to up to 460-fold (based on mean reported values) - far from the 10,000-fold difference observed in *in vivo* potency. This discrepancy suggests that increased receptor affinity alone cannot explain CAR's extreme potency *in vivo*, implying that additional pharmacodynamic factors contribute to its exceptional efficacy.

Nevertheless, the combination of high μOR affinity and rapid CNS penetration of highly potent opioids accelerates their physiological effects, including analgesia, sedation, and, most critically, respiratory depression [88-90]. Consequently, the medical use of fentanyls is often impaired, not only by a wide range of side effects [6], but their extreme potency and toxicity, especially that of CAR, which contributes to the significant risks of misuse and overdose associated with fentanyls [91]. Adding to CAR's danger is the lack of understanding of its μOR interactions and the mechanisms underlying its exceptional toxicity [92].

3.1.3. Associated risks

Clinically, opioid intoxications are characterized by a triad of symptoms: pinpoint pupils, respiratory depression, and coma [93,94]. Among these, opioid-induced respiratory depression poses the most significant risk, particularly with more potent opioids, as it can result in fatal outcomes in cases of overdose [95]. This condition arises from the stimulation of μORs in key respiratory control centers, such as the brainstem, insula and the preBötzinger complex [96-98]. Activation of these receptors leads to increased arterial carbon dioxide levels and reduced respiratory parameters, like tidal and minute volumes [99,100], causing respiration to slow, become irregular, and, in severe cases, cease altogether [101]. While the risk of respiratory depression is relatively low under medical supervision (e.g. postoperative care) [102], illicit opioid abuse - especially of high-potency substances - significantly increases the danger of fatal outcomes [103]. Furthermore, the potent euphoric effects of fentanyls contribute to the widespread issue of psychological dependence, further complicating their use [104]. Prolonged use can additionally lead to physical tolerance, where the drugs lose

effectiveness over time, and dependence, marked by withdrawal symptoms when use is stopped [105]. These effects are thought to stem from receptor desensitization, downregulation and adaptations in intracellular signaling pathways [106]. Consequently, particularly highly potent synthetic opioids like fentanyls, present considerable challenges for the healthcare system.

These risks associated with fentanyls have been highlighted by the ongoing opioid crisis, which has resulted in extensive addiction, a rise in overdose fatalities and significant consequences for public health, particularly in the US [107,108]. The crisis was exacerbated by aggressive marketing campaigns in the 1990s that promoted prescription opioids for a wide range of conditions, from menstrual discomfort to anxiety and coughs. Purdue Pharma's promotion of OxyContin exemplifies this era [109]. By 2010, an estimated 15.5 million people worldwide were dependent on opioids [110] and opioid prescription rates in the US peaked in 2012, reaching 81.3 prescriptions per 100 inhabitants [111]. This excessive availability of prescription opioids set the stage for misuse and a sudden increase in opioid-related overdose deaths (the “first wave”), followed by a rise in heroin use (the “second wave”). The “third wave” began in 2016 when fentanyls overtook heroin as the leading cause of drug overdoses [112].

Illicit non-pharmaceutical fentanyls (NPF) are often mixed with other substances, such as cocaine or pressed into counterfeit pills, frequently without the user’s knowledge [113]. Their prevalence is driven by their extreme potency, low production costs and ease of manufacturing [114]. Between 2016 and 2021, drug overdose deaths involving fentanyls increased by nearly 300% and in 2023 and 2024 approximately 80% of overdose deaths involved NPF, with an estimated 72,000 deaths attributed to FEN in 2023 alone [115]. More alarmingly, CAR has emerged on the illicit market and is used as an adulterant of other street drugs. Due to its extraordinary toxicity, deaths involving CAR have risen approximately sevenfold since 2023, with hundreds of fatalities reported in North America and Europe [115]. Consumption of CAR frequently occurs unknowingly, as many drug users are aware of its extreme potency and deadly risks [114]. Known by street names such as “elephant tranquilizer”, “gray death”, “drop dead” and “serial killer” [116], CAR significantly heightens the risk of overdose and death, even among individuals with high opioid tolerance [117]. The availability of online synthesis

instructions and its low manufacturing costs make CAR a particularly devastating addition to the illicit drug market [45,118]. Its appearance in drug supplies outside the US, including Germany, underscores its global reach and the escalating challenges it poses [119-121].

Another significant public health concern regarding highly potent opioids like CAR is their potential use as chemical weapons. The use of fentanyls was already investigated in the 1990s as part of a US program which aimed at developing incapacitating agents [122]. CAR´s toxicity is estimated to resemble that of some nerve agents [123], with calculations suggesting that one kilogram of CAR could account for 20 million lethal doses. This extraordinary lethality makes CAR presumably 2,000 times deadlier than a thermonuclear bomb [124].

In 2002, the Moscow dubrovka theatre hostage crisis underscored the risks associated with the weaponization of fentanyls. During the incident, Chechen terrorists held more than 800 hostages, causing russian special forces to introduce an immobilizing aerosol into the building's ventilation system to terminate the siege. CAR, alongside REMI, was identified as one of the active agents in the gas [125,126]. Due to its extreme toxicity and the delayed identification of the substance, coupled with inadequate medical countermeasures, 127 hostages lost their lives and over 600 were hospitalized as a result [127].

Although the WHO recommends the strictest level of international control for synthetic opioids like CAR, it is not explicitly listed in the Chemical Weapons Convention (CWC) [128,129]. However, CAR could fall under the CWC's broader category of pharmaceutically active substances, which, despite not being classified as chemical warfare agents, are listed due to their high toxicity [130]. In theory, this should prohibit its development, production, stockage and use. However, its potential application as a high-impact weapon remains a significant public health threat [124].

In conclusion, while FEN derivatives are highly effective for pain management, their extreme strength also increases the risk of severe adverse effects. CAR is particularly concerning due to its pronounced toxicity, posing a high risk of fatal

overdose and accidental exposure when misused as an illicit drug or chemical weapon.

3.1.4. Endogenous opioid system

Endogenous opioid peptides play a central role in the body's physiological pain regulation system. Acting as agonists at ORs, they trigger a cascade of cellular processes that ultimately inhibit the transmission of pain signals to the central nervous system [131]. Beyond their role in pain modulation, endogenous opioids influence a wide range of physiological processes. These include the regulation of stress [132], respiration [133-136], appetite [137-140], cardiovascular function [141-146], intestinal motility [147,148] and endocrine processes [149] as well as reward and mood [150,151], which underlines their significance for emotional wellbeing.

More than 30 opioid peptides are derived from three precursor proteins: pro-opiomelanocortin (pro-OMC), proenkephalin (pro-ENK) and prodynorphin. These precursors undergo post-translational modifications, resulting in variations in the distribution and concentration of opioid peptides across different regions of the central and peripheral nervous system [152]. While they are ubiquitously expressed, their concentrations differ depending on the specific neural region [131,153,154]. This regional specificity is crucial for explaining the diverse effects of opioids in different parts of the nervous system [155].

The primary peptides in this system include β-endorphin, met-enkephalin, leu-enkephalin and dynorphins. They all share a characteristic amino acid sequence (Tyr-Gly-Gly-Phe), known as the "opioid motif," which is essential for receptor binding [156]. However, their receptor affinities differ [156]. For instance, β-endorphin primarily targets the μOR, whereas met- and leu-enkephalin exhibit a stronger affinity for the delta-OR (δOR). Dynorphins, on the other hand, preferentially bind to kappa-OR (κOR) [157].

Endomorphin-1 (ENDO) and -2 are endogenous opioid-related peptides, that have been identified in the human CNS [158]. Even though their precursor and gene have not been identified, endomorphins play a remarkable role for the physiological antinociceptive system [156,159]. Among all endogenous compounds, ENDO demonstrates the highest specifity and affinity for μOR [160].

Unlike traditional opioid peptides, endomorphins lack the typical opioid sequence and have a unique structure - characterized by a distinctive N-terminal sequence, shorter peptide length, and C-terminal amidation (Figure 1: Chemical structure of OR agonists) [161]. This further supports their role as key endogenous modulators of OR activity. Hence, for the purposes of this study, ENDO was selected as a representative endogenous opioid peptide.

3.1.5. Opioid receptors

Through agonism at OR, all exogenous opioids mimic endogenous opioid peptides and induce comparable physiological effects [162,163]. However, the binding affinity and specificity for the receptor is differentially pronounced depending on the opioid substance [164].

OR belong to the large family of G protein-coupled receptors (GPCRs), which are coupled to heterotrimeric $G_{i/o}$ proteins. These receptors consist of a single polypeptide chain that traverses the cell membrane seven times, forming the characteristic seven-transmembrane domain structure [165]. Their architecture includes an extracellular ligand-binding pocket, where agonist binding results in interactions with intracellular signaling partners, such as heterotrimeric G proteins and arrestins, thereby facilitating diverse cellular responses [166-168].

OR are classified into four subtypes: μOR, δOR, κOR and nociceptin/orphanin FQ receptor (NOR), also known as opioid receptor-like 1 (ORL-1). The naming of OR subtypes reflects their historical discovery contexts: μOR, named after its high affinity for MOR; κOR, after the selective ligand ketocyclazocine and δOR, after the vas deferens tissue where it was first identified [169]. These subtypes are pharmacologically distinguished by their varying affinities for different ligands [170,171]. NOR, which binds the endogenous peptide ligand nociceptin/orphanin FQ [172-174], is structurally similar to traditional OR like μOR, δOR and κOR [175,176]. However, it differs significantly in its ligand-binding domain and activation mechanisms compared to other subtypes and exerts distinct physiological roles [177]. Notably, NOR does not bind traditional opioid agonists and is therefore not typically involved in the effects of widely used opioids such as MOR and FEN [178,179].

Among these subtypes, μORs are particularly significant because they mediate the central effects of opioids, including analgesia and respiratory depression [180,181]. Furthermore, most clinically relevant opioids, such as MOR and fentanyls, exert their effects predominantly via the μOR [9,182]. δOR and κOR share similar intracellular signaling pathways but differ in their distribution within the nervous system and their physiological roles [183,184]. Table 2 provides an overview of opioid effects, the corresponding receptor subtype and specific agonists.

OR subtype	**Physiological effects**	**Agonists**
μOR	Analgesia (central and peripheral), respiratory depression, euphoria, constipation, sedation, physical dependence, miosis	MOR, FEN, heroin, endomorphin-1 and -2, β-endorphine, methadone, DAMGO[1]
δOR	Analgesia (central and peripheral), convulsions, anxiolysis, constipation, modulation of mood and emotions, antidepressant effects	Enkephalines, Deltorphins DPDPE[2]
κOR	Analgesia (central and peripheral), diuresis, dysphoria, sedation	U-50488, Salvinorin A, Ketocyclazocine, Dynorphins
NOR	Modulation of pain processing, stress response, anxiety	Nociceptin, Nocistatin

Table 2: Outline of OR subtypes, their physiological effects and specific agonists

Adapted from Stein et al. [157] and data compiled from [169,184]. [1]DAMGO: [D-Ala2, N-MePhe4, Gly-ol]-enkephalin, [2]DPDPE: [D-Pen2,D-Pen5]enkephalin

3.2. μOR pharmacology and modes of actions

As a member of the GPCR family, the μOR facilitates the transmission of extracellular signals into the cell, primarily via intracellular guanine nucleotide binding proteins (G proteins) and β-arrestins [185]. The agonist-induced activation of the μOR in the CNS therefore plays a pivotal role in mediating the main physiological opioid effects like analgesia, euphoria and respiratory depression [21].

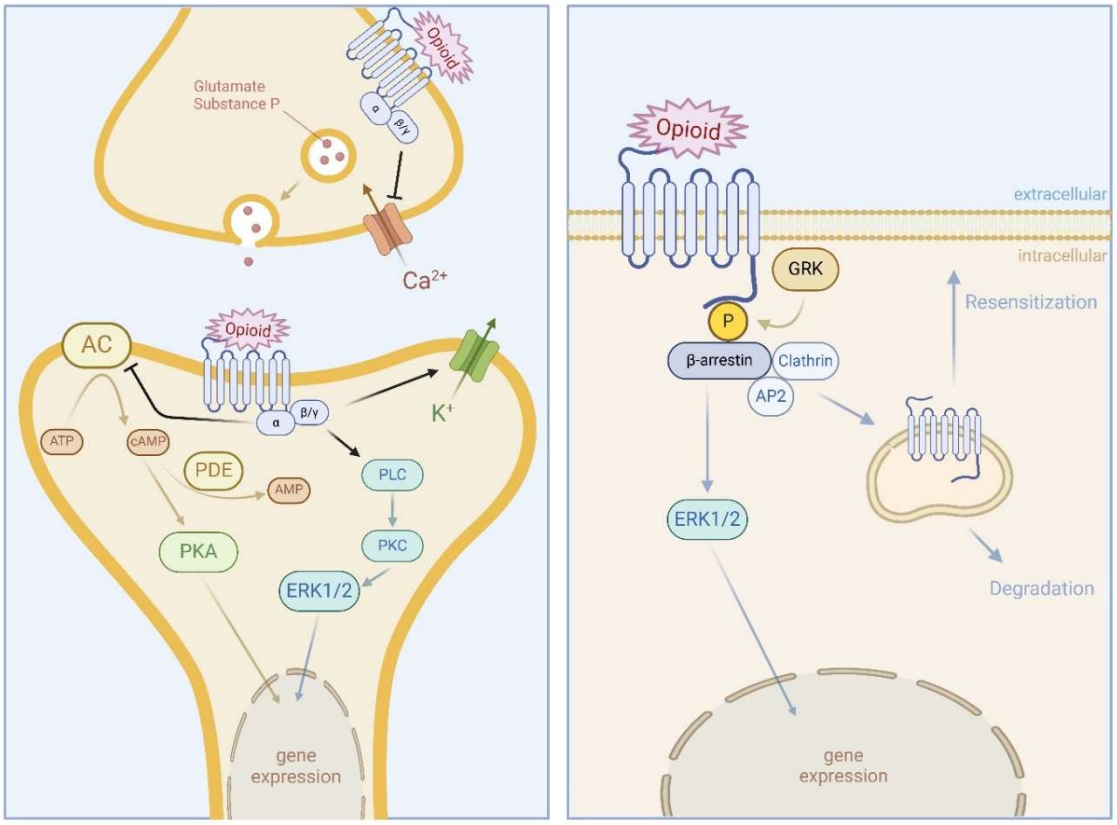

Figure 2: G protein- and β-arrestin-mediated signaling pathways of the μOR

Upon ligand binding, μOR activates both G protein-dependent ($G_{i/o}$-mediated) pathways (left), leading to modulation of ion channels and inhibition of adenylate cyclase, reduced cAMP levels and modulation of downstream effectors, as well as β-arrestin-dependent pathways (right), which regulate receptor desensitization and alternative signaling cascades.

As discussed earlier, a substance's *in vivo* potency is likely influenced by its pharmacodynamics at the receptor level. While the high μOR affinity of FEN analogs, especially CAR, is thought to contribute to its extreme toxicity, the extent to which μOR activation itself plays a role remains unclear. The following sections

provide an overview of the signaling pathways activated by μOR agonists, with a particular focus on what is currently known about CAR-specific signaling.

3.2.1. G protein-dependent signaling pathways

G proteins are heterotrimers consisting of two functional components: a βγ-dimer and an α-subunit. In the inactive state, the βγ-dimer remains tightly associated to the α-subunit, which holds guanosine diphosphate (GDP). Upon activation, the μOR engages with the heterotrimeric G protein at its intracellular domain, specifically at the highly conserved DRY motif. This motif, located between the third transmembrane helix and the second intracellular loop, comprises the amino acids aspartic acid, arginine and tyrosine [186]. This interaction involves the G_{α}-GDP and $G_{\beta\gamma}$ subunits [187]. Activation triggers the exchange of GDP for guanosine triphosphate (GTP) on the G_{α} subunit through conformational changes. The ligand-bound μOR therefore functions as a guanine nucleotide exchange factor (GEF), facilitating the release of GDP from the G_{α} subunit. As a result, the G protein dissociates into two functional components: G_{α}-GTP and the $G_{\beta\gamma}$-dimer. Both components independently initiate distinct signaling pathways [165,188]. The G protein signaling activity is terminated by its intrinsic GTPase activity, which hydrolyzes GTP back to GDP [189,190]. This restores the G_{α} subunit to its inactive, GDP-bound state, ready for another activation cycle [190,191].

3.2.1.1. Modulation of second messenger cAMP

The G-alpha-iota/-omicron subunit ($G_{\alpha I/0}$) is a member of the inhibitory G protein family for which μORs exhibit strong preference [192]. A key result of this signaling cascade is the inhibition of adenylate cyclase (AC), the enzyme responsible for converting adenosine triphosphate (ATP) into cyclic adenosine monophosphate (cAMP) [193,194]. This inhibition leads to a reduction in intracellular cAMP levels. The regulation of intracellular cAMP levels is further influenced by phosphodiesterases (PDEs), enzymes that degrade cAMP into adenosine monophosphate (AMP) [195]. As a second messenger molecule, cAMP plays a critical role in intracellular signal transduction. A key consequence of reduced cAMP formation is the decreased activation of protein kinase A (PKA), the primary cAMP-regulated protein. PKA, in turn, regulates various substrates - including ion channels, enzymes and transcription factors - through

phosphorylation, thus playing a vital role in modulating gene expression [196]. The AC-cAMP-PKA pathway following μOR activation has been shown to contribute to opioid-induced effects, including analgesia [197-201], tolerance [202,203] and respiratory depression [204,205]. In particular, the cAMP signaling pathway plays a central role in controlling respiratory rhythm, helping to maintain the self-generated rhythmic activity of pre-inspiratory neurons in the brainstem and thereby regular and stable breathing [206]. Suppression of this pathway by opioids has been linked to decreased neuronal excitability and disrupted respiratory drive [207]. Studies have shown that pharmacological agents that restore cAMP levels, such as PDE inhibitors or D1-dopamine receptor agonists, can counteract opioid-induced respiratory depression [208,209].

Given the role of this signaling pathway for opioid effects, the extent to which a substance inhibits cAMP formation may impact its *in vivo* potency and toxicity - especially its potential to cause respiratory depression. While some studies suggest that CAR exhibits an increased potency for cAMP inhibition compared to other opioids [75,210], others have reported that CAR is not particularly effective in G protein activation [211]. The broader implications of these findings remain unclear, highlighting the need for a deeper understanding of CAR's mechanism of action and its contribution to its disproportionate toxicity.

3.2.1.2. Modulation of ion channels

The $G_{\beta\gamma}$ subunit mediates the modulation of cell membrane proteins and ion channels [212]. Postsynaptic G protein-gated inwardly rectifying potassium channels (GIRK) are opened, allowing potassium to exit the cell. This results in a change in membrane potential, specifically a hyperpolarization leading to an increased distance between the resting membrane potential and the threshold for action potential generation [213,214]. Furthermore, voltage dependent calcium channels are closed, blocking calcium from entering the cells [215]. In combination with the inhibition of a protein complex called vesicle SNAP receptors (SNAREs) this results in a decreased exocytosis of excitatory, pro-nociceptive neurotransmitter (e.g. glutamate, substance P) [216,217]. Ultimately, this results in a decrease of the excitability of neurons and attenuation of afferent neuronal transmission of pain signals to central processing units [218-220].

3.2.1.3. G protein-dependent ERK1/2 phosphorylation

Another main signaling pathway downstream of the μOR involves the activation of extracellular signal-regulated kinases 1/2 (ERK1/2) [34]. ERK1 and ERK2 are members of the mitogen-activated protein kinase (MAPK) family and are substantial for the regulation of cellular processes such as proliferation, growth and differentiation [221]. Once activated and phosphorylated (pERK1/2), these kinases can phosphorylate various downstream signaling molecules, further propagating intracellular signals [222]. For instance, pERK1/2 can translocate into the nucleus, where it phosphorylates transcription factors like the cAMP response element-binding protein (CREB), significantly influencing gene expression [223-225].

Several mechanisms have been proposed for ERK1/2 activation downstream of OR. Opioid-induced ERK1/2 phosphorylation has been shown to be sensitive to pertussis toxin, indicating that it occurs - among other pathways - via $G_{i/o}$ protein-mediated signaling [226-228]. In this context, the $G_{\beta\gamma}$ subunit plays a central role by activating phospholipase C (PLC) [229-231]. Upon activation, PLC hydrolyzes phosphatidylinositol-4,5-bisphosphate (PIP_2) into two secondary messengers: inositol-1,4,5-trisphosphate (IP_3) and diacylglycerol (DAG). DAG subsequently activates protein kinase C (PKC), which can phosphorylate cytosolic ERK1/2 [232,233]. This signaling cascade has been proposed as the main route for G protein-dependent ERK1/2 activation in HEK293 cells following opioid stimulation [234,235]. In addition, $G_{\beta\gamma}$-dependent phosphorylation of ERK1/2 can occur via tyrosine kinase activation [236-238], e.g. through transactivation of the epidermal growth factor receptor (EGFR) [239]. Beyond these mechanisms, there is also evidence suggesting that ERK1/2 phosphorylation can occur through G_{α}-mediated pathways [240].

The role of ERK1/2 in OR signaling is both multifaceted and complex. Chronic opioid treatment and opioid withdrawal have been associated with elevated levels of pERK1/2 [241], suggesting a possible link to the development of opioid tolerance [242]. Similarly, PKC has been implicated in mechanisms underlying opioid tolerance [243,244]. PLC signaling itself appears to play a role in modulating opioid-induced antinociception, as inhibition of this pathway enhances the analgesic potency of opioid agonists [245,246]. Conversely, there

are indications that ERK1/2 contributes to opioid-induced antinociception [247], suggesting that its role in opioid-mediated analgesia may be divergent and context-dependent.

3.2.2. μOR phosphorylation

The μOR contains eleven serine and threonine residues at its intracellular C-terminus [248], which can be phosphorylated upon receptor activation. This phosphorylation can either occur in an agonist-independent manner via second messenger-regulated protein kinases, such as PKA and PKC, which phosphorylate the receptor regardless of its activation state (heterologous) [249,250]. Alternatively, specific GPCR kinases (GRKs) mediate phosphorylation in response to agonist binding (homologous) [251]. Unlike PKA and PKC, GRKs are specifically recruited to agonist-activated OR and mediate phosphorylation in a ligand-dependent manner [252,253]. Notably, GRK phosphorylation exhibits ligand specificity, meaning that the binding of different ligands to the same receptor can lead to signal transduction through distinct GRK pathways [250,254,255].

Among the C-terminal residues, S363 is a prominent site for basal, agonist-independent phosphorylation by PKC [256]. In contrast, the residues S375, T370, T376 and T379 are the major sites of agonist-induced phosphorylation [257-260]. This homologous phosphorylation primarily occurs within a conserved 10-residue sequence (^{370}TREHPSTANT^{379}) in the receptor's cytoplasmic tail [257,260-262]. The phosphorylation process is hierarchical, beginning at S375, which acts as the initiating site for subsequent phosphorylation at T370, T376 and T379. Notably, phosphorylation at these residues is mediated by GRK2/3 isoforms, with S375 additionally being phosphorylated by GRK5/6 in an agonist-dependent manner and T370 by PKC [258,263-265].

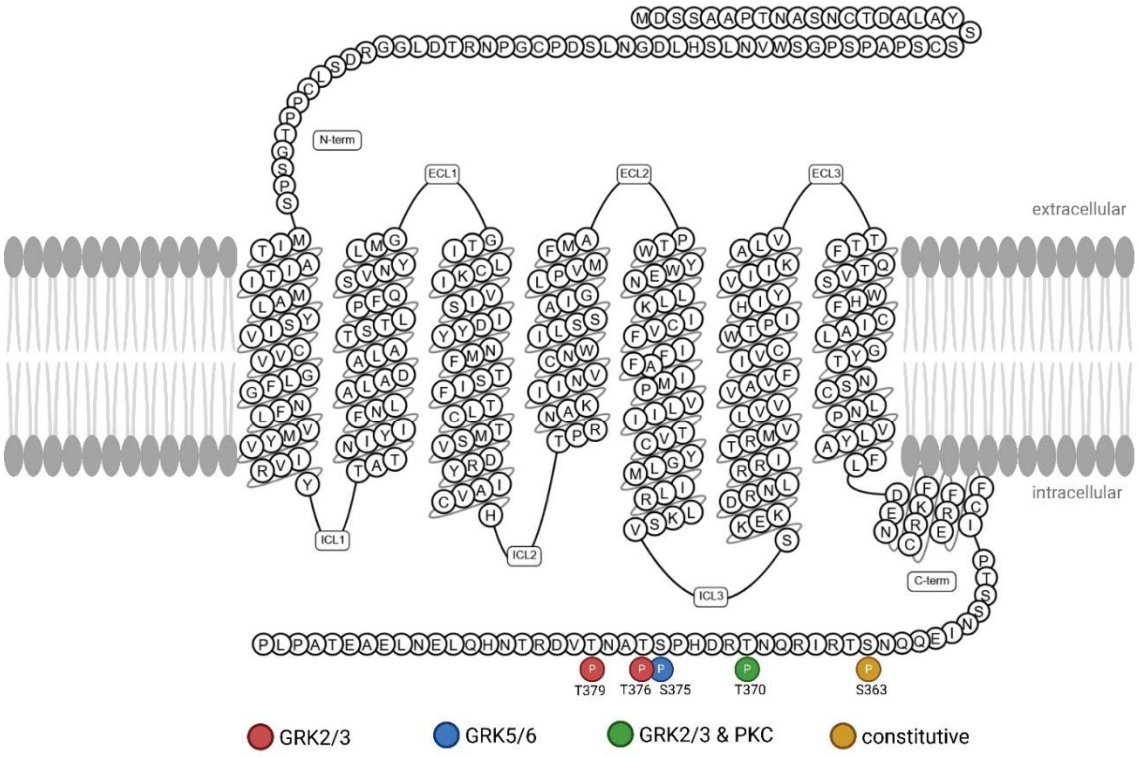

Figure 3: μOR with C-terminal phosphorylation sites and corresponding kinases

Adapted from GPCRdb (https://gpcrdb.org/protein/oprm_human/) [266,267] and modified using BioRender.com

C-terminal phosphorylation of the μOR is a requirement for the recruitment of β-arrestins, which bind to the phosphorylated residues [268]. This interaction uncouples G proteins from the receptor, terminating signal transduction in a process known as desensitization [269,270]. In addition to desensitization, receptor phosphorylation facilitates internalization, a key mechanism for regulating μOR activity and cellular responsiveness to agonists (see chapter 3.2.3).

3.2.3. β-Arrestin dependent signaling pathways

Arrestins are a family of proteins that play a crucial role in regulating GPCR function. Among them, β-arrestin-1 and β-arrestin-2 (non-visual arrestins) are ubiquitously expressed throughout the central and peripheral nervous system and serve as key regulators of OR [271-273]. Activated μOR interact with β-arrestins through recognition of C-terminal GRK phosphorylation, leading to

receptor desensitization and internalization [248,274]. In homologous GPCR desensitization, β-arrestins sterically hinder G protein interaction, effectively preventing further signaling [275-277]. Additionally, they act as scaffolds for enzymes that degrade downstream second messengers, further limiting G protein signaling [278,279].

Restoring GPCR sensitivity requires receptor removal from the cell surface following agonist activation, a process mediated by endocytosis [280,281]. β-arrestins facilitate this by serving as adaptors for clathrin and adapter protein 2 (AP2), which are essential for forming clathrin-coated pits [282-285]. These pits undergo dynamin-dependent vesicle formation, leading to receptor internalization from the plasma membrane [286]. Once internalized, receptors fuse with early endosomes, where they are sorted into one of two pathways. They can either be recycled back to the plasma membrane, a process known as resensitization, allowing continued receptor signaling, or trafficked to lysosomes for degradation, leading to receptor down-regulation and a decrease in receptor availability [287].

Besides their roles in desensitization and endocytosis, β-arrestins also play a crucial role in μOR signaling by acting as adapter proteins for various downstream effectors, including Src, Raf and ERK1/2 [288-291]. Thereby, β-arrestin-mediated signaling forms a second integral component of μOR signaling through the MAPK pathway, beyond G protein signaling [292,293]. Receptor-bound β-arrestin-2 functions as a scaffold, bringing together the kinases cRaf, MEK1 (Mitogen-activated protein kinase kinase 1) and ERK1/2 in an optimal conformation for efficient phosphorylation [294]. Within this complex, cRaf phosphorylates and activates MEK1, which in turn phosphorylates ERK1/2, leading to further downstream signaling, transcriptional regulation and gene expression modulation [289,295]. Notably, β-arrestin-mediated ERK1/2 activation occurs with a delay compared to G protein-dependent activation, suggesting distinct temporal signaling dynamics [235].

The physiological and therapeutic relevance of β-arrestin in opioid signaling is complex and context-dependent. Studies have demonstrated that β-arrestin-2 negatively regulates μOR-mediated analgesia, yet its impact on opioid-induced pain relief appears to be agonist-dependent. In β-arrestin-2 deficient mice, MOR-

induced analgesia is significantly enhanced and prolonged [296-298] whereas FEN-mediated analgesia remains unchanged [299].

Beyond its effects on analgesia, β-arrestin-2 through its role in μOR desensitization and internalization, contributes to the development of opioid tolerance, following μOR phosphorylation by GRKs [257,300]. However, this regulatory effect also varies between different opioid agonists [301]. While the absence of β-arrestin-2 significantly reduces MOR-induced tolerance, FEN-induced tolerance remains unchanged [299]. Interestingly, FEN induces stronger internalization and desensitization of the μOR compared to MOR [302]. A possible reason is that MOR-bound μORs are not optimal substrates for GRK-mediated phosphorylation or β-arrestin binding, leading to a generally slower development of tolerance [303,304]. However, MOR-induced minimal receptor internalization and recycling may contribute to a more pronounced long-term tolerance. In contrast, FEN-induced μOR internalization facilitates receptor recycling and resensitization, potentially mitigating long-term tolerance despite its initially stronger desensitization [305]. In addition to its role in opioid analgesia and tolerance, β-arrestin-2 was also shown to contribute to opioid-induced respiratory depression [306].

While processes like μOR phosphorylation by GRKs, β-arrestin recruitment with subsequent receptor desensitization and endocytosis are known to influence opioid effects, their specific contribution to the extreme potency and toxicity of highly potent opioids like CAR remains unclear. CAR's impact on μOR phosphorylation has not been specifically studied, however, CAR has been shown to induce pronounced receptor internalization [211]. One possible hypothesis suggests that extensive μOR phosphorylation, leading to rapid internalization and efficient receptor recycling to the cell surface, could enhance opioid potency and toxicity by ensuring the receptor remains available for ongoing signaling [307].

Notably, to date, no studies have specifically examined CAR-induced ERK1/2 phosphorylation, whether through β-arrestin- or G protein-dependent pathways, highlighting a critical gap in understanding its pharmacodynamics at the μOR.

3.2.4. Biased agonism

Biased agonism, also referred to as functional selectivity, occurs when different ligands selectively engage distinct intracellular signaling pathways upon binding to the same receptor. This means that a ligand can favor specific downstream effects while minimizing others [308]. In the context of GPCRs, this selectivity can be so pronounced that activation is predominantly mediated through either G proteins or β-arrestins [309]. For opioids, β-arrestin signaling has long been hypothesized to mediate many of the undesirable side effects, including respiratory depression and opioid tolerance [296,306], while G protein signaling is primarily responsible for the desired analgesic effects [310]. Based on this assumption, significant research efforts have been dedicated to developing opioid ligands that preferentially activate G protein signaling while reducing β-arrestin recruitment [311,312]. The goal has been to create opioids that provide strong analgesia while reducing the risk of respiratory suppression and tolerance [313,314]. However, more recent studies suggest that both G protein- and β-arrestin-mediated pathways contribute to opioid side effects [315-318]. These findings challenge the initial assumption that opioid-induced respiratory depression is dependent on a single signaling pathway. Instead, evidence indicates that the severity of respiratory depression is primarily determined by the overall strength of receptor activation, rather than a specific signaling bias [319]. A key example illustrating this is Oliceridine, a G protein-biased opioid, which was FDA-approved in 2020 after initially being rejected in 2018 [320]. Its safety profile has been reported to be similar to that of other opioid derivatives, suggesting that G protein bias alone may not be sufficient to eliminate opioid-induced respiratory depression [321].

These insights highlight the complexity and therapeutic relevance of biased agonism in OR signaling, as well as the intricate interplay between distinct signaling pathways. Understanding how different opioids - especially highly potent compounds like CAR - engage these pathways can be crucial for improving the safety and efficacy of opioid-based therapies.

3.3. Therapeutic interventions of fentanyl intoxication

3.3.1. Opioid receptor antagonists

The standard therapy for opioid overdose and intoxication involves the administration of non-specific, BBB permeable OR antagonists, such as naloxone (NLX) or nalmefene (NLM). Antagonists usually carry large hydrocarbon residues at the amine group [322], which alter their interaction with the receptor´s orthosteric binding site and do not promote receptor activation (Figure 4) [323]. NLX and NLM, both US Food and Drug Administration (FDA) approved agents, counteract opioid toxicity by competing with opioid agonists for μOR binding, preventing further receptor activation and reversing opioid-induced respiratory depression and other opioid effects [324]. Another opioid antagonist, Naltrexone, is primarily used for the treatment of opioid dependence and misuse rather than for acute overdose reversal [325,326].

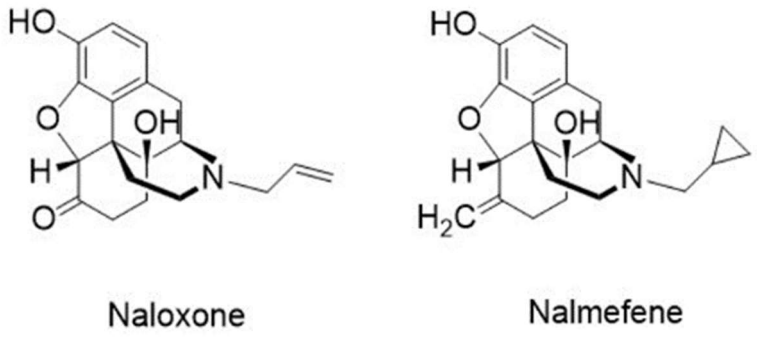

Figure 4: Chemical structure of opioid receptor antagonists

NLX is a moderately hydrophilic opioid antagonist, rapidly metabolized into naloxone-3-glucuronide, a pharmacologically inactive metabolite that cannot cross the BBB [327-329]. Due to its short half-life of approximately 1-2 hours [329] and its rapid onset of action within minutes [330], NLX is the preferred emergency treatment for opioid-induced respiratory depression, restoring normal respiration and consciousness [322,331,332]. NLX is available in multiple formulations, including intravenous and intramuscular injections, as well as nasal sprays designed for non-clinical, on-site and over-the-counter use [333]. The Narcan® nasal spray (4 mg NLX) was first approved by the FDA in 2015 for the treatment of opioid overdoses. In March 2023, the FDA granted approval for its over-the-

counter sale [334]. In the European Union, the Nyxoid® nasal spray received approval in 2017 [335].

Despite its proven efficacy in reversing overdoses from common opioids such as MOR, NLX faces significant challenges when counteracting highly potent synthetic opioids. Studies indicate that NLX reverses respiratory depression induced by MOR more effectively than that caused by FEN [89]. Hence, reports suggest that multiple doses of NLX are frequently required for FEN intoxications [336-339]. Several factors contribute to the high lethality of FEN analogs and the limited efficacy of NLX in these cases. Notably, most fentanyls exhibit prolonged pharmacokinetics compared to frontline antagonists [64,65,340]. This pharmacokinetic discrepancy increases the risk of delayed or inadequate responses and raises concerns regarding renarcotization, the phenomenon where opioid effects return after an initial reversal [102,341]. However, some evidence suggests that, beyond pharmacokinetics, highly potent synthetic opioids may also exhibit a form of pharmacodynamic resistance to NLX's effects [336,342]. This issue is of particular concern with CAR [210,341], which poses a significant challenge to the healthcare system due to its extreme toxicity and the limited efficacy of opioid antagonists against it [337,343-345]. As a result, the question has arisen whether NLX is the ideal antidote for intoxications with highly potent synthetic opioids such as CAR [346,347].

NLM was initially developed for the treatment of alcohol use disorders due to its ability to reduce cravings and block opioid-induced rebound phenomena. It was approved as a nasal spray (Opvee®) for opioid intoxication in the US in May 2023, with an active dose of 2.7 mg, producing effects within 2.5 to 5 minutes [348]. Unlike NLX, NLM exhibits an extended half-life of approximately 11 hours, which is hoped to provide longer-lasting opioid reversal and reduced risk of renarcotization, however it exhibits a slower onset of action [349,350]. While the longer duration of action could theoretically offer advantages, its clinical benefit remains debated, as no convincing evidence currently demonstrates that longer-acting antagonists are superior to NLX in practice [348,351,352]. Additionally, longer-acting antagonists may increase the risk of severe withdrawal symptoms, which can complicate treatment and patient management [348]. While OR antagonists such as NLX and NLM are highly effective and indispensable for

counteracting respiratory depression caused by classical low-potency opioids like MOR, their efficacy against highly potent synthetic opioids such as CAR appears to be significantly limited. This highlights the urgent need for alternative approaches for opioid intoxication management.

3.3.2. Anti-fentanyl antibodies

An alternative strategy to counteract the effects of highly potent opioids is their neutralization through specific antibodies, which would ideally remove the drug from the bloodstream and prevent it from binding to its receptor. One of the main advantages of antibodies is their customization to target specific opioid derivatives, as well as their extended half-life of approximately 21 days in humans [353,354]. Furthermore, antibodies have the potential for prophylactic vaccination, offering protection against future opioid exposure, which could be particularly relevant in scenarios such as opioid use in warfare [355,356].

Since the formation of antibodies against a target molecule depends on its recognition by the immune system, the development of antibodies against highly potent opioids poses significant challenges. Opioids are small, non-peptide molecules, which are poorly recognized by the immune system [357,358]. To overcome this, carrier proteins like KLH (keyhole limpet hemocyanin), BSA (bovine serum albumin) or BgG (bovine gamma globulin) are often conjugated to opioids to enhance immunogenicity [359-363]. This labeling induces an immune reaction by cross-linking B-cell receptors and activating T-cells, enabling the generation of antibodies against the target molecule [364]. The antibodies used in present study were generated using this approach. In total, eight antibodies were obtained from Medix Biochemica and one from Invitrogen. As outlined in Chapter 4.6, these antibodies differ in clonality, the species in which they were raised, and the immunogen used for their generation. Six antibodies were monoclonal and produced either in mice or mouse hybridoma cells, while three were polyclonal, raised in sheep or rabbits.

Another approach to generating antibodies against highly potent opioids involves the utilization of highly immunogenic carrier systems, such as the variant surface glycoprotein (VSG) of African trypanosomes, to enhance the immune response against conjugated opioid molecules [365].

The first investigations into immunization with antibodies to mitigate the effects of FEN were conducted as early as 1975 [366]. Since then, murine, chimeric and human anti-FEN antibodies have demonstrated effectiveness against FEN [367,368] as well as against CAR in rodent models [359,369,370]. Active immunization through vaccination aims to induce the production of endogenous antibodies that bind to the target drug in the bloodstream, thereby limiting its ability to cross the BBB. This approach has already reached clinical trials in humans [371]. However, despite ongoing research, no antibodies for passive immunization against opioids have yet progressed to clinical trials [365]. Recent clinical studies have demonstrated the efficacy and safety of monoclonal antibodies targeting methamphetamine [372] and cocaine [373]. These promising findings indicate that similar antibodies could be developed for opioids, opening new avenues for therapeutic intervention.

3.4. Research objectives

This study aimed to investigate the pharmacodynamics of CAR at the μOR *in vitro*, focusing on cellular mechanisms that might contribute to its exceptional toxicity. Additionally, potential countermeasures, including OR antagonists and anti-FEN antibodies, were evaluated for their ability to neutralize OR binding and activation. By providing a comprehensive pharmacodynamic characterization of CAR, this project sought to deepen the understanding of the molecular basis of its extreme toxicity and explore potential therapeutic interventions.

To achieve these goals, the following key steps were undertaken:

- Generation of a stable HEK293 cell line constitutively expressing μOR, ensuring reproducible experimental conditions. Receptor expression was validated through [^{3}H]-naloxone binding assays and the selected cell line was characterized for binding affinity and total receptor capacity.
- Comparative analysis of CAR's pharmacodynamics and signaling properties against other opioids, including FEN, REMI, MOR and ENDO, by assessing:
  - μOR binding affinity
  - Potency and intrinsic activity for cAMP inhibition
  - Potency and intrinsic activity for ERK1/2 phosphorylation
  - Receptor efficacy across the two signaling pathways
  - Phosphorylation patterns of μOR and cellular proteins
- Evaluation of OR antagonists (NLX, NLM) regarding their ability to neutralize opioid-induced receptor activation
- Assessment of anti-FEN antibodies for their capacity to neutralize FEN- and CAR-induced receptor binding and activation as well as their cross-reactivity with other opioids.

4. Materials

4.2. Instruments

Instrument	Manufacturer
cAMP columns	Available in the laboratory, provided by Dr. Breit
Cell culture incubator PHCbi	PHC, Etten-Leur
Cell harvester	Brandel, Glasgow
Centrifuge Heraeus Biofuge Stratos	ThermoFisher, Waltham
Centrifuge Heraeus Fresco21	ThermoFisher, Waltham
Centrifuge Labofuge 400	ThermoFisher, Waltham
ChemiSmart 5000	Peqlab, Erlangen
Gel electrophoresis Mini-PROTEAN Tetra Cell	BioRad, Hercules
Hellma® TrayCell™	Hellma GmbH & Co. KG, Müllheim
Incubated orbital shaker MaxQ 6000	ThermoFisher, Waltham
Light microscope CKX31	Olympus, Hamburg
Magnetic stirrer MR 3000	Heidolph, Schwabach
Micro pipettes	Peqlab, Erlangen
Mini TransBlot ® tank transfer system	BioRad, Hercules
Multi-channel pipette	Thermo Scientific, München
Neon® electroporation system	ThermoFisher, Waltham
Neubauer chamber	Brand, Wertheim
Optima XL 100k Ultracentrifuge	Beckman Coulter, Brea
Orbital shaker Polymax 1040	Heidolph, Schwabach
pH-Meter FiveEasy F20	Mettler Toledo, Columbus

Photometer BioPhotometer Plus	Eppendorf, Hamburg
Pipetus®	Hirschmann Laborgeräte, Eberstadt
Plate Reader CLARIOstar Plus	BMG Labtech, Ortenberg
Plate Reader FluoStar Omega	BMG Labtech, Ortenberg
Scale EG620	Kern, Balingen
Scintillation counter WinSpectral 1414	PerkinElmer, Rodgau-Jügesheim
Sonopuls™ Ultrasonic Homogenizer	Bandelin, Berlin
Sterile laminar flow hood HERAsafe KS18	ThermoFisher, Waltham
Thermo shaker TS-100	Peqlab, Erlangen
Trans-Blot Turbo Transfer System	BioRad, Hercules
Ultra Turrax T18 basic	Ika, Staufen
Vortex REAX1DR	Heidolph, Schwabach
Water bath HI 1210	Memmert, Schwabach

4.3. Consumables

Material	**Manufacturer**
20 ml syringe	Braun, Tuttlingen
Cell culture 12-well plates	Sarstedt, Nürnbrecht
Cell culture 48-well plates	Sarstedt, Nürnbrecht
Cell culture 6-well plates	Sarstedt, Nürnbrecht
Cell culture 96-well plates	Corning, Kennebunk
96-well plates, white bottom	Sarstedt, Nürnbrecht
Cell culture dishes 5 mL / 22 cm^2	Sarstedt, Nürnbrecht
Cell culture flask, 175 cm^2	Sarstedt, Nürnbrecht

Cleaning wipes	Kimberly-Clark Professional,
Cell scraper	Corning, Kennebunk
Cryo pure tubes	Sarstedt, Nürnbrecht
Filter paper 2.45 mm	BioRad, Hercules
Neon™ Transfection System 100 µL Kit	ThermoFisher, Waltham
Nitrocellulose membrane 0.45 µm	GE Healthcare Life science,
Immunblot PVDF Membrane	BioRad, Hercules
NucleoBond Xtra Midi Kit for plasmid DNA	MACHEREY-NAGEL GmbH &
NucleoBond Finalizer	MACHEREY-NAGEL GmbH &
Pasteur pipettes	VWR, Darmstadt
Pipette tips	Sarstedt, Nürnbrecht/ Starlab, Hamburg
Reagent reservoirs	Corning, Durham
Safe seal micro tubes	Sarstedt, Nürnbrecht
Screw cap tubes	Sarstedt, Nürnbrecht
Serological pipettes	Sarstedt, Nürnbrecht
Open-Top Thinwall Ultra-Clear Tube	Beckman Coulter, Brea
Surgical disposable scalpels	Braun, Tuttlingen
Whatman Filter Paper Grade GF/C Microfiber Glass Filter	Cytiva, Marlborough

4.4. Cell culture media and supplements

Reagent, Catalogue number	**Manufacturer**
DMEM + GlutaMAX™ (Dulbecco's modified eagle medium), 61965026	ThermoFisher, Waltham

Penicillin Streptomycin, 15070-063	ThermoFisher, Waltham
Poly-L-Lysine, P1274	Sigma-Aldrich, St. Louis
SeraPlus FCS (fetal calf serum), P30-3033	PAN-Biotech, Aidenbach
MycoRazor®, M040-100	Biontex Laboratories GmbH, München
Phosphate buffered saline (PBS), J61196.AP	ThermoFisher, Waltham
Zeocin™, 460072	ThermoFisher, Waltham

HEK293 cells were provided by Dr. Andreas Breit. Rat μOR cDNA was obtained from Höllt et al. [374] and human μOR cDNA was purchased from OriGene Technologies (RC210383).

4.5. Reagents

Reagent, Catalogue number[1]	**Manufacturer**
[2,8-^{3}H]-Adenine, NET811250UC	PerkinElmer, Boston
[N-Allyl-2,3-^{3}H]-Naloxone, NET719250UC	PerkinElmer, Boston
μOR Phosphorylation Assay kits pS375-MOP, 7TM0319C-PA	7TM antibodies, Jena
μOR Phosphorylation Assay kits pT370-MOP, 7TM0319B-PA	7TM antibodies, Jena
μOR Phosphorylation Assay kits pT379-MOP, 7TM0319E-PA	7TM antibodies, Jena
3-Isobutyl-1-methylxanthin, I5879	Sigma-Aldrich, St. Louis
4-(2-hydroxyethyl)-1-piperazineethanesulfonic acid (HEPES)	Carl Roth, Karlsruhe
AlphaScreen cAMP detection kit, 6760635D	Revvity Germany Diagnostics, Lübeck
Ammonium persulfate (APS)	Sigma-Aldrich, St. Louis

Aprotinin, 9087-70-1	Tocris Bioscience, Bristol
Biomol BLUEplus Protein Ladder (10-180kDa)	Biomol, Hamburg
Bovine Serum Albumine	Carl Roth, Karlsruhe
Carfentanil-D5 Oxalate, C-163	Cerilliant Corporation, Round
Clarity WesternBlot substrate	BioRad, Hercules
cOmplete™, EDTA-free proteaseinhibitor-cocktail	Roche Diagnostics, Mannheim
Coomassie Brilliant Blue	BioRad, Hercules
DH5α competent E.coli	Thermo Fisher, Waltham
Endomorphin-1, SCP0132	Sigma-Aldrich, St. Louis
Ethanol	Carl Roth, Karlsruhe
Fentanyl, F-013	Sigma-Aldrich, St. Louis
Forskolin, F3917	Sigma-Aldrich, St. Louis
Glycine	Carl Roth, Karlsruhe
Isopropanol	Carl Roth, Karlsruhe
Leupeptin hemisulfate, 103476-89-7	Tocris Bioscience, Bristol
Methanol	Carl Roth, Karlsruhe
Milk powder	Carl Roth, Karlsruhe
Morphine, M-005	Sigma-Aldrich, St. Louis
N,N,N',N'- Tetramethylethylendiamin (TEMED)	Carl Roth, Karlsruhe
Nalmefene, SML2956	Sigma-Aldrich, St. Louis
Naloxone, BP-048	Sigma-Aldrich, St. Louis
Pepstatin A, 26305-03-3	Tocris Bioscience, Bristol
Ponceau S	Sigma Aldrich, St. Louis
Proteome profiler human phospho-kinase array	R&D Systems, Minneapolis

Remifentanil hydrochlorid, R-024	Sigma-Aldrich, St. Louis
Rotiphorese®Gel 30	Carl Roth, Karlsruhe
Rotiszint®Filter	Carl Roth, Karlsruhe
Sodium dodecyl sulfate (SDS)	Carl Roth, Karlsruhe
Tris(hydroxymethyl)aminomethan (TRIS)	Carl Roth, Karlsruhe
Tryptone/peptone	Carl Roth, Karlsruhe
TurboFect™ Transfection Reagent	Thermo Fisher, Waltham
Yeast extract	Carl Roth, Karlsruhe

[1]Catalogue numbers are provided only for reagents that are potentially important for ensuring experimental reproducibility.

4.6. Antibodies

Western blot

Primary antibody	**Species**	**Manufacturer, purchase number**
Histone H3	Rabbit	Abcam, Cambridge; ab1791
pERK1/2	Mouse	Santa Cruz Biotechnology, Dallas; sc-7383

Secondary antibody	**Species**	**Manufacturer, purchase number**
Anti-rabbit-IgG	Goat	BioRad, Hercules; 1706515
Anti-mouse-IgG	Goat	BioRad, Hercules; 1706516

Anti-Fentanyl antibodies

Antibody	**Species**	**Antigen**	**Manufacturer, purchase number**
Ab1 (monoclonal)	Mouse	Fentanyl-KLH	Medix biochemica, Espoo, HM1132

Ab2 (monoclonal)	Mouse	Fentanyl-BSA	Medix biochemica, Espoo, HM004
Ab3 (monoclonal)	Mouse	Fentanyl-KLH	Medix biochemica, Espoo, HM628
Ab4 (monoclonal)	Mouse	Fentanyl-KLH	Medix biochemica, Espoo, HM1133
Ab5 (monoclonal)	Mouse hybridoma	Fentanyl-BSA	Medix biochemica, Espoo, 100974
Ab6 (monoclonal)	Mouse hybridoma	Fentanyl-BSA	Medix biochemica, Espoo, 100998
Ab7 (polyclonal)	Rabbit	Fentanyl-BgG	Medix biochemica, Espoo, P01-99-
Ab8 (polyclonal)	Rabbit	Fentanyl-BgG	Medix biochemica, Espoo, P01-99-
Ab9 (polyclonal)	Sheep	Fentanyl-BSA	Thermo Fisher Scientific, Waltham;

5. Methods

5.2. Plasmid isolation

5.2.1. Bacterial transformation

Transformation refers to the process of introducing recombinant DNA into a prokaryotic cell, where it is propagated [375]. This DNA can then be used for transfection into eukaryotic cells. For transformation and plasmid propagation, DH5α competent E. coli (Thermo Fisher) were used. Two 500 µL aliquots of bacteria stored at -80°C were slowly thawed on ice and transferred into sterile, round-bottom transformation tubes. The required amount of plasmid (typically 100 ng) or an equal amount of phosphate-buffered saline (PBS) (negative control) was then added to the bacterial suspension under sterile conditions, followed by a 30-minute incubation on ice. The bacterial suspensions were subjected to a 5-minute heat shock at 37°C in a water bath to temporarily destabilize the cell membrane, facilitating the uptake of foreign DNA. Immediately afterwards, the tubes were returned to ice. The bacteria were then plated onto antibiotic agar plates and spread evenly with a Drigalski spatula. Plates were incubated overnight at 37°C. If the plasmid carrying the antibiotic resistance gene was successfully taken up, visible bacteria colonies grew on the plates, indicating successful transformation. These colonies were then ready for further processing.

LB medium
1% Trypton/Pepton
0.5% Yeast extract
85.5 mM NaCl
0.5 mM NaOH
100 mg/mL Antibiotic supplement
(1.5% Agar for LB agar plate)

5.2.2. cDNA extraction

Single bacterial clones were carefully picked from the plate using a sterile pipette tip and transferred into a round-bottom tube containing 2 mL of LB medium (Luria-Bertani medium [376] or lysogenic broth) supplemented with the respective antibiotic (concentration 100 mg/mL). The culture was incubated for 24 hours at 37°C with shaking at 250 rpm. Following this, the bacterial suspension was transferred into 200 mL of LB medium for another 24-hour incubation at the same temperature and shaking speed.

Plasmid isolation was performed using the “NucleoBond® Xtra Midi kit for transfection-grade plasmid DNA” from Macherey-Nagel, following the manufacturer’s protocol. All reagents were supplied by the manufacturer. The bacterial culture was diluted until it reached an optical density (OD) of approximately 2 at 600 nm. Subsequently, 200 mL of the culture was centrifuged at 5,000 × g for 15 minutes at 4°C and the supernatant was discarded. The pellet was resuspended in 8 mL of resuspension buffer, and 8 mL of lysis buffer was added, followed by incubation at room temperature for 5 minutes. During this step, the cell wall and membrane are broken down, releasing plasmid DNA, genomic DNA and other cellular components into the solution. Meanwhile, the column and the NucleoBond® Xtra column filter were equilibrated with 12 mL of equilibration buffer.

The lysate was neutralized by adding 8 mL of neutralization buffer and the tube was inverted several times until the solution became colorless. This step facilitates the renaturation of chromosomal DNA and the aggregation of cellular proteins, allowing their subsequent separation. Meanwhile, the plasmid DNA remains dissolved in the solution. The bacterial lysate was loaded onto the filter, taking care not to block it with solid cell fragments. This step clarified the solution by removing aggregated cell debris. After washing with 5 mL of equilibration buffer, the filter was discarded. The column was then washed with 8 mL of washing buffer and the plasmid DNA was eluted into a falcon tube using 5 mL of elution buffer. To precipitate the plasmid DNA, 3.5 mL of isopropanol was added to the eluate, followed by vigorous vortexing and a 2-minute incubation at room temperature. The resulting solution was transferred into a syringe equipped with the NucleoBond® Finalizer and pressed through. Subsequently, 2 mL of 70%

ethanol was added as a washing step and the filter was dried by pressing air through it at least six times. Finally, the plasmid DNA was eluted into an Eppendorf tube with 200-800 µL of provided TRIS-buffer. The concentration of the plasmid DNA was measured using a spectrophotometer at 260 nm and the plasmids were stored in aliquots at -20°C for long-term storage and at 4°C for short-term storage.

5.3. Cell culture

5.3.1. Cell cultivation

For this study, HEK293 cells were chosen as the experimental model. HEK293 cells are immortalized human embryonic kidney cells derived from an aborted or miscarried female fetus [377]. They are a widely used model in biomedical research due to several advantageous characteristics. Due to their transfection with fragmented adenovirus 5 DNA and the stable expression of viral proteins that inhibit apoptosis and promote cell division (E1A and E1B 55 kDa), HEK293 cells exhibit rapid proliferation and can grow indefinitely under appropriate conditions [377-380]. Additionally, they are easy to cultivate and are highly suitable for transfection, making them ideal for expressing recombinant proteins [381].

Cells were cultured in adherence within growth medium on T175 flasks (surface area of 175 $cm^{2)}$. The growth medium consisted of DMEM (Dulbecco's Modified Eagle Medium) with high glucose, supplemented with GlutaMAX™ supplement, 10% fetal calf serum (FCS), 100 U/mL penicillin/streptomycin and 5 µg/mL MycoRazor®. Flasks were held in a humid incubator maintaining 5% CO_2 atmosphere at 37°C. Upon reaching around 80% confluency, the cells underwent subculturing to prevent overgrowth. This process, along with cell seeding, occurred under aseptic conditions within a sterile laminar flow hood. Solutions required for subcultivation were preheated to 37°C in a water bath. The cell medium was carefully aspirated and cells were rinsed with 5 ml of PBS. Subsequently, 5 ml of PBS was introduced into the flask to allow cells to dissociate from the plastic surface. The absence of bivalent cations (Mg^{2+}, Ca^{2+}) in PBS served to attenuate intercellular interactions and reduce cell adhesion to the plastic surface, facilitating detachment of the cells. Once detachment was

confirmed through microscopic examination, 5 ml of growth medium was added to the flask. Cell conglomerates were seperated by gentle pipetting and 10 mL suspension was transferred to a 15 mL tube. Centrifugation for 5 minutes at 800 rpm was performed, followed by the removal of the supernatant and resuspension of the cell pellet in 10 mL of medium. A portion of this suspension (usually 1 mL) was transferred to a new T175 flask containing 25 mL of growth medium to achieve 80% confluence within 3-4 days. The remaining cell suspension was utilized for experimental purposes. The cell count in the suspension was determined by applying 10 µL of the cell suspension to a Neubauer counting chamber. The number of cells present within a single gridded square (equivalent to 0.1 µL) was ascertained under a microscope and then multiplied by 10^4 to compute the number of cells per mL within the suspension. Cells were seeded onto culture plates in quantities optimized for the specific experimental requirements and incubated at 37°C for 24 hours to allow proper adherence and growth. To synchronize the cells to the same cell cycle phase, they were usually serum starved over night before performing experiments. For this purpose the growth medium was replaced with FCS-free medium.

5.3.2. Cryoconservation of cells

Cells were detached and quantified as outlined in section 5.3.1. They were transferred to a 15 mL falcon tube and centrifuged at 800 rpm for 5 minutes. Supernatant was removed and the pellet was resuspended in icecold FCS supplemented with 10% dimethyl sulfoxide (DMSO) to prevent frost-induced damage. 1 mL FCS/DMSO mixture was prepared per 500,000 cells. Notably, these procedural steps were executed under ice-cooled conditions. 1 mL of cell suspension was transferred into cryo-tubes and promptly placed in a freezing apparatus set at -80°C, specifically calibrated to achieve an optimal cooling rate of -1°C per minute. After 24 hours, the cryo-tubes were transferred into the liquid phase of a nitrogen tank (-196°C), ensuring long-term preservation.

5.3.3. Thawing of cells

Following removal from the nitrogen tank, cryo-tubes underwent rapid warming at 37°C in a water bath and were then moved to a T175 culture flask with 25 mL preheated growth medium. This rapid procedure ensured the efficient thawing of

the cells [382]. Subsequently, after 24 hours, the medium was replaced with fresh growth medium to eliminate DMSO.

5.3.4. Transfection for stable μOR expression

In the course of this work, a recombinant HEK293 cell line, stably expressing the μOR was established by transfection and subsequent selection. HEK293 cells are known for their high transfection efficiency and ease of cultivation [381,383,384] and are therefore a valuable tool for studying receptor-ligand interactions and cellular processes. In addition to providing a homogeneous cell population that eliminates clonal variability, the approach of transfection with stable protein expression, also offers the advantage of experimental simplicity. The steps of transfection and the waiting time until sufficient protein expression were thereby saved.

5.3.4.1. Transfection

HEK293 cells were thawed in FCS-supplemented DMEM growth medium as described in chapter 5.3.3. Upon reaching around 80% confluency, one million cells each were seeded on five 20 mL cell culture plates in growth medium. After 24 hours, cells were co-transfected with cDNA encoding the rat or human μOR (rμOR or hμOR) along with the pcDNA4 plasmid, which contains a gene for resistance to Zeocin™. Zeocin™ is an antibiotic from the bleomycin/phleomycin family, known for its cytotoxic effects on vaious cells including bacterial and mammalian cells [385]. Resistance to Zeocin™ is conferred by the *Sh ble* gene from *Streptoalloteichus hindustanus*. This gene encodes a 13.7 kDa protein that binds to Zeocin™, preventing it from breaking DNA strands [386]. As a result, cells expressing this resistance protein can survive in the presence of Zeocin™, making it a useful tool for selecting successfully transfected cells. To determine the transfection protocol that yields the highest protein expression levels, several concentrations of cDNA were introduced to the cells.

5.3.4.1.1. Rat μOR

Cells were transfected with a pEAK10 expression vector carrying the rμOR using TurboFect® (Thermo Scientific) [374]. TurboFect® contains a small, cationic polymer which forms highly diffusible complexes with DNA. These complexes are

easily endocytosed by the cells and enable translocation of the DNA into the nucleus.

The plasmid combinations were chosen to investigate the effect of varying ratios of μOR-cDNA to pcDNA4 on the expression efficiency of the μOR. The balance between the plasmid carrying the gene of interest (μOR) and the plasmid with the selection marker (pcDNA4), as well as the ratio between the total plasmid amount and the cationic polymer, are crucial for transfection efficiency and subsequent gene expression [387]. High concentrations of pcDNA4 might compete with the μOR-cDNA plasmid for transcriptional and translational resources, potentially reducing μOR expression. On the other hand, a higher concentration of μOR-cDNA could enhance receptor expression, but may also decrease transfection efficiency due to the overall plasmid load.

Transfection approach	**Gene of interest (rμOR) [μg]**	**Selection marker (pcDNA4) [μg]**
1.	5	2
2.	10	5
3.	5	5
4.	-	5
5.	-	-

Transfection approach 4 was included as a negative control for the gene of interest, while approach 5 served as a negative control for transfection success. The required volumes of corresponding cDNA quantities were dissolved in 500 μL of DMEM without antibiotic supplement. A further 500 μL of medium were mixed with twice the amount of TurboFect® (in relation to the amount of total cDNA). The TurboFect® dilutions were slowly pipetted into the cDNA mixture and incubated for 1 hour at room temperature. 1 mL of transfection solution was then introduced to the cells by gently dropping it onto the cell culture plates. Cells were subsequently incubated for 24h.

5.3.4.1.2. Human μOR

Cells were transfected with the hμOR via electroporation using the Neon™ Nxt transfection system (Invitrogen). This method involves applying short electric pulses to the cells, creating pores in the cell membrane that allow plasmids to enter. The buffers utilized were supplied by the manufacturers. Cells were detached, counted and a volume containing 15 million cells was centrifuged for 5 minutes at 1000 rpm. The supernatant was aspirated and the cell pellet was resuspended in 450 µL of resuspension buffer. The cell suspension was divided into three equal parts, each supplemented with different amounts of plasmids to determine the optimal ratio.

Transfection approach	**Gene of interest (hμOR) [µg]**	**Selection marker (pcDNA4) [µg]**
6.	1.5	0.5
7.	5	2
8.	2	2

100 µL of each transfection approach was electroporated with 1100 V for 20 ms and 2 pulses. Cells were subsequently seeded on 20 mL plates in DMEM without antibiotic supplement and incubated for 24 hours. No negative controls were included in this experiment as it was already incorporated during the transfection of the rat receptor.

5.3.4.2. Zeocin™ selection and single cell cloning

To select cotransfected cells, plates were cultured for about two weeks with regular medium exchange with DMEM supplemented with 400 µg/mL Zeocin™ every 2-3 days.

When cell colonies became visible to the naked eye, single-cell cloning was performed to isolate individual cell clones. For this purpose growth medium was aspirated. Cloning rings were carefully placed on the plate, with the cell clone in the center. 200 µL PBS was added into the ring and incubated for 5 minutes at room temperature. Cells were detached from the plate by gentle pipetting within the cloning rings. Subsequently the cell suspensions were transferred into wells

of a 6-well culture dish together with 2 mL growth medium supplemented with 200 µg/mL Zeocin™. After reaching ~80% confluency, cells were ready for further experiments.

Single cell clones derived from rµOR transfection approach 3 were designated as 3A, 3B, 3C, and so on. Cell clones of rat µOR transfection approaches 1 and 2 were united through detachment and unified cultivation and further investigated as cell pools (pool 1 and pool 2).

Single cell clones derived from hµOR transfection approach 7 were designated as 7A, 7B, 7C and so on, clones derived from approach 8 were designated as 8A, 8B, 8C etc.

5.3.5. Transfection for transient µOR expression

Transient transfection is the process of introducing foreign DNA into a cell, enabling the expression of the desired protein. Unlike stable transfection, the foreign DNA is not integrated into the cell's genome, resulting in temporary protein expression. One advantage of transient transfection is that it often leads to higher levels of target protein expression compared to stable transfection. Additionally, transient transfection is typically more efficient and successful in a shorter time frame [388,389]. In this study, transient transfection was performed as a positive control for the expression of the hµOR and served as a comparison to the stable expression (discussed in 6.2)

50,000 HEK293 cells were seeded on 6 wells of a 48-well plate in 400 µL growth medium and cultivated for 24 hours. A total of 150 µL DMEM without antibiotic additives was mixed either with 0.9 µg of hµOR plasmid or with double the amount of Turbofect® (1.8 µL). The Turbofect® dilution was added dropwise to the plasmid solution and incubated at room temperature for 1 hour. 50 µL of the mixture was then carefully added to each of the 6 wells, and the cells were cultured for 24 hours. Subsequently, cells were ready for screening in the binding assay (see 5.4.1).

5.3.6. Stimulation procedure

Individual experiments required distinct stimulation protocols and reagent concentrations, as detailed in the accompanying method descriptions and

reflected in the figure captions. Whenever reagents were dissolved in solvents besides water, control samples were supplemented to prevent any misinterpretation arising from solvent-related influences on the data.

Table 3 offers a summary of the dissolving agents and stock concentrations prepared for each reagent.

Two equally effective stimulation procedures were employed in this work. Typically, the growth or starvation medium was aspirated and replaced with a stimulation dilution of the desired concentration, prepared in FCS-free medium. Alternatively, the medium was first replaced with 90% of the final volume of FCS-free medium and incubated for at least 30 minutes before adding 10% of a tenfold concentrated stimulation dilution.

Stimulant	**Solvent**	**Stock concentration [µM]**
Carfentanil	Methanol	204
Endomorphin-1	H_2O	5000
IBMX	DMSO	500,000
Fentanyl	Methanol	2970
Forskolin	DMSO	50,000
Morphine	Methanol	3500
Nalmefene	H_2O	10,000
Naloxone	H_2O	10,000
Remifentanil	Methanol	266

Table 3: Stimulants used with corresponding solvent and stock concentration

5.3.7. Preparation of total membrane fraction

Total membrane preparation was conducted as previously described [390]. Up to four T175 flasks containing µOR HEK293 cells grown to ~80% confluency were harvested through PBS-washing and detachment as described in section 5.3.1. The cell suspension was transferred to 15 mL falcon tubes and centrifuged at

1000 rpm for 5 minutes at room temperature. Each pellet was resuspended in 10 mL icecold membrane buffer (5 mM TRIS-HCl, 2 mM EDTA, pH 7.4, 50 mL supplemented with one protease inhibitor tablet (Roche)). Further steps were performed on ice to preserve the integrity of cellular membranes and prevent enzymatic degradation of membrane components [391]. With an ultra turrax cells were shredded mechanically for 10-20 seconds. To separate nuclei and other unwanted cell fragments from the membrane fraction, the suspension was centrifuged at 1000 rpm for 10 minutes at 4°C. The supernatant was transferred into round bottom ultra centrifuge tubes and balance was adjusted, if necessary, by adding membrane puffer. Membranes were precipitated through ultracentrifugation (41,000 rpm, 1 hour, 4°C). Resulting pellets were mixed with 500-1000 µL of membrane buffer and resuspended through vigorous pipetting. Following protein quantification (5.3.8), membranes were cryopreserved as aliquots (0.5-2 mg) by immersing them into liquid nitrogen and subsequently transferring them to -80°C freezer.

5.3.8. Quantification of membrane protein content

Total protein content in isolated membrane fractions was determined using the Bradford/Coomassie Brilliant Blue assay. While this method typically measures overall protein concentration, it was used here to normalize membrane preparations, ensuring consistent amounts for subsequent experiments. Coomassie Blue is a dye commonly used to quantify protein concentrations [392-394]. Upon non-covalently interacting with amino and carboxyl side chains of proteins, the coomassie dye undergoes conformational changes (switches to its anionic form) and its absorption maximum shifts from 465 nm to 595 nm [395]. The intensity of blue color is directly proportional to the amount of protein in the sample and can be detected spectrophotometricly [396]. The exact protein concentration was determined by interpolation from a standard curve generated with protein standards of known concentrations. Bovine serum albumin (BSA) was used as standard protein. For this purpose a 10 mg/mL stock solution was prepared with deionized water as solvent and diluted to one order of magnitude higher concentrations than the desired concentrations. 360 µL of Coomassie Brilliant blue were mixed with 40 µL of the above dilutions and absorption at 585 nm of the resulting solutions was measured in triplicates (100 µL) on a 96-well

plate with transparent bottom. Since the Coomassie dye was relatively old, its absorption maximum was determined by measuring optical densities (OD) across a range of wavelengths. Due to chemical alterations in the dye, the absorption maximum had shifted to 585 nm, so protein measurements were conducted at this adjusted wavelength. The corresponding OD values were plotted against the final concentrations of the solutions and a linear regression was used to create a linear equation.

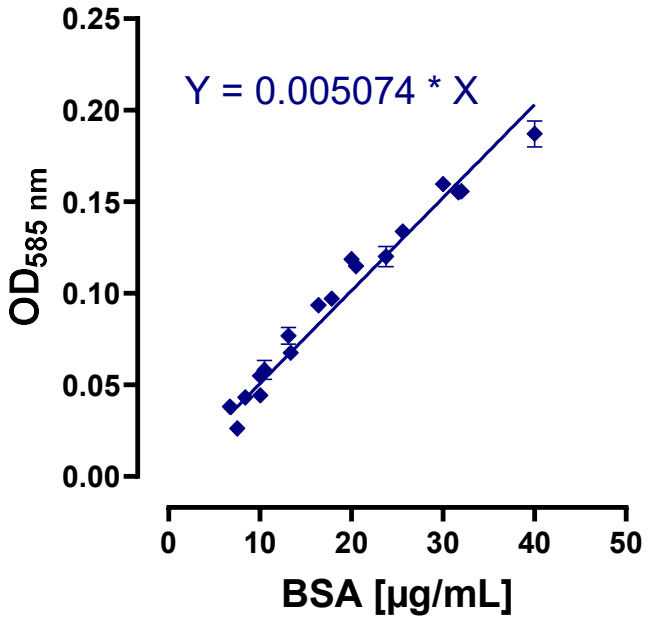

Figure 5: BSA - Coomassie standard curve and corresponding linear equation

To determine protein concentrations of membrane preparations, 5 µL membrane preparation were mixed with 45 µL of deionized water. 40 µL of this 1:10 dilution was given to 360 µL of Coomassie Blue. For blank, 40 µL of deionized water was used accordingly. 100 µL were pipetted in triplicates on a 96-well plate with transparent bottom and OD at 585 nm was measured. Protein concentration of the initial membrane preparation was obtained by inserting it into the linear equation and taking the dilution factors into account.

5.4. Ligand-receptor binding studies

Radiobiochemical assays are used to observe cellular processes like receptor-ligand interaction or formation of molecules of interest. By binding or incorporating radioactive tracers (in) to target molecules, their behavior can be tracked and

their quantitative measurement is enabled. The readout of the radiobiochemical experiments described in this work - specifically the ligand binding assays (described below) and the cAMP assay (section 5.5.1) - was performed using a liquid scintillation counter. The measured variable was the radioactive β-decay of the [^{3}H]-labeled tracer, either in form of disintegrations per minute (dpm) or counts per minute (cpm), with cpm being divided by the efficiency factor to obtain dpm. The efficiency factor of a scintillation counter represents the ratio between the actual radioactive decay of a sample and the measured decay. To determine this factor, a radioactive standard with a precisely known activity at a specific time point was used. By considering the half-life of the radioisotope and the time passed since the reference point, the current radioactivity expected at the time of measurement was calculated. This calculated value was then compared to the actual measurement of the standard, which allowed for the determination of the efficiency factor, defined as the ratio between the measured and expected value. Measured cpm values were divided by this factor to obtain the corresponding dpm.

Ligand binding assays provide a direct method for measuring interactions between GPCRs and ligands and are one of the earliest *in vitro* techniques developed to study receptor function, with the first assay established in 1965 [397,398]. They play a crucial role in the assessment of natural and synthetic ligands such as neurotransmitters, hormones or pharmaceutical drugs and therefore pose fundamental tools in GPCR biology and pharmaceutical industry [399,400].

In this work, ligand binding assays were performed with [^{3}H]-naloxone ([^{3}H]-NLX) as a tracer. As a non-selective OR antagonist, NLX binds and therefore labels OR. Receptor preparations were stimulated in triplicates with [^{3}H]-NLX to obtain total tracer binding, which consists of both specific and non-specific binding. Non-specific binding occurs when [^{3}H]-NLX binds not only to the receptors but also, to a lesser extent, to other binding sites like the cell membrane or the filter. Measuring non-specific binding is crucial to accurately reflect how much [^{3}H]-NLX is truly bound to the receptors themselves. It was determined by coincubation of the receptor with [^{3}H]-NLX and an excess of unlabeled (cold) NLX. This surplus of cold ligand competes with the radioligand for receptor binding sites and is

expected to saturate over 99% of available receptors. However, non-specific binding sites (e.g. membrane or filter binding) are typically regarded as linear and non-saturable, meaning that excess unlabeled ligand does not displace the radioligand bound non-specifically [399,400]. Through subtraction of non-specific binding from the total binding, specific μOR receptor binding was calculated [401].

$$total\ [^3H]NLX\ binding = specific\ [^3H]NLX\ binding + nonspecific\ [^3H]NLX\ binding$$

$$specific\ [^3H]NLX\ binding = total\ [^3H]NLX\ binding - nonspecific\ [^3H]NLX\ binding$$

Equation 1: Calculation of specific [³H]-NLX binding

A receptor preparation was offered to the tracer in three formats: as a cell monolayer, cell suspension or membrane preparation. Tracer binding enabled quantification and the resulting data were used to calculate parameters such as receptor expression levels and binding affinities.

Membrane preparation or cell suspension

To prepare the membrane preparation for the experiment, a cryopreserved aliquot was thawed in the required volume of binding buffer. To create a suspension of whole cells, HEK293-μOR cells were washed and detached using PBS. The cells were then counted and the volume was adjusted to achieve the desired cell concentration before centrifuging at 1000 rpm for 5 minutes. The resulting cell pellet was resuspended in the required amount of binding buffer. Usually, 75 or 100 μL of tracer solution, four times higher concentrated than the desired final concentration, was pipetted into the wells of a 96-deepwell plate. 75 or 100 μL of four-times concentrated ligand solutions were added to the wells. The reaction was started by the addition of 150 or 200 μL cell suspension or diluted membrane preparation. The 96-well plate was then incubated for defined time periods at specific temperatures to enable the formation of an equilibrium between the association and dissociation of the receptor-ligand complex [402,403]. This equilibrium was disrupted by rapid aspiration of the receptor preparations onto a glass fiber filter using a cell harvester, which effectively separates the bound ligand from the free ligand. Three washes with 500 μL PBS

served to separate remaining free ligand from the filter. Filter patches were then transferred into scintillation vials, mixed with 5 mL scintillation cocktail (Rotiscint® Filter) and measured with the liquid scintillation counter.

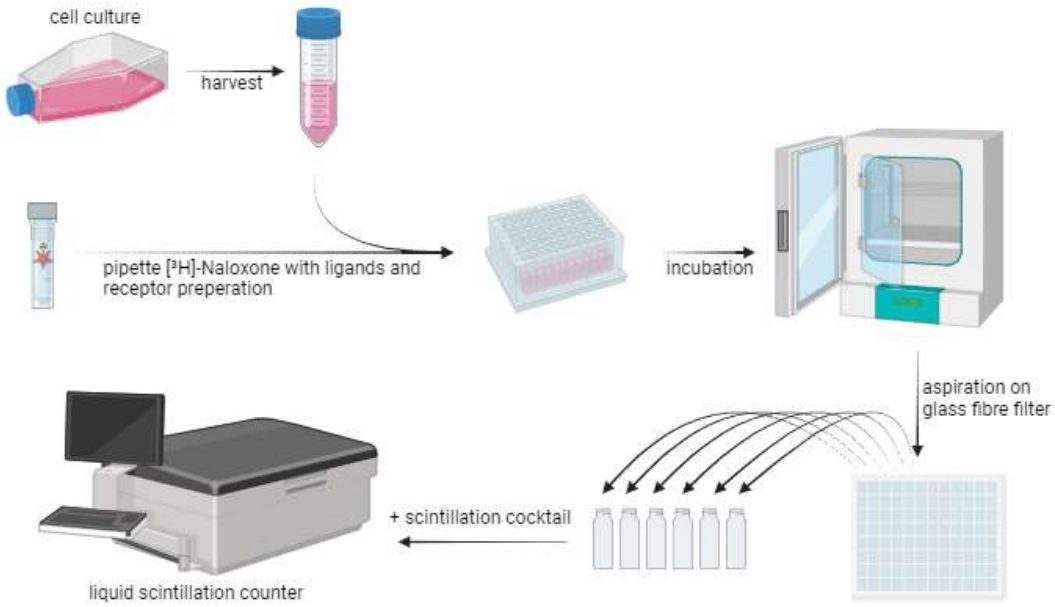

Figure 6: Experimental setup of a ligand binding assay with cell suspension or membrane preparation

Cell monolayer

For assays using cell monolayers, cells were stimulated and lysed directly in the wells where they were seeded, eliminating the filtration step. Cells were seeded at 80-100,000 cells/well on poly-L-lysine coated (50 µg/mL) 48-well plates in 400 µL/well growth medium and cultured for 24 hours. Poly-L-lysine coating transfers a positive charge to the plastic surface and was used to enhance cell attachment. Cells were then starved for an additional 24 hours before stimulation. The medium was replaced with 250 µL of stimulation dilutions per well, prepared in the respective binding buffer as detailed in the corresponding chapter. After a one-hour incubation at room temperature, stimulation dilutions were aspirated, and cells were washed twice with 400 µL PBS. Subsequently, cells were lysed with 250 µL lysis buffer (0.1 N NaOH, 0.1% SDS) per well. Lysates were transferred into scintillation vials, mixed with 5 mL scintillation cocktail and read for radioactive decay.

Further experimental details and specific setups are provided in the respective sections.

5.4.1. Screening HEK293 cells for receptor expression

Transfected HEK293 cells obtained through Zeocin™ selection and single cell cloning (see chapter 5.3.4.2) were investigated with regard to their μOR expression. The following approaches were assessed in the experiments: Cells derived from single-cell cloning, generating rμOR clones (e.g. 3A, 3B, ...) as well as two pooled cell populations (labeled pool 1 and pool 2), alongside native HEK293 cells as a control. For hμOR expression, two rounds of transfection followed by single-cell cloning resulted in clones such as 7B, 7C, 8C, 8D and others were included. Transiently transfected cells and two rat-derived clones with the highest [³H]-NLX binding were incorporated as references, with native HEK293 cells serving as control. The goal was to identify the transfection approach and cell clone with the highest receptor expression. One clone with optimal expression was then selected for further characterization in subsequent experiments.

For the assays, cell monolayers of the clones and pools were incubated with 10 nM [³H]-NLX to measure total binding and 10 μM NLX was used to determine non-specific binding. These solutions were prepared in DMEM supplemented with 50 mM HEPES as a buffering agent. Specific [³H]-NLX binding was calculated using Equation 1 and the data were plotted as the mean ± SEM of dpm.

5.4.2. Assay optimization

5.4.2.1. Incubation parameters

Temperature variations within the assay can significantly affect both the binding affinity and the stability of the receptor-ligand complex, as changes in temperature may alter the strength of the interaction as well as the duration of the binding [404,405]. To determine optimal incubation parameters, temperature and time dependency of the [³H]-NLX receptor binding in the stable HEK293-μOR cell line was investigated. For this purpose, ligand binding was measured at several time points, both at room temperature and at 37°C. 250,000 whole intact cells per well were incubated with 5 nM [³H]-NLX in a total volume of 200 μL for

15-minute intervals up to two hours, either at room temperature or in a temperature-controlled 37°C incubator. The concentration of 5 nM [³H]-NLX was chosen based on preliminary saturation experiments, where this concentration approximated the affinity range of the tracer, allowing for optimal measurement of binding without excessive use of radioactive material. Non-specific binding was determined by co-incubation with 10 µM unlabeled NLX. The binding buffer used in the assay was DMEM supplemented with 50 mM HEPES.

Upon terminating the reaction by filtration and washing, filter patches were evaluated regarding their [³H]-NLX binding by measuring their radioactivity. Specific binding was determined using Equation 1. Dpm at 120 minutes was set as 100% and other values were normalized to this time point. The data of 3-4 individual experiments were plotted as the mean ± SEM of specific [³H]-NLX binding, expressed as a percentage of the dpm at 120 minutes, against time.

5.4.2.2. Methanol influence

Research has shown, that solvents can influence the solubility and stability of ligands and also impact binding dynamics by changing receptor shape or the ionic environment in the assay [406]. The choice of solvent can therefore impact the binding of radiolabeled ligands to receptors. To investigate the impact of methanol on [³H]-NLX binding in HEK293-µOR cells, 250,000 adherent cells per well were incubated in either 50 mM TRIS-HCl buffer (pH 7.4) or DMEM supplemented with 50 mM HEPES, together with 5 nM [³H]-NLX and varying concentrations of methanol, for 30 minutes at 37°C. Co-incubation with 10 µM unlabeled NLX was performed to assess non-specific binding for each condition. Specific binding was calculated using Equation 1, and data from three independent experiments were plotted as the mean ± SEM of [³H]-NLX binding (dpm) against the methanol dilution factor.

5.4.3. Saturation binding assay – Determination of [³H]-naloxone affinity

Saturation binding assay is a common tool to characterize receptors with regard to the binding affinity of ligands and the receptor density/quantity in a preparation [400,403,407,408]. Determining the [³H]-NLX saturation curve is a useful method for understanding key characteristics of the HEK293-µOR cell line and the

receptors it expresses. This method helped to find the right tracer concentrations to optimize receptor binding while keeping non-specific binding to a minimum.

20 µg/well of HEK293-µOR membrane preparation was incubated with 0 to 15 nM of [³H]-NLX enabling the formation of receptor ligand complexes in a total volume of 400 µL/well. For each concentration of tracer, non-specific binding was determined by co-incubation of 10 µM cold ligand. Either 50 mM TRIS-HCl buffer (pH 7.4) or DMEM + 50 mM HEPES served as the binding buffer. After a 30-minute incubation in a 37°C incubator, filtration and washing, radioactivity bound to the filter was measured with a scintillation counter. Total and non-specific binding determined in three individual experiments were either plotted together as mean ± SEM of [³H]-NLX binding in dpm or specific [³H]-NLX binding was determined using Equation 1. Using the specific activity of the tracer (specification by the manufacturer) and the amount of membrane used, the specific binding was calculated as fmol of receptor per mg of total protein.

$$receptor\ quantity\ \left(\frac{fmol}{mg}\right) = \frac{specific\ [^3H]NLX\ binding\ [dpm]}{222{,}000\ x\ \alpha\ x\ m}\ x\ 1{,}000{,}000$$

Equation 2: Calculation of receptor quantity per total protein

Specific [³H]-NLX binding refers to the amount of ligand that specifically bound to the receptors. *222,000* is a scaling factor that converts dpm into Curie units. *α* denotes the specific activity of the tracer and *m* represents the mass of the membranes in milligrams. The final result is then multiplied by *1,000,000* to express the quantity in fmol per mg of membrane.

Specific tracer binding was then plotted as mean ± SEM against logarithmic tracer concentration and a hyperbolic saturation curve was observed, which asymptotically approaches the maximum binding (B_{max}). The B_{max} indicated the receptor density or availability of specific binding sites in the cell line. Moreover, from the saturation curve, the dissociation constant (K_d) of [³H]-NLX to the receptor could be calculated. The K_d value indicates the stability of a ligand-receptor complex, representing the ratio of free receptors and free ligands compared to the receptor-ligand complex. Specifically, K_d is defined as the concentration of ligand at which 50% of the available receptor sites are occupied. Therefore, a lower K_d value suggests a higher affinity between the ligand and the receptor. K_d and B_{max} values were determined using GraphPad Prism 10.3.1 (Non-linear regression one-site specific binding).

5.4.4. Competitive binding assay – Determination of opioid affinity

Competitive binding assays were performed to assess the binding affinities of non-radiolabeled ligands, specifically opioid agonists and antagonists. In these assays, increasing concentrations of the test ligand compete with a fixed concentration of [³H]-NLX. As the concentration of the non-labeled ligand increases, the radioactive ligand is progressively displaced from the receptor.

For competitive binding experiments, 20 µg of HEK293-µOR membrane preparation per well were incubated with 5 nM [³H]-NLX and varying concentrations of OR agonists and antagonists, as specified in the accompanying graphs. The total volume was 400 µL per well and the incubation took place for 30 minutes at 37°C.

In addition to membrane-based assays, some affinity measurements were also performed in intact HEK293-µOR cells (Figure 17). For this, 80,000 cells per well were seeded, starved as previously described and then incubated with [³H]-NLX and the respective ligands under the same conditions as the membrane preparations.

To minimize variance and reduce errors, tracer binding at the lowest opioid concentration was set to 100% and the raw data (in dpm) was normalized to the percentage of [³H]-NLX binding. This normalization made it easier to visualize the data by putting all maximum tracer binding values on the same scale, which enhanced comparability across different conditions and helped reduce any potential distortions from buffer effects. However, it's important to note that the goal of normalization wasn't to change or misrepresent the underlying data. It was guaranteed that the variables (halfmaximal inhibitory concentration, IC_{50}) remain predominantly consistent before and after normalization to prevent any manipulation of the results.

Specific binding, determined from 3-4 individual experiments, was plotted as the mean ± SEM against the logarithmic concentration of the unlabeled ligand, resulting in an inverse sigmoidal curve. The IC_{50} value, representing the concentration of an unlabeled agonist or antagonist that inhibits 50% of radioligand binding, was calculated using GraphPad Prism 10.3.1 (Non-linear regression one site - fit log IC_{50}). The IC_{50} value depends on the experimental

conditions, specifically the concentration of the radioligand used [409]. Thus, K_i values of the opioids were calculated using the equation of Cheng-Prusoff [410], where [L] represent the radioligand concentration and K_d represents its binding affinity (determined in section 5.4.3).

$$Ki = \frac{IC50}{1 + \frac{[L]}{Kd}}$$

Equation 3: Calculation of inhibition constant

5.4.5. Neutralizing effect of antibodies on opioid-induced [³H]-naloxone displacement

The neutralizing effect of nine anti-FEN antibodies on opioids´ μOR binding was assessed by examining the inhibition of opioid-induced [³H]-NLX-displacement. When a neutralizing antibody inhibits the opioid from binding to the receptor, it is no longer able to displace the radioligand, resulting in increased radioactive binding at the receptor. Therefore, in the presence of neutralizing antibodies, the radioactivity bound to the receptor rises compared to the presence of the opioid alone.

All dilutions were prepared in 50 mM TRIS-HCl (pH 7.4). Opioids at the appropriate concentrations were pre-incubated with the antibodies for 30 minutes at 37°C. Following this, [³H]-NLX was added alongside the opioid-antibody mixture in a 96-deepwell plate, and the reaction was initiated by adding 20 µg of HEK293-μOR membrane preparation per well. The resulting final volume was 300 µL/well. After an additional 30-minute incubation at 37°C, the reaction was terminated as previously described, and the radioactivity of the filter patches was measured. For each experiment, total [³H]-NLX binding was set to 100%. The opioid-induced displacement and displacement in the presence of 500 nM antibody were then normalized to this value and plotted as the mean ± SEM of 3-5 individual experiments.

5.5. Measurement of intracellular cAMP level

cAMP is a key signaling molecule downstream of GPCRs, e.g. by modulation of effector proteins like PKA. The measurement of intracellular cAMP levels can be

a pivotal tool to investigate OR activity [411,412]. Upon agonist binding, AC activity is inhibited in a G_i protein-dependent manner, reducing the conversion of ATP to cAMP. By artificially accumulating cAMP in the cell, the inhibition of AC through opioid stimulation can be measured. Stimulation with forskolin (FSK), an activator of the AC and 3-Isobutyl-1-methylxanthine (IBMX), a PDE-inhibitor to prevent cAMP degradation, results in a rise of cAMP levels in the cell. This enables the observation of significant decline in cAMP concentration and thus AC activity in the cells, which can be a helpful tool to assess potencies of ligands.

5.5.1. Radiometric cAMP assay

The decrease in previously accumulated cAMP level can be measured radiobiochemically through metabolic labeling with a precursor for radiolabeled nucleotide synthesis. Cells are incubated overnight with [^{3}H]-adenine, which is taken up by the cell and metabolized into radiolabeled ATP and subsequently into cAMP. Formed [^{3}H]-cAMP can be isolated in the cell extract by sequential column chromatography and quantified with a scintillation detector [413-416].

For this purpose, 12-well cell culture plates were coated with poly-L-lysine (50 µg/mL) for 5 minutes. After aspiration and drying for approximately 15 minutes, HEK293-µOR cells (300,000/well) were seeded to reach confluence in 1 mL FCS-supplemented DMEM. After a 24-hour incubation (37°C), the medium was exchanged with 500 µL/well of FCS-free DMEM supplemented with 1 µCi/mL [^{3}H]-adenine. To avoid measurement interference, caused by residual, unincorporated [^{3}H]-adenine activity in the cell supernatant, on the next day [^{3}H]-adenine solution was aspirated and exchanged with 400 µL of IBMX solution (500 µM). All subsequent dilutions were prepared in IBMX solution to maintain a constant final concentration of 500 µM. Cells were further stimulated with 100 µL of five-fold concentrated stimulants. The final concentrations are indicated in the respective graphs and figure captions. After 20 minutes of incubation at 37°C, the supernatant was aspirated, and the cells were extracted with 1 mL/well of ice-cold 5 % trichloroacetic acid (TCA). [^{3}H]-cAMP purification was carried out as follows:

Dowex® resin (ion exchange resin) columns were prepared by washing with 10 mL of 1 M HCl to remove impurities and protonate the functional groups, facilitating ion exchange. This was followed by a rinse with 10 mL of deionized water to eliminate excess HCl. Similarly, aluminum oxide columns were washed with 10 mL of 0.1 M imidazole buffer (pH 7.4) to stabilize the pH and prepare the surface for selective binding to phosphate groups. TCA extracts were loaded onto the Dowex® resin columns, where nucleotides were expected to bind. A subsequent wash with 4 mL of water removed weakly bound nucleotides, such as [³H]-ATP and the eluate was discarded. The Dowex® columns were then placed on top of aluminum oxide columns and eluted with 10 mL of water, transferring [³H]-cAMP to the aluminum oxide columns. The aluminum oxide columns, now binding [³H]-cAMP, were first washed with 1 mL of water to remove non-specific impurities, followed by elution with 5 mL of 0.1 M imidazole buffer (pH 7.4) into scintillation vials. The eluates were mixed with 10 mL of scintillation cocktail and analyzed using a liquid scintillation counter.

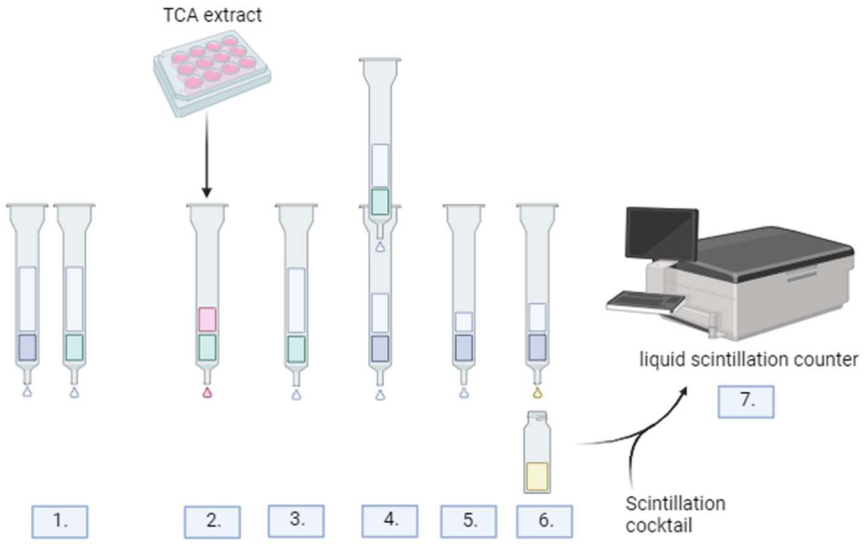

Figure 7: Illustration of [³H]-cAMP purification with Dowex®-resin and aluminiumoxid columns

Dowex®-resin columns are shown in green, aluminiumoxid columns in dark blue. 1. Washing steps of columns, 2. Loading of TCA extracts on Dowex®-resin column, 3. Washing step, 4. Elution of Dowex® on aluminiumoxid column, 5. Washing step, 6. Elution of aluminiumoxid columns into scintillation vial, 7. Read out

5.5.1.1. Determination of opioids´ EC_{50} values

As mentioned above, the measurement of opioid-induced, µOR-transmitted cAMP attenuation can be utilized to determine opioid potencies to activate the receptor. The potency is expressed as the halfmaximal effective concentration (EC_{50}), which represents the concentration of an opioid needed to produce 50 % of its maximum effect in reducing cAMP levels. A lower EC_{50} values indicates higher potency, because lower concentrations are required to achieve half maximal receptor activation.

In the experiment, HEK293-µOR cells were stimulated with 500 µM IBMX, either alone or supplemented with 10 µM FSK, or 10 µM FSK combined with varying opioid concentrations. Following the established protocol, the resulting dpm values were baseline-corrected (IBMX-only signal as baseline) and normalized to the percentage of the maximum signal. Data from three independent experiments were plotted as the mean ± SEM of FSK-induced cAMP signal [%] against the logarithmic concentrations of opioids. EC_{50} values were derived from the resulting sigmoidal curves using GraphPad Prism 10.3.1 (Non-linear regression one-site fit log IC_{50}).

5.5.1.2. Inhibitory potency of antagonists

When opioids are inhibited by an antagonist, the opioid-induced reduction in FSK-stimulated cAMP accumulation is prevented. The following increase in cAMP signal can be measured using the radioactive cAMP assay.

For this purpose, HEK293-µOR cells were stimulated as described above, either with 10 µM FSK alone, or with 10 µM FSK and defined opioid concentrations or 10 µM FSK, the respective opioid concentration and NLX or NLM in varying concentrations. Opioid concentrations were adjusted to approximately match their receptor affinity in DMEM, ensuring that around 50% of the receptors were occupied by each opioid. This normalization provided a consistent pharmacological baseline, allowing the antagonists to compete under comparable conditions for receptor binding and opioid displacement. After incubation and extraction of the cells, [^{3}H]-cAMP was purified using the above mentioned procedure. Obtained dpm values were corrected for basal levels

(IBMX signal as the baseline) and cellular cAMP levels were calculated as fmol cAMP/well using following Equation.

$$\boldsymbol{cellular\ cAMP}\ \left[\frac{\boldsymbol{fmol}}{\boldsymbol{well}}\right] = \frac{[^{\boldsymbol{3}}\boldsymbol{H}]\boldsymbol{cAMP}\ [\boldsymbol{dpm}]}{\boldsymbol{\alpha}\left[\frac{\boldsymbol{Ci}}{\boldsymbol{mmol}}\right]\ \boldsymbol{x\ 2220}}$$

Equation 4: Calculation of cellular cAMP levels in fmol/well

[³H]-cAMP [dpm] represents the measured radioactivity for a single well. The parameter α denotes the specific activity of the [³H]-Adenine used in the assay. The factor 2220 is applied to convert Ci/mmol into dpm/fmol for the calculation.

Data were plotted either as mean ± SEM of cAMP levels (fmol/well) from three independent experiments or as percentage inhibition of opioid-induced suppression by antagonists. For the latter, the difference between FSK and opioid signals was set to 100%, and the differences between antagonist and opioid signals were normalized to this value. These percentages were plotted as mean ± SEM against logarithmic antagonist concentrations. The IC_{50} of each antagonist against the respective opioid was determined from the resulting curves using GraphPad Prism 10.3.1 (Non-linear regression log (agonist) vs. response (three parameters)). The IC_{50} indicates the antagonist concentration required to inhibit 50% of the opioid's effect, with lower IC_{50} values reflecting higher antagonist potency.

Notably, in experiments testing NLX's effects on CAR, FEN, and REMI (Figure 27A-C), initially an older aliquot of the radioactive tracer was used. Since this tracer may have degraded over time, its specific activity might have been lower than expected or it might not have incorporated well into the cells. This could account for the noticeably reduced cAMP levels that were seen in those early measurements. When the experiments were conducted with fresh tracer, cAMP levels were about ten times higher. However, the ratio of the FSK signal to those induced by opioids and NLX/NLM remained the same, indicating that these variations in absolute counts did not impact the overall results.

5.5.2. AlphaScreen

The amplified luminescent proximity homogeneous assay (Alpha) is a non-radioactive, highly sensitive technology designed to study biomolecular interactions, including the measurement of intracellular cAMP levels. The

experiments were conducted using the AlphaScreen cAMP detection kit from Revvity. It utilizes streptavidin-coated donor beads carrying a photosensitizer (*phythalocyanine*). When excited by light at a wavelength of 680 nm, the photosensitizer can generate reactive singlet oxygen (single excited electron). Reactive oxygen molecules can diffuse up to 200 nm before they electrochemically relax to their ground state. Acceptor beads contain *thioxene*-derivatives and, if brought in close proximity, react with singlet oxygen under the emission of light (520-620 nm). To bring the beads into proximity, biotinylated cAMP was used as a tracer. The biotin moiety binds to the streptavidin on the donor beads, while the acceptor beads are labeled with an anti-cAMP antibody that specifically binds cAMP. Unlabeled, external cAMP can compete with the tracer for the anti-cAMP antibody. Consequently, the amount of external cAMP can be quantified based on the decrease in emitted light. When cAMP is artificially accumulated in cells through IBMX and FSK stimulation, opioid-induced μOR activation can be detected by a rise in the AlphaScreen signal, indicating a decrease in cAMP levels.

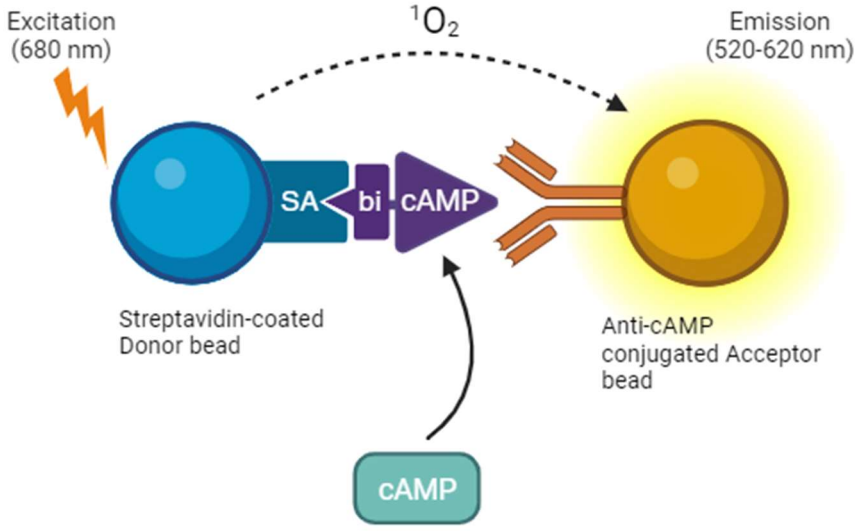

Figure 8: Outline of AlphaScreen principle

20,000 HEK293-μOR cells per well were seeded on a poly-L-lysine (50 μg/mL) coated 96-well plate and grown in 200 μL growth medium at 37°C for 24 hours before serum starving the cells for another 24 hours. Cells were pre-stimulated with 50 μL of IBMX (500 μM) in FCS-free DMEM for 5 minutes. Subsequently, 50

µL of two-fold concentrated stimulation solutions were added, and the cells were incubated at 37°C for 20 minutes. The stimulation solutions included IBMX alone, or IBMX combined with one of the following: 1µM FSK, FSK with opioids, or FSK with opioids and antibodies. Before stimulation, antibodies were pre-incubated with opioids at 37°C for 30 minutes to allow binding equilibrium to be achieved. Details regarding the respective final opioid and antibody concentrations are provided in the accompanying graphs and figure legends. Next, stimulation solutions were aspirated and cells were lysed with 40 µL of 1x assay buffer (prepared by diluting the 10x assay buffer provided by the manufacturer). The lysates were then supplemented with biotinylated cAMP (diluted 1:16,000) and acceptor beads (diluted 1:400). For generating the cAMP standard curve, 40 µL of diluted cAMP standard solution (provided in the kit) in 1x assay buffer was used instead of cell lysate. Subsequently the plate was incubated at room temperature for one hour under light exclusion. 10 µL of donor beads (1:100 dilution) were added to the wells resulting in final dilutions of 1:20,000 for the tracer and 1:500 for acceptor and donor beads (corresponds to 12.5 µg/mL). Following a 25 minute incubation at room temperature and light exclusion, the plate was placed in the instrument (CLARIOstar Plus) and incubated for another 5 minutes in the dark to prevent any light interference caused by moving the plate. The measurements were carried out with the following parameters: 0.4 s excitation (680 ± 40 nm), 0.41 s resting phase, 2.00 s emission measurement (570 ± 100 nm).

5.6. Phospho-kinase array

Protein phosphorylation regulates protein activity, localization and interactions and thereby influences critical cellular processes like signal transduction, cell division and apoptosis [417-419]. This modification is mediated by kinases, which transfer phosphate groups to specific amino acids (serine, threonine or tyrosine), and reversed by phosphatases, which remove these groups. Both kinases and phosphatases are tightly regulated, with phosphorylation itself inducing conformational changes that affect their activity [417,420,421]. Herein the focus was specifically on measuring kinase phosphorylation, providing insights into the activation state of these signaling molecules. Understanding these complex

signaling pathways requires simultaneous identification and measurement of protein phosphorylation patterns.

A proteome profiler human phospho-kinase array (R&D systems) was used to concurrently detect the phosphorylation levels across multiple proteins in a single experiment. The purpose of the human phospho-kinase array in this study was to investigate the changes and differences in phosphorylation patterns in HEK293-μOR cells following stimulation with opioid solutions. Comparing protein phosphorylation profiles between stimulated cells and control groups could give insights into signaling pathways activated by μOR and potentially help to identify key kinases that drive opioid-induced cellular responses.

The array utilized two nitrocellulose membranes (part A and B), which were labeled with a total of 39 phospho-kinase-specific antibodies, each in duplicate. These kinases differed in their cellular functions, subcellular locations, and their activation or inactivation status due to phosphorylation. The specific positions of each kinase on the membrane, along with their phosphorylation sites (amino acid residues), are detailed in Figure 9 and Table 4. This information allowed it to accurately assign each membrane spot to its respective kinase. On each membrane, PBS was included as a negative control.

Upon incubation with a cell lysate, phosphorylated proteins bind to their corresponding antibodies. Detection was achieved using a biotinylated secondary antibody, followed by a streptavidin-HRP (horseradish peroxidase) mediated substrate reaction. This allowed for the quantification of protein phosphorylation through the measurement of chemiluminescence.

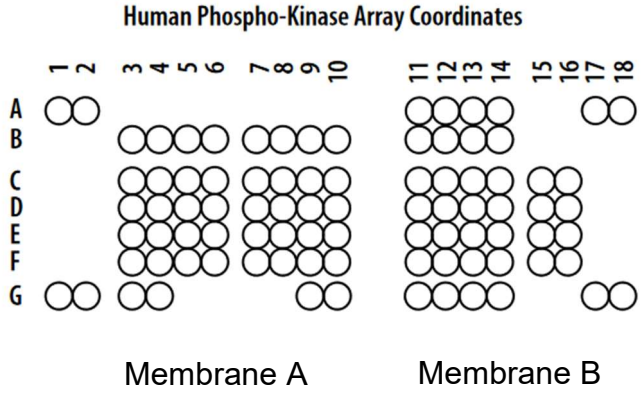

Figure 9: Coordinate map of phospho-kinase-specific antibody locations on the membrane

Adapted from the R&D Systems human phospho-kinase array protocol (Catalogue number ARY003C)

Membrane, coordinate	Target/Control	Phosphorylation site
A, A1-A2	Reference spot	-
B, A11-A12	Akt 1/2/3	T308
B, A13-A14	Akt 1/2/3	S473
B, A17-A18	Reference spot	-
A, B3-B4	CREB	S133
A, B5-B6	EGFR	Y1086
A, B7-B8	eNOS	S1177
A, B9-B10	ERK1/2	T202/Y402, T185/Y187
B, B11-B12	Chk-2	T68
B, B13-B14	c-Jun	S63
A, C3-C4	Fgr	Y421
A, C5-C6	GSK-3α/β	S21/S9
A, C7-C8	GSK-3β	S9
A, C9-C10	HSP27	S78/S82
B, C11-C12	p53	S15
B, C13-C14	p53	S46
B, C15-C16	p53	S392
A, D3-D4	JNK 1/2/3	T182/Y185, T221/Y223
A, D5-D6	Lck	Y394
A, D7-D8	Lyn	Y397
A, D9-D10	MSK1/2	S376/S360
B, D11-D12	p70 S6 kinase	T389

B, D13-D14	p70 S6 kinase	T421/S424
B, D15-D16	PRAS40	T246
A, E3-E4	p38α	T180/Y182
A, E5-E6	PDGF Rβ	Y751
A, E7-E8	PLC-γ	Y783
A, E9-E10	Src	Y419
B, E11-E12	PYK2	Y402
B, E13-E14	RSK1/2	S221/S227
B, E15-E16	RSK 1/2/3	S380/S386/S377
A, F3-F4	STAT2	Y689
A, F5-F6	STAT5a/b	Y694/Y699
A, F7-F8	WNK1	T60
A, F9-F10	Yes	Y426
B, F11-F12	STAT1	Y701
B, F13-F14	STAT3	Y705
B, F15-F16	STAT3	S727
A, G1-G2	Reference spot	-
A, G3-G4	β-Catenin	-
A, G9-G10	PBS (negative control)	-
B, G11-G12	STAT6	Y641
B, G13-G14	HSP60	-
B, G17-G18	PBS (negative control)	-

Table 4: Membrane sections and coordinates with corresponding target molecules and phosphorylation sites

Adapted from the R&D Systems human phospho-kinase array protocol (Catalogue number ARY003C)

All used buffers were provided in the array kit by the manufacturer. To perform the array, HEK293-μOR cells were cultured in 5 mL cell culture dishes. Each dish was seeded with 2 million cells. After 24 hours, the cells were subjected to a starvation period of 24 hours. Following starvation, the cells were stimulated with 5 mL of opioid dilution or the corresponding solvent control prepared in FCS-free DMEM at 37°C for 10 minutes, to account for any potential effects of the solvent itself. To ensure maximum receptor engagement and maximal effect, each opioid was applied at concentrations well above its K_I. The exact concentrations used are provided in the accompanying graph. The stimulation was rapidly stopped by placing the dishes on ice, to inhibit further kinase activity and the cells were washed with 1 mL of PBS. For cell lysis, 500 μL of cell lysis buffer, freshly supplemented with protease inhibitors (aprotinin, leupeptin, and pepstatin, each at 10 μg/mL) to prevent protein degradation, were added to each plate. Lysates were scraped if necessary to ensure complete collection, transferred to Eppendorf tubes, incubated on ice for 30 minutes, and centrifuged at 14,000 × g for 5 minutes to remove debris. The supernatants, containing soluble proteins including phosphorylated kinases, were collected (300 μL) and mixed with 2100 μL of array buffer 1, then kept on ice until further use.

Nitrocellulose membranes, pre-blocked for 1 hour in 1 mL of array buffer 1 at room temperature, were incubated with 1 mL of the respective cell lysates overnight at 4°C on a shaker set at 200 rpm, allowing target molecules to bind to the immobilized antibodies. The following day, the membranes were washed three times with 20 mL of 1x wash buffer for 10 minutes each to remove unbound protein. Biotinylated detection antibodies A and B, reconstituted in 100 μL of deionized water and diluted 1:2000 in array buffer 2/3, were then added to the respective membranes and incubated for 2 hours at room temperature. After separate washes with 10 mL of wash buffer (three times, 10 minutes each), the membranes were treated with streptavidin-HRP, diluted per the manufacturer's instructions. This was followed by a 30-minute incubation at room temperature and three additional washes with 20 mL of wash buffer to remove excess streptavidin-HRP.

For chemiluminescent detection, membranes were placed on a plastic cover, and a 1:1 mixture of chemiluminescent reagents 1 and 2 was applied for 1 minute.

HRP catalyzed a reaction with the reagents, producing light. The luminescence, directly correlating to the amount of phosphorylated kinase, was measured with a luminescence reader. Phosphorylation of specific kinases was identified by an increased chemiluminescence signal compared to solvent control-treated cells. This allowed for the comparison of phosphorylation patterns between opioid-stimulated and basal states, providing insights into opioid-induced kinase modulation.

Luminescence signals were quantified densitometrically as the area under the curve (AUC) using Fiji ImageJ software and normalized to the reference spot on the respective membrane. Opioid-induced changes in kinase activity were calculated as a percentage of the control.

5.7. Target protein detection via Western Blot

Western Blot was used for the detection and characterization of proteins, specifically pERK1/2 in cell lysates [422]. It involved the separation of proteins by electrophoresis, transfer to a membrane and detection using specific antibodies [423]. In this study, the Western Blot aimed to investigate an additional signaling pathway activated by opioids via the μOR, complementing the cAMP inhibition studies.

5.7.1. Sample preparation

250,000 HEK293-μOR cells were seeded on poly-L-lysine (50 μg/mL) coated 6-well plates and grown in 2 mL cell culture medium for 24 hours, before serum starving the cells for another 24 hours. Starvation media exchange was performed with 900 μL per well at least 1 hour prior to stimulation. The cells were then stimulated by addition of 100 μL of ten times concentrated ligand dilution for the desired period of time. Reactions were stopped by placing the plates on ice. Stimulation solution was aspirated and cells were lysed in 200 μL 1x Laemmli buffer. 4x Laemmli buffer was supplemented with deionized H_2O to generate 1x Laemmli buffer. Laemmli buffer contains sodium dodecyl sulfate (SDS) and β-mercaptoethanol [424]. SDS breaks non-covalent protein bonds and ultimately disrupts secondary and tertiary structures. Further, the SDS bound to the protein and therefore the protein´s acquired negative charge is proportional to its molecular weight and chain length [425]. β-mercaptoethanol carries a reducing

thiol group and thus cleaves disulfide bridges, resulting in the destabilization of quaternary protein structures. Consequently, Laemmli buffer denaturates and linearizes cellular proteins, enabling their separation and detection on a polyacrylamide gel. The cell lysates were transferred into Eppendorf tubes and treated with a sonicator for ~10 s, followed by heating for 5 minutes at 65°C to degrade genomic DNA and reduce viscosity. Subsequently the lysates were stored at -20°C. Upon usage, lysates were thawed at room temperature and centrifuged for 5 minutes at 14,000 rpm to precipitate solid cell fragments.

4x Laemmli buffer

Bromphenol blue	0.2 % (w/v)
Glycerin	40 % (v/v)
SDS	8% (w/v)
TRIS-HCl pH 6.8	200 mM
β-Mercaptoethanol	20% (v/v)

5.7.2. SDS-polyacrylamide gel electrophorese (SDS-PAGE)

SDS-PAGE is a common technique to separate proteins based on their molecular size and facilitates various downstream applications including Western Blot. It utilized the property of SDS to denature proteins and transmit a negative charge to them proportional to their length. A polyacrylamide gel serves as a chemical sieve, where small proteins travel faster through the gel pores than larger ones, when an electrical field is applied, resulting in size-based separation. In this study, two different, but equally suitable types of gels were used. For both variants, the components were mixed in a falcon. Upon addition of Tetramethylethylendiamin (TEMED), polymerization started and the solution was quickly poured into the gel apperature, supplied with the comb to form wells for subsequent sample addition and waited for polymerization.

Discontinuous gel system

This system utilizes two different gels with varying acrylamide concentrations to achieve efficient protein separation [424,426,427]. The upper layer, known as the

stacking gel, contains a lower acrylamide concentration (5.4%) and features larger pore sizes. Beneath it lies the running gel, which has a higher acrylamide concentration (10%) and smaller pore sizes. This arrangement serves a specific purpose: the stacking gel initially concentrates the protein samples into a narrow band, which then migrates into the running gel for separation. The pH difference between the gels alters the charge and mobility of the proteins, which improves the resolution.

	Stacking gel, pH 6.8	**Running gel, pH 8.8**
TRIS	0.13 M	0.38 M
SDS	0.1%	0.1%
Acrylamide	5.4%	10%
Bisacrylamide	0.14%	0.3%
TEMED	0.001%	0.001%
Ammonium persulfate	0.001%	0.001%

After polymerization of the gel, it was assembled in the Mini-PROTEAN Tetra Cell electrophoresis system from BioRad. The chamber was filled with SDS running buffer, which had been prepared by diluting a 10x concentrated stock solution with deionised water. 20 µL of lysate was carefully pipetted into each well of the gel, with 4 µL of a loading control (ladder) occupying one well per gel. Subsequently, a voltage of 80 V was applied until the lysates reached the running gel, at which point the voltage was increased to 120 V. The presence of bromphenol blue in the Laemmli buffer allowed for the visual tracking of the lysates, ensuring they did not run out of the gel.

10x SDS running buffer	
TRIS-HCl	25 mM
SDS	0.1%
Glycine	190 mM

Continuous gel system

In this configuration, a single, continuous polyacrylamide gel (8%) was used for protein separation. This method was simpler and faster to prepare, however, it may provide lower resolution for proteins with similar molecular weights compared to the stacking/running gel system [428]. It was performed according to Jiménez-Soto [429].

Continuous 8% acrylamide gel

TRIS-HCl	80 mM
Glycine	0.1 M
Serine	0.1 M
Asparagine monohydrate	0.1 M
Acrylamide	8.0%
TEMED	0.08%
Ammonium persulfate	0.001%

Following the polymerization of the gel, it was installed in the BioRad Mini-PROTEAN Tetra Cell electrophoresis system. The chamber was filled with 1x SDS running buffer and the gel was loaded with 7 µL of lysate per well. Additionally, each gel was loaded with one well containing 7 µL of protein ladder. To ensure the proteins entered the gel gradually, the voltage was initially set to 90 V for 10 minutes, followed by 240 V for 20 minutes to achieve separation.

10x SDS running buffer, pH 8.3

TRIS	25 mM
Glycine	1.92 M
SDS	0.1%

5.7.3. Protein transfer to the membrane and detection

To detect proteins previously separated by SDS-PAGE, they were transferred from the acrylamide gel to a membrane using the Western Blot technique, either with the wet blot or semi dry blot method. Both transfers were performed using a Mini TransBlot ® tank transfer system. On the membrane, the proteins were exposed to specific antibodies, followed by a HRP-labeled secondary antibody and subsequent enzyme reaction that enabled quantification through luminescence measurement.

Wet blot method

The wet blot method was used for protein transfer following the discontinuous SDS-PAGE. The membrane, gel and filter papers were first equilibrated in TGM buffer (Tris-glycine methanol buffer). The assembly began by placing the gel on top of the nitrocellulose membrane (GE Healthcare Life science), followed by layering filter papers on both sides. Any trapped air bubbles were carefully removed with a roller to ensure proper contact between the layers. The entire stack was then placed between foam pads and inserted into a gel holder cassette. To avoid air bubbles during the process, all components were covered in TGM buffer. Two cassettes were placed into a tank filled with TGM and an electric current was applied. The negatively charged proteins migrated toward the anode, transferring them from the gel to the membrane. The transfer was performed at 250 V and 350 mA for 2 hours at 4°C. Upon blocking non-specific binding sites (described below), the protein transfer was checked by staining them with Ponceau S, followed by decolorization with TRIS-buffered saline (TBST).

1x TGM	**10x TBST (pH 7.4)**	**Ponceau S**
25 mM TRIS	10 mM TRIS	0.1% Ponceau
192 mM Glycine	150 mM NaCl	5% Acetic acid
20% Methanol	0.05% Tween (v/v)	

Semi dry method

The semi dry Western Blot utilizes less buffers and mostly works faster. It was used for proteins previously separated with the continuous SDS-PAGE and performed according to [430] with the Trans-Blot® turbo transfer system from BioRad.

Methanol is used to activate the PVDF membrane (BioRad) for 15 seconds prior to use, reducing its hydrophobicity and enhancing protein binding efficiency. Following this, the membrane was transferred to anode II buffer. Two filter papers were wetted with anode I buffer and placed onto the transfer cassette. Above these, two additional filter papers, each soaked in anode II buffer, were positioned, followed by the membrane itself. The gel was then carefully placed on top of the membrane. Stacking was completed by adding four filter papers soaked in cathode buffer. Care was taken to avoid trapping air bubbles, which were removed if present using a roller. The cassette was then closed and placed into the BioRad device. The transfer was conducted for 7 minutes at 1.3 A and 25 V for one gel, or 2.5 A and 25 V for two gels. After the transfer, the membrane was dried either for one hour at 37°C or overnight at room temperature. Before blocking non-specific binding sites (described below), the membrane was reactivated in methanol.

	Anode I (pH 10.4)	**Anode II (pH 10.4)**	**Cathode (pH 9.4)**
TRIS	0.3 M	25 mM	25 mM
Methanol	10%	10%	10%
6-Amino-n-Caproic acid			40 mM

Detection using specific antibodies

Using the protein ladder for orientation, the membranes were horizontally cut with a scalpel to ensure that the protein of interest remained on the membrane. For each membrane, the detection of a loading control was included to account for variability independent of cell stimulation. In this study, histone H3 was used as

the loading control. It is found in the chromatin of all eukaryotic cells and its expression is not significantly altered by the experimental conditions. To block non-specific binding sites on the membrane, the membranes were incubated with an appropriate blocking solution for 30 minutes at room temperature. Following this, the membranes were incubated overnight on a shaker at 4°C with the primary antibody (solvents and dilutions are outlined below). The next day, membranes were washed three times for 10 min each with TBST. Subsequently, the membranes were treated with the appropriate HRP-labeled secondary antibody for 1 hour at room temperature followed by another three washing steps with TBST. A 1:1 mixture of hydrogen peroxide solution and luminol was then pipetted onto the membranes. The enzymatic reaction was allowed to proceed for approximately one minute. During this time, HRP, in the presence of H_2O_2, catalyzed the conversion of luminol to its active form, which was then measured as light emission with a luminescence imager.

		Primary antibody		**Secondary antibody**	
Protein	Molecular weight	Blocking solution/solvent	dilution	species	dilution
Histon H3	17 kDa	3% milk powder	1:40,000	rabbit	1:10,000
pERK1/	42 kDa	5% milk powder	1:500	mouse	1:5000

Quantification

Images obtained with the ChemiSmart 5000 camera were subjected to densitometric analysis using the Fiji ImageJ software, where the area under the curve (AUC) was calculated. The AUC of the target protein was then normalized to that of the respective histone band.

For kinetic studies of opioid-induced ERK1/2 phosphorylation (Figure 21), AUC ratios of pERK1/2 to Histone H3 were normalized to the percentage of the 2.5-minute value and plotted as mean ± SEM against time from six individual experiments. To assess concentration-dependent ERK1/2 phosphorylation (Figure 22), AUC ratios were directly plotted as mean ± SEM against logarithmic

opioid concentrations. EC_{50} values, indicating opioid potency, were calculated from the resulting curves using GraphPad Prism 10.3.1 (Non-linear regression, log (agonist) vs. response, three parameters).

5.8. Determination of opioid receptor phosphorylation via ELISA

Ligand-dependent receptor phosphorylation is a key post-translational modification that influences receptor activity and downstream signaling. Investigating μOR phosphorylation can provide critical insights into opioid-induced receptor regulation and signaling pathways, making it a valuable tool for understanding pharmacological response and receptor function [257,270,431]. In this study, μOR phosphorylation was measured to investigate opioid-induced receptor modulation alongside classical signaling pathways, providing a more comprehensive understanding of opioid effects.

For that purpose, μOR phosphorylation was measured using an enzyme-linked immunosorbent assay (ELISA) kit (7TM antibodies). μOR in cell lysates were captured using magnetic beads conjugated with anti-hemagglutinin (anti-HA) antibodies. The use of a magnet allowed their immobilization, washing and ultimately the separation of μOR from other proteins. The phosphorylated receptors were then detected using phosphosite-specific antibodies, followed by the application of a secondary antibody and an enzyme-dependent colorimetric reaction, which was quantified photometrically.

20,000 HEK293-μOR cells were seeded on a poly-L-lysine (50 μg/mL) coated 96-well plate. After 24 hours of incubation at 37°C, the cells were serum-starved for an additional 16-24 hours. At least one hour before stimulation, the starvation medium was replaced with 180 μL of fresh starvation medium. Cells were then stimulated by adding 20 μL of a tenfold concentrated ligand solution in FCS-free DMEM for 5 minutes at 37°C. All buffers used were provided by the manufacturer and prepared or diluted according to the instructions. Post-stimulation, the supernatant was aspirated, and the cells were washed three times with 100 μL PBS. Lysis was performed with 150 μL detergent buffer containing protease and phosphatase inhibitors for 30 minutes at 4°C, to prevent the degradation of

proteins of interest and the loss of phosphate groups. The plate was centrifuged at 3000 rpm for 20 minutes at 4°C to remove cell debris.

Subsequently, 60 µL of the supernatant was transferred to a U-bottom plate, mixed with 40 µL of HA-tagged magnetic bead suspension and incubated for 2 hours at 4°C to ensure µOR binding to the beads. The beads were washed three times with 100 µL PBST (PBS with 0.1% Tween 20) under magnetic force, then 60 µL of a primary phosphosite-specific antibody solution was added and incubated overnight at 4°C, enabling the specific binding to phosphorylated amino acid residues. The following day, the beads were washed three times with PBST on a magnet and 60 µL of secondary, enzyme labeled antibody solution was added, followed by a 2-hour incubation at room temperature. After three additional washes with PBST under magnetic force, 100 µL of detection solution was added and the OD was measured at 405 nm until values ranged between 0.2 and 1.2. The enzymatic reaction was stopped with 100 µL of stop solution and the plate was placed on the magnet. 140 µL of the solution was transferred to a fresh flat-bottom plate for a final OD measurement at 405 nm. To exclude background interference from the substrate itself, a blank without beads was included for each measurement. The measured values were corrected by subtracting the blank and then normalized to the respective solvent control. Opioid-induced µOR phosphorylation [OD_{405nm} or % of solvent control] was plotted as the mean ± standard error of the mean (SEM) from 4-5 individual experiments.

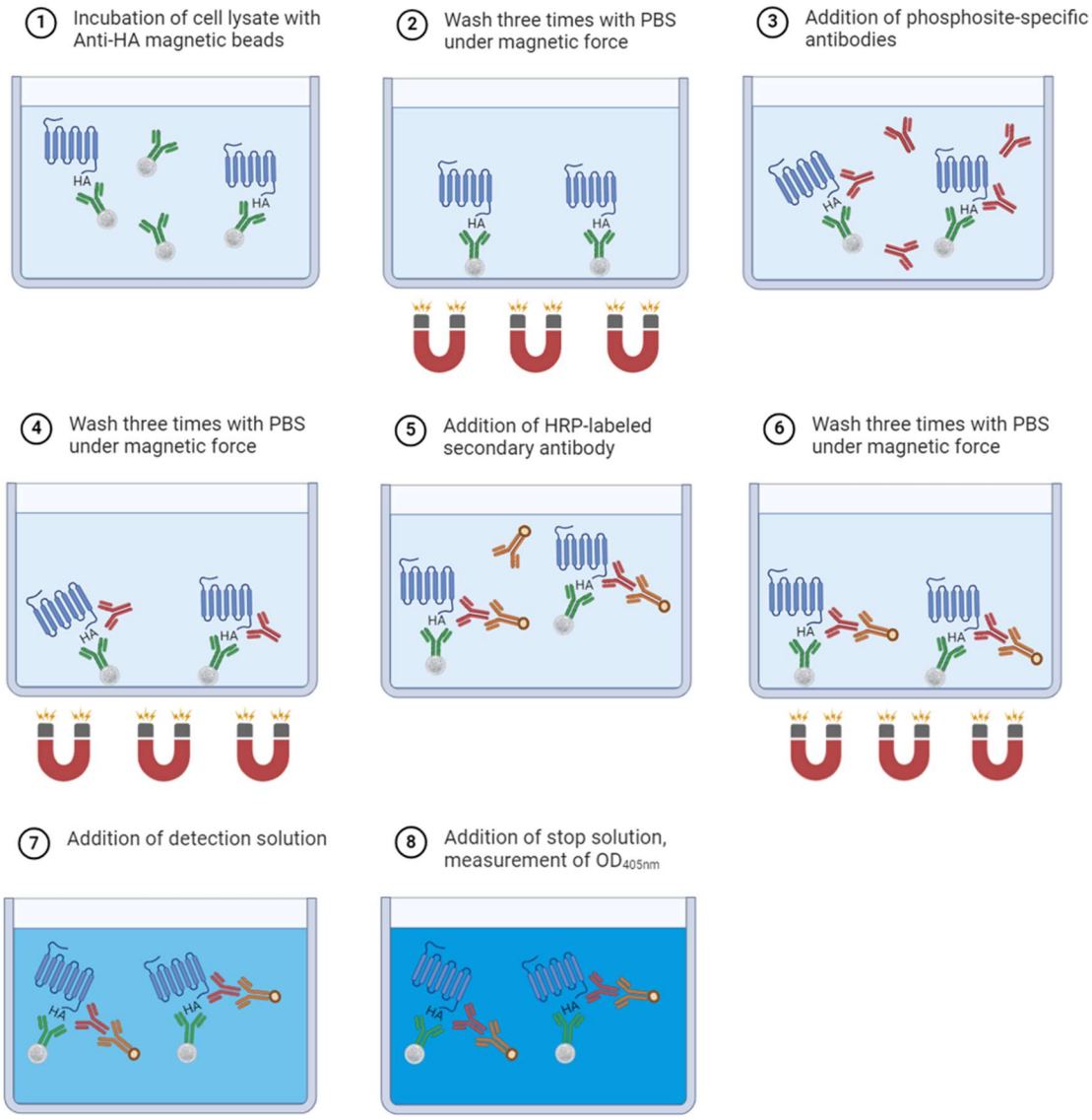

Figure 10: Outline of phosphorylation assay based on ELISA principle

The workflow includes cell lysate incubation, washing steps, phosphosite-specific antibody binding, HRP-labeled secondary antibody detection and absorbance measurement at 405 nm.

5.9. Calculations

5.9.1. Receptor occupancy for halfmaximal receptor activation

The determination of receptor occupancy (RO) for half-maximal receptor activation of opioid ligands enables the estimation and comparison of their efficacy in inducing a specific signaling pathway, while also considering their receptor binding affinity. RO was calculated using the method developed by Kenakin et al. [432], applying the following formula, where K_i represents the opioids binding affinity and EC_{50} is the concentration required for the ligand to

induce half-maximal receptor activation or trigger half-maximal signal (i.e. potency for the signaling pathway of interest).

$$Receptor\ occupancy\ [\%] = \frac{EC50}{EC50 + Ki} \times 100$$

Equation 5: Calculation of a ligand´s receptor occupancy for half-maximal receptor activation

5.9.2. Bias factor

The bias factor quantifies the extent to which one agonist activates one specific signaling pathway over another in relation to a reference ligand, when binding a receptor. It is therefore a measure for biased agonism. While multiple methods exist for calculating the bias factor, in this work, it was calculated following the approach outlined in [433]. Two important pharmacological parameters are required: The EC_{50} value**,** which reflects the concentration of the compound needed to produce a half-maximal effect and the intrinsic activity (E_{max}), which represents the maximal response minus the minimal response. Both parameters can be derived from dose-response curves, which typically display a sigmoidal shape. First, the ratio of EC_{50} and E_{max} of the reference and the ligand of interest for one signaling pathway is calculated and their difference is build. Then, the Δlog (E_{max}/EC_{50}) value for one pathway is subtracted from the Δlog (E_{max}/EC_{50}) value of another pathway to evaluate the bias activity. The bias factor is then calculated as the inverse logarithmic value of this difference.

$$\Delta\log\frac{Emax}{Ec50} = (\log\frac{Emax}{EC50})opioid - (\log\frac{Emax}{EC50})reference\ opioid$$

$$\Delta\Delta\log\frac{Emax}{Ec50} = (\Delta\log\frac{Emax}{EC50})pathway1 - (\Delta\log\frac{Emax}{EC50})pathway\ 2$$

$$bias\ factor = 10^{\Delta\Delta\log\frac{Emax}{EC50}}$$

Equation 6: Calculation of bias factor

5.10.Statistical methods

The experiments were autonomously conducted a minimum of three times, with the specific count detailed in the associated chapters and figure legends. Results are presented as the mean along with the SEM. Statistical analyses were executed using GraphPad Prism 10.3.1, employing distinct statistical hypothesis testing approaches. Significance levels were categorized into four groups: * $p<0.05$, ** $p<0.01$, *** $p<0.001$, and **** $p<0.0001$. A two-sample t-test was employed to analyze significant distinctions between two mean values. To compare multiple means, a one-way analysis of variance (ANOVA) was conducted. Depending on the comparison, either Tukey's post-hoc test was used to identify which specific groups differed, comparing all possible pairs of means, or Dunnett's multiple comparison test was employed to assess significant differences relative to a single reference group. Notably, statistical tests on normalized data were exclusively executed subsequent to verifying the statistical significance of the raw data.

5.11. Supportive computational tools

Each section of this work was researched, drafted and written by the author. For some sections, the AI-based tool ChatGPT (OpenAI) was used to assist with linguistic optimization, refinement of English language, checking for spelling mistakes and supplementary literature searches. For translations of single words or sections between German and English, the translation tool DeepL was used. Figures 2, 3, 6, 7, 8, 10, 30, 41, 42 and 43 were created or adapted using BioRender.com. The tool was used to generate schematic representations of experimental designs and molecular interactions for better visualization and understanding.

All scientific content, interpretations, and conclusions presented in this work were independently developed and critically reviewed.

6. Results

6.2. Establishment of recombinant HEK293-μOR cell line

HEK293 cells are frequently used in research on receptor expression, especially in studies on GPCRs [381,434]. Although HEK293 cells do not endogenously express the μOR [435], they are a preferred choice for developing recombinant cell lines, particularly in the study of OR pharmacology [436,437]. Therefore, following Zeocin™-selection (described in 5.3.4), transfected HEK293 cells were screened for μOR expression using a ligand binding assay with radiolabeled OR antagonist [³H]-NLX as a tracer.

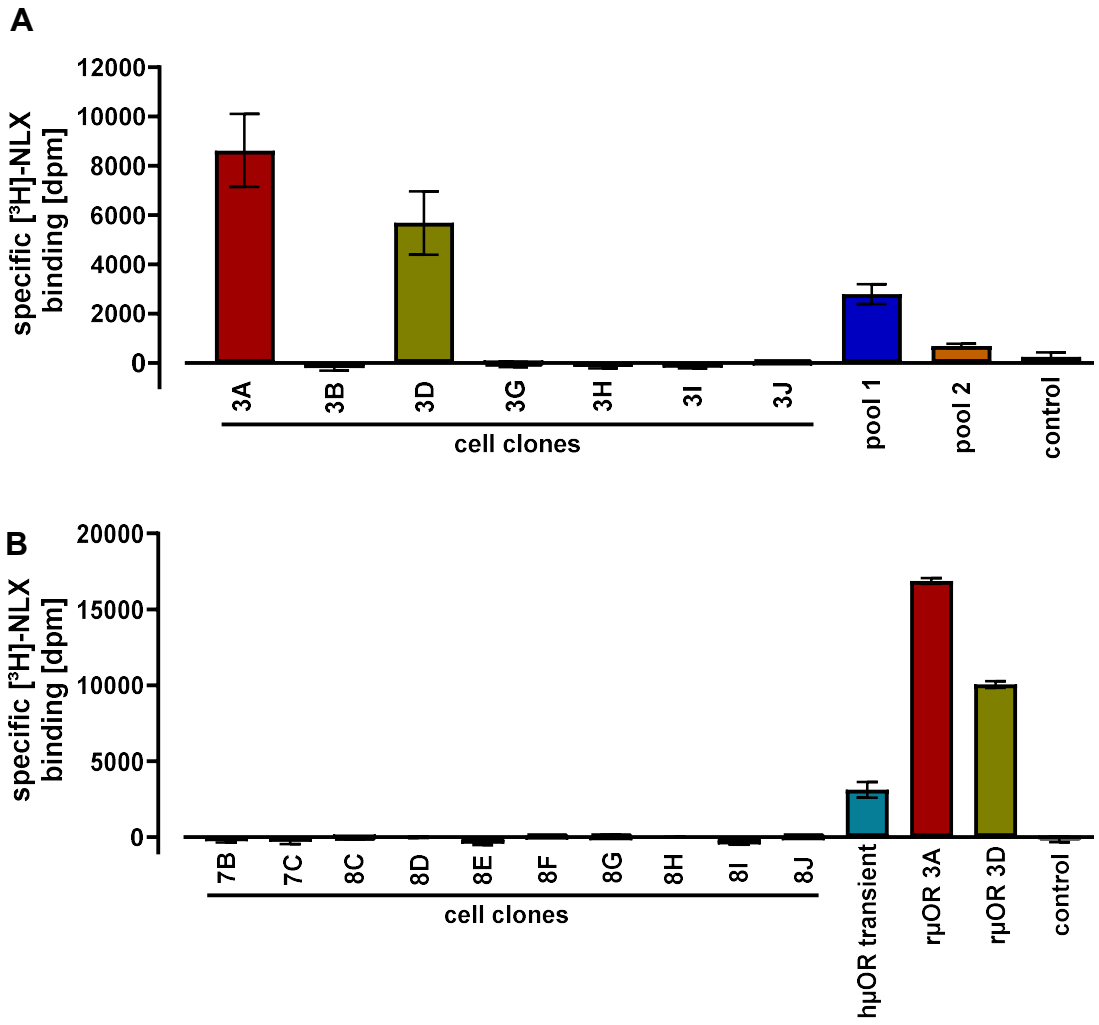

Figure 11: Assessment of μOR expression in rat and human μOR HEK293 clones

For each isolated cell clone or pool, 100,000 cells per well were seeded on 48-well plates and cultured for 48 hours. Cells were stimulated in triplicates with 10 nM [³H]-NLX to measure total tracer binding, while non-specific binding was assessed by co-incubation with 10 μM unlabeled NLX. Cell culture medium DMEM + 50 mM HEPES served as the assay buffer. Cell lysates were measured for their radioactive

decay. Specific [³H]-NLX binding was determined with Equation 1 and is displayed as mean ± SEM of dpm. n=3. The experiment utilized five transfection approaches. **A:** Three for the rμOR: one involved single-cell cloning, generating clones (e.g. 3A, 3B), while two produced unified cell pools (labeled as pool 1 and 2), native HEK293 cells as control. **B:** For the hμOR, two transfections with subsequent single-cell cloning resulted in clones such as 7B, 7C, 8C, 8D and so on. Transient transfection and two rμOR clones with highest [³H]-NLX binding are shown as refererence, native HEK293 cells as control.

As expected, native, untransfected HEK293 cells did not exhibit notable [³H]-NLX binding, demonstrating the absence of endogenously expressed OR. RμOR clones 3A and 3D, as well as cell pools 1 and 2, revealed increased [³H]-NLX binding, indicating measurable expression of the receptor (Figure 11A). In contrast, none of the tested stable human μOR clones demonstrated detectable tracer binding. However, transient transfection of the hμOR resulted in significant receptor expression, confirming the functionality of the plasmid itself (Figure 11B).

Prior studies have demonstrated that rat and human μORs share 95% sequence homology and exhibit comparable ligand affinity and selectivity [72,438,439]. Given the importance of consistent and high-level receptor expression for this study, clone 3A, which expresses the rμOR, was selected as the most suitable cell model for subsequent experiments. It is referred to here as HEK293-μOR.

6.3. Characterization of selected HEK293-μOR cell clone

Ligand binding assays using [³H]-NLX as a tracer were conducted to comprehensively characterize the newly established HEK293-μOR cell line and ensure precise interpretation of subsequent experimental results.

6.3.1. Temperature dependency of [³H]-naloxone equilibrium

To determine the optimal conditions for [³H]-NLX binding in HEK293-μOR cells, binding assays were conducted at multiple time points and under two different temperature settings.

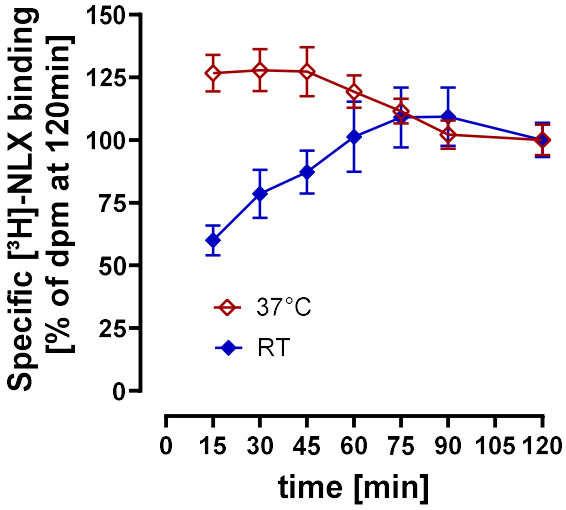

Figure 12: Temperature and time dependency of [³H]-NLX association

250,000 HEK293-μOR cells per well were incubated in triplicates with 5 nM [³H]-NLX for up to two hours either at room temperature or 37°C. For each time point, non-specific binding was determined through co-incubation of 10 μM unlabeled NLX. Dilutions were made in DMEM + 50 mM HEPES. Radioactive decay of the filter patches was measured. Specific binding was calculated using Equation 1 and plotted as mean ± SEM of % of the respective 2-hour value against time. n=3-4

At room temperature, tracer binding increased gradually, reaching a plateau after approximately 75 minutes. In contrast, at 37°C, maximal [³H]-NLX binding was achieved within the first 15 minutes, reflecting the faster kinetics and quicker achievement of equilibrium between bound and unbound states at the higher temperature [440]. However, after 45 minutes at 37°C, [³H]-NLX binding began to decrease, eventually stabilizing around the 120-minute mark. This decline could be attributed to temperature-related changes in the tracer, such as potential dissociation of the tritium label. To optimize assay conditions and ensure consistency across experiments, while preventing any decrease in [³H]-NLX binding, a 30-minute incubation at 37°C was selected as the optimal setup for subsequent assays.

6.3.2. Methanol influence on [³H]-naloxone binding

Binding assays are typically designed to mimic physiological conditions, which is why they are often performed using whole, intact cells in blood-like media, such

as cell culture medium or simple TRIS or HEPES buffers supplemented with ions at appropriate concentrations [441,442]. However, for technical reasons - such as simplifying experiments, increasing throughput and improving reproducibility - membrane preparations are frequently used instead of whole cells [443,444]. This approach was also employed in most binding assays in this study. Since membrane preparations lack the intracellular-extracellular ion gradient, some compromises in physiological relevance must be accepted.

Nevertheless, typically for most studies, the ionic composition of the used assay buffer should not significantly impact receptor-ligand binding behavior. In the case of opioid binding to the μOR, however, the choice of binding buffer plays a crucial role, as it can directly influence ligand affinity [445]. Therefore, although membrane preparations were used in several experiments in this study - meaning some physiological relevance was lost - particular attention was given to the choice of buffer. 50 mM TRIS-HCl (pH 7.4) was used for the binding assays in this study, as it provides the most reference values in the literature (see Table 1). Alongside, cell culture medium DMEM supplemented with 50 mM HEPES as a buffering agent was used. This choice also ensured consistency with subsequent experiments investigating opioid signaling (e.g. cAMP assay), making it crucial to understand opioid binding behavior in DMEM.

Before membrane preparations were established as the standard approach in this study, the influence of methanol on [^{3}H]-NLX binding was initially tested in whole cells to account for potential matrix effects. This was particularly relevant since some opioids used in subsequent experiments were dissolved in methanol (Table 3). The experiments were conducted in both binding buffers.

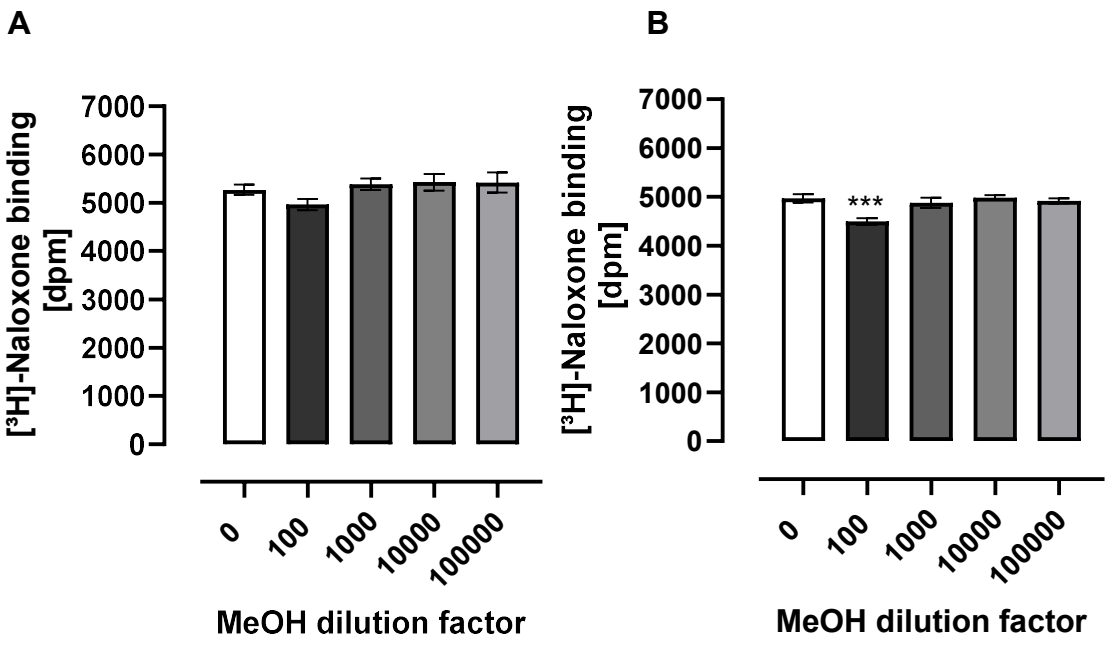

Figure 13: Methanol influence on [³H]-NLX binding in two different buffer systems

250,000 HEK293-μOR cells per well were incubated in triplicates in 50 mM TRIS-HCl buffer (pH 7.4) or DMEM + 50 mM HEPES with the indicated methanol dilutions and 5 nM [³H]-NLX. Non-specific binding was assessed by co-incubation with 10 μM unlabeled NLX. After an incubation of 30 minutes at 37°C, radioactive decay of the filter patches was measured. Specific binding was calculated with Equation 1 and plotted as mean ± SEM of dpm against methanol dilution. **A**: Methanol influence on [³H]-NLX binding in 50 mM TRIS-HCl (pH7.4) **B**: Methanol influence on [³H]-NLX binding in DMEM + 50 mM HEPES. Statistical analysis was performed using one-way ANOVA followed by Dunnett's multiple comparisons test to compare each group to the control value. Asterisk indicate significant difference to control, ***p<0.001.

Methanol, at the tested concentrations, had no effect on [³H]-NLX binding when the assay was performed in TRIS-buffer (Figure 13A). However, a 1:100 dilution of methanol significantly reduced [³H]-NLX binding in assays conducted in DMEM (Figure 13B). In this study, the only relevant methanol dilution falling in this range was 1:35, used alongside 100 μM MOR. Since methanol has a low molecular weight, this dilution results in a concentration of about 700 mM - much higher than any other substance in the assay. Solvents influence the solubility and stability of ligands and can also affect binding dynamics by altering receptor conformation or ionic conditions in the assay environment [446]. Methanol might disrupt receptor-ligand interactions by altering the polarity of the receptor's environment and destabilizing cell membranes, which can affect receptor conformation and accessibility. This high methanol level could potentially influence receptor interactions, so it’s important to keep this in mind when

interpreting the results. However, since this is the only methanol concentration considered relevant for this study, it can be concluded that no additional effects on [³H]-NLX binding are expected beyond this concentration.

Additionally, some opioids are dissolved in water. As water is the main component of the binding buffers, no influence of water on [³H]-NLX binding was assumed and it was therefore not included as a solvent control in the experiments.

6.3.3. Determination of K_d and B_{max} of [³H]-naloxone

To determine key parameters of the used cell line - K_d and B_{max} of [³H]-NLX - a saturation binding assay was conducted using HEK293-µOR membrane preparations, as described in 5.4.3.

Total and non-specific binding of [³H]-NLX were analyzed in the two buffer systems previously employed to examine the effect of methanol on [³H]-NLX binding. These measurements were then used to calculate specific µOR binding, resulting in the generation of a saturation curve.

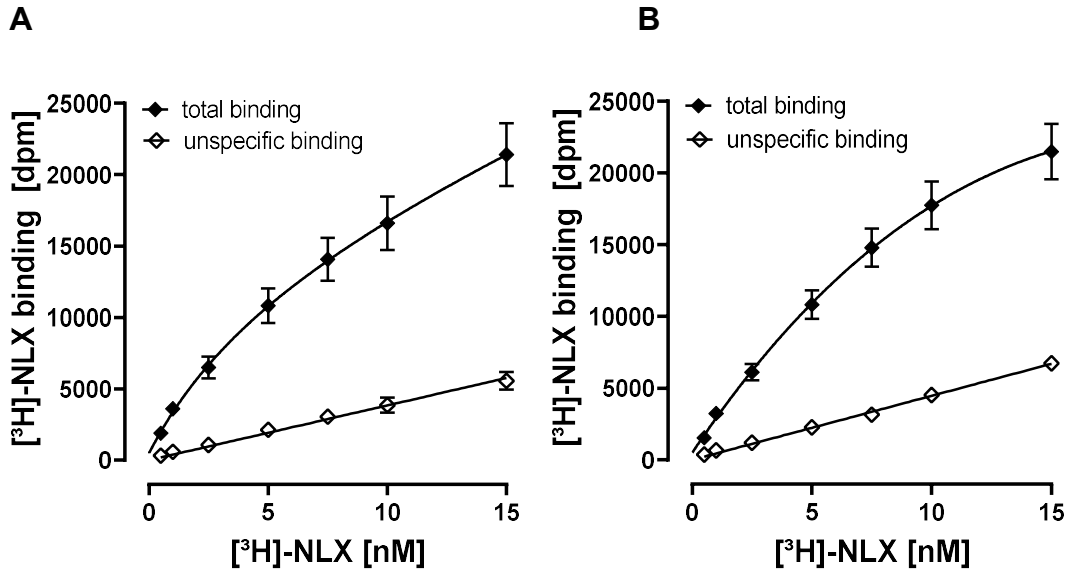

Figure 14: Total and non-specific [³H]-NLX binding in HEK293-µOR cells

20 µg of HEK293-µOR membrane preparation per well were incubated in triplicates with the indicated concentrations of [³H]-NLX for 30 minutes in a 37°C incubator in either 50 mM TRIS-HCl, pH7.4 or DMEM supplemented with 50 mM HEPES. For each concentration, non-specific binding was examined through coincubation of 10 µM unlabeled NLX. Radioactivity of the individual filter patches was measured. Total and non-specific binding were plotted as mean ± SEM of dpm against [³H]-NLX concentration using GraphPad Prism 10.3.1 (Non-linear regression one-site total binding and simple linear regression). n=3 **A**: Total and non-specific [³H]-NLX

binding assessed in TRIS-buffer **B**: Total and non-specific [³H]-NLX binding assessed in DMEM.

In both buffer systems, as total binding of [³H]-NLX reaches its peak, the relationship between tracer concentration and non-specific binding stays linear - the more tracer present, the more non-specific sites become occupied. In contrast, receptor binding is limited by the number of available receptors, meaning that specific binding has a defined maximum capacity.

To better identify the relevant receptor population for tracer interaction in the HEK293-µOR cell line, specific [³H]-NLX binding was determined using Equation 1. When specific [³H]-NLX binding was plotted against linear concentrations of [³H]-NLX, a hyperbolic saturation curve was obtained with an asymptotic approach to the maximum binding (B_{max}).

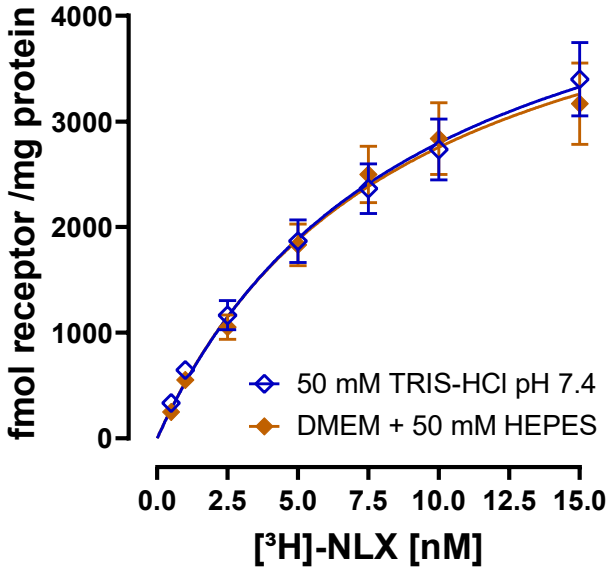

Figure 15: Specific [³H]-NLX binding in HEK293-µOR cells

Specific binding was calculated based on data shown in Figure 14 using Equation 1 for each [³H]-NLX concentration. From obtained dpm values, receptor quantity was calculated as fmol receptor per mg of total protein (Equation 2) and plotted as mean ± SEM against [³H]-NLX concentration. n=3

	TRIS-buffer	**DMEM**
K_d [nM]	9.73 ± 1.81	8.61 ± 0.99
B_{max} [fmol/mg]	5425 ± 1010	5199 ± 1404

Table 5: K_d and B_{max} of [³H]-NLX

K_d and B_{max} values were determined from the data shown in Figure 15 using GraphPad Prism 10.3.1 (Non-linear regression one-site specific binding). Values represent the mean ± SEM from three independent experiments. Differences in K_d and B_{max} between buffers were analyzed using an unpaired t-test, but no significant differences were observed.

In both buffer systems, the measured K_d value of NLX was approximately 9 nM, consistent with values reported in the literature [82,408]. Although tracer affinity in DMEM - which contains a complex mixture of ions - displayed a slightly lower K_d than in TRIS-buffer, this difference was not statistically significant. Nevertheless, this observation aligns with literature suggesting that sodium enhances antagonist binding [447-449]. Similarly, the B_{max} values were comparable across both conditions. The receptor density, approximately 5 pmol per mg of total protein, is notably high, significantly exceeding levels typically observed in endogenous cell lines [408,450]. Interestingly, even previously established recombinant HEK293 cell lines displayed receptor expression levels that were roughly tenfold lower [451]. This underscores the exceptionally high receptor expression in the recombinant HEK293-μOR cell line. This observation was further supported during the screening process, where the clone utilized in this study demonstrated the highest [^{3}H]-NLX binding levels (Figure 11A).

The high μOR expression and strong tracer affinity in the established HEK293-μOR cells are likely to facilitate robust signals and simplify data interpretation. Consequently, HEK293-μOR cells represent a suitable model for further studies investigating opioid-receptor interactions and opioid-induced cellular processes.

6.4. Comparative pharmacodynamic analysis of carfentanil, fentanyl, remifentanil, morphine and endomorphin-1

As outlined in the introduction, a substance's toxicity is likely reflected at the receptor level through its pharmacodynamics. This chapter presents a comprehensive characterization of CAR's pharmacodynamic properties - including affinity, potency, intrinsic activity and receptor efficacy - comparing it to other opioids to uncover features that may underlie its extreme toxicity. Several opioids were selected for comparison based on their pharmacological relevance, diverse characteristics, and significance in both clinical and illicit contexts. The aim was to better understand how CAR interacts with and activates receptors compared to other exogenous and endogenous opioids and to explore potential links to its exceptional *in vivo* effects.

6.4.1. Analysis of μOR binding affinities

μOR binding affinities of opioid antagonists (NLX and NLM) and agonists (CAR, FEN, REMI, MOR and ENDO) were measured using a competitive ligand binding assay with HEK293-μOR membranes. In accordance with the previous chapter, these measurements were conducted in two different buffer systems to evaluate how varying buffer conditions could affect antagonist and agonist receptor binding.

K_i values, calculated from IC_{50} values as described in chapter 5.4.4, indicate the concentration of ligands required to occupy half of the available receptors, independent of the tracer concentration. Table 6 summarizes the IC_{50} and K_i values for agonists and antagonists determined in both buffers.

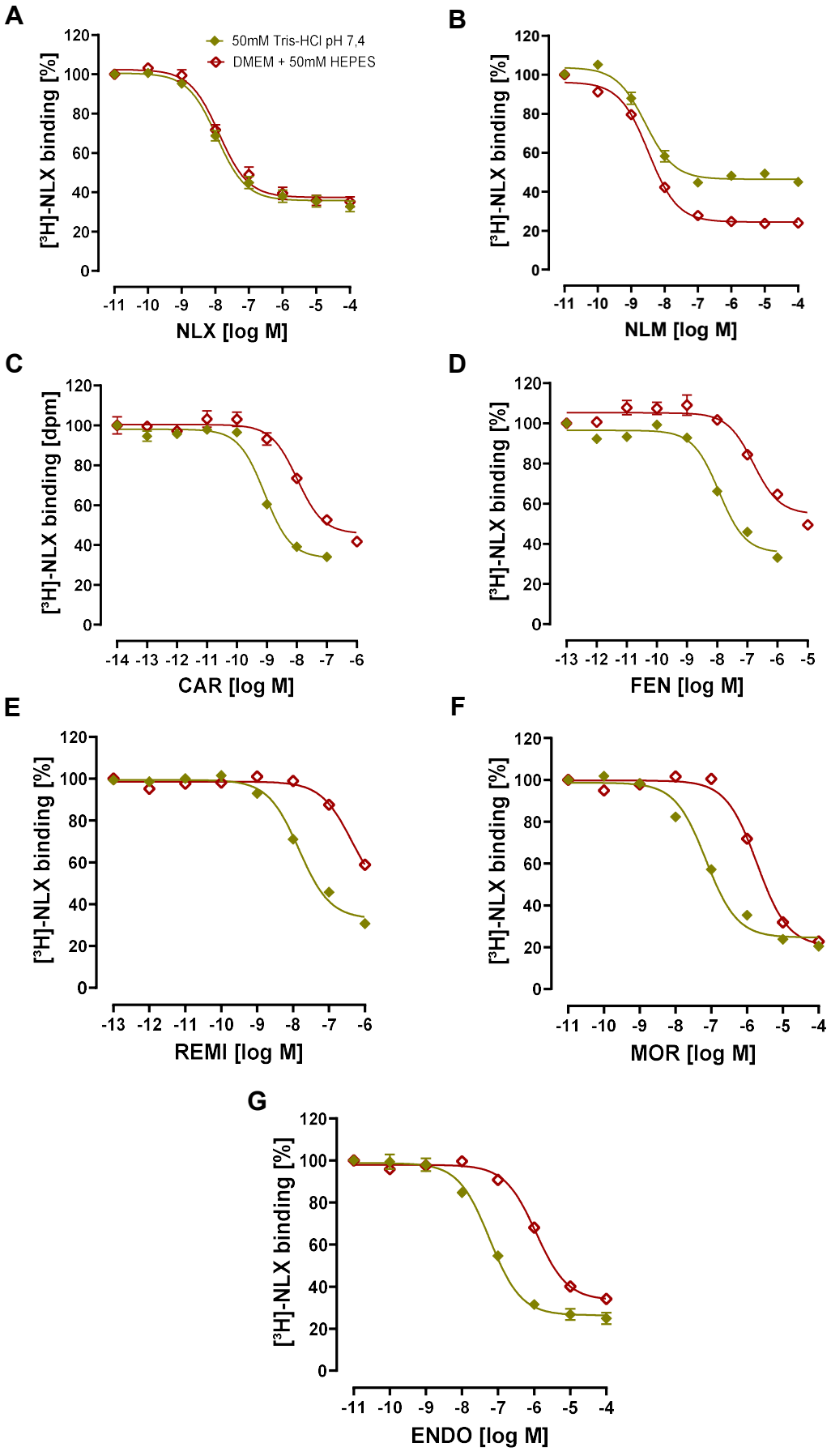

Figure 16: Competitive binding curves of OR agonists and antagonists

20 µg of HEK293-µOR membrane preparation was incubated in triplicates with 5 nM [³H]-NLX and the indicated concentrations of ligands diluted in either 50 mM TRIS-HCl (pH7.4) or DMEM + 50 mM HEPES. After an incubation period of 30 minutes in a 37°C incubator, radioactive decay of the filter patches was measured. Raw data were normalized by setting [³H]-NLX binding at lowest ligand concentations to 100%. Percentage of [³H]-NLX binding in presence of NLX (**A**), NLM (**B**), CAR (**C**), FEN (**D**), REMI (**E**), MOR (**F**) or ENDO (**G**) was plotted as mean ± SEM of % [³H]-NLX binding against the corresponding concentration of agonist or antagonist. n=3-4

	TRIS-buffer		**DMEM**	
	IC_{50} [nM]	**K_i [nM]**	**IC_{50} [nM]**	**K_i [nM]**
NLX	11.7 ± 1.82	7.79 ± 1.21	14.7 ± 3.96	9.78 ± 2.64
NLM	2.75 ± 0.43	1.83 ± 0.29	3.31 ± 0.13	2.20 ± 0.09
CAR	1.07 ± 0.24	0.71 ± 0.16	10.7 ± 1.95	7.10 ± 1.30**
FEN	11.7 ± 2.28	7.81 ± 1.52	147.7 ± 20.4	98.4 ± 13.6**
REMI	14.8 ± 1.66	9.86 ± 1.11	>504 ± 166	>336 ± 110*
MOR	72.4 ± 5.51	48.3 ± 3.67	1913 ± 272	1276 ± 182**
ENDO	59.5 ± 6.23	39.7 ± 4.15	1119 ± 96.1	746 ± 64.1***

Table 6: K_i values of OR agonists and antagonists determined in different buffer systems

IC_{50} values were specified based on data shown in Figure 16 using GraphPad Prism 10.3.1 (Non-linear regression one site - fit log IC_{50}). K_i values were calculated from IC_{50} values using Equation 3 as outlined in chapter 5.4.4. Values represent the mean ± SEM from individual experiments. Statistical analysis was performed using an unpaired t-test. Asterisks indicate significant difference between K_i values determined in the two different buffers. *p<0.05, **p<0.01, ***p<0.001

Derivatives of the FEN group exhibited clearly higher receptor binding affinities compared to MOR and ENDO in both buffer systems. Among the FEN derivatives, CAR exhibited the highest µOR binding affinity, with K_i values below 1 nM in TRIS-buffer and below 7 nM in DMEM, highlighting its strong binding to the µOR among these compounds. FEN and REMI followed with K_i values of approximately 8-10 nM in TRIS-buffer, while MOR and ENDO showed the lowest affinities (40-50 nM). It is important to note that there were difficulties when determining the K_i value for REMI in DMEM. Achieving a plateau in [³H]-NLX displacement would have required to test one additional, higher concentration of REMI. However, due to limitations in the stock concentration and concerns about

the excessive methanol content, a concentration of 1 µM for REMI could not be exceeded. As a result, the K_i value is reported as > 336 ± 110 nM, indicating that the actual K_i is likely higher.

Overall, affinities fell within the range of published values when assessed in TRIS-buffer, considering the variability typically introduced by differences in methodological approaches (Table 6, Table 1). Notably, no direct reference values for opioid affinities in DMEM exist. The rank order of affinities observed was CAR > FEN = REMI > ENDO = MOR in TRIS-buffer and with CAR > FEN > REMI > ENDO > MOR similar in DMEM. However, agonists binding affinities measured in DMEM were significantly lower than those in TRIS-buffer (Table 6). DMEM significantly reduced the affinities of all tested µOR agonists, aligning with reports about ion influence in the literature [445].

The K_i values for NLX and NLM were consistent with literature values across both buffer systems (Table 5, Table 6) [72,73,76,82,452]. Notably, NLM displayed lower K_i values than NLX, indicating a higher µOR affinity, which is in line with previous findings [74,453]. These results also align with saturation curve data shown earlier in this work, where the K_d value for [^{3}H]-NLX binding was approximately 9 nM - falling within the same range as the K_i values measured for NLX here. In line with the saturation binding assays (6.3.3), no significant differences in antagonist affinity were observed between the two binding buffers.

Overall, these findings indicate that the buffer composition does play a role in influencing agonist but not antagonist binding affinity. However, importantly, the use of different buffers did not affect the ranking of opioid affinities.

As previously described, membrane preparations in ligand binding assays compromise physiological relevance due to the loss of the intact cell surface and disruption of the intra- and extracellular ion gradient, even when using DMEM as a binding buffer. To address this, the affinity of CAR and FEN was exemplarily determined with whole, adherent cells in DMEM, providing conditions closer to physiology.

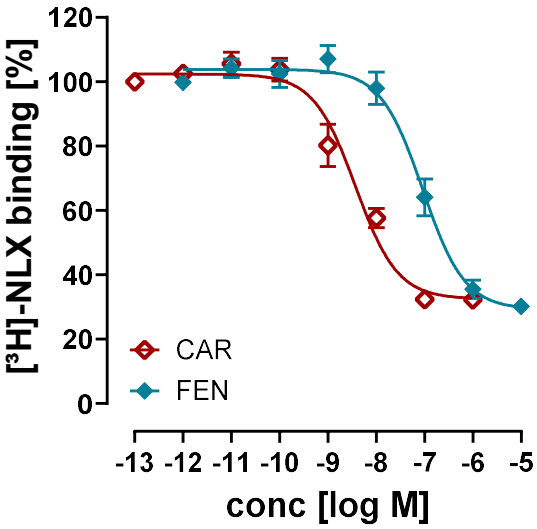

Figure 17: Competitive binding curves of CAR and FEN determined with whole cells in DMEM

80,000 HEK293-μOR cells per well were seeded on poly-L-lysine coated 48-well plates. After a 24-hour starvation period, cells were stimulated with 5 nM [³H]-NLX and the indicated concentrations of CAR and FEN for 30 minutes at 37°C. DMEM + 50 mM HEPES served as the binding buffer. Radioactive decay of cell lysates was measured and raw data were normalized by setting [³H]-NLX binding at lowest ligand concentation to 100%. Percentage of [³H]-NLX binding in presence of CAR and FEN was plotted as mean ± SEM of % [³H]-NLX binding against the corresponding concentration of agonist. n=3

	IC_{50} [nM]	K_i [nM]
CAR	3.78 ± 1.43	2.39 ± 0.90
FEN	101 ± 55.9	63.8 ± 35.4

Table 7: K_i values of CAR and FEN determined with whole cells in DMEM

IC_{50} values were specified based on data shown in Figure 17 using GraphPad Prism 10.3.1 (Non-linear regression one site - fit log IC_{50}). K_i values were calculated from IC_{50} values using Equation 3 as outlined in chapter 5.4.4. Values represent the mean ± SEM from individual experiments.

The K_i values determined in whole cells closely match those from membrane preparations (Table 6), suggesting that membrane use does not significantly affect opioid binding behavior in DMEM. Typically, intact cells in a blood-like medium, such as DMEM, are considered the preferred physiological model, while membrane preparations are often regarded as less representative of *in vivo* conditions. However, the similarity in binding data between these two systems

suggests that membrane-based assays in DMEM may more closely approximate physiological conditions than previously assumed.

6.4.2. Assessment of opioid potency in cAMP inhibition

To complement the μOR binding studies, radioactive cAMP accumulation assays were conducted to compare the potencies of CAR, FEN, REMI, MOR and ENDO in reducing cellular cAMP levels, providing insights into the relative performance of these opioids in receptor activation.

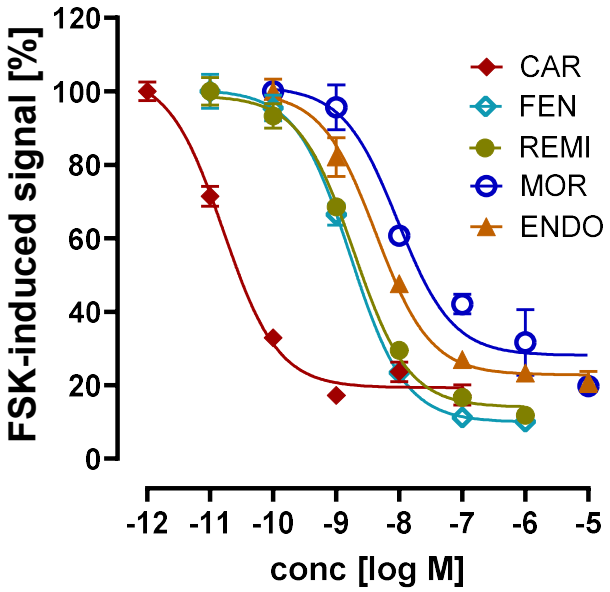

Figure 18: Potencies of μOR agonists to attenuate FSK-induced cAMP accumulation

300,000 HEK293-μOR cells per well were cultivated on 12-well plates and labeled with 1 μCi/mL [³H]-adenine for 24 hours. Cells were stimulated in triplicates with 500 μM IBMX, 50 μM FSK and the indicated concentrations of opioids prepared in FCS-free DMEM for 20 minutes at 37°C. Cell lysates were purified using column chromatography as described in 5.5.1. Radioactive decay of the eluates was measured. Signal at lowest opioid concentration was set to 100%. Nomalized data was plotted as mean ± SEM of percentage of FSK-induced signal against logarithmic opioid concentration. n=3

Opioid-induced cAMP attenuation was concentration-dependent and resulted in sigmoidal curves. From these dose-response curves, EC_{50} values of the ligands were determined. The EC_{50} value provides a measure of the ligand's potency in modulating the cAMP signaling pathway, while the E_{max} represents the maximum signal induction at saturated concentrations (intrinsic activity). The EC_{50} values, along with the E_{max} values of the opioids, are summarized below.

	EC_{50} [nM]	E_{max}[%]
CAR	0.016 ± 0.001	80.7 ± 3.29
FEN	1.70 ± 0.23**	90.1 ± 1.25
REMI	1.94 ± 0.33**	86.1 ± 0.94
MOR	9.93 ± 1.24**	72.0 ± 3.09
ENDO	4.17 ± 0.48***	77.1 ± 2.09

Table 8: EC_{50} values and intrinsic activities of μOR agonists determined using radioactive cAMP assay

EC_{50} values were determined using data shown in Figure 18 and GraphPad Prism 10.3.1 (Non-linear regression one site - fit log IC_{50}). Intrinsic activities were calculated as the difference between top and bottom of the curves (Figure 18). Values represent the mean ± SEM of individual experiments. Statistical analysis was performed using unpaired t-tests, to compare each EC_{50} and E_{max} to the corresponding value of CAR. Asterisk indicate significant difference to CAR (**p<0.01, ****p<0.0001).

All tested opioids exhibited intrinsic activities ranging from 70% to 90%. While the FEN derivatives tended to show higher intrinsic activities compared to MOR and ENDO, with FEN exhibiting the highest value, no significant differences were observed among the opioids regarding their maximum effect.

FEN analogs demonstrated lower EC_{50} values compared to MOR and ENDO, suggesting higher potencies. Among all tested opioids, CAR exhibited the highest potency, with an EC_{50} value of less than 20 picomolar, making it approximately 620 times more potent than MOR in inhibiting cAMP production. These findings are consistent with existing research. While no comprehensive study to date has systematically compared this particular selection of opioids for their potency in the cAMP signaling pathway, previous work has demonstrated a higher potency of CAR in such assays [75].

6.4.3. Evaluation of receptor efficacy in cAMP signaling modulation

To investigate the relationship between μOR binding and activation by individual opioids, data from ligand binding assays and cAMP accumulation assays were combined. This allowed for the determination of receptor efficacy, reflecting how efficiently a single receptor-bound opioid translates its binding into a cellular response. It is important to note that the binding assays revealed variations in

ligand affinity based on the buffer system used. Therefore, a comparative analysis of potency and affinity was included for both buffer systems. The combined presentation of the data from the binding assays and the cAMP assays is shown below.

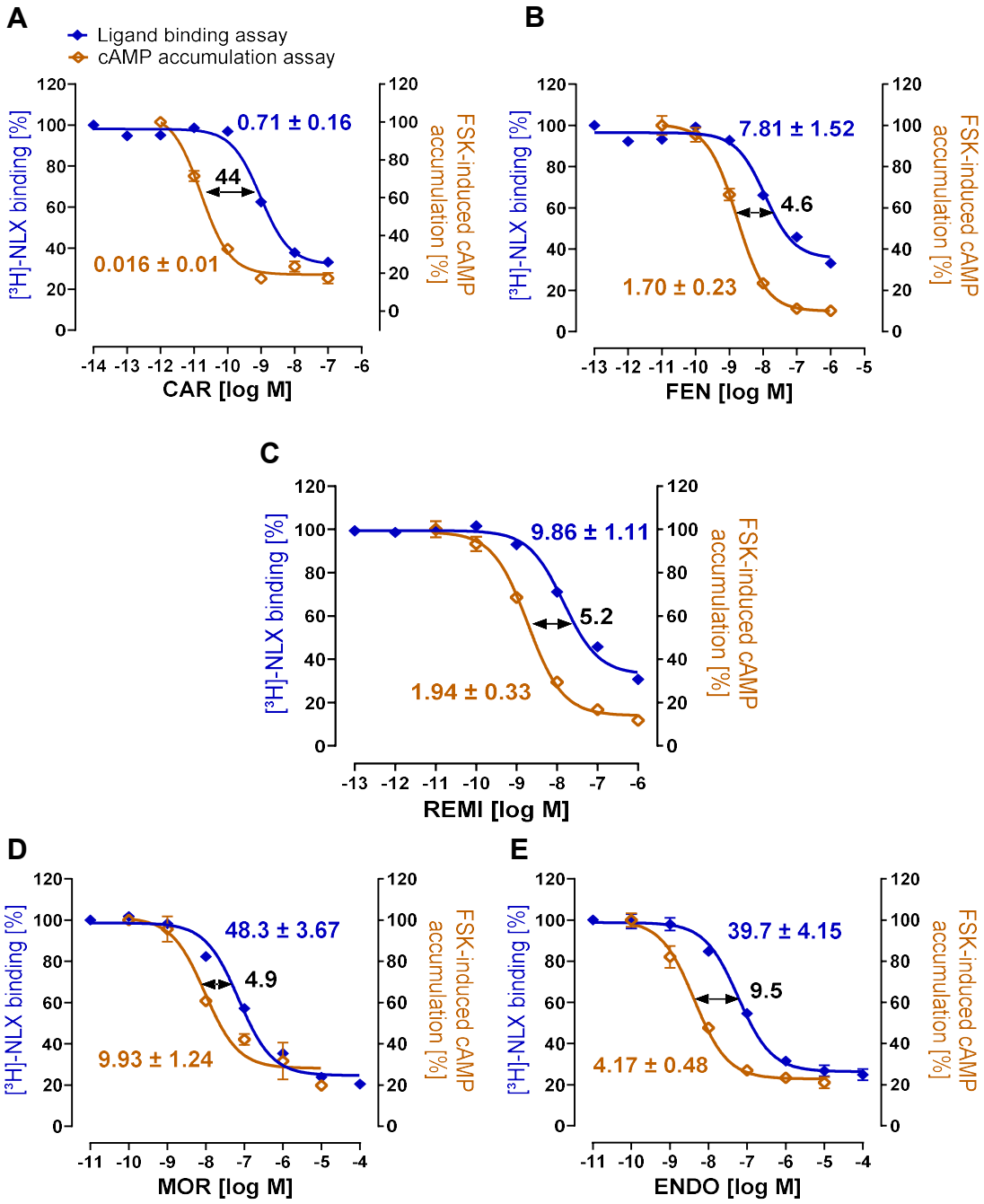

Figure 19: Combined representation of opioid μOR binding affinities (TRIS- buffer) and their potencies for cAMP inhibition

Data from competitive ligand binding assay conducted in 50 mM TRIS-HCl (pH 7.4) shown in Figure 16 as well as data from cAMP accumulation assays shown in Figure 18 were plotted together as mean ± SEM of percentage of [³H]-NLX binding or percentage of FSK-induced cAMP accumulation against indicated concentrations of

CAR (**A**), FEN (**B**), REMI (**C**), MOR (**D**) or ENDO (**E**). Corresponding K_i and EC_{50} values are specified in nM and represent the mean ± SEM of individual experiments. Arrows and associated numbers indicate ratios between K_i and EC_{50} (affinity-to-potency ratio, APR).

The collective data representation revealed a leftward shift in the potency curves for all tested agonists, indicating that lower opioid concentrations were required to achieve half-maximal inhibition of cAMP levels compared to half-maximal receptor binding. This well-documented phenomenon in overexpressing cell systems is commonly attributed to receptor reserve, where the EC_{50} value of a ligand does not directly correspond to 50% receptor binding [454].

In this study, receptor reserve was quantified using the affinity-to-potency ratio (APR), which reflects the efficiency of signal transduction per bound receptor (receptor efficacy). Based on APR values, opioids fell into three distinct groups: FEN, MOR and REMI demonstrated similar ratios of approximately 5 (Figure 19 B-D), while ENDO displayed a higher APR of around 10, indicating greater efficacy (Figure 19E). Notably, CAR stands out markedly with a ratio of 44, far exceeding all other agonists (Figure 19 A). This suggests that, in view of its affinity, CAR is exceptionally active in inhibiting FSK-induced cAMP accumulation, underscoring its exceptionally strong effects compared to other opioids.

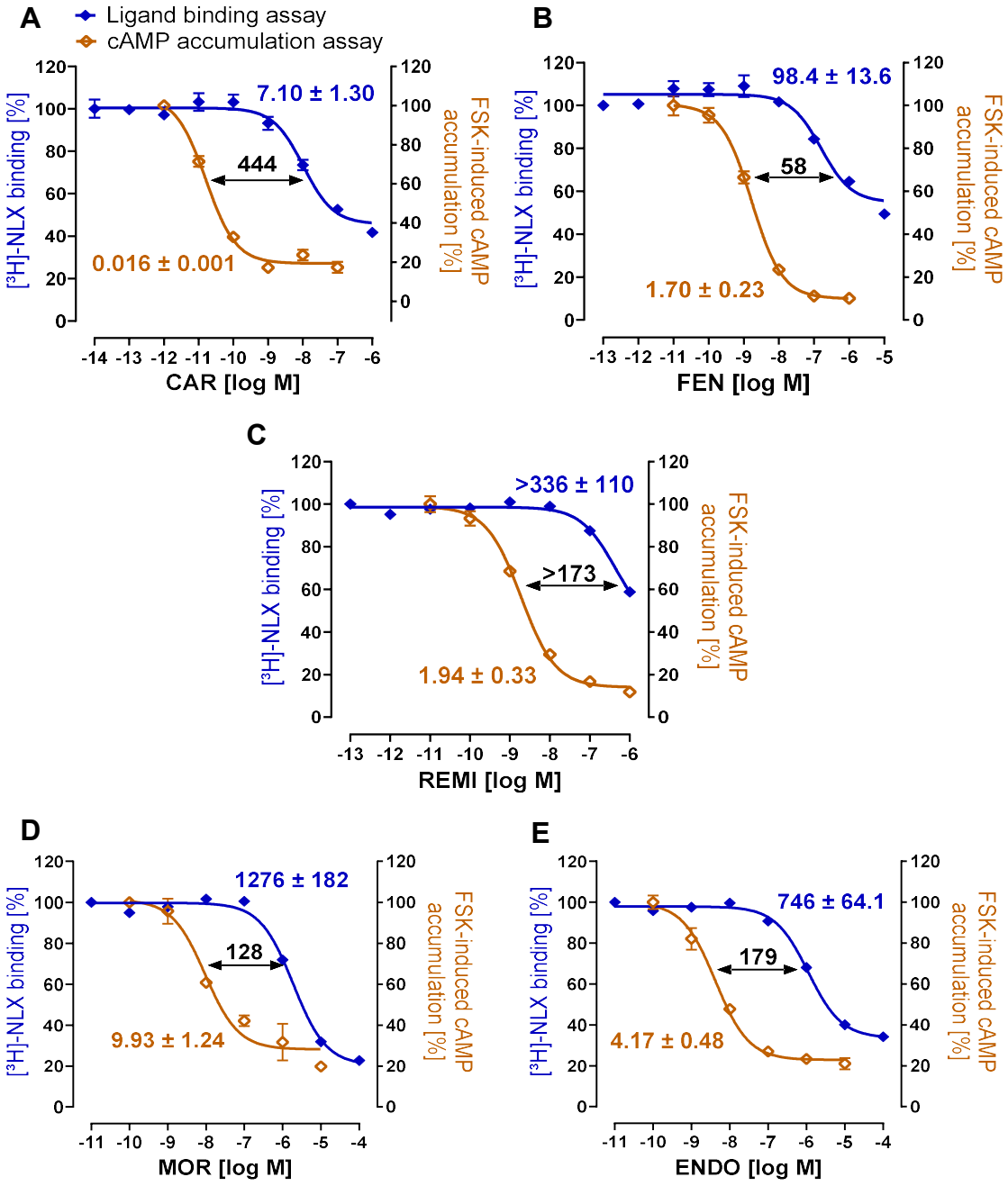

Figure 20: Combined representation of opioid μOR binding affinities (DMEM) and their potencies for cAMP inhibition

Data from competitive ligand binding assay conducted in DMEM + 50 mM HEPES shown in Figure 16 as well as data from cAMP accumulation assays shown in Figure 18 were plotted together as mean ± SEM of percentage of [³H]-NLX binding or percentage of FSK-induced cAMP accumulation against indicated concentrations of CAR (**A**), FEN (**B**), REMI (**C**), MOR (**D**) or ENDO (**E**). Corresponding K_i and EC_{50} values are specified in nM and represent the mean ± SEM of independent experiments. Arrows and associated numbers indicate APRs.

When measured in DMEM, tested OR agonists showed lower affinities, further increasing the divergence between affinity and potency when plotted together. Consequently, this also led to higher APR values. Nonetheless, three distinct

groups emerged again: This time, MOR, ENDO, and REMI displayed ratios of around 130-180, while FEN showed a notably lower ratio of approximately 60. For REMI, the ratio is listed as >173 due to its likely higher true K_i value, suggesting this factor might be somewhat underestimated. Importantly, CAR stands out once more with a strikingly high ratio of 444, reaffirming that, across experimental conditions, CAR takes an exceptional role in cAMP signaling.

In addition to calculating the APRs, another approach was used to evaluate and compare opioids´ receptor efficacies. By considering both an opioid´s ability to activate the μOR and its binding affinity, receptor occupancy for half-maximal receptor activation (RO) was calculated. In this section, it describes the proportions of receptor-binding required for half maximal inhibition of FSK-stimulated cAMP accumulation. A summary of K_i values for both binding buffers, EC_{50} values and ROs, calculated using each K_i value respectively is shown below.

	EC_{50} [nM]	K_i [nM]	RO [%]	K_i [nM]	RO [%]
		TRIS-buffer		DMEM	
CAR	0.016 ± 0.001	0.71 ± 0.16	2.2 ± 0.7	7.10 ± 1.30	0.22 ± 0.06
FEN	1.70 ± 0.23	7.81 ± 1.52	17.9 ± 4.9*	98.4 ± 13.6	1.70 ± 0.46*
REMI	1.94 ± 0.33	9.86 ± 1.11	16.4 ± 3.9*	336 ± 110	0.58 ± 0.32
MOR	9.93 ± 1.24	48.3 ± 3.67	17.1 ± 2.8*	1276 ± 182	0.77 ± 0.21
ENDO	4.17 ± 0.48	39.7 ± 4.15	9.5 ± 1.9	746 ± 64.1	0.56 ± 0.11

Table 9: Summary of binding affinities determined in different buffer systems, potencies and receptor occupancies of opioid agonists for half maximal cAMP inhibiton

K_i values were determined in 6.4.1, EC_{50} values were determined in 6.4.2. Receptor occupancies (RO) were calculated using Equation 5 as described in 5.9.1. The error was estimated by calculating RO at the lower and upper limits of K_i and EC_{50} values. The final uncertainty was taken as half the difference between these values. Statistical analysis was performed using a one-way ANOVA, followed by Dunnett's multiple comparison test to determine significant differences in RO values compared to CAR's RO (*$p<0.05$).

RO correlates closely with APRs when ranking the opioids. Based on affinities measured in TRIS-buffer, FEN, REMI and MOR required the highest RO, with 16-18% needed to achieve half-maximal inhibition of cAMP. In comparison, ENDO needed only about 10% occupancy to produce similar effects. CAR, however, stood out with remarkable efficacy, achieving 50% activation of the receptors with just around 2% receptors bound. Notably, the RO of CAR was significantly lower than that of all other tested opioids except for ENDO, further highlighting its distinct efficacy in receptor activation.

In DMEM, where K_i values were higher, RO requirements were generally lower and the rankings shifted slightly. FEN showed the highest RO requirement at 1.7%, which was significantly higher than that of CAR. REMI, MOR and ENDO required around 0.6-0.8% occupancy for half-maximal activation, with no significant differences between them. CAR continued to require the lowest RO with only 0.2%.

This analysis compared affinity, potency, intrinsic activity and receptor efficacy (expressed as APR and RO) for the tested opioids. In conclusion, CAR showed the highest affinity among the tested opioids, along with exceptionally high potency and receptor efficacy in cAMP pathway activation. This indicates that, relative to its affinity, CAR is significantly more effective in translating receptor binding into a cellular response, specifically cAMP inhibition, than the other opioids. Notably, this observation was consistent across different buffer conditions used for affinity determination.

6.4.4. Investigation of receptor efficacy in ERK1/2 phosphorylation

Previous results showed that CAR exhibits extraordinarily high efficacy in cAMP inhibition, a G protein-dependent pathway. Given that ERK1/2 phosphorylation can occur through both G protein- and β-arrestin-dependent mechanisms, examining this pathway could provide further insights into potential signaling bias among the tested opioids. Therefore, after determining potency and receptor efficacy in the cAMP pathway, these parameters were also analyzed in the context of another opioid-induced signaling pathway.

6.4.4.1. Kinetic analysis of opioid-induced ERK1/2 phosphorylation

To investigate potential differences in ERK1/2 signaling and to identify the optimal conditions under which the phosphorylation profiles of the opioids could be assessed, initially, the time course of ERK1/2 phosphorylation was examined for CAR, FEN, REMI, MOR and ENDO. This included both the early, G protein-mediated phase and the later, β-arrestin-mediated phase, which are associated with distinct signaling pathways [292,455]. The graphs below illustrate the time-dependent ERK1/2 phosphorylation induced by the selected opioids.

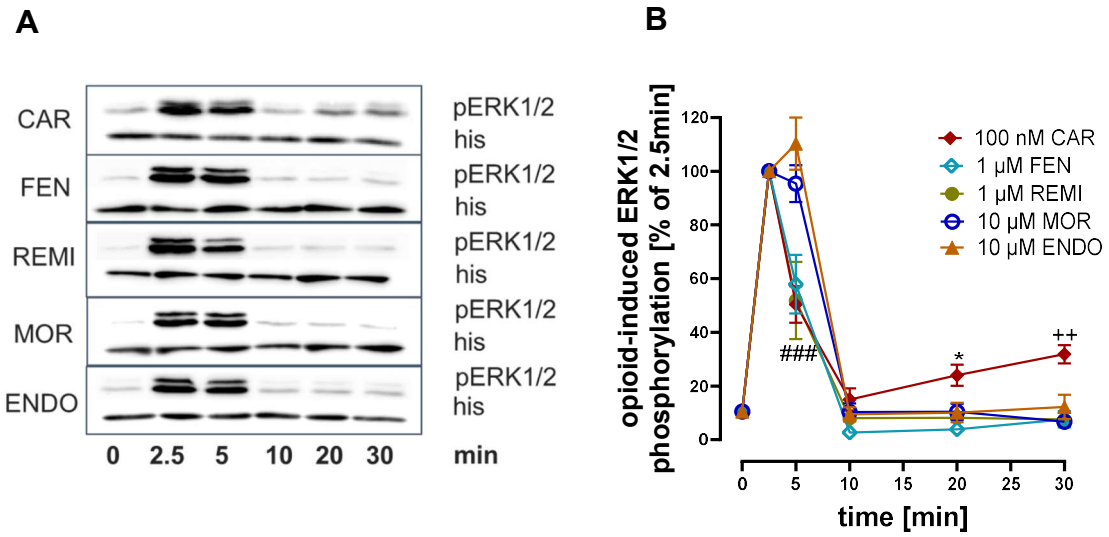

Figure 21: Time course of opioid-induced ERK1/2 phosphorylation from 0 to 30 minutes

HEK293-µOR cells (300,000/well) were stimulated on 6-well plates with saturated opioid concentrations (100 nM CAR, 1 µM FEN, 1 µM REMI, 10 µM MOR, 10 µM ENDO) in FCS-free DMEM over the indicated time intervals at 37°C. Protein levels of phosphorylated ERK1/2 (42/44 kDa) and loading control Histone H3 (17 kDa) were determined using Western Blot (see section 5.7). n=6 **A:** Representative Western blot images are shown for each opioid condition. **B:** AUC ratios of pERK1/2 to Histone H3 levels were calculated and normalized to the percentage of ERK1/2 phosphorylation observed at 2.5 minutes. Normalized pERK1/2 levels are plotted as the mean ± SEM as % of 2.5-minute baseline over time. Statistical analysis was performed using a one-way ANOVA followed by Dunnett's multiple comparisons test, comparing CAR values at each time point with those of all other opioids. Diamond symbols indicate significant difference to ENDO and MOR ($^{###}p < 0.001$), asterisks denote significant differences to FEN, REMI and MOR ($^{*}p < 0.05$), and plus symbols indicate significant differences to all other opioids ($^{++}p < 0.01$).

The cells were stimulated with saturated opioid concentrations to ensure that most receptors were bound, producing a maximal ERK1/2 signaling response. All tested opioids induced a rapid ERK1/2 phosphorylation response, with peak levels observed between 2.5 and 5 minutes, suggesting a G protein-dependent mechanism. CAR did not show significantly higher phosphorylation levels

compared to other opioids, suggesting that the maximal ERK1/2 response induced by CAR is similar to that of the other opioids.

By the 5-minute mark, an interesting difference appeared: cells treated with FEN derivatives showed lower pERK1/2 levels than those treated with MOR and ENDO, suggesting a rapid drop in phosphorylation after the initial peak. This rapid decline with CAR, FEN and REMI contrasts with the more sustained phosphorylation seen with MOR and ENDO.

Interestingly, CAR was the only opioid to maintain significant, though diminished, β-arrestin-mediated ERK1/2 phosphorylation at 20 to 30 minutes - a late-phase activity absent in other opioids. This suggests unique phosphorylation dynamics for CAR, potentially involving distinct regulatory pathways or specific β-arrestin interactions, although this aspect was not further investigated in this study. Despite this, CAR did not demonstrate a significant advantage over other opioids in terms of early, G protein-mediated ERK1/2 phosphorylation.

6.4.4.2. Comparison of opioid-induced ERK1/2 phosphorylation potency

In addition to examining the timing and duration of ERK1/2 phosphorylation induced by opioids, their dose-response relations were assessed. Thereby, the potencies (EC_{50} values) of CAR, FEN, REMI, MOR and ENDO could be determined enabling a comprehensive comparison of each opioid's performance in activating ERK1/2. This analysis focused on the early, G protein-mediated phase of ERK1/2 phosphorylation.

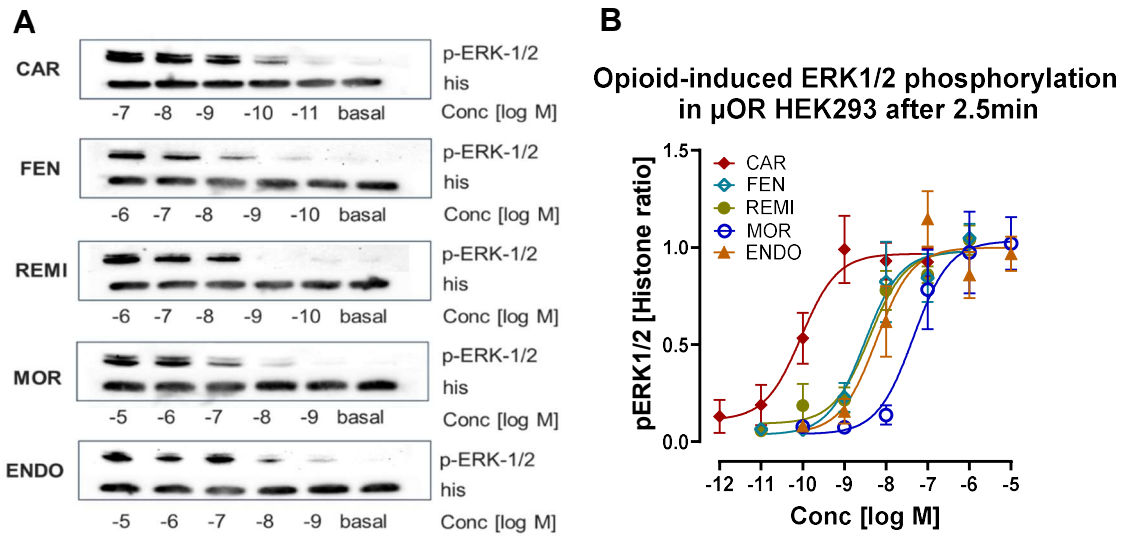

Figure 22: Dose-response curves of opioids for ERK1/2 phosphorylation

HEK293-μOR cells (300,000/well) were stimulated on 6-well plates with the indicated concentrations of opioids for 2.5 minutes at 37°C. Protein levels of pERK1/2 (42/44kDa) and loading control Histone H3 (17kDa) were determined using Western Blot (see section 5.7). n=6 **A:** Representative Western blot images are shown for each opioid condition. **B:** AUC ratios of pERK1/2 to Histone H3 levels were calculated and ERK1/2 phosphorylation induced by opioids was plotted as the mean ± SEM of Histone ratio against logarithmic opioid concentrations.

As expected, lower opioid concentrations resulted in reduced pERK1/2 levels, with all dose-response curves starting near baseline. At higher concentrations, each opioid reached a similar maximum phosphorylation level, stabilizing at a Histone H3 ratio of approximately 1. Given the comparable maximum phosphorylation levels reached by each opioid at higher concentrations, the intrinsic activities of the opioids were not separately listed, as they appeared relatively consistent across the tested compounds. CAR, in particular, did not show distinct effects in this regard, which is consistent with the findings from the kinetic analysis, where CAR exhibited a maximal ERK1/2 response similar to that of the other opioids.

From the dose-response curves, the EC_{50} values of the opioids were determined, allowing for the comparison of their potencies. Furthermore, as with the cAMP signaling pathway analysis, receptor efficacy was assessed by calculating the RO required to achieve half-maximal ERK1/2 phosphorylation, using the affinity constants obtained from the two different buffer conditions.

	EC_{50} [nM]	K_i [nM]	RO [%]	K_i [nM]	RO [%]
		TRIS-buffer		DMEM	
CAR	0.21 ± 0.11	0.71 ± 0.16	22.8 ± 13.2	7.10 ± 1.30	2.87 ± 2.03
FEN	6.57 ± 4.32	7.81 ± 1.52	45.7 ± 22.0	98.4 ± 13.6	6.26 ± 4.71
REMI	5.06 ± 2.43	9.86 ± 1.11	33.9 ± 13.4	336 ± 110	1.48 ± 1.31
MOR	41.0 ± 11.3	48.3 ± 3.67	45.9 ± 8.8	1276 ± 182	3.11 ± 1.28
ENDO	5.80 ± 1.42	39.7 ± 4.15	12.7 ± 3.9	746 ± 64.1	0.77 ± 0.26

Table 10: Summary of binding affinities determined in different buffer systems, potencies and receptor occupancies of opioid agonists for ERK1/2 phosphorylation

K_i values were obtained from Table 6, EC_{50} values were obtained from data shown in Figure 22B using GraphPad Prism 10.3.1 (Non-linear regression log (agonist) vs. response (three parameters)). Values represent the mean ± SEM of individual experiments. ROs were calculated using Equation 5 and describe proportions of receptor-binding required for half maximal ERK1/2 phosphorylation induced by opioids. The error was estimated by calculating RO at the upper and lower limits of K_i and EC_{50} values, with the final uncertainty defined as half of the resulting range. Statistical analysis was conducted using a one-way ANOVA, followed by Dunnett's multiple comparison test to assess significant differences in RO values relative to CAR's RO. No significant difference was observed.

Among the opioids tested, CAR demonstrated the highest potency (0.7 nM), followed by FEN, REMI and ENDO, which showed similar EC_{50} values ranging from 5 to 7 nM. MOR exhibited the lowest potency, with an EC_{50} value around 41 nM. This ranking of potency aligns with the data obtained from the cAMP assays. Notably, the potencies for ERK1/2 phosphorylation were consistently lower across all opioids compared to their ability to inhibit FSK-induced cAMP accumulation.

As a result, the RO values calculated for ERK1/2 phosphorylation were considerably higher than those observed in the cAMP pathway, regardless of the buffer system used to determine the K_i values. This indicates a lower receptor efficacy for ERK1/2 activation, meaning a greater proportion of μOR must be occupied to trigger ERK1/2 signaling compared to what is required for cAMP inhibition. Based on the lower K_i values measured in TRIS-buffer, ROs for half-maximal ERK1/2 activation ranged between 13% and 46%. ENDO required the least receptor occupancy (13%) and was therefore the most efficient at inducing

pERK1/2, followed by CAR (23%), REMI (34%), and finally MOR and FEN, both requiring around 46%. Interestingly, the phenomenon observed with cAMP inhibition - where CAR achieved similar effects with significantly lower RO - did not apply to ERK1/2 phosphorylation.

When ROs were calculated using higher K_i values from DMEM, the occupancy levels required were predictably lower. In this condition, ENDO required the least receptor binding, with an occupancy of 0.8% to achieve half-maximal ERK1/2 phosphorylation, followed by REMI, CAR and then MOR and FEN. Here also, CAR´s receptor efficacy did not stand out as uniquely as it did in the cAMP pathway, with its RO of around 3% falling within the mid-range of the group.

6.4.5. Bias assessment of opioid signaling towards the cAMP pathway

To further compare the effects of opioids on the cAMP and pERK1/2 signaling pathways, the ratio of ROs was calculated. Additionally, the bias factor was determined, which indicates the preference of a ligand to activate one signaling pathway over another relative to a reference ligand. ENDO was used as the reference ligand in these calculations.

	Ratio of RO (pERK/cAMP) TRIS-buffer	**Ratio of RO** (pERK/cAMP) DMEM	**Bias factor relative to ENDO** (cAMP/pERK)
CAR	8.44	3.18	10.8
FEN	2.55	2.71	3.33
REMI	2.11	2.50	2.10
MOR	2.68	5.44	2.73
ENDO	1.34	1.04	1.00

Table 11: Ratio of ROs required for ERK1/2 phosphorylation versus cAMP inhibition, along with the bias factor for cAMP inhibition relative to ENDO

Ratio between ROs required for half maximal ERK1/2 phosphorylation (Table 10) and cAMP inhibition (Table 9) were build either with values arising from calculation

with K_i values determined in TRIS-buffer or DMEM (Table 6). Bias factor was calculated using Equation 6 and ENDO as the reference ligand.

The RO ratios were relatively consistent across the two buffer systems used to determine K_i values. ENDO had ratios around 1, indicating that it required similar levels of RO to achieve either 50% inhibition of cAMP signaling or 50% ERK1/2 phosphorylation. This finding suggests that ENDO does not show a preference for one signaling pathway over the other, making it an excellent reference ligand for calculating the bias factor. In contrast, FEN and REMI exhibited ratios between 2 and 3, indicating a slight preference for cAMP signaling over ERK1/2 phosphorylation when binding to the receptor. MOR had a ratio of nearly 3 based on its K_i in TRIS-buffer and around 5 when measured in DMEM, making it the highest recorded value in that buffer system. This data suggests that under the DMEM conditions, MOR shows a stronger bias toward the cAMP pathway compared to the other opioids, with CAR closely following at a factor of 3. When measured in TRIS-buffer, CAR exhibited an even higher ratio of more than 8, indicating a strong bias toward the cAMP signaling pathway compared to the other opioids.

This bias was further supported by the calculated bias factor, which helps isolate pathway preference from binding affinity, eliminating any differences that might arise from the experimental conditions used for measuring affinity. While FEN, REMI and MOR had bias factors of only 2-3 relative to ENDO, CAR demonstrated a significant bias factor of almost 11, highlighting its strong preference for the cAMP pathway.

Consequently, although all tested opioids exhibited some degree of pathway bias favoring cAMP signaling over ERK1/2 phosphorylation, CAR stood out with a markedly stronger bias, distinguishing it from the other tested opioids.

6.5. Screening of opioid-induced phosphorylation patterns in cellular proteins

Findings of this study indicate that CAR demonstrates a pronounced bias toward cAMP signaling, in addition to the documented bias toward β-arrestin signaling observed in previous studies [211]. However, beyond these pathways, little is known about CAR's signaling profile, underscoring the need for further

investigation. Despite extensive research on opioids, no studies to date have systematically examined multiple signaling pathways of CAR in parallel. A comprehensive analysis of its broader signaling network could provide valuable insights into whether CAR occupies a unique role in opioid signaling.

A particularly effective method for such thorough analysis was the use of a phospho-kinase array. This technique enabled the simultaneous screening of multiple cellular proteins to evaluate their activation or inactivation in response to opioid stimulation. To optimize the assay kinetics for opioid-induced protein phosphorylation, the initial experiment aimed at finding the ideal incubation time for opioids with the cells. FEN was chosen for this purpose, as it is well-characterized in terms of its effects on specific protein phosphorylation, making it an effective positive control for the kinetic analysis. The results presented focus on three kinases: CREB, ERK1/2 and Lck.

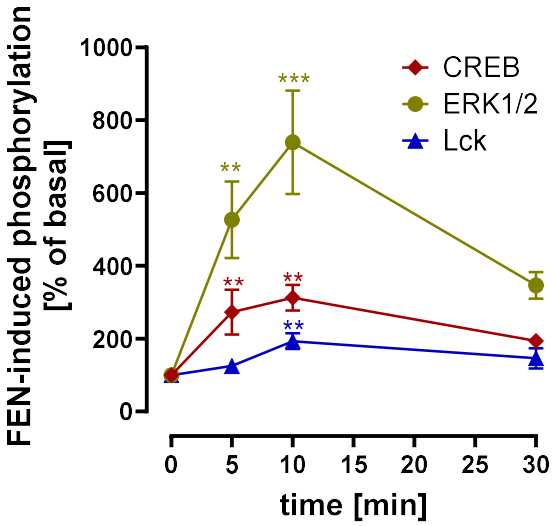

Figure 23: Kinetics of FEN-induced CREB, ERK1/2 and Lck phosphorylation

Three million HEK293-μOR cells were stimulated on 5 mL cell culture dishes with 1 μM FEN or an equivalent concentration of MeOH as a control for the specified time intervals. A phospho-kinase array was performed per protocol (section 5.6.), and the luminescence of each nitrocellulose membrane was measured. The area under the curve for each luminescence spot was normalized to the reference spot of the respective membrane and adjusted for the basal value. FEN-induced protein phosphorylation is presented as the mean ± SEM of the percentage of basal over time. Statistical significance for each time point relative to basal was assessed by one-way ANOVA with Dunnett's multiple comparison test (**p<0.01, ***p<0.001, ****p<0.0001)

All three assessed kinases exhibited time-dependent phosphorylation in response to FEN stimulation, using a saturated concentration to ensure maximal activation. The phosphorylation of CREB and ERK1/2 in response to FEN is well-established [293,456-458] and was replicated here. While Lck phosphorylation at Y394 has not been specifically investigated in the context of FEN, research suggests that μOR activation can influence Lck activity [459]. In this experiment, significant Lck phosphorylation at Y394 following FEN stimulation for 10 minutes was observed.

Interestingly, the phosphorylation levels of all kinases - CREB, ERK1/2, and Lck - peaked at 10 minutes before declining. This time point demonstrated the highest statistical significance, making it optimal for producing robust and interpretable assay results. However, it is important to note that the analysis of ERK1/2 phosphorylation in this assay did not align with the previous Western Blot results, which indicated that FEN-induced ERK1/2 phosphorylation peaked as early as 2.5 minutes (Figure 21). This discrepancy may stem from differences in experimental design and the kinetics of the assays used. Despite not being able to directly correlate the assays, the overall FEN-induced phosphorylation of ERK1/2 was successfully reproduced. Since this section focused on comparing the signaling pathways differentially activated by opioids, 10 minutes were chosen as a suitable incubation time for subsequent experiments.

Next, the phosphorylation patterns of the proteins listed in Table 4 were analysed in HEK293-μOR cells after stimulation with saturated concentrations of CAR, FEN, REMI and ENDO. To ensure sufficient comparability, each opioid was tested three times against every other opioid, resulting in a total of nine experiments per opioid stimulation. An example of the resulting nitrocellulose membrane readings, following cell lysate processing and development, is shown below.

In earlier experiments, MOR was included alongside the other opioids to thoroughly compare CAR with other opioids. For this particular assay, however, MOR was left out. Since ENDO had proven to be a reliable reference in prior studies, as it showed no bias in cAMP assays or ERK1/2 phosphorylation, its

inclusion alongside the FEN derivatives was considered a strong foundation for evaluating how CAR modulates kinases in comparison to other opioids.

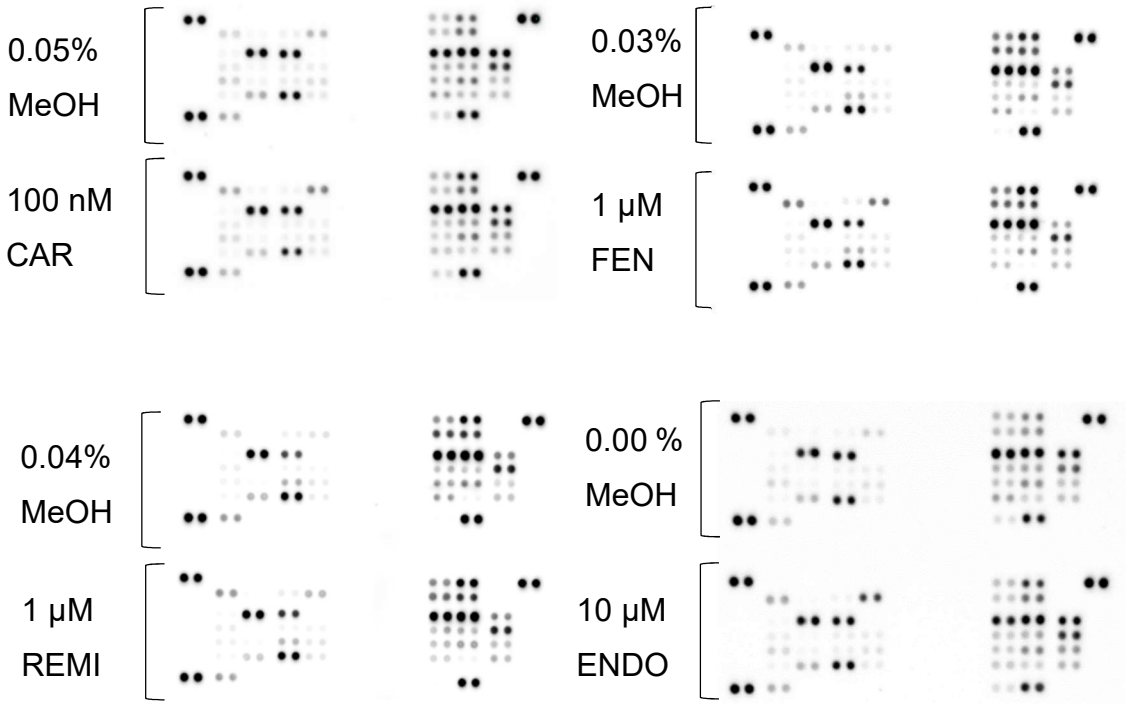

Figure 24: Exemplary phospho-kinase array membranes for each opioid stimulation and respective solvent control, recorded via chemiluminescence detection

Three million HEK293-µOR cells were stimulated in 5 mL culture dishes with the specified opioid concentrations for 10 minutes at 37°C. Phospho-kinase array was conducted as outlined in Chapter 5.6 and kinase phosphorylation was detected on nitrocellulose membranes using chemiluminescence. A representative set of membranes is shown as captured by the BioRad ChemiDoc system.

As already mentioned, some phosphorylation events, such as opioid-induced CREB phosphorylation, are well-documented in the literature [456,457]. The visible changes observed in many spots after opioid stimulation clearly indicated that the assay was working as intended. However, to ensure accurate quantification, standardization and interpretation of these signals, further processing of the collected data was required. The heat map below illustrates the modulation of protein activity (phosphorylation or dephosphorylation) in response to saturated opioid concentrations, compared to the solvent control.

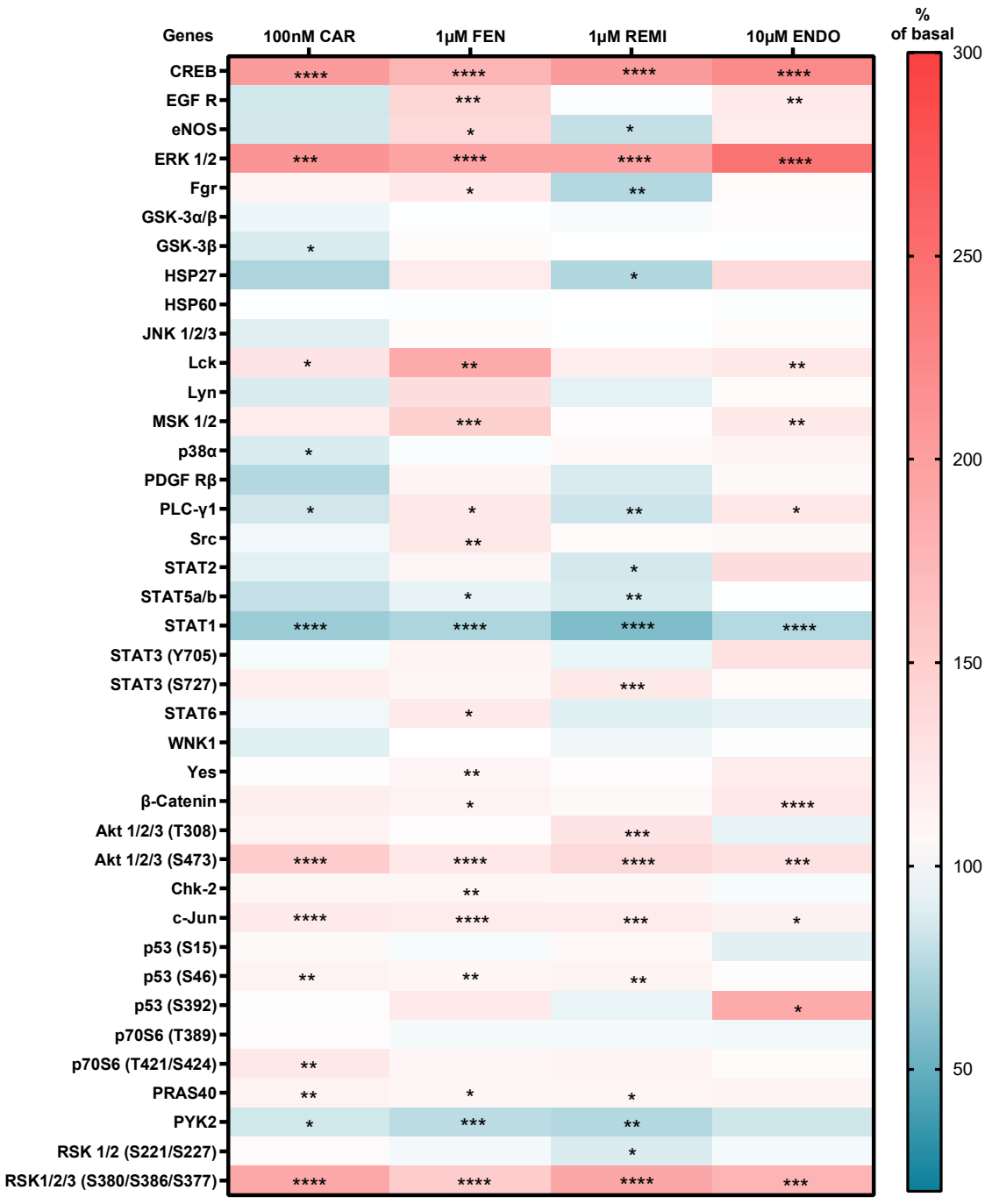

Figure 25: Phosphorylation pattern of cellular proteins induced by opioids

Three million HEK293-µOR cells were stimulated in 5 mL culture dishes with the indicated opioid concentrations for 10 minutes at 37°C. The phospho-kinase array was performed as described in Chapter 5.6, and kinase phosphorylation was detected on nitrocellulose membranes via chemiluminescence. Luminescence signals from individual spots on the membranes were quantified densitometrically using the Fiji ImageJ software. AUC values were normalized to the reference spot on each membrane and adjusted relative to the corresponding basal values. In this heat map, phosphorylation and dephosphorylation events are represented by color: red indicates phosphorylation, while blue indicates dephosphorylation. Opioid-induced modulation of each protein is presented as the mean percentage relative to the basal value. n=9. Statistical significance of kinase modulation with and

without opioid stimulation was analyzed using unpaired t-tests (*p<0.05, **p<0.01, ***p<0.001, ****p<0.0001).

Several targets, such as CREB, ERK1/2, STAT1, AKT1/2/3 (S473), cJun and RSK1/2/3 (S380/S386/S377), showed similar modulation across all the opioids tested. In contrast, other targets were uniquely modulated by only one or a specific subset of opioids - for example, AKT1/2/3 (T308) by REMI, Src, Yes and Chk4 by FEN, p70S6 (T421/S424) by CAR and p53 (S392) by ENDO. FEN-induced Lck phosphorylation after 10 minutes was consistently observed, as previously seen in Figure 23. In addition, CAR and ENDO also demonstrated Lck phosphorylation in this analysis.

To further explore differences between the opioids and identify any potential top-performers, the number of modulated proteins was counted for each opioid stimulation. During the experiments, it was observed that differences with low statistical significance ($p > 0.01$) varied widely between individual experiments. Therefore, the analysis was conducted using two significance levels as cut-offs to enhance reliability.

	All significance levels			**Significance levels p<0.01**		
	Modulated (of 39)	Phosphorylated	Dephosphorylated	Modulated (of 39)	Phosphorylated	Dephosphorylated
CAR	14	9	5	9	8	1
FEN	21	18	3	14	12	2
REMI	18	9	9	13	8	5
ENDO	12	11	1	9	8	1

Table 12: Number of modulated proteins through opioid stimulation

Number of proteins modulated, phosphorylated and dephosphorylated, as determined from data shown in Figure 25. The analysis was performed including all significance levels or only those with $p < 0.01$.

The choice of significance levels included in the analysis played a crucial role. When all significance levels were considered, all opioids displayed modulation of a larger number of proteins. In this context, FEN appeared to be the top performer, modulating a total of 21 proteins, with only 3 showing

dephosphorylation. Close behind was REMI, which modulated 18 proteins, but had an equal split between phosphorylation and dephosphorylation. CAR and ENDO modulated 14 and 12 proteins, respectively, with both showing more phosphorylation events than dephosphorylation.

When the lowest significance level was excluded, thereby increasing the reliability of the results, the number of modulated proteins across all opioids decreased. Nevertheless, the overall trends from the first numerical analysis remained consistent. FEN continued to modulate the highest number of proteins, totaling 14, of which 12 were phosphorylated. REMI followed closely with 13 proteins modulated, but nearly 40% of these showed dephosphorylation, the highest proportion among the opioids. CAR and ENDO each modulated 9 proteins, with over 90% of those showing phosphorylation. It's important to note that the similarity in the number of modulated proteins doesn’t mean that the target proteins or their modulation patterns were identical. Despite major overlaps, such as the phosphorylation of CREB, ERK1/2, Akt1/2/3 (S473) and RSK1/2/3 (S380/S386/S377), as well as the dephosphorylation of STAT1, there were also notable differences. Table 13 below highlights these significant differences in protein modulation in FEN-, REMI- and ENDO-stimulated cells compared to CAR-stimulated cells. To ensure statistical robustness, only significance levels of $p<0.01$ or lower were considered and only proteins with significant modulation differences are included in the table.

	FEN	**REMI**	**ENDO**
EGF-R	****	ns	ns
eNOS	**	ns	ns
MSK1/2	**	ns	ns
Src	**	ns	ns
Akt1/2/3 (S473)	ns	**	ns
RSK1/2 (S221/S227)	ns	**	ns

Table 13: Comparison of cellular protein modulation following stimulation with CAR, FEN, REMI and ENDO

Data presented originate from the same experiment as Figure 25. Statistical significance of individual protein phosphorylation was assessed using one-way ANOVA followed by Dunnett's multiple comparison test to evaluate differences in protein modulation in cells stimulated with FEN, REMI and ENDO, compared to CAR stimulation (**p<0.01, ****p<0.0001).

For the majority of proteins in this array, CAR-induced modulation did not significantly differ from that induced by other opioids. However, FEN uniquely increased phosphorylation of EGF-R, eNOS, MSK1/2 and Src, while REMI promoted phosphorylation of AKT1/2/3 (S473) and dephosphorylation of RSK1/2 (S21/S227) - both patterns not observed with CAR. Figure 25 revealed specific distinctions between CAR and ENDO: for example, β-catenin phosphorylation was exclusive to ENDO, while CAR uniquely stimulated PRAS40. However, Table 13 shows no statistically significant differences between CAR and ENDO, suggesting an overall similarity in their protein modulation profiles within this analysis. These results highlight the complexity of interpreting opioid-induced protein modulation, seen in this assessment.

Overall, CAR did not show a distinctly different effect on the kinase network. It neither phosphorylated significantly more proteins nor demonstrated statistically unique modulation compared to the other opioids tested. However, it notably induced specific phosphorylation of p70S6 at residues T421 and S424 - a modification previously described for MOR [460] and other opioids not analyzed in this study [461,462]. This analysis successfully reproduced several protein modulations previously documented in the literature while also uncovering new modulation patterns unique to this study.

6.6. Analysis of opioid-induced μOR phosphorylation at S375, T370 and T379

To investigate μOR modulation by opioids beyond traditional signaling assays, additionally, agonist-induced receptor phosphorylation was examined. Specifically, phosphorylation patterns induced by CAR, FEN, REMI, MOR and ENDO were examined at three C-terminal amino acids: Serine 375 (S375), Threonine 370 (T370) and Threonine 379 (T379). For this, a magnetic-bead-based immunoprecipitation method followed by detection using the ELISA principle was used.

It is well established that opioids can induce receptor phosphorylation with varying efficacy [300,463]. While μOR phosphorylation has been extensively studied for MOR, a review of the literature suggests that no data are available regarding CAR-induced phosphorylation. Therefore, this analysis provides novel insights into the phosphorylation profile of CAR in comparison to other opioids.

The graphs below illustrate the opioid-induced phosphorylation of the respective residues compared to the corresponding solvent control, presented as either raw or normalized data.

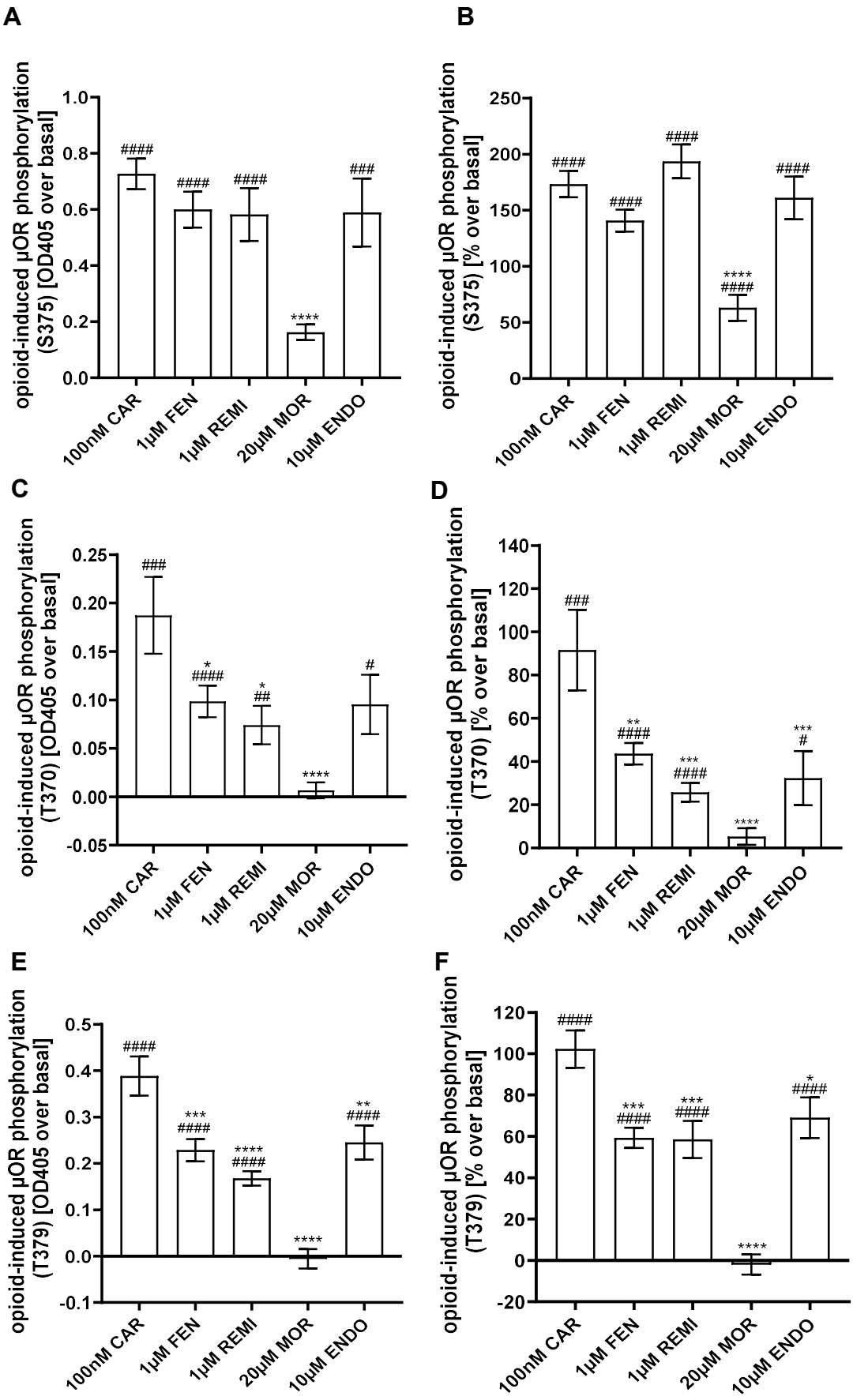

Figure 26: Opioid-induced µOR phosphorylation at S375, T370 and T379

HEK293-μOR cells (80,000/well) were stimulated in triplicates on 96-well plates with the indicated concentrations of each opioid, alongside corresponding solvent controls for 5 minutes at 37°C. Phosphorylation assays were performed as described in section 5.8. n=4-5 **A, C, E:** Optical density at 405 nm (OD_{405}) was measured and adjusted by subtracting the OD_{405} values of the respective solvent controls. Opioid-induced μOR-phosphorylation at specific residues is presented as the mean ± SEM of OD_{405} values over basal. **B, D, F:** Basal-corrected OD_{405} values were normalized as percentage above basal. Opioid-induced μOR-phosphorylation at specific residues is shown as the mean ± SEM of % increase over basal. Statistical analyses were conducted using a one-sample t-test to evaluate significant phosphorylation ($^{\#}p<0.05$, $^{\#\#}p<0.01$, $^{\#\#\#}p<0.001$, $^{\#\#\#\#}p<0.0001$) or one-way ANOVA followed by Dunnett's multiple comparisons test, where CAR-induced phosphorylation was compared to that induced by all other opioids (*p<0.05, **p<0.01, ***p<0.001, ****p<0.0001).

To ensure maximum signal detection, saturated opioid concentrations were used for this analysis. All tested opioids induced significant phosphorylation at S375, generating the highest ELISA signals among the examined residues. Given that S375 is a primary phosphorylation site of the μOR, this likely contributes to the consistently high levels of phosphorylation observed at this residue across all opioids tested. Most opioids produced a similar response at S375, with phosphorylation levels around 150% above baseline, except for MOR, which had significantly lower phosphorylation levels at about 50% above baseline. Given that MOR shows reduced phosphorylation at this key site, it’s reasonable to think that phosphorylation at downstream residues is also diminished. This is reflected in the results for T370 and T379, where MOR showed minimal to no phosphorylation. This pattern is consistent with existing literature [258,300,464] and was successfully reproduced in the course of this work.

Interestingly, CAR induced significantly higher phosphorylation at both T370 and T379 compared to all other opioids tested, with phosphorylation levels reaching approximately 90% over basal for T370 and 100% over basal for T379. In contrast, phosphorylation levels at these residues for the other opioids, with the exception of MOR, were relatively consistent, ranging from 30-40% above baseline for T370 and 60-70% above baseline for T379.

6.7. Evaluation of antagonists and antibodies targeting carfentanil and other opioids

Numerous reports indicate that receptor antagonists often prove insufficient in cases of CAR intoxications [18,344,465]. It has been demonstrated in this study that CAR stands out among the opioids tested, exhibiting ultra-efficient cAMP signaling, which may contribute to its unique pharmacological profile. This led to an examination of how this phenomenon might influence the effectiveness of standard receptor antagonists at the cellular level. Additionally, the potential of specific antibodies as an alternative method to block the effects of FEN analogs was explored.

6.7.1. Comparison of naloxone and nalmefene potency against carfentanil and other opioids

Two clinically approved OR antagonists, NLX and NLM, widely used in the treatment of opioid intoxications, were tested for their ability to inhibit the effects of CAR, FEN, REMI, MOR and ENDO. To assess the effectiveness of these antagonists, radioactive cAMP assays were conducted to determine the IC_{50} values for each antagonist against these opioids. Opioid concentrations were adjusted to match their receptor affinity, ensuring an equal pharmacological basis for comparing the antagonists. Since the cAMP assays were carried out using DMEM as the buffer for cell stimulation, the opioid affinities were normalized based on K_i values determined with the binding assays conducted in DMEM + 50 mM HEPES (Table 6).

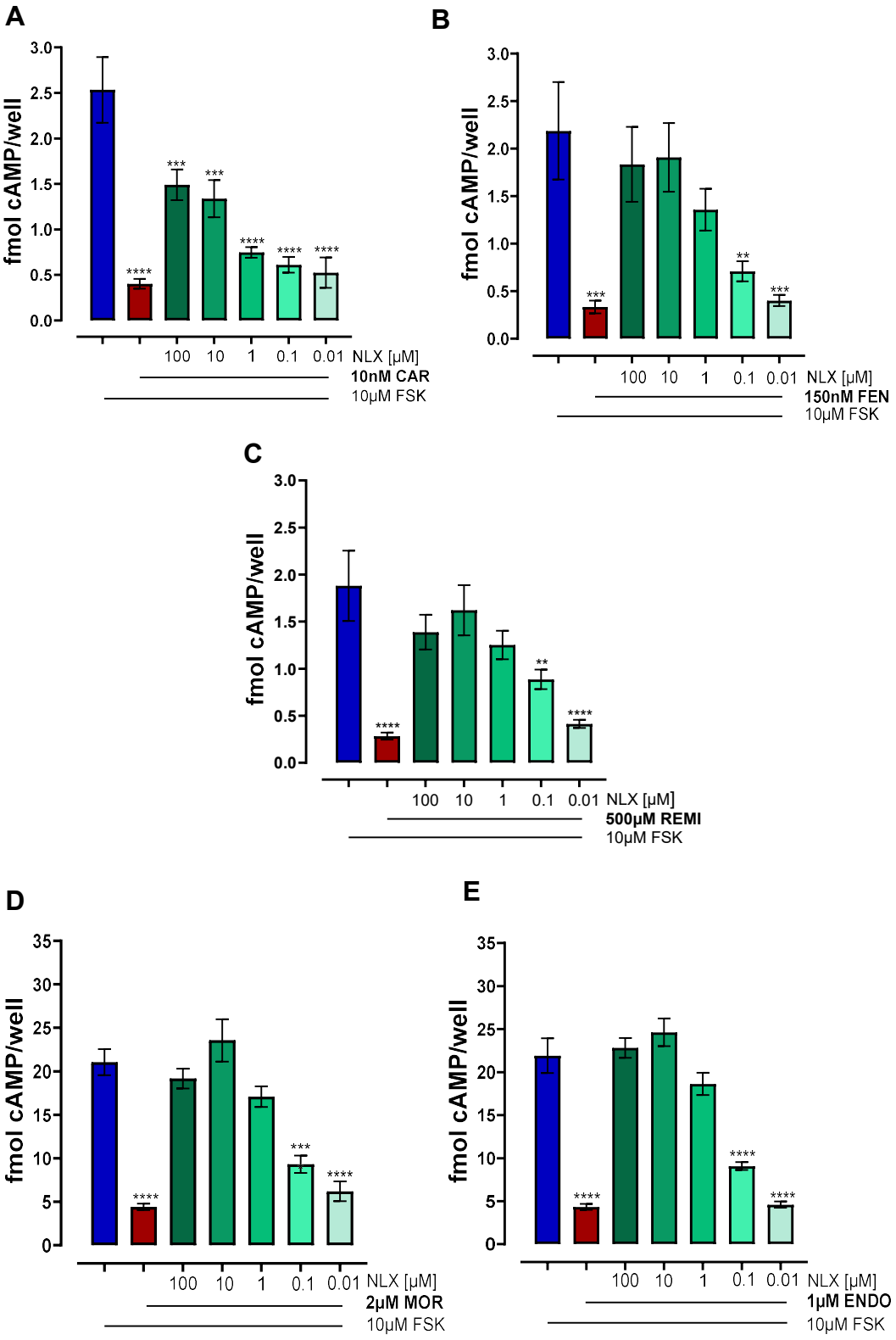

Figure 27: Neutralizing effect of NLX on opioid-induced attenuation of FSK-mediated cAMP accumulation

300,000 HEK293-µOR cells per well were labeled overnight with 1 µCi/mL [^{3}H]-adenine. The following day, cells were stimulated in triplicates at 37°C for 20 minutes with 500 µM IBMX, 50 µM FSK, the specified opioid concentrations and increasing concentrations of NLX. The radioactivity of purified cell lysates was then

measured using a liquid scintillation counter. Fmol cAMP per well were calculated from measured dpm values with Equation 4. Calculated values were adjusted by subtracting the basal signal (IBMX only). Bars represent the FSK signal (blue), the FSK signal in the presence of an opioid (red) or the FSK signal with both an opioid and the corresponding NLX concentration (green). n=4. Statistical analysis was conducted with one-way ANOVA, followed by Dunnett's multiple comparison test to determine significant differences relative to cells stimulated with FSK alone (*p<0.05, **p<0.01, ***p<0.001, ****p<0.0001).

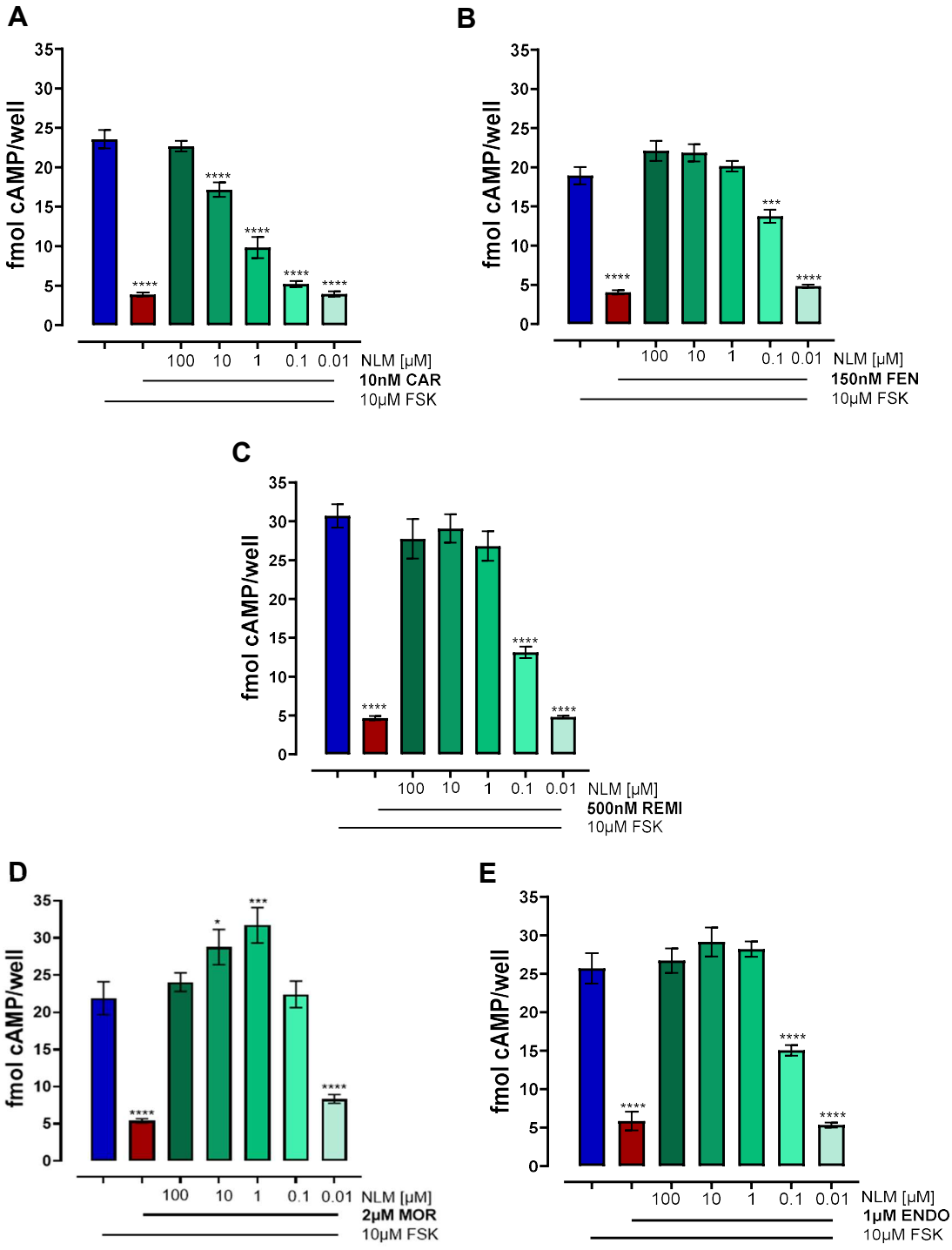

Figure 28: Neutralizing effect of NLM on opioid-induced attenuation of FSK-mediated cAMP accumulation

300,000 HEK293-μOR cells per well were labeled overnight with 1 μCi/mL [³H]-adenine. The following day, cells were stimulated in triplicates at 37°C for 20 minutes with 500 μM IBMX, 50 μM FSK, the specified opioid concentrations and increasing concentrations of NLM. The radioactivity of cell lysates was then measured using a liquid scintillation counter. Fmol cAMP per well were calculated from measured dpm values with Equation 4. Calculated values were adjusted by subtracting the basal signal (IBMX only). Bars represent the FSK signal (blue), the FSK signal in the presence of an opioid (red) or the FSK signal with both an opioid and the corresponding NLM concentration (green). n=4. Statistical analysis was conducted with one-way ANOVA, followed by Dunnett's multiple comparison test to to identify significant differences relative to cells stimulated with FSK alone (*p<0.05, **p<0.01, ***p<0.001, ****p<0.0001).

All tested opioids significantly reduced the FSK-induced signal, which correlates with a decrease in intracellular cAMP levels. The FSK inhibition consistently ranged between 80% and 85% across all opioids, which is in alignment with the observations presented in Figure 18. Both antagonists reversed the opioids' effects on cAMP in a concentration-dependent manner. While the lowest NLX concentration tested (10 nM) had no effect on FSK inhibition by any opioid, at 100 μM, NLX completely blocked the effects of all opioids, except for 10 nM CAR. This is indicated by the remaining significant difference between the highest NLX concentration and the FSK baseline (Figure 27A).

NLM exhibited similar effects to NLX; it significantly blocked opioid-induced signals. However, unlike NLX, NLM was able to fully inhibit the CAR-induced cAMP attenuation at the highest tested concentration, indicating a higher maximal antagonization of CAR. This was evident from the fact that there was no significant difference between the signal induced by 10 nM CAR in the presence of 100 μM NLM and the baseline FSK signal. At higher concentrations (10 and 1 μM), NLM unexpectedly seemed to increase cAMP levels in cells stimulated with MOR. This effect may reflect an enhancement of FSK or AC activity specifically within the context of MOR signaling, as no similar response was observed with other opioids. This effect is intriguing but remains unclarified within the scope of this study.

To provide a more quantitative comparison of the effectiveness of both antagonists against the opioids, their IC_{50} values were determined.

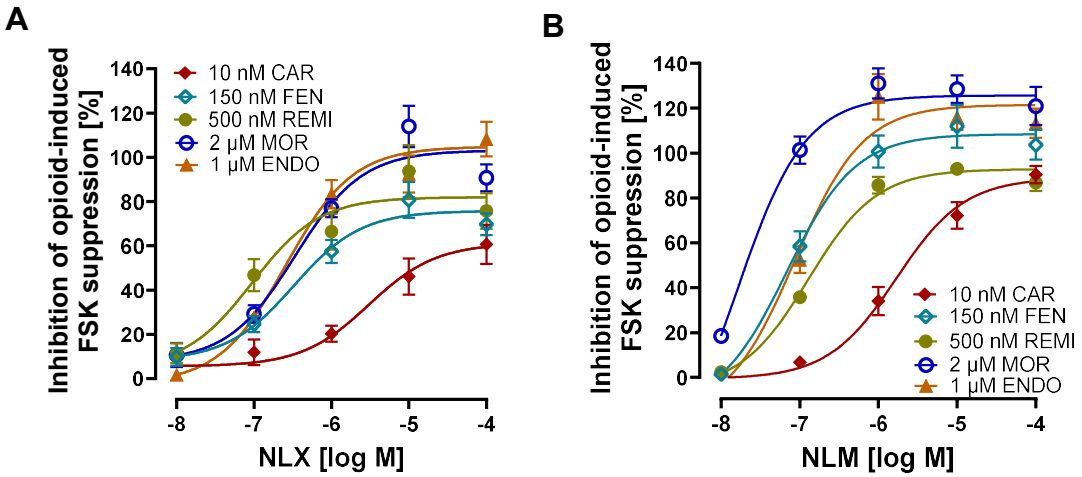

Figure 29: Inhibitory potencies of NLX and NLM against opioid concentrations of equal affinity

See Figure 27 and Figure 28 for details on experimental procedure. Measured dpm values were baseline-corrected by subtracting the signal from IBMX alone. The difference between the FSK and opioid signals was defined as 100% and differences between the antagonist and opioid signals were then normalized relative to this value. The resulting values represent the percentage inhibition of the opioid-induced suppression of FSK, which were plotted as mean ± SEM against logarithmic concentrations of the antagonist.

	NLX		NLM	
	EC_{50} [nM]	Max. inhibition [%]	EC_{50} [nM]	Max. inhibition [%]
CAR	4664 ± 1668	64.3 ± 14.4	3840 ± 1982	95.3 ± 4.84
FEN	459 ± 244 ***	73.9 ± 5.74	83.8 ± 14.9*	112 ± 12.3
REMI	149 ± 78.1 ***	80.5 ± 14.1	135 ± 28.2*	91.7 ± 2.89
MOR	330 ± 61.2 ****	103 ± 10.2	33.9 ± 13.1*	145 ± 9.80**
END	388 ± 57.7 ****	119 ± 15.4*	101 ± 15.8*	125 ± 11.1

Table 14: IC_{50} values and maximal inhibtion of NLX and NLM against opioid concentrations of equal affinity

IC_{50} values were determined from data in Figure 29 using GraphPad Prism 10.3.1 (Non-linear regression log (agonist) vs. response (three parameters)). Maximal inhibition was calculated as the difference between top and bottom of curves. Values represent the mean ± SEM of individual experiments. Statistical analysis was conducted using a one-way ANOVA followed by Dunnett's multiple comparison test to evaluate differences in the performance of NLX and NLM, specifically their IC_{50} values and maximal inhibition, when tested against CAR compared to other

opioids. Asterisks indicate significant differences compared to CAR: *p<0.05, **p<0.01, ***p<0.001, ****p<0.0001.

While the IC_{50} value reflects the antagonist's potency against each opioid, the maximal inhibition describes the highest level of antagonism achievable at increased antagonist concentrations. The observed sigmoidal curves align with the results in the column diagrams, indicating consistent trends. NLX generally demonstrated lower maximal inhibition against FEN derivatives compared to MOR and ENDO, though this difference was statistically significant only for ENDO. Notably, NLX´s maximal antagonism observed for CAR was was lower than its capacity against the other opioids, reaching only 64%.

NLM showed high maximal inhibition of MOR and ENDO, though this may have been influenced by its low-concentration effect of increasing cAMP signals, as described earlier. Nevertheless, at its highest concentration, NLM fully inhibited all opioids, including CAR, achieving nearly 100% efficacy.

Since opioid concentrations were normalized to their affinity - assuming 50% receptor occupancy in each setup - similar antagonist performance would have been expected across opioids, as the competitive environment for receptor binding was standardized. For NLX, this expectation held true for FEN, MOR and ENDO, where IC_{50} values ranged from 330 to 460 nM. Although NLX showed a slightly lower IC_{50} value of 150 nM for REMI, it still fell within a comparable range. In contrast, NLX exhibited a substantially lower potency against CAR, with an IC_{50} value of over 4.5 µM, indicating not only reduced maximal inhibition but also markedly lower potency against CAR. The difference in NLX potency between MOR and CAR was approximately 14-fold.

A similar trend was observed with NLM. NLM's IC_{50} values were somewhat lower (34-135 nM) than those of NLX, suggesting a slightly better overall performance. However, NLM also displayed significantly lower potency against CAR than against the other opioids, with an IC_{50} value nearing 4 µM. The difference in potency against MOR and CAR was even more pronounced with NLM, exceeding 110-fold, highlighting that while NLM was generally more potent against all tested opioids, its relative potency against CAR was even lower than that of NLX.

These findings align with CAR's high potency and highlight that NLX, in particular, struggles to counter CAR-induced cAMP reduction. Specifically, NLX appeared to have a reduced maximal capacity in antagonizing CAR compared to the other opioids tested. Although NLM proved more effective than NLX, it also showed significantly reduced potency against CAR when compared to the other opioids.

6.7.2. Screening of neutralizing antibody effects on μOR binding of carfentanil and other opioids

The findings of present study indicate that once CAR binds to the μOR, it is highly effective in activating certain signaling pathways. Furthermore, they suggest that using OR antagonists to block CAR's binding to the μOR may not be the most effective strategy. An alternative approach could involve neutralizing CAR directly with specific antibodies before it interacts with the receptor. The following section explores antibodies originally developed against FEN, examining their effects on μOR binding by both FEN and CAR, as well as their cross-reactivity with [^{3}H]-NLX, REMI, MOR and ENDO by performing competitive ligand binding assays.

In earlier experiments, binding assays were used to assess the affinity and binding behavior of μOR ligands by directly measuring the displacement of the tracer [^{3}H]-NLX. To indirectly evaluate the neutralizing effect of antibodies on opioid-receptor binding, it was examined whether μOR agonists could still displace the tracer in the presence of these antibodies. Since this experimental approach was, according to current knowledge, entirely novel, it was approached gradually, with each component being tested carefully to validate the methodology.

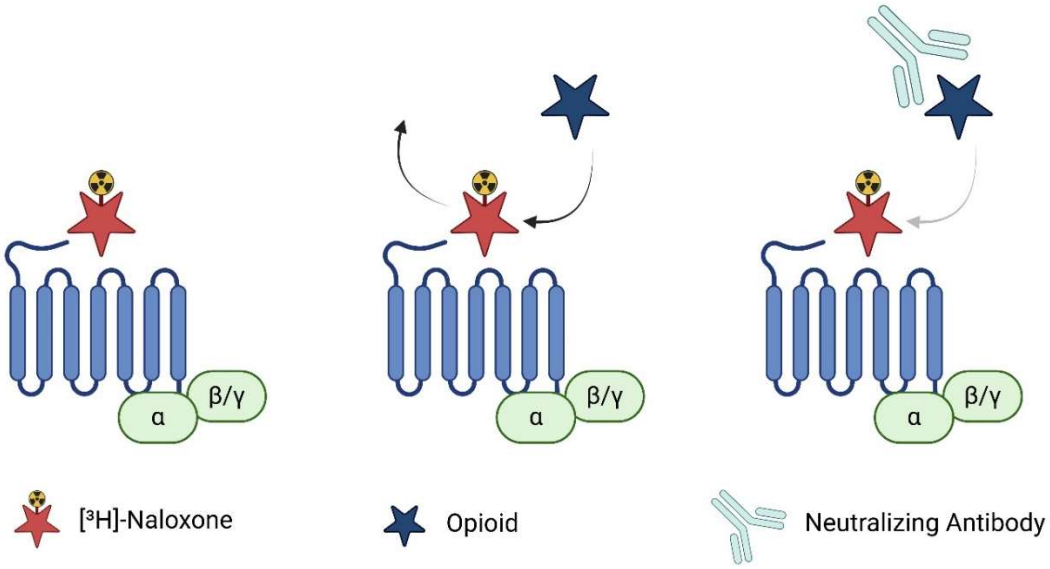

Figure 30: Principle of ligand binding assay for investigating neutralizing antibody effects on opioids´ receptor binding

The radiolabeled tracer [³H]-NLX binds to μORs expressed in HEK293-μOR cell membranes and total tracer binding is measured by radioactivity. In the presence of an opioid that can bind to the receptor, the tracer is displaced, resulting in decreased radioactivity. If an antibody neutralizes the opioid and prevents its receptor binding, more tracer remains bound, leading to an increase in measured radioactivity.

6.7.2.1. Antibodies´ effect on [³H]-naloxone binding

Initially, the effect of 500 nM antibody (listed in 4.6) on [³H]-NLX binding alone was assessed, to rule out any potential interference from the antibodies on the tracer itself, ensuring accurate interpretation in subsequent experiments.

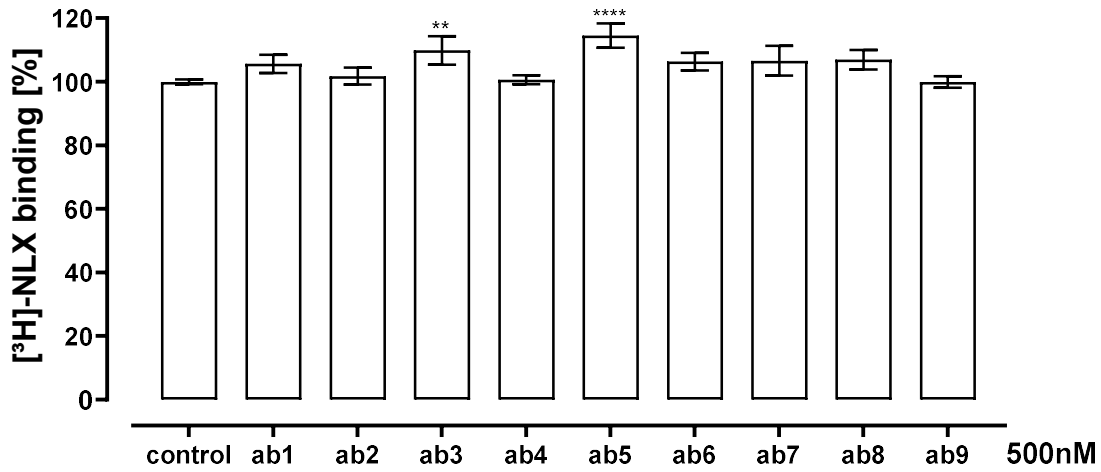

Figure 31: Antibodies´ effect on [³H]-NLX binding

20 µg HEK293-µOR membrane preparation was incubated in triplicates with 5 nM [³H]-NLX, either alone or in combination with 500 nM of the indicated antibodies, diluted in 50 mM TRIS-HCl (pH 7.4) for 30 minutes at 37°C. Radioactive decay of filter patches was measured and the resulting dpm values were normalized to the percentage of the control condition ([³H]-NLX alone). Results of three individual experiments are presented as mean ± SEM of percentage tracer binding. Statistical analysis was performed using one-way ANOVA followed by Dunnett's multiple comparison test to determine significant differences between antibody-stimulated membranes and control (**p<0.01, ****p<0.0001).

With the exception of antibodies ab3 and ab5, none of the tested antibodies significantly influenced [³H]-NLX binding to the receptor, underscoring their specificity in distinguishing between agonists and antagonists. Ab3 and ab5 however, significantly increased measured radioactivity by approximately 10-15%. This increase might suggest an enhancing effect on tracer binding, which should be considered when interpreting later results, as it may lead to an overestimation of ab3 and ab5's performance against opioids. Though the real cause of this effect remains unclear and was not further investigated in this study. Importantly, however, none of the antibodies - including ab3 and ab5 - displaced the tracer from the receptor. Such displacement would have prevented the evaluation of the opioid effect and, by extension, the antibodies' influence on the opioid effect, thereby complicating the interpretation of subsequent experiments.

6.7.2.2. Antibodies´ effect on fentanyl receptor binding

All nine antibodies investigated in this study were originally generated against FEN, primarily for laboratory applications such as ELISA experiments. To date, these antibodies have not been tested for their ability to bind FEN in a biological system, nor have they been evaluated in the context of µORs. To assess the suitability of the ligand-binding assay for evaluating the neutralizing effects of these antibodies on opioids, the following section explored their neutralizing potential on FEN binding at the receptor level.

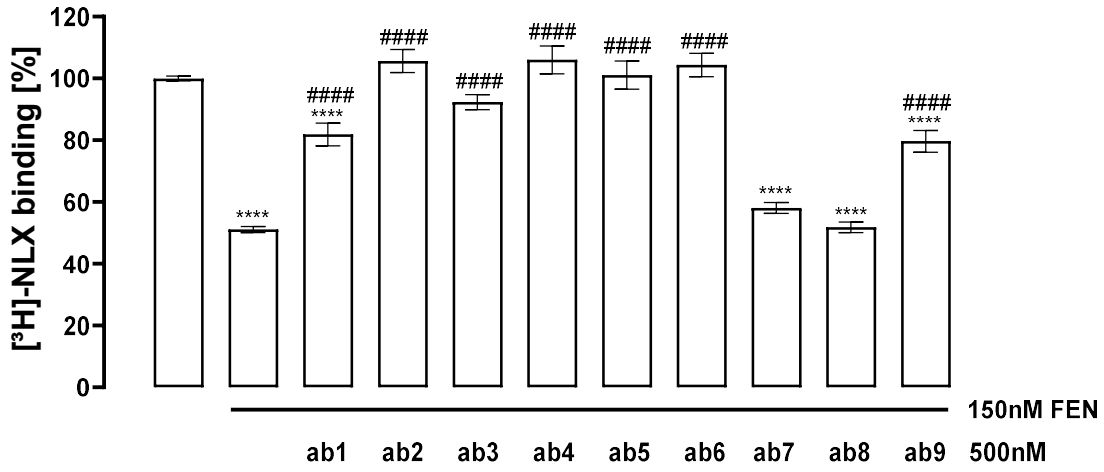

Figure 32: Antibodies´ effect on FEN binding

20 µg HEK293-µOR membrane preparation was incubated in triplicates with 5 nM [³H]-NLX either alone, in combination with 150 nM FEN, or with 150 nM FEN and 500 nM of the indicated antibodies for 30 minutes at 37°C. All dilutions were made in 50 mM Tris-HCl (pH 7.4). Radioactive decay was measured and the resulting dpm values were normalized to the percentage of the control condition ([³H]-NLX alone). Data from 3-5 independent experiments are presented as mean ± SEM. Statistical analysis was performed using one-way ANOVA followed by Dunnett's multiple comparison test. Asterisks indicate significant differences between FEN and antibody-stimulated membranes compared to the control (****p<0.0001), while diamond symbols indicate significant differences between antibody-stimulated membranes and FEN stimulation alone (####p<0.0001).

As expected, FEN significantly reduced tracer binding by approximately 50%, creating a suitable measure for evaluating the subsequent effects of the antibodies. This result aligns with the displacement observed in the competitive binding curves, which were used to assess FEN's binding affinity in TRIS-buffer (Figure 16D). Of the nine anti-FEN antibodies tested, seven demonstrated functionality in this assay. At a concentration of 500 nM, these antibodies effectively inhibited FEN-induced tracer displacement, with ab2, ab4, ab5, and ab6 achieving complete inhibition (100%) and restoring the control signal (see also Table 15). In contrast, ab1 and ab9 were unable to fully inhibit FEN, as indicated by a remaining significant difference compared to the control value of [³H]-NLX alone. Antibodies ab7 and ab8, however, did not affect FEN-induced [³H]-NLX displacement at all, as shown by the absense of a significant difference from the FEN signal alone, suggesting they were not functional against FEN within the tested concentration range in this assay.

6.7.2.3. Antibodies´ effect on carfentanil receptor binding

In this chapter it was evaluated, whether anti-FEN antibodies could also inhibit CAR-μOR binding by assessing their ability to neutralize CAR's [³H]-NLX displacement.

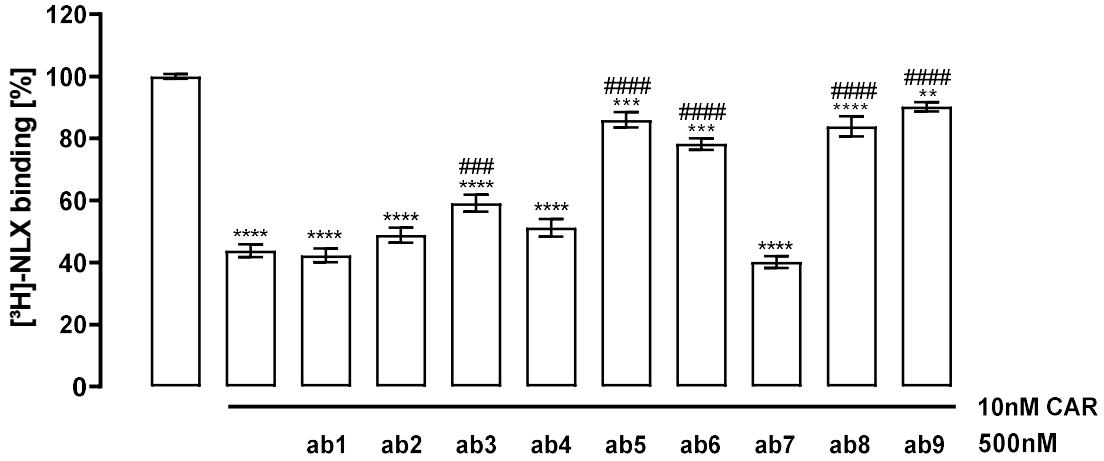

Figure 33: Antibodies´ effect on CAR binding

20 μg membrane preparation of HEK293-μOR cells was incubated in triplicates with 5 nM [³H]-NLX, either alone, combined with 10 nM CAR, or with 10 nM CAR and 500 nM of the specified antibodies for 30 minutes at 37°C. Further procedure was as outlined in Figure 32. Data from 3-5 independent experiments are presented as mean ± SEM of percentage tracer binding. Statistical analysis was performed using one-way ANOVA followed by Dunnett's multiple comparison test. Asterisks label significant differences between CAR and antibody-stimulated membranes compared to the control (***p<0.001, ****p<0.0001), while diamond symbols indicate significant differences between antibody-stimulated membranes and FEN alone (###p<0.001, ####p<0.0001).

At a concentration of 10 nM, CAR displaced the tracer by approximately 60%, which was consistent with the results observed in the competitive binding curves used for affinity assessment (Figure 16C). Besides FEN, antibodies ab3, ab5, and ab6 also inhibited CAR's [³H]-NLX displacement, demonstrating notable impacts on its receptor binding. While ab3 exhibited a modest inhibitory efficacy of around 20%, the other functional antibodies showed stronger effects, with efficacies between 50% and 80% (Table 15). Notably, ab3 and ab5 were shown to increase tracer binding (Figure 31), potentially leading to a slight overestimation of their inhibitory effect. Although ab8 did not affect FEN-receptor binding, it significantly inhibited CAR's effects, suggesting that it is CAR-specific in this assay, despite being initially developed against FEN.

6.7.2.4. Antibodies´ crossreactivity towards remifentanil, morphine and endomorphin-1 receptor binding

To assess the specificity of the antibodies in neutralizing opioid-receptor interactions - particularly concerning FEN and CAR - their effects on other opioid groups, including natural, endogenous and further FEN-like opioids, were also examined. For this reason, the antibodies were tested against REMI, MOR and ENDO. Since antibody ab7 did not show significant effects on FEN or CAR and was therefore deemed irrelevant to this study, it was excluded from further analysis.

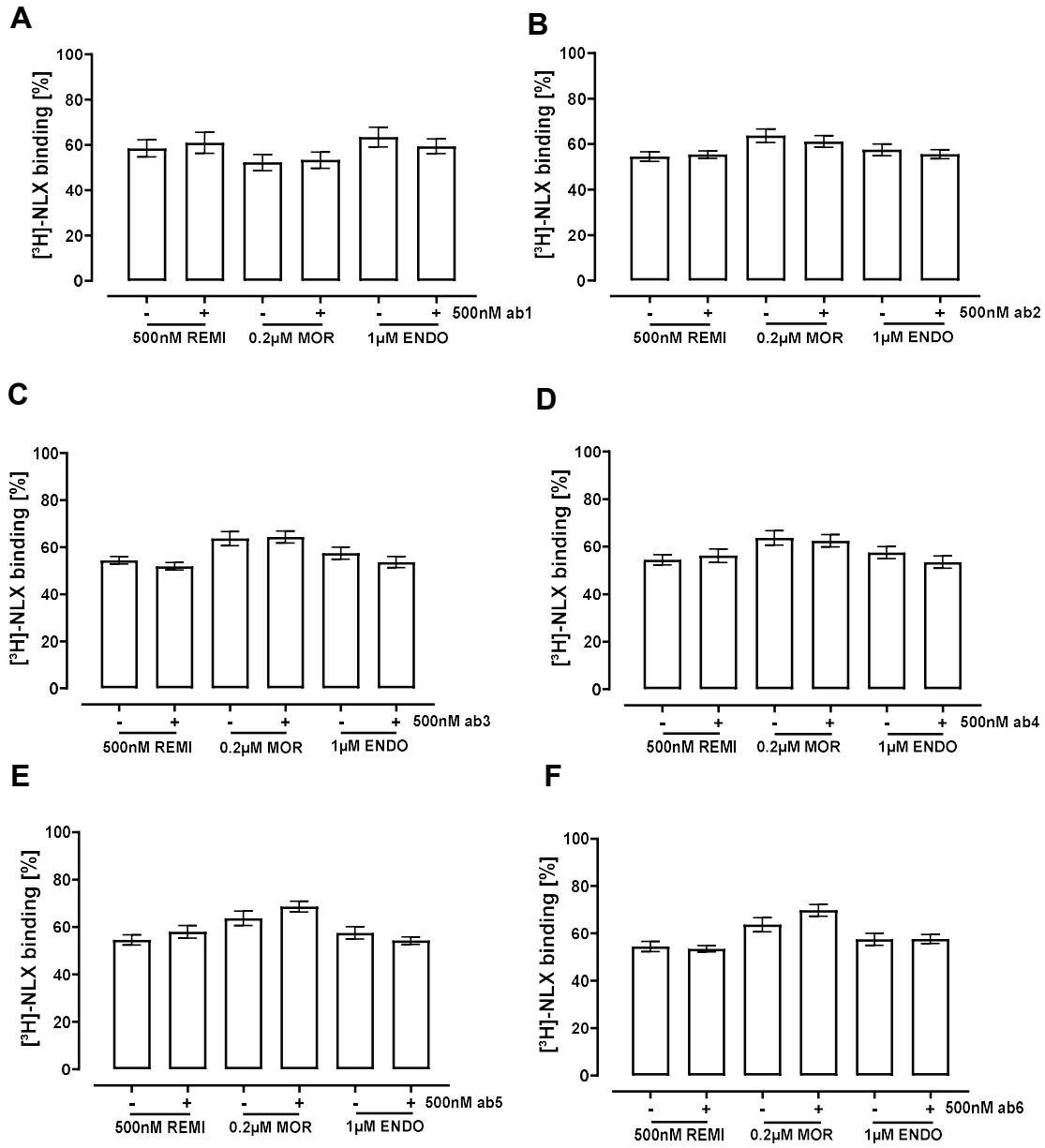

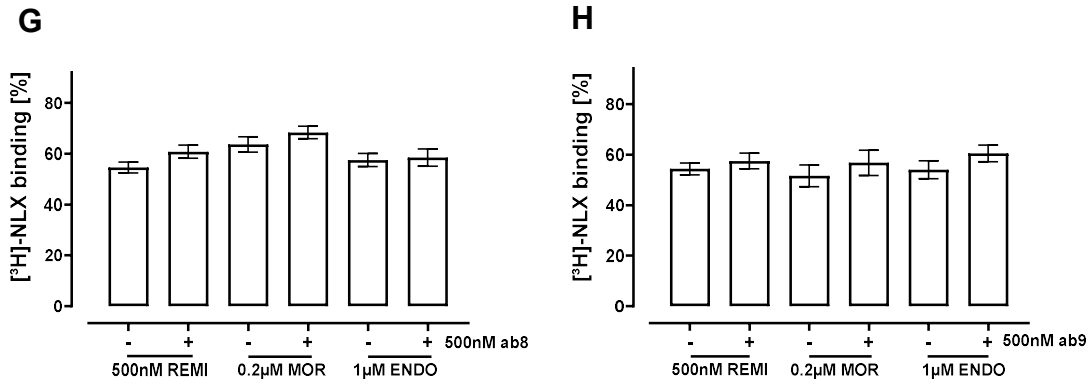

Figure 34: Antibodies´ effect on REMI, MOR and ENDO binding

20 µg membrane preparation of HEK293-µOR was incubated in triplicates with 5 nM [³H]-NLX, either alone, combined with the respective opioid concentration, or with the indicated opioid concentration and 500 nM of the specified antibodies for 30 minutes at 37°C. All dilutions were made in 50 mM TRIS-HCl (pH 7.4). Radioactive decay was measured and the resulting dpm values were normalized to the percentage of the control condition ([³H]-NLX alone). Data from 3-4 independent experiments are presented as mean ± SEM of percentage tracer binding. Statistical analysis was performed using one-way ANOVA followed by Dunnett's multiple comparison test to assess significant antibody effects on opioid tracer displacement. No significant antibody effects were observed.

REMI at 500 nM displaced [³H]-NLX by approximately 40-50%, aligning with previous competitive binding data observed in this study (Figure 12E). Similarly, 0.2 µM MOR displaced the tracer by 35-50%, which also corresponded well with prior results (Figure 16F). At 1 µM, ENDO produced a slightly lower displacement of 40-50%, compared to the expected 70% based on earlier data (Figure 16G). Although the reason for this variation remains unclear, it was not significant for this experiment, as the primary goal was to compare [³H]-NLX displacement of opioids in the presence or absence of antibodies. For this purpose, the reduced displacement by ENDO posed no issue. None of the antibodies significantly affected REMI, MOR or ENDO-induced tracer displacement, suggesting they do not interfere with these opioids´ receptor binding within the tested concentration range.

To quantify the effects of the antibodies, their maximal inhibitions at 500 nM against each opioid are summarized in the table below.

	150 nM FEN	10 nM CAR	500 nM REMI	200 nM MOR	2 µM ENDO
ab1	60.2 ± 7.91	0.49 ± 2.10	6.98 ± 9.09	4.91 ± 3.04	-14.7 ± 4.98
ab2	112.0 ± 7.71	-9.67 ± 5.41	1.10 ± 4.11	-8.19 ± 3.83	-4.86 ± 2.54
ab3	84.1 ± 5.17	8.66 ± 9.92	-6.29 ± 4.51	0.75 ± 4.46	-9.94 ± 5.12
ab4	111.2 ± 8.72	-4.77 ± 6.41	3.06 ± 5.95	-4.33 ± 4.74	9.79 ± 4.80
ab5	101.4 ± 9.45	70.3 ± 5.91	8.01 ± 3.53	11.9 ± 5.26	-8.86 ± 4.58
ab6	108.3 ± 7.68	53.5 ± 4.43	-3.07 ± 3.31	16.3 ± 3.90	-0.06 ± 2.47
ab7	16.2 ± 3.80	5.06 ± 2.31	-	-	-
ab8	3.00 ± 5.04	66.4 ± 6.03	13.9 ± 4.52	12.2 ± 3.95	2.78 ± 4.63
ab9	55.3 ± 7.38	82.8 ± 2.80	13.8 ± 8.82	9.27 ± 9.87	13.6 ± 5.41

Table 15: Maximal inhibition of µOR binding by 500 nM antibodies [%]

This table shows the maximal inhibition of each antibody at a concentration of 500 nM in blocking opioid-induced [³H]-NLX displacement. The tracer displacement observed without antibodies was normalized to 100% and the antibody effects are reported as percent inhibition of this baseline. Values are presented as mean ± SEM, calculated from data shown in Figure 32, Figure 33 and Figure 34. Antibodies that significantly reduced opioid-induced [³H]-NLX displacement are highlighted in green.

While four antibodies (ab2, ab4, ab5 and ab6) achieved complete inhibition of FEN-receptor binding, none of the tested antibodies fully blocked CAR-receptor interaction. However, five out of the nine antibodies did show significant neutralization of CAR's binding to the µOR, including ab8, which appeared to be CAR-specific in this assay.

6.7.3. Assessment of selected antibodies for neutralization of receptor activation by carfentanil and fentanyl

To determine whether the antibodies could inhibit not only FEN- and CAR-induced µOR binding but also µOR activation, additional cAMP accumulation assays were conducted. For this purpose, an alternative method to the traditional radioactive cAMP assay - the AlphaScreen assay - was established and optimized over the course of this study.

6.7.3.1. Establishment of an alternative cAMP accumulation assay – AlphaScreen

Initially, a cAMP standard curve was created, as recommended by the manufacturer, to determine the assay's sensitivity (IC_{50} value) and to enable extrapolation of the absolute amount of cAMP produced by the cells. However, the focus of this study was not on absolute cAMP concentration values. Instead, the primary objective was to investigate the opioid-induced reduction in cAMP levels, with a secondary goal of inhibiting this reduction using antibodies. Therefore, the standard curve was used primarily to assess assay functionality and sensitivity and to monitor relative changes in cAMP under the specified assay conditions. The following graphs illustrate both the raw and normalized data.

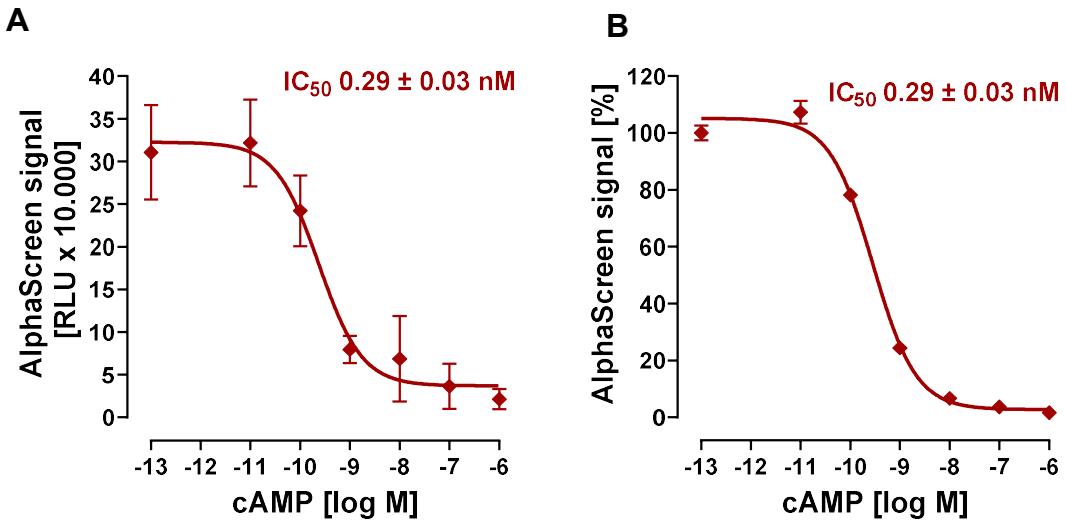

Figure 35: cAMP standard curve determined using AlphaScreen

Dilutions of cAMP standard were prepared in assay buffer in triplicates and AlphaScreen was performed as described in 5.5.2. n=3 **A:** Random light units (RLU) were plotted against logarithmic cAMP concentrations. **B:** Highest AlphaScreen signal was set to 100% and other values were normalized to this control. Values represent the mean ± SEM from individual experiments. IC_{50} values were specified using GraphPad Prism 10.3.1 (Non-linear regression log (inhibitor) vs. response (three parameters)).

As expected for a competitive immunoassay, the AlphaScreen cAMP standard curve displayed a sigmoidal relationship between the log-transformed cAMP concentrations and the AlphaScreen signal. IC_{50} values around 0.3 nM were observed, approximately tenfold lower than those reported in the manufacturer's manual, suggesting that specific assay parameters used herein (including bead and tracer dilutions, as well as measurement settings) resulted in enhanced

sensitivity. Importantly, normalization of the data had no impact on the calculated IC_{50} value (Figure 35B), ensuring that data processing did not alter the true values or artificially influence assay sensitivity.

The assay was validated and familiarity with the newly implemented AlphaScreen technology was established by determining the EC_{50} value of FSK. This served not only to confirm that FSK effectively elevates cAMP levels, as expected, but also to provide insights into optimal assay conditions.

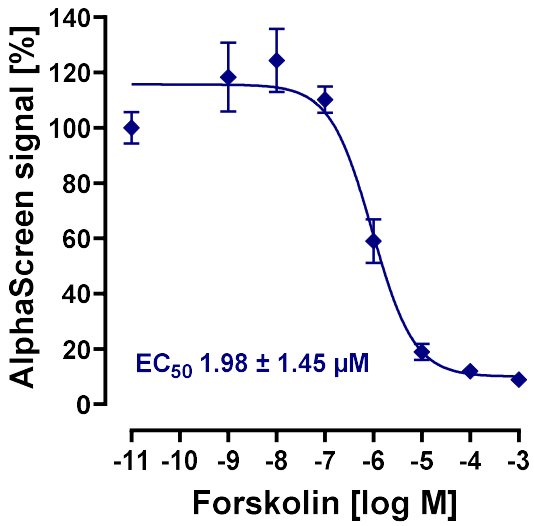

Figure 36: Potency of FSK determined using AlphaScreen

20,000 HEK293-µOR cells per well were stimulated in triplicates with either 500 µM IBMX alone (basal signal) or in combination with specified FSK concentrations for 20 minutes at 37°C. The AlphaScreen assay was performed as described in 5.5.2. Measured RLU values were normalized to baseline (IBMX alone, plotted here as log M -11) and are presented as mean ± SEM from three independent experiments, expressed as a percentage of the AlphaScreen signal. The EC_{50} was calculated using GraphPad Prism 10.3.1 (Non-linear regression, log (agonist) vs. response with three parameters).

FSK induced a concentration-dependent increase in cAMP levels, displaying a characteristic sigmoidal dose-response curve consistent with its role as an AC activator. As FSK concentrations increased, cAMP production correspondingly rose and consequently, AlphaScreen signal descreased. However, the AlphaScreen signal eventually reached a plateau, likely due to assay limitations, as the finite amount of beads and tracer in the system restricts the detection of further increases in cAMP levels.

The EC_{50} value of approximately 2 µM for FSK observed in this assay aligns perfectly with the values specified in the manufacturer's application note for this assay [466]. Understanding FSK's potency was essential for selecting an optimal concentration for subsequent opioid and antibody testing. Excessively high concentrations of FSK could lead to elevated cAMP levels that overshadow the effects of opioid-induced attenuation, making it difficult to detect subtle changes in cAMP. By establishing the EC_{50} value, a FSK concentration within the assay's dynamic range could be selected, which enabeled the effective detection of opioid-mediated reductions in cAMP. For subsequent assays, 1 µM FSK was selected as the optimal concentration.

To ensure consistency and comparability between different assay formats, the EC_{50} values of the tested opioids were also determined using the AlphaScreen method, in addition to the radiometric cAMP accumulation assay. This approach allowed for direct comparison of potency and intrinsic activity across platforms.

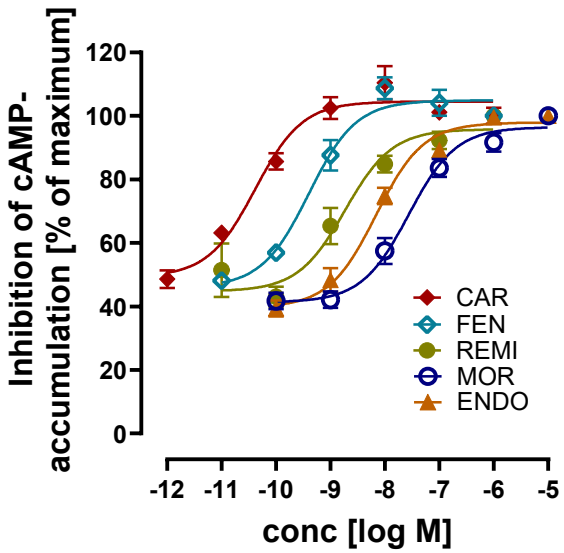

Figure 37: Potencies of µOR agonists to attenuate FSK-induced cAMP accumulation determined using AlphaScreen

20,000 HEK293-µOR cells per well were stimulated in triplicates with either 500 µM IBMX alone (baseline signal), 1 µM FSK or 1 µM FSK together with varying concentrations of opioids, resulting in the specified final concentrations for 20 minutes at 37°C. The AlphaScreen assay was performed as described in section 5.5.2. Measured RLU values were baseline-corrected (IBMX alone). The difference between the baseline signal (IBMX alone) and the FSK-stimulated signal was taken as control. Opioid effects were normalized to the maximal FSK signal reduction induced by opioids, with the reduction at the highest opioid concentration set to

100%. Data are presented as mean ± SEM from three independent experiments plotted against logarithmic opioid concentrations.

	AlphaScreen		Radiometric assay	
	EC_{50} [nM]	E_{max} [%]	EC_{50} [nM]	E_{max} [%]
CAR	0.066 ± 0.033	50.3 ± 3.81	0.016 ± 0.001	80.7 ± 3.29
FEN	0.53 ± 0.19 *	55.1 ± 2.90	1.70 ± 0.23	90.1 ± 1.25
REMI	1.73 ± 0.59	58.2 ± 7.17	1.94 ± 0.33	86.1 ± 0.94
MOR	29.2 ± 8.72	59.0 ± 4.57	9.93 ± 1.24	72.0 ± 3.09
ENDO	6.55 ± 1.19	60.7 ± 5.13	4.17 ± 0.48	77.1 ± 2.09

Table 16: Summary of EC_{50} values and intrinsic activities of opioids determined in different cAMP assays

EC_{50} values and intrinsic activities (E_{max}) were calculated based on the data presented in Figure 37, representing the ability of μOR agonists to attenuate FSK-induced cAMP accumulation. EC_{50} and E_{max} values were determined with GraphPad Prism 10.3.1 (Non-linear regression, log (agonist) vs. response (three parameters)). Results are shown as the mean of three independent experiments. For comparison, results from radiometric cAMP assays (Table 8) were also included. Statistical analysis was performed using an unpaired t-test to evaluate significant differences between the EC_{50} values obtained from the two methods (*$p < 0.05$). Unpaired t-tests were performed to evaluate significant differences between opioids´ E_{max} values determined in AlphaScreen (no significant differences).

Opioids inhibited FSK-induced cAMP accumulation in a concentration-dependent manner, as expected. By including the lowest FSK inhibition observed at minimal opioid concentrations, the E_{max} of each opioid (the difference between maximal and minimal cAMP attenuation) could be assessed. The calculated E_{max} values, presented in Table 16, ranged from 50% to 60% and showed no significant differences between the opioids, consistent with observations from the radiometric assay. Interestingly, these values were markedly lower than those determined in the radiometric cAMP assay and their rankings differed as well. For instance, while MOR and ENDO exhibited the lowest E_{max} in the radioactive assay, they showed the highest in the AlphaScreen. It is important to note that several methodological parameters differed between the assays, including assay sensitivity, FSK concentration, cell count, assay volume and lysis buffer

composition. Additionally, in the AlphaScreen assay, the amount of tracer (biotinylated cAMP) plays a crucial role, as it influences the potency and intrinsic activity of the tested opioids. These differences likely contribute to the observed discrepancies and complicate direct comparisons between the methods.

Nonetheless, a reliable measure for comparing the relative performance of opioids within a single signaling pathway is their potency. EC_{50} values of the opioids (shown in Table 16) were in the subnanomolar to nanomolar range, with FEN analogs showing higher potencies compared to MOR and ENDO, while CAR exhibited the highest potency. This potency ranking was consistent with the radioactive cAMP measurements. The EC_{50} values were very similar between the two methods, with no significant differences observed, except for FEN. However, the observed difference, while measurable, was minimal in terms of significance. It's important to note that in the AlphaScreen assay, 1 µM FSK was used, while the radiometric assay used a 10 µM FSK concentration. Despite this 10-fold difference in FSK concentration, as long as it remains within the dynamic range of the method, it should not significantly impact the opioid's ability to inhibit FSK-stimulated cAMP accumulation. This was confirmed in the course of this study, highlighting the importance of considering FSK's potency. Although the FSK concentration was higher in the radiometric assay, its potency was not specifically examined in this study. However, based on the findings, it is likely within the dynamic range of the assay.

In conclusion, while there were differences in the absolute efficiency and in the comparison of opioid effects between the two methods, the similar potency values for the opioids make the AlphaScreen and the radiometric assays highly comparable. The AlphaScreen assay, in addition to being safer - since it doesn't involve radioactivity - offers the advantages of using a tenfold lower reaction volume, which also reduces reagent consumption tenfold. Furthermore, with the use of 96-well plates, it allows for higher throughput in experiments. Given these advantages, the AlphaScreen assay is also well-suited for investigating antibodies targeting opioids, specifically in terms of their neutralizing effect on opioid-induced µOR activation, even though opioid antagonists were initially tested using the radiometric assay.

6.7.3.2. Determination of antibody IC_{50} values for neutralization of fentanyl and carfentanil

Anti-FEN antibodies were previously tested in the binding assay to evaluate their ability to neutralize FEN and CAR receptor binding. Based on these results, a selection was made for further testing of their neutralizing effect on opioid-induced receptor activation. Antibodies ab2 and ab4 were selected as highly efficient FEN-specific antibodies. Antibodies ab5, ab6 and ab9 were chosen for their ability to inhibit both FEN and CAR receptor binding and ab8 was selected for its specificity towards CAR. These selected antibodies were tested at ascending concentrations against 15 nM FEN and 1 nM CAR in the AlphaScreen. Below are column diagrams that present the raw data and illustrate the underlying principle of the assay setup.

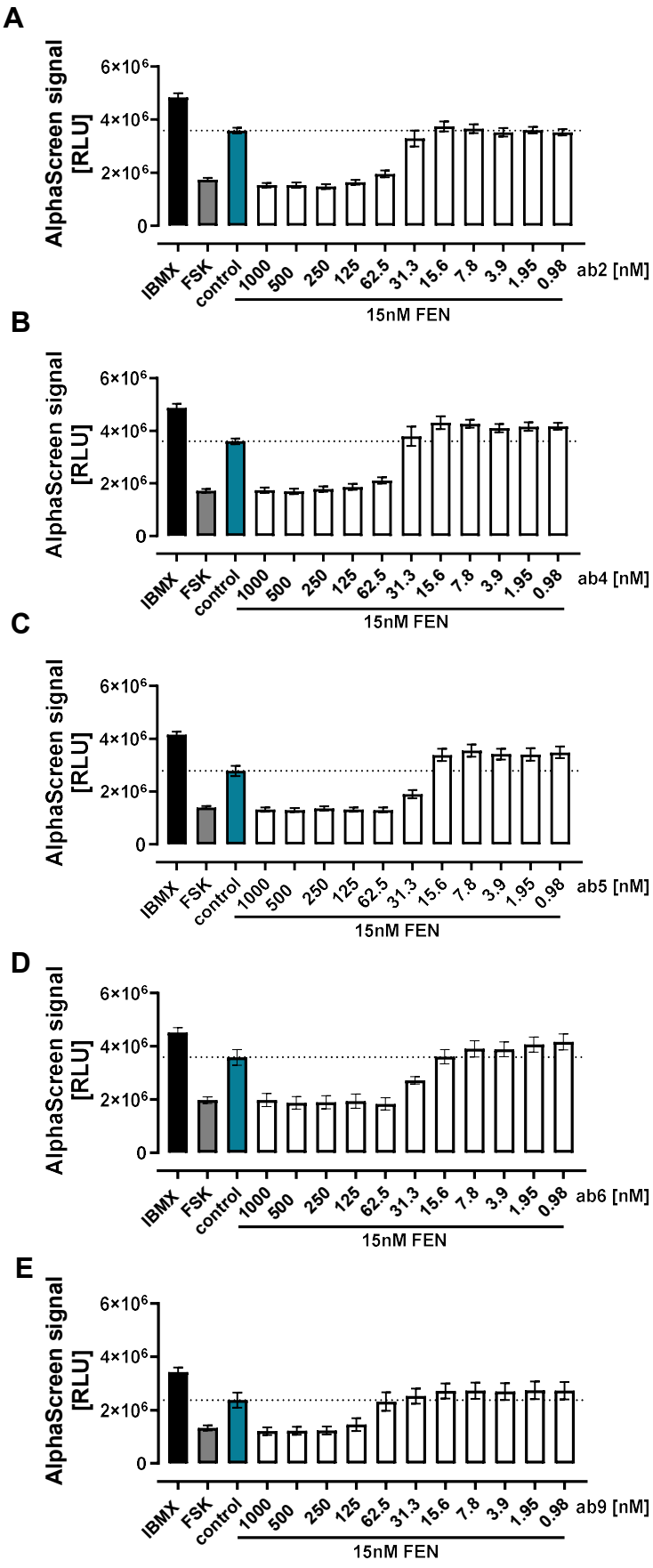

Figure 38: Inhibition of FEN-induced cAMP attenuation through Anti-FEN antibodies

20,000 HEK293-μOR cells were stimulated in triplicates with one of the following conditions to result in final concentrations: 500 μM IBMX alone (baseline signal), 1 μM FSK alone or together with 15 nM FEN or with 15 nM FEN combined with antibody dilutions at the specified final concentrations (**A**: ab2, **B**: ab4, **C**: ab5, **D**: ab6, **E**: ab7). The antibodies were pre-incubated with the other stimulants for 30 minutes at 37°C to allow for binding equilibrium before being added to the cells. The AlphaScreen assay was performed as described in section 5.5.2. Measured random light units (RLU) are plotted as the mean ± SEM of five individual experiments.

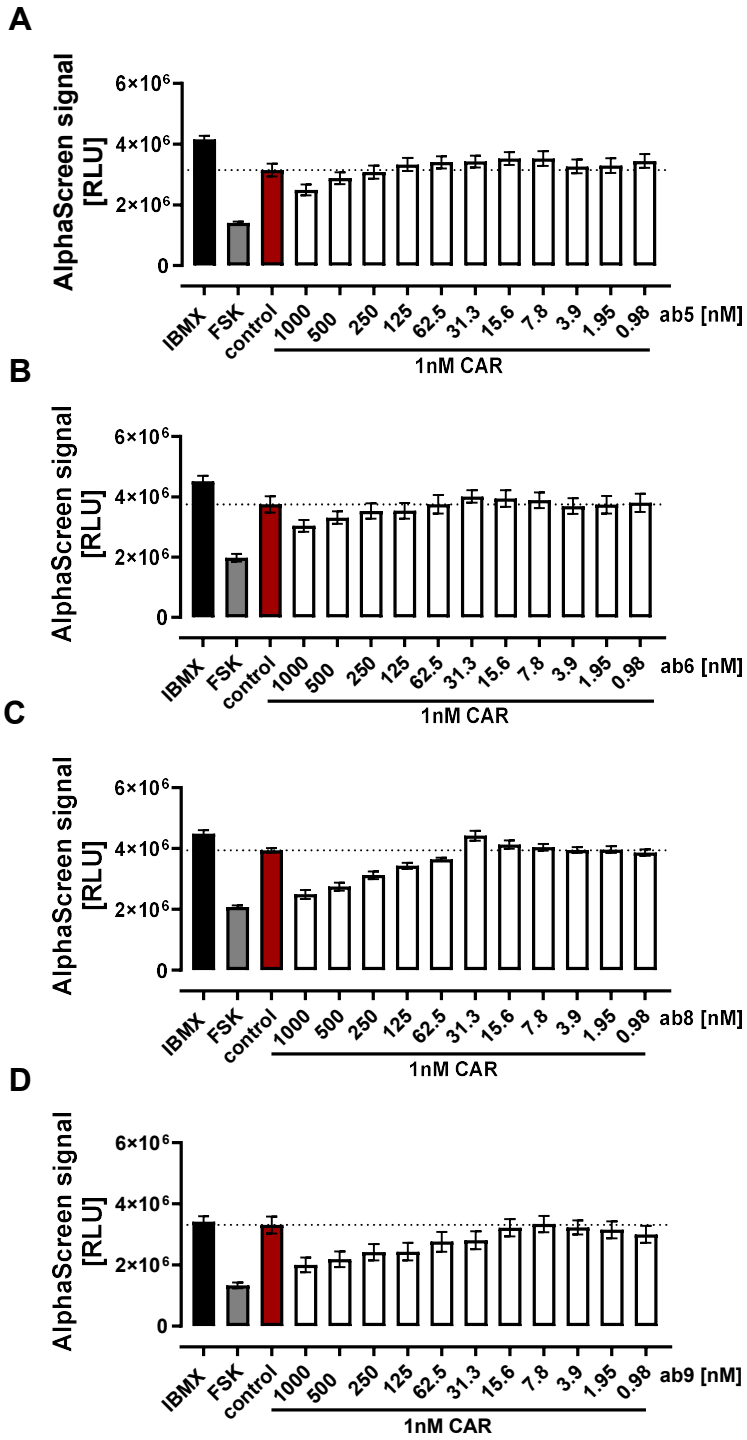

Figure 39: Inhibition of CAR-induced cAMP attenuation through Anti-FEN antibodies

20,000 HEK293-μOR cells were stimulated in triplicates with one of the following conditions to result in final concentrations: 500 μM IBMX alone (baseline signal), 1 μM FSK alone or together with 1 nM CAR or with 1 nM CAR combined with antibody dilutions at the specified final concentrations (**A**: ab5, **B**: ab6, **C**: ab8, **D**: ab9). The antibodies were pre-incubated with the other stimulants for 30 minutes at 37°C to allow for binding equilibrium before being added to the cells. The AlphaScreen assay was performed as described in section 5.5.2. Measured random light units (RLU) are plotted as the mean ± SEM of five individual experiments.

The IBMX signal serves as the baseline, reflecting the basal cAMP level in the cells, while its degradation is prevented by PDE inhibition. Stimulation with 1 μM FSK activates AC, increasing cAMP levels, which leads to a decrease in the AlphaScreen signal. This FSK signal was reduced by approximately 50% with 15

nM FEN, consistent with previously determined potency measurements (Figure 37A).

In the presence of antibody, the AlphaScreen signal decreased in a concentration-dependent manner, with higher antibody concentrations causing a greater reduction in the signal, indicating an increase in cAMP levels. This suggests that the antibody inhibited the opioid-induced attenuation of cAMP production and thus blocked their receptor activation. At antibody concentrations above 62.5-125 nM, the FSK signal was restored for most of the tested antibodies, indicating complete inhibition of the FEN effect (Figure 38). Interestingly, in all cases except for ab2 (Figure 38A) at lower antibody concentrations, the AlphaScreen signal exceeded the baseline signal observed with FEN alone, suggesting an unexpected enhancement of FEN's effect rather than inhibition.

1 nM CAR inhibited the FSK signal by approximately 60%, slightly more than the 50% inhibition observed at higher concentrations in Figure 37A. Even at the highest antibody concentration of 1 µM, CAR-induced cAMP attenuation was not fully reversed (Figure 39). The overshoot of the AlphaScreen signal at low antibody concentrations was also observed with CAR for the majority of antibodies, though it was less pronounced than with FEN.

Overall, FSK inhibition by opioids varied considerably between experiments. To address this variability, antibody effects were normalized to the opioid response in each corresponding experiment. This normalization ensured consistent and reliable assessment of antibody performance. From the resulting dose-response curves, IC_{50} values for the antibodies could be determined, enabling a direct and comparable evaluation of their inhibitory efficacy.

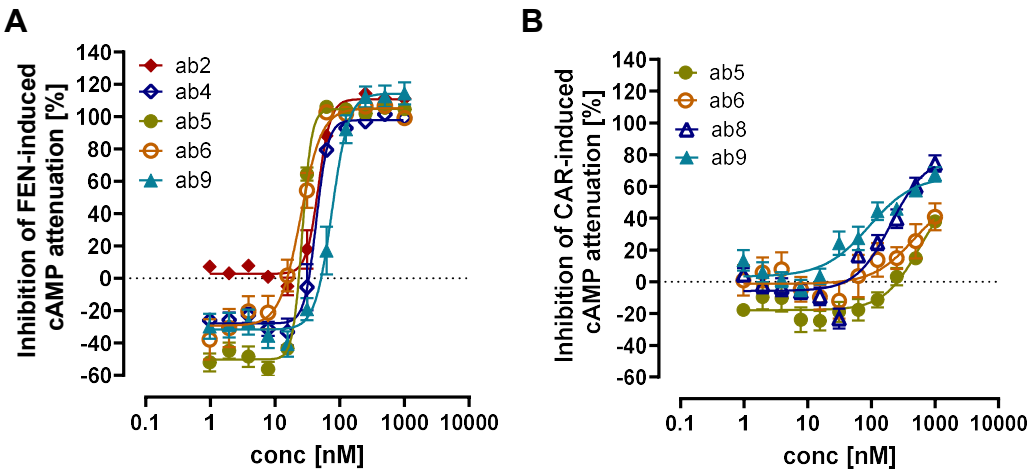

Figure 40: Potencies of selected antibodies to inhibit FEN and CAR induced μOR activation

For details on experimental procedure see Figure 38 and Figure 39. From measured RLU values the FSK effect was calculated as the difference between the FSK-stimulated signal and the baseline. The opioid effect was determined as the reduction in FSK signal caused by the addition of the opioid (difference between FSK alone and FSK + opioid). The antibody effect was calculated as the difference between the signal in the presence of FSK, opioid and antibody, and the FSK + opioid signal. This antibody effect was then normalized to the opioid effect and plotted as the mean ± SEM, expressed as a percentage of inhibition of opioid-induced cAMP attenuation against logarithmic antibody concentrations.

	15 nM FEN				1 nM CAR			
	IC_{50} [nM]	Hillslope	Effect at 1 µM [%]	Effect at 1 nM [%]	IC_{50} [nM]	Hillslope	Effect at 1 µM [%]	Effect at 1 nM [%]
ab2	45.5 ± 8.76	4.59	111	2.72	-	-	-	-
ab4	42.6 ± 7.27	4.79	97.8	-28.0	-	-	-	-
ab5	26.9 ± 1.53	6.03	105	-50.3	494 ± 50.3***	1.59	60.2	-17.9
ab6	25.7 ± 3.65	2.67	105	-29.4	904 ± 473*	1.31	54.1	-1.33
ab8	-	-	-	-	224 ± 73.9	1.55	79.0	-5.76
ab9	73.5 ± 19.2	3.34	114	-31.8	121 ± 57.1	1.23	66.6	3.19

Table 17: Potencies of selected antibodies to inhibit opioid-induced µOR activation, hillslopes, and effects at 1 µM and 1 nM

IC_{50} values of antibodies, corresponding hillslopes of the curves and effects at 1 µM and 1 nM were determined based on data shown in Figure 40 using GraphPad Prism 10.3.1. Non-linear regression analysis was performed using the "agonist vs. response" model with a variable slope (four parameters). IC50 values are presented as mean ± SEM from 3-5 independent experiments. Hillslopes and antibody effects at 1 µM and 1 nM are reported as the values derived from the combined curve generated from 3-5 experiments. Unpaired t-tests were performed to evaluate significant differences in IC_{50} values of each antibody between FEN and CAR conditions (*p<0.05, ***p<0.001).

All tested antibodies inhibited 15 nM FEN and 1 nM CAR in a concentration-dependent manner, reaching saturation at higher antibody concentrations. The IC_{50} values against FEN ranged between 25 and 70 nM, demonstrating high potency of the antibodies against FEN. Notably, all antibodies completely inhibited FEN-induced μOR activation at concentrations above 100 nM, achieving 100% neutralization.

As mentioned previously and indicated in Figure 40 and Table 17, all dose response curves, except for ab2´s, exhibited a shift of values towards the negative at low antibody concentrations. This phenomenon was more pronounced in the inhibition of FEN compared to CAR inhibition (Table 17) and suggests that low antibody concentrations do not inhibit the opioid's effect on cAMP inhibition but rather enhance it.

Analysis of the hillslope provided insights into the cooperativity of binding between the antibodies and the opioids. A hillslope greater than 1 suggests positive cooperativity, where the binding of one molecule facilitates the binding of additional molecules [467]. Antibodies ab2, ab4 and ab5 showed particularly high hillslopes between 4.5 and 6, indicating strong positive cooperativity. This could indicate, that the binding of one antibody molecule to FEN enhances subsequent FEN binding. Ab6 and ab9 exhibited slightly lower Hill slopes (2.7–3.3) but still demonstrated notable cooperativity.

Against 1 nM CAR, the potency of ab5 and ab6, with IC_{50} values between 500 and 900 nM, was substantially lower than those observed for FEN. Ab8, which exhibited specificity for CAR in binding assays, had a moderate IC_{50} value of approximately 200 nM. Ab9 showed the highest potency against CAR, with an IC_{50} of around 120 nM, which did not significantly differ from its potency against FEN. This indicates that ab9 is similarly effective at inhibiting μOR activation by both FEN and CAR. However, the antibodies' maximal inhibition of CAR was markedly lower compared to FEN. None of the tested antibodies achieved complete inhibition of 1 nM CAR, even at the highest concentration tested (1 μM). The maximal inhibition ranged between 40% and 70%. Furthermore, hillslopes for CAR were generally just above 1 for all antibodies, suggesting that the strong positive cooperativity observed for FEN binding was largely absent for CAR.

These findings indicate that antibodies capable of blocking FEN and CAR binding to the receptor can also inhibit their receptor activation. Overall, the antibodies demonstrated higher potency and maximal inhibition against FEN compared to CAR. An exception was ab9, which exhibited similar potency but reduced maximal inhibition against CAR. These results highlight both the potential and limitations of these antibodies in neutralizing μOR activation by FEN and CAR.

7. Discussion

This study established a recombinant HEK293 cell line for stable μOR expression to assess the pharmacodynamics of CAR, alongside FEN, REMI, MOR and ENDO. The data presented here reveal a pronounced bias of CAR toward cAMP signaling. Furthermore, CAR was found to promote μOR hyperphosphorylation at T370 and T379, distinguishing it from other opioids. Additionally, CAR exhibited reduced sensitivity to antagonists like NLX and NLM, suggesting that it stabilizes a distinct μOR conformations that favors cAMP signaling, enhances phosphorylation and diminishes antagonist efficacy. Anti-FEN antibodies investigated in this study demonstrated the ability to neutralize CAR receptor binding and activation, highlighting the therapeutic potential of specific antibodies for managing or preventing FEN and CAR intoxications.

7.2. Carfentanil stabilizes unique μOR conformation

The extreme toxicity of CAR can stem from either its pharmacodynamics or pharmacokinetics. While pharmacokinetics involve factors such as absorption, distribution, half-life and elimination, the present study focused on the pharmacodynamics at the μOR. Specifically, it examined μOR binding affinities, potencies across two distinct signaling pathways with corresponding receptor efficacies, kinase phosphorylation and opioid-induced receptor phosphorylation.

To assess CAR's pharmacodynamic profile relative to other opioids, several derivatives were selected for pharmacodynamic comparison based on their pharmacological relevance and differing properties. MOR, a well-established natural opioid, served as a reference due to its extensive medical history. Furthermore, it is often used as a reference point for comparing the analgetic potency of other opioid derivatives [25]. ENDO shows the highest affinity and selectivity for μOR among endogenous peptide ligands, making it a valuable model for understanding naturally occurring opioid interactions with receptors [160]. In addition to CAR, two FEN derivatives were also included to broaden the scope of the comparison. FEN itself, the prototype of this synthetic opioid class, was selected due to its widespread clinical and illicit use. REMI, a short-acting FEN analogue used in anesthesia, was included for its role in poisoning incidents alongside CAR [125]. By comparing these opioids, this study aimed to elucidate

the unique μOR binding and activation properties of CAR, particularly in relation to both endogenous and synthetic opioids, with the overarching goal of identifying potential links between these pharmacodynamic properties and CAR's exceptional toxicity.

7.2.1. Carfentanil-bound μOR conformation shows cAMP bias

7.2.1.1. Influence of binding buffers on μOR affinity of opioids: Carfentanil as a high-affinity ligand in focus

In this study, binding affinities were evaluated using radioligand binding assays with HEK293-μOR membranes in two buffer systems: TRIS-buffer and cell culture medium DMEM. CAR exhibited the highest μOR binding affinity among the opioids, regardless of the buffer system used in the analysis, a finding consistent with the literature (Table 1). The binding affinity of a ligand to its receptor is determined by the stability of the ligand-receptor complex. This stability arises from specific interactions between the functional groups of the ligand and the amino acid residues within the receptor's binding pocket [468]. Consequently, modifying or introducing new functional groups on a molecule can significantly influence its binding affinity by altering these interactions [469,470]. This is especially relevant for synthetic opioids, as variations in their chemical structures can lead to distinct binding modes, which in turn influence receptor affinity and activation, potentially explaining the diverse pharmacological effects of opioid derivatives [56,87]. CAR´s elevated binding affinity is likely attributed to the 4-carbomethoxy group, which enhances interactions within the μOR binding pocket [471].

The results further affirmed the importance of buffer composition for this assessment, with DMEM significantly reducing the binding affinities of all tested μOR agonists, aligning with literature reports on the effects of ions on receptor interactions (Table 6). Notably, sodium ions are well-documented to modulate μOR binding: they reduce agonist binding [472], while increasing antagonist binding [448,473]. Mechanistically, sodium ions inhibit agonist binding by raising K_d values or reducing the number of binding sites [440,447,474-477], while they enhance antagonist binding by lowering K_d values [447,448] and increasing B_{max} [449]. The absence of a significant difference in NLX and NLM affinity depending on the used buffer (Table 6) suggests that this factor did not substantially affect

antagonist binding, contrasting with reports that sodium enhances binding [447-449]. This discrepancy may stem from other ions in DMEM, which also contains magnesium, calcium and potassium, making it difficult to isolate individual contributions. This complicates interpretations of sodium's role as an allosteric μOR modulator [473,478-480]. Nevertheless, understanding receptor binding in DMEM was essential for later opioid signaling experiments to adjust opioid concentrations accordingly (e.g. chapter 6.7.1). Surprisingly, despite this well-known effect of ions on opioid affinity, most of the published works have utilized sodium-free buffers such as TRIS or HEPES for binding assays with opioids (Table 1) [72,73,80,81]. Only a few have investigated binding under more physiologically relevant conditions [82,83] (~140 mM sodium in extracellular fluid [481]).

However, importantly, in present study the general rank order of binding affinities remained unchanged across the two buffer systems (Table 6), indicating that while buffer conditions affected the absolute binding affinities, they did not substantially alter the relative affinities of the opioids tested.

Given CAR's extreme toxicity, a straightforward hypothesis would be that its significantly higher μOR affinity directly translates to *in vivo* potency. However, the observed difference in binding affinity between CAR and MOR - approximately 70-fold in TRIS-buffer and up to 180-fold in DMEM - does not fully explain the extreme discrepancy in their toxicity profiles. Despite CAR's significantly higher μOR affinity, its *in vivo* potency is reported to be up to 10,000-fold greater than that of MOR. This indicates that CAR's increased toxicity cannot be attributed solely to its stronger binding at the μOR. These findings reinforce existing evidence that μOR binding affinity does not always serve as a reliable predictor of μOR activation, either *in vitro* or *in vivo* [92,482-484].

7.2.1.2. Carfentanil-bound μOR conformation is ultraefficient in cAMP inhibition but not ERK1/2 phosphorylation

While binding affinity is a key determinant of receptor-ligand interactions, the pharmacodynamics of an opioid also include its potency and intrinsic activity in initiating intracellular signaling pathways. To determine whether CAR exhibits distinct receptor activation behavior compared to other opioids, μOR binding

affinities were complemented by assessments of the opioids´ potencies and intrinsic activities for cAMP inhibition and ERK1/2 phosphorylation. Additionally, receptor efficacy was assessed using two key parameters: the APR and RO, which together describe how efficiently a single receptor-bound ligand translates its binding into a functional response.

Among the tested opioids, CAR demonstrated the highest potency for cAMP inhibition (Figure 18), aligning with previous studies [59]. Moreover, what distinguishes CAR is its extraordinarily high receptor efficacy. The pronounced gap between its binding affinity and functional potency, reflected in its exceptionally high APR, indicates that CAR converts receptor binding into an intracellular effect - specifically cAMP signaling - far more efficiently than other opioids (Figure 19, Figure 20). Similarly, CAR required far fewer occupied receptors to achieve the same level of cAMP inhibition (Table 9).

Notably, these findings remained consistent regardless of the buffer system used for affinity measurements. CAR exhibited 5 - 8 times higher receptor efficacy than other opioids when affinities measured in TRIS-buffer were considered. When affinities measured in DMEM were used for calculations, CAR remained 3 - 8 times more efficient than the other opioids. This observation suggests that while the choice of binding buffer influences the absolute affinities of the opioids, it has little effect on their relative receptor efficacy and that this phenomenon is intrinsic to the ligand-receptor interaction rather than an artifact of experimental conditions. However, a particularly interesting observation in this study was that affinity values measured in DMEM, using membrane-based assays, closely aligned with those obtained from whole-cell experiments (Figure 17). Given that intact cells in a blood-like medium are often considered a more physiologically relevant model, this suggests the analyses including affinities measured in DMEM may better reflect *in vivo* opioid-receptor interactions than previously assumed. Consequently, CAR's already exceptional receptor efficacy appears even more pronounced under these conditions, with an APR exceeding 400 and an RO as low as 0.2% for half-maximal cAMP inhibition.

μOR activation triggers conformational changes and $G_{\alpha i}$ protein translocation, leading to AC inhibition and reduced cAMP production - a key G protein-

dependent pathway [193,194]. As a crucial second messenger, cAMP plays a well-documented role in opioid-induced analgesia [197-199] and respiratory depression [205,207]. While the intrinsic activity for cAMP inhibition was comparable across opioid subgroups, indicating similar maximal effects, FEN derivatives - particularly CAR - exhibited significantly higher potency than MOR and ENDO. This aligns with their stronger analgesic and respiratory depressive effects [89,451,485] (Figure 18 and Table 8).

The analysis highlights the extraordinary potency and receptor efficacy of CAR in modulating cAMP signaling. While a comparative analysis of opioids that incorporates affinity, potency and receptor efficacy (expressed as APR and RO) has not been conducted before, the relationship between *in vitro* measures of opioid μOR binding and activation, and the corresponding *in vivo* opioid-like effects, has already been explored. Glatfelter et al. found that μOR binding affinity values from rat brain tissues did not correlate with *in vitro* functional potencies or *in vivo* effects in mice [482]. Instead, a strong positive correlation was observed between *in vitro* μOR functional potencies - specifically in the cAMP assay - and *in vivo* opioid-like effects, including antinociception, locomotor activity and temperature change. Although respiration was not assessed in their study, these findings suggest that functional assays measuring μOR activation, rather than simply binding affinity, can reliably predict *in vivo* opioid effects relevant to toxicity. This aligns with the present study, where CAR, despite its higher affinity compared to MOR, exhibited an even more striking potency difference (~620-fold) in cAMP inhibition. While this alone does not fully explain CAR's extreme *in vivo* potency - up to 10,000 times higher - it provides a mechanistic basis, particularly when considering its exceptionally high receptor efficacy in cAMP signaling. It suggests that CAR not only suppresses cAMP at lower concentrations but also translates binding into cellular responses far more efficiently than other opioids, potentially contributing to its severe pharmacological effects.

When evaluating opioid potency and receptor efficacy in ERK1/2 phosphorylation as a secondary signaling pathway, CAR once again demonstrated the highest potency among the tested opioids. However, unlike its extreme receptor efficacy in cAMP inhibition, CAR did not exhibit a similar outstanding efficiency in ERK1/2

activation. The RO values required for half-maximal phosphorylation were lower for CAR and ENDO compared to other opioids, yet the differences between opioids were far less pronounced than in the cAMP pathway (Table 10). This indicates that CAR, despite its superior potency, does not act as an ultra-efficient agonist in ERK1/2 signaling.

This raises the question of how a ligand can translate receptor binding more efficiently into one signaling pathway than another. What determines the differences in receptor efficacy across pathways? ORs are GPCRs that mediate intracellular signaling in response to agonist binding, propagating external stimuli into the cell. Traditionally, it was believed that the receptor exists in only two states (ternary complex model): an active conformation that interacts with G poteins and induces signaling pathways and an inactive conformation that does not [486]. Agonists were thought to have high affinity for the active conformation, driving signaling, whereas antagonists were believed to maintain the receptor's equilibrium, favoring the inactive state [487]. However, findings by Samama et al. demonstrated that receptors can adopt active conformations independently of agonist binding, challenging this model and paving the way for the multi state receptor model, which proposes the existence of multiple active receptor conformations, each with subtle differences in their signaling profiles [488-492]. This model also explains the phenomenon of biased agonism, where differences in the molecular structure of ligands lead to distinct interactions with the receptor’s binding pocket, stabilizing specific conformations that favor certain signaling pathways over others [493].

In this context, a key observation from this study is the signaling bias favoring the cAMP pathway across most tested opioids. CAR exhibited the most pronounced bias, suggesting that it stabilizes a receptor conformation that is highly efficient in activating the cAMP pathway but not the ERK1/2 pathway. This is reflected in the ratio of RO values required for cAMP inhibition versus ERK1/2 phosphorylation. Specifically, CAR required 3- to 8-fold fewer RO for cAMP inhibition than for ERK1/2 activation, depending on the buffer system used for affinity assessment (Table 11). In contrast, ENDO showed minimal differences between the two pathways, with RO ratios around one for both calculations, indicating no significant pathway preference. The calculated bias factors further quantified

CAR´s pathway preference. While all opioids showed some degree of bias toward cAMP signaling, CARs bias factor of approximately 11 was significantly higher than the 2 - 3 observed for other opioids (Table 11). Notably, the bias factor provides the advantage of eliminating the influence of binding affinities, ensuring that observed differences are independent of experimental conditions such as buffer composition. This strengthens the conclusion that CAR intrinsically favors G protein-mediated signaling, regardless of affinity variations across buffer systems.

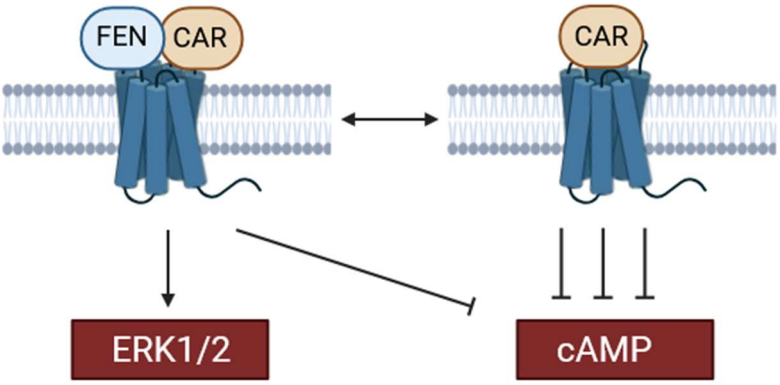

Figure 41: CAR-induced μOR conformation favors cAMP inhibition over ERK1/2 activation

CAR binds and stabilizes unique μOR conformations that are not recognized by other opioids such as FEN. These receptor states are characterized by ultra-efficient cAMP inhibition, indicating CAR´s signaling bias toward this pathway.

A bias of CAR toward G protein activation has not been observed in previous studies. Ramos-Gonzales et al. investigated CAR´s G protein activation using a BRET (Bioluminescence Resonance Energy Transfer) assay, which measures the dissociation of G protein subunits by detecting changes in energy transfer from a luminescent donor molecule to a fluorescent acceptor molecule [211]. This method requires the overexpression of specific G protein subunits in the cell line used. In their study, no G protein activation bias was observed relative to the synthetic opioid peptide DAMGO. These findings contradict those of the present study, where a cAMP signaling bias - and thus a bias toward a G protein-dependent pathway - was identified. Similarly, in present study, no G protein bias was observed at the level of early ERK1/2 phosphorylation, which is thought to

be primarily $G_{\beta\gamma}$-dependent. Given that G protein activation leads to the simultaneous release of both G_{α} and $G_{\beta\gamma}$ subunits, the absence of a similar bias in ERK1/2 phosphorylation is unexpected. These discrepancies suggest that cAMP inhibition may involve distinct $G_{\alpha i}$ subunits that were neither assessed by Ramos-Gonzales et al. nor implicated in the ERK1/2 activation monitored here. Moreover, the overexpression of G protein subunits may saturate the system, enabling receptor coupling to G proteins even when the receptor's natural preference for G protein signaling over β-arrestin is only moderate. Under these conditions, biases could be masked. Another explanation for the missing G protein bias in ERK1/2 phosphorylation could be the involvement of alternative signaling pathways. It has been suggested that, in HEK293 cells, μOR can activate ERK1/2 through a calmodulin-dependent transactivation of EGFR [234]. If this pathway contributed to the ERK1/2 activation measured in this study, it might have obscured the G protein bias at this level. Alternatively, CAR-induced cAMP inhibition may not be solely dependent on G protein activation. Instead, the observed bias might arise from alternative receptor-mediated signaling upstream of cAMP inhibition. Future studies could explore which specific G protein subunits contribute most significantly to the observed differences between opioids or investigate the precise mechanisms by which CAR induces cAMP inhibition beyond G protein activation.

Although it was long believed that opioid side effects were mediated through arrestin signaling, this notion has been refuted. Instead, both G protein- and β-arrestin-mediated pathways have been shown to contribute to opioid side effects [315-318]. Additionally, research has established that G protein signaling in respiratory network neurons is a primary mechanism behind opioid-induced respiratory depression [319,494]. Similarly, evidence indicates that respiratory depressive effects of opioids are primarily determined by the overall strength of receptor activation [319]. Considering the well-established link between cAMP inhibition and opioid-induced respiratory depression [204,205,495-497], the observations in present study suggest that CAR's pharmacodynamic profile - characterized by its extreme potency and receptor efficacy in the cAMP pathway - may contribute to its severe toxicity. This assumption is further supported by previous findings demonstrating that CAR exhibits exceptionally strong activation

of ion channels, another G protein-dependent process closely linked to opioid-induced respiratory depression [498].

Taken together, CAR demonstrated ultra-efficient cAMP signaling but showed comparable effectiveness to other opioids in ERK1/2 phosphorylation. This signaling bias suggests that CAR stabilizes a unique μOR conformation, distinct from those engaged by other opioids. These observations reinforce the hypothesis that CAR's unique signaling properties, particularly its profound ability to suppress cAMP signaling, underlie its extreme pharmacological effects and potential lethality.

7.2.2. Carfentanil-bound μOR conformation shows hyperphosphorylation

The characterization of CAR's unique pharmacological profile was extended by investigating its effects on μOR phosphorylation. Given that differences between CAR and other opioids had already been observed, the goal was to see if these distinctions were also reflected in the receptor phosphorylation patterns. Notably, GRK-mediated receptor phosphorylation has been shown to be dependent on the bound agonist and the receptor conformation [250,254]. Its examination was therefore useful to gain further insights into the unique receptor conformation potentially induced by CAR.

Experiments employed in this work revealed that robust phosphorylation at S375 was a consistent feature across all opioids tested (Figure 26). S375 represents the initial phosphorylation site on the μOR, acting as a trigger for subsequent phosphorylation events at additional receptor sites and is predominantly targeted by GRK2/3 and GRK5 [262]. MOR exhibited significantly weaker phosphorylation at this site compared to other opioids and showed negligible phosphorylation at T370 and T379. This pattern aligns with prior findings [258,261,303,499] and might result from the exclusive involvement of GRK5 in phosphorylating S375 on MOR-bound μOR, while phosphorylation by other opioids and at other residues also requires contributions from additional GRK subtypes [500].

While - except for MOR - opioids produced comparable phosphorylation levels at T370 and T379, CAR induced significantly higher phosphorylation at both residues. Given CAR's increased potency in both cAMP inhibition and ERK1/2

phosphorylation, the observed enhancement in μOR phosphorylation may, at first glance, not be surprising. It could be hypothesized that CAR is simply more effective at recruiting kinases to the receptor, thereby driving higher maximal phosphorylation levels. In this scenario, CAR would behave as a full agonist in the context of receptor phosphorylation, while other opioids function more as partial agonists, unable to drive maximal phosphorylation. However, this explanation is challenged by the observation that this effect is not uniformly present across all phosphorylation sites. While FEN, REMI and ENDO induced phosphorylation at T370 and T379 at levels only 10-40% of their respective S375 phosphorylation efficiency, CAR reached 50-60%. This disproportionate enhancement suggests that CAR does not only induce a stronger overall phosphorylation response but instead stabilizes a distinct receptor conformation that selectively favors phosphorylation at certain sites. The fact that phosphorylation at T370 and T379 is known to be highly agonist-dependent and predominantly mediated by GRK2/3 and GRK5/6 - with additional PKC involvement reported for T370 - further supports this interpretation. It implies that CAR-bound μOR adopts a conformation that either makes it especially accessible to kinases or activates pathways that enhance receptor phosphorylation.

As described previously, the phosphorylation of the μOR facilitates the recruitment of β-arrestins, which in turn promotes receptor internalization. Previous studies have shown that CAR exhibits a bias towards β-arrestin signaling [211]. The results of present study support and expand those findings, as the observed increase in μOR phosphorylation with CAR is likely to enhance β-arrestin recruitment. Moreover, it is established, that the activation of ERK1/2 through μOR is dependent on receptor phosphorylation, which facilitates β-arrestin binding, initiating the signaling cascade leading to ERK1/2 phosphorylation [293,458]. Hence, data from experiments analyzing the kinetics of opioid-induced ERK1/2 phosphorylation support this hypothesis. Among the tested opioids, CAR uniquely exhibited a second, weaker peak at 20-30 minutes (Figure 21) and this sustained or later-phase ERK1/2 phosphorylation is often linked to β-arrestin-mediated signaling pathways [292,455]. Consequently, the β-arrestin bias of CAR might contribute to both enhanced receptor phosphorylation and the delayed ERK1/2 signaling observed. Given that β-arrestin signaling was

shown to play a key role in opioid-induced respiratory depression, this pharmacodynamic distinction may further amplify CARs severe toxicity [306,313]. However, β-arrestin bias has also been reported for ENDO [264], a finding that could not be replicated in the present study in the context of enhanced receptor phosphorylation and late-phase ERK1/2 phosphorylation.

The involvement of β-arrestin for opioid-driven μOR phosphorylation and ERK1/2 phosphorylation was not further investigated in the course of this study. Determining whether CAR preferentially engages specific kinases or scaffolding proteins that promote these phosphorylation events would add valuable insights. Additionally, examining the downstream effects of CAR-induced phosphorylation patterns could reveal potential functional differences in μOR-mediated signaling.

To the best of current knowledge, no studies have specifically examined the phosphorylation of μOR or ERK1/2 resulting from CAR binding before. Given the connection between agonist-induced receptor phosphorylation and receptor conformation, the heightened CAR-induced GRK-dependent μOR phosphorylation further supports the hypothesis that the receptor conformation stabilized by CAR is distinct from those stabilized by other opioids.

7.2.3. Carfentanil exhibits no distinct protein phosphorylation profile compared to other opioids

While CAR's bias toward G protein signaling was demonstrated in this study, there were also indications of its previously established β-arrestin bias, which has been documented elsewhere [211]. However, beyond these well-characterized pathways, little is known about CAR’s broader signaling effects, particularly in relation to kinase phosphorylation. Given that opioids can differentially modulate intracellular signaling cascades, a deeper understanding of CAR’s kinase interactions is essential. Using a phospho-kinase array, the modulation of 39 proteins was analyzed simultaneously, confirming and supplementing several known findings from the literature.

The results revealed that CAR does not exhibit a distinct protein phosphorylation pattern compared to other opioids. Several kinases, including CREB (cAMP response element-binding protein), ERK1/2, STAT1 (Signal transducer and activator of transcription 1), AKT1/2/3 (Protein kinases B subtypes 1/2/3) and

RSK2/3 (ribosomal protein S6 kinases 1, 2, and 3) were modulated in a largely consistent manner across all tested opioids (Figure 25). These findings align with existing literature, which has well-documented the phosphorylation of CREB and ERK1/2 in response to opioids like MOR, FEN, REMI and synthetic opioid peptide DAMGO [227,293,456,457,501-506]. This study extends these observations to CAR and ENDO, suggesting that the phosphorylation of these kinases is a conserved feature of opioid signaling rather than a unique property of any specific compound.

CREB phosphorylation, in particular, was robustly detected across all opioids (Figure 25). As a transcription factor critical for neuronal plasticity and gene expression [507], CREB is typically activated via PKA. However, although opioids reduce cellular cAMP levels by inhibiting AC and consequently decreasing PKA activity, CREB can still undergo phosphorylation through alternative signaling pathways, such as calcium-dependent kinases (PKC, calmodulin-dependent kinase II) or ERK1/2 signaling [225,508,509].

Similarly, ERK1/2 phosphorylation, often associated with both G protein and β-arrestin-mediated signaling, was observed for CAR and all other opioids. Moreover, robust ERK1/2 phosphorylation was also observed during Western Blot analysis for all tested opioids (Figure 21), providing validation for the assay's functionality. Evidence suggests that the mechanisms underlying ERK1/2 activation may vary between different opioids [458]. Notably, while FEN and ENDO also promoted EGFR phosphorylation - one possible upstream regulator of ERK1/2 [226,510,511] - CAR and REMI did not. This discrepancy suggests that CAR may activate ERK1/2 through alternative mechanisms or that EGFR modulation by CAR follows distinct kinetics that could not be resolved within the scope of this analysis. Both possibilities warrant further investigation. Overall, the findings confirm ERK1/2 phosphorylation for several opioids and extend this observation to additional opioids not previously investigated.

STAT1 dephosphorylation was observed for CAR, FEN, REMI and ENDO, aligning with previous reports for MOR [457], though some studies have reported conflicting results for opioid-induced STAT1 modulation [512-514]. AKT1/2/3 phosphorylation at S473 was also consistent across all opioids, in agreement with

existing literature on MOR and FEN [515-519]. These kinases are involved in cell proliferation and growth and are typically activated in response to growth factors, e.g. through ERK1/2 signaling, which was also found to be activated by opioids in prior studies [517,520]. Similarly, RSK1/2/3 phosphorylation was detected for all opioids, extending previous findings on MOR to additional derivatives [247,521]. Since RSK functions downstream of ERK, its activation further supports opioid-induced ERK1/2 involvement in cellular signaling [522,523]. While these kinases have been studied in the context of other opioids, their modulation by CAR has not been previously reported.

Although CAR did not exhibit a completely distinct signaling profile, some protein modulation patterns varied among opioids. For instance, while most kinases were modulated similarly, CAR was the only opioid to phosphorylate p70S6 at T421/S424, a modification previously linked to opioid signaling but not specifically associated with CAR before [524]. However, this isolated observation is insufficient to conclude that CAR displays a uniquely different pattern of protein phosphorylation. Numerical analysis of kinase modulation revealed that FEN and REMI exhibited the highest number of modulated kinases, while CAR and ENDO showed fewer events (Table 12). Notably, REMI was the only opioid derivative associated with substantial dephosphorylation (~40%), whereas the others predominantly induced phosphorylation (~90%). CAR and ENDO displayed a similar balance between phosphorylation and dephosphorylation, with no significant differences in individual protein targets (Table 13). However, some divergences emerged when considering the overall modulation pattern, such as ENDO phosphorylating EGFR while CAR did not (Figure 25). This highlights the complexity of opioid-induced kinase signaling and the difficulties of this array-based approach in capturing subtle differences.

That said, the limitations of the kinase array approach must be considered. While this method effectively captures broad kinase activity, it may overlook dynamic or transient signaling events. For example, β-arrestin-mediated effects can exhibit complex kinetics that may not be fully captured in a single time-point analysis. Additionally, while ERK1/2 phosphorylation was detected across all opioids, the mechanism driving its activation may vary, as suggested by the differing EGFR phosphorylation results.

Overall, CAR did not exhibit a distinct kinase phosphorylation profile compared to other opioids, and its bias agonism was not directly reflected in this analysis. This suggests that CAR's effects on kinase signaling may be more nuanced or context-dependent than what this approach can capture. Nevertheless, this study successfully reproduced known opioid-induced protein modulations while extending these findings to CAR, but does not support the hypothesis of uniquely distinct kinase signaling. While CAR exhibits bias toward G protein and β-arrestin signaling, its effects on kinase phosphorylation remain largely comparable to those of other opioids, with only minor differences. Further research is needed to determine whether its bias agonism influences more specialized signaling cascades.

7.2.4. Carfentanil-bound μOR conformation exhibits resistance to approved opioid antagonists

Even though the administration of OR antagonists is the standard therapy for opioid intoxication, this approach often proves insufficient against highly potent opioids such as CAR. Based on data from this study, it is hypothesized that CAR stabilizes receptor conformations distinct from those stabilized by other opioids. To investigate this further, the effectiveness of approved antidotes, NLX and NLM, against opioid concentrations of comparable receptor affinities was determined. This setup ensured consistent pharmacodynamic conditions, theoretically enabling NLX and NLM to exhibit similar effectiveness against all opioids. However, the results revealed otherwise.

Both NLX and NLM exhibited significantly reduced potencies against CAR compared to other opioids, with 10- to 100-fold higher IC_{50} values (Table 14). Notably, even at a 10,000-fold molar excess, NLX was unable to fully reverse CAR-induced cAMP suppression, suggesting a reduced maximal efficacy. Additionally, the bar chart revealed a potential plateau effect around 1.5 fmol cAMP/well, with the slope flattening at higher NLX concentrations (Figure 27). This implies that even higher NLX doses might not fully counteract CAR-induced receptor activation, pointing to a potential form of NLX resistance.

In contrast, NLM achieved complete CAR-inhibition at its highest concentration and displayed lower IC_{50} values overall, indicating greater potency. This superior

performance may be attributed to NLM's higher receptor affinity (Table 6), enhancing its ability to compete with CAR for receptor binding.

The reduced potency and efficacy of frontline antagonists against CAR suggest mechanisms beyond simple receptor affinity. NLX, and to a lesser extent NLM, appear to have difficulty targeting the unique receptor conformation stabilized by CAR - a state highly efficient in cAMP signaling. This distinct conformation seems inherently resistant to conventional antagonists, potentially explaining the observed limitation of NLX´s effectiveness in clinical settings.

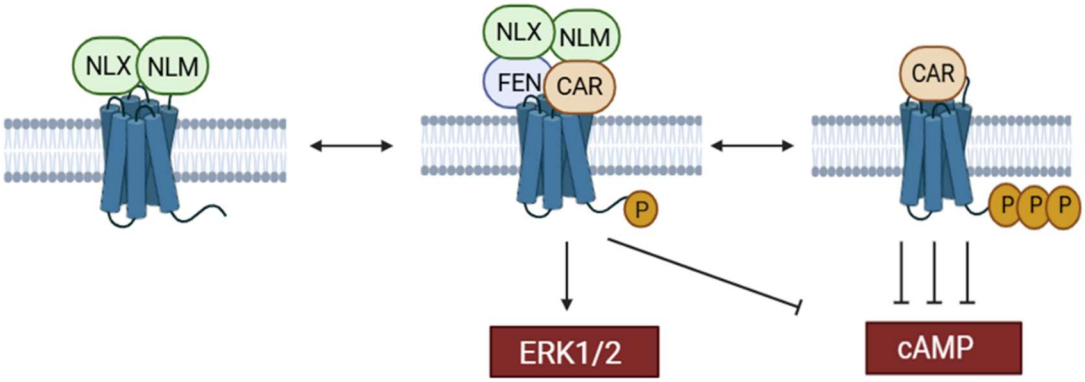

Figure 42: CAR-induced μOR conformation favors cAMP inhibition, promotes hyperphosphorylation and reduces antagonist sensitivity

μOR exist in active and inactive conformations that either activate or fail to activate downstream signaling pathways. The receptor antagonist NLX does not differentiate between these conformational states. Agonists such as FEN bind to active conformations that do not preferentially mediate cAMP inhibition or ERK1/2 phosphorylation. In contrast, CAR binds to distinct receptor states that inhibit cAMP ultra-efficiently without promoting ERK phosphorylation and are characterized by enhanced phosphorylation at the C-terminus. These CAR-bound receptor conformations are not recognized by other opioids, including FEN, MOR, REMI and ENDO, nor by antagonists like NLX and NLM. Consequently, antagonists have difficulty inhibiting CAR-induced cAMP inhibition.

Notably, NLX resistance of CAR has been previously documented. Feasel et al. demonstrated that NLX's potency against CAR at EC_{90} concentrations was reduced tenfold compared to FEN [210], aligning closely with the findings of this study. Similarly, Flynn et al. observed that Naltrexone – a distinct antagonist commonly used for opioid dependence treatment - was less effective against CAR than FEN [525]. These observations support the hypothesis that CAR

induces receptor conformations that limit the effectiveness of standard opioid antagonists, posing a challenge for conventional treatment approaches.

These findings underscore the importance of further exploring the structural and functional characteristics of receptor conformations stabilized by potent opioids, as well as the development of more effective therapeutic strategies to counteract their effects. Additionally, it would be valuable to systematically screen alternative OR antagonists for their potential to exhibit greater efficacy against CAR than NLX or NLM.

7.3. Characterization of antibodies: Potential for neutralizing highly potent opioids at the receptor level

The concept of using an immunological approach to counteract opioid toxicity is not new. Both passive and active immunization strategies against opioids - particularly highly potent FEN analogs - have been explored in research [366,369,526]. However, their clinical application remains a challenge, particularly due to the rapid onset and extreme potency of synthetic opioids.

This study aimed to assess whether commercially available anti-FEN antibodies could neutralize CAR and cross-react with other opioids. The primary focus was to determine whether these antibodies could inhibit opioid binding and activation of the μOR. While used antibodies were originally developed for laboratory applications such as ELISA, lateral flow (LF) or fluorescence immunoassays (FIA), they had never been tested in a biological system or at the receptor level. To current knowledge, this is the first study to evaluate these antibodies in this context.

7.3.1. Several antibodies inhibit μOR binding of fentanyl and carfentanil

One potential *in vivo* application of antibodies is their administration to patients before they are exposed to a potent opioid. This approach could be particularly beneficial for soldiers deployed on missions where they might face the risk of opioid exposure. In this context, their specificity is particularly important. Ideally, the antibodies should effectively neutralize highly toxic opioids like CAR while still allowing the use of medically necessary opioids like MOR for pain management.

At the same time, they must not interfere with endogenous opioids, which exhibit essential physiological functions [527].

To assess their neutralizing potential, nine antibodies were screened for their ability to inhibit opioid-induced displacement of the radiolabeled tracer [³H]-NLX in HEK293-μOR membranes. Seven of the nine antibodies significantly inhibited FEN actions, with four (ab2, ab4, ab5, ab6) achieving complete inhibition (Figure 32). This suggests that the majority of anti-FEN antibodies were effective in this assay and effectively neutralized FEN's μOR binding. Notably, ab7 and ab8 showed no significant effects, suggesting they were non-functional in this assay. Both antibodies are polyclonal and the only ones raised in rabbits using FEN-BgG as the immunogen (see chapter 4.6.). Their lack of functionality in this assay could be due to specific factors in their production process that affected their ability to bind FEN. Alternatively, it is possible that even when bound to the antibody, FEN could still interact with the receptor - perhaps because key functional groups remained exposed, allowing it to bind the receptor's orthosteric binding site.

The cross-reactivity of the antibodies with CAR was particularly relevant given its extreme potency and resistance to standard opioid antidotes. While FDA-approved treatments like NLX and NLM are effective against most opioids, they have limited efficacy against CAR both *in vitro* and *in vivo* due to its exceptionally strong receptor activation. Once CAR binds to the μOR, these antagonists struggle to fully block its effects. Antibodies, however, could provide a promising alternative by neutralizing CAR before it reaches the receptor. Five antibodies (ab3, ab5, ab6, ab8 and ab9) significantly inhibited CAR binding, although none achieved complete neutralization (Figure 33, Table 15). This finding suggests that some anti-FEN antibodies possess cross-reactivity with CAR, likely due to shared structural features between the two opioids. As observed by Eubanks et al. [369], these antibodies likely target the core phenylethyl and piperidinyl groups - structural elements shared by FEN and CAR. This overlap in molecular features could explain their ability to bind both substances (Figure 1: Chemical structure of OR agonists). Notably, ab3, ab5 and ab6 are monoclonal antibodies generated in mice or mouse hybridoma cells, while ab8 and ab9 are polyclonal antibodies raised in rabbits or sheep. Consequently, no direct link can be established

between the observed reduction in specificity and certain antibody specifications. Interestingly, ab8 was ineffective against FEN but displayed notable activity against CAR, indicating a certain degree of CAR specificity in this assay. Ab8 shares the same specifications as ab7, yet only ab8 showed activity against CAR. The polyclonality of ab8 and ab9 may enable them to bind multiple epitopes of a single antigen, which could explain their reduced specificity for FEN while increasing their ability to recognize shared structural features between FEN and CAR. Although CAR differs from FEN by the addition of a quaternary methoxy group at position 4 of the piperidine ring - a feature absent in FEN - this broader epitope recognition might account for ab8's cross-reactivity with CAR.

The manufacturers had previously evaluated the cross-reactivity of certain anti-FEN antibodies with FEN derivatives, including CAR. According to the product data sheets, ab1 exhibited 1% cross-reactivity with CAR, ab2 showed less than 0.1%, ab3 demonstrated 5% and ab4 showed 1%. These data align with the findings of this study, where none of these antibodies - except for ab3 - showed significant inhibition of CAR receptor interaction. Ab3 inhibited approximately 9% of CAR binding (Table 15). For ab5, ab6, ab7, ab8 and ab9, no manufacturer data regarding CAR cross-reactivity were available. Therefore, the observed functionality of these antibodies cannot be directly compared to any pre-existing specifications.

Importantly, none of the antibodies interfered with MOR and ENDO at the tested concentrations, suggesting that their selectivity is limited to FEN and CAR and does not extend to other opioid classes. While this specificity helps minimize side effects, it also raises concerns about their potential inefficacy against structurally distinct synthetic opioids. MOR, an alkaloid with a morphinan skeleton and ENDO, a tetrapeptide, differ structurally from FEN derivatives and lack the characteristic anilidopiperidine core, which might be essential for antibody recognition. Surprisingly, none of the antibodies recognized REMI either, despite its anilidopiperidine structure. Unlike FEN and CAR, REMI lacks the alkylbenzyl substituent on the nitrogen atom of the piperidine ring, instead featuring a methyl ester group at this position. This structural difference could explain the lack of binding, suggesting that the alkylbenzyl group might be a key determinant for antibody recognition. Alternatively, the higher concentration of REMI used in this

assay compared to FEN and CAR may have played a role. If the antibodies do bind REMI, but an excess of unbound molecules was still available to displace [^{3}H]-NLX, a neutralizing effect might have been masked in this experiment.

This said, the effectiveness of neutralizing agents strongly depends on the ligand concentrations used in the assay. In this study, opioid concentrations were selected based on those used in antagonist experiments: 150 nM FEN, 10 nM CAR, 10 µM ENDO and 500 nM REMI. The only exception was MOR, which was tested at 200 nM to reflect physiologically relevant therapeutic plasma levels [528]. This concentration was chosen to simulate real-life scenarios where patients treated with anti-FEN or anti-CAR antibodies might still require MOR for pain management. While the lower MOR concentration slightly reduced the challenge for antibody binding, it still ensured that most receptors were occupied (Figure 19), making it easier to assess potential antibody effects on MOR. For FEN analogs, concentrations approximated lethal plasma levels. CAR's exact lethal concentration remains unknown, but post-mortem analyses following CAR intoxication have reported plasma levels between 0.2 and 3.4 ng/mL (0.5-8.6 nM) [61,529-531]. For FEN, concentrations above 20 ng/mL (60 nM) are associated with loss of consciousness, according to [532]. Gill et al. and Edinboro et al. reported FEN concentrations of around 25 ng/mL (74 nM) in intoxication victims [533,534]. Olson et al. reported a range from 5 to 26 ng/mL, corresponding to 15-77 nM [535]. Determining lethal REMI concentrations is more challenging due to its rapid metabolism; in some cases, only its metabolites were detectable post-intoxication [536]. However, target plasma concentrations for REMI-induced anesthesia are typically 3-5 ng/mL (8-13 nM) [537]. Based on these data, the selected concentrations of 150 nM FEN, 10 nM CAR and 500 nM REMI likely fall within ranges that would be lethal or, at the very least, cause severe respiratory depression in opioid-naive individuals.

It's important to note, however, that unlike the antagonist experiments conducted in DMEM buffer (radioactive cAMP assay, see section 6.7.1) this assay was performed in TRIS-buffer. As demonstrated in section 6.4.1, opioids generally exhibit higher binding affinities in TRIS-buffer. Given that the selected concentrations were approximately 10 to 20 times higher than each opioid's respective K_i, it's estimated that over 90% of the receptors are already bound by

the opioids. This increased receptor occupancy presents a more challenging environment for the antibodies to inhibit opioid binding. However, the advantage of using TRIS-buffer was twofold: it not only reduced the amount of opioid required, but also, consequently, the necessary amount of antibodies. Despite the high receptor occupancy across the chosen concentrations, these conditions still provide a suitable framework for screening the antibodies' neutralizing effects against the opioids, as they strike a balance, allowing sufficient tracer displacement for effective measurement, while also conserving both opioid and antibody resources.

7.3.2. Antibodies exhibit reduced potency and maximal inhibition against Carfentanil

Beyond receptor binding, the ability of antibodies to inhibit opioid-induced receptor activation was assessed using cAMP accumulation assays. For this analysis the antibodies, which showed the best effect in opioid inhibition in the binding assays were selected. However, the concentrations used to assess the antibody potencies were selected to be tenfold lower than those used in the antagonist experiments conducted with the radioactive assay. This decision was based on the higher sensitivity of the AlphaScreen assay, which allowed the usage of lower concentrations of both the antibodies and FSK. In fact, the FSK concentration in the AlphaScreen assay was also reduced by a factor of ten. Initial trials using the same concentrations as in the antagonist experiments (150 nM FEN and 10 nM CAR) did not yield any detectable neutralizing effect of the antibodies. This lack of effect indicated that the opioid response was already saturated. Even when receptor binding was presumably significantly inhibited by the antibody, sufficient cAMP inhibition still occurred, making it impossible to detect any antibody effects under these conditions. As a result, the concentrations were adjusted to be tenfold lower, specifically 15 nM FEN and 1 nM CAR, which still resulted in sufficient FSK inhibition, so subsequent antibody effects could be detected.

Compared to their effects on FEN, the antibodies exhibited lower potency and maximal inhibition against CAR. While ab2, ab4, ab5, ab6 and ab9 demonstrated high potency against 15 nM FEN (IC_{50} values: 20-70 nM), their potency against 1 nM CAR was markedly lower. The IC_{50} values of ab5 and ab6 were between

500 and 900 nM, and ab8 showed moderate potency (IC_{50} ~ 200 nM). Ab9 was the only antibody with similar potency against both FEN and CAR, though its maximal inhibition of CAR remained incomplete.

The reduced efficacy against CAR is likely due to its high receptor affinity and ability to activate the μOR efficiently, even at low occupancy levels (Table 9). Additionally, the strong positive cooperativity observed in FEN-neutralizing antibodies - evident from high hillslopes (Table 17) - was absent in CAR inhibition, further supporting the notion that these antibodies were optimized for FEN rather than CAR. The phenomenon positive cooperativity, where binding of one molecule enhances the binding of additional molecules, is well-documented in proteins with multiple binding sites, such as hemoglobin [538]. However, for antibodies, which typically have two identical Fab regions, the situation is more complex. Some studies suggest that under specific conditions - such as the formation of large antigen-antibody complexes - conformational changes in the antibody might influence binding properties [539]. Also, there are reports that ligands can influence the overall conformation of antibodies [540]. Furthermore, there is evidence for allosteric cooperativity in IgG antibodies, where ligand binding to the variable region impacts the constant region's effector functions [541,542]. However, these effects differ from the classical cooperativity seen in hemoglobin and are not directly comparable. Importantly, no direct evidence supports the notion that ligand binding to one Fab fragment facilitates binding to the other Fab fragment of the same antibody. The positive cooperativity-like effects observed in this study appear to be a unique and novel aspect of antibody functionality at the receptor level. However, the underlying mechanisms remain unclear and require further investigation. Despite this, these findings highlight the need for CAR-specific antibodies to achieve more effective neutralization.

An unexpected phenomenon was observed at low antibody concentrations (<30 nM), where FEN-induced cAMP inhibition was enhanced, with dose-response curves dipping below baseline. For most antibodies (except ab2), this effect was particularly pronounced at 10 nM, where FEN-induced cAMP attenuation was enhanced by up to 50%. A similar, though less pronounced, effect was observed with ab5 and ab8 against 1 nM CAR, enhancing cAMP attenuation by up to 20%. Interestingly, this effect varied opioid-dependent; for example, ab6 exhibited this

behavior with FEN but not with CAR. This specificity rules out the possibility that the phenomenon is an intrinsic property of the antibodies, independent of their interaction with the ligand.

In the literature, there are reports of ligand-antibody complexes enhancing receptor activation [543]. At low antibody concentrations, distinct antibody-ligand complexes, such as one-to-one configurations may form, potentially increasing ligand affinity or concentrating the ligand near the receptor. Additionally, low antibody concentrations have been associated with enhanced receptor activation in other contexts [544] and physiological anti-receptor antibodies have been proposed to exert receptor-regulatory functions [545]. These findings may explain the receptor-activating effect observed in this study, where low antibody concentrations seem to promote receptor activation either through unique antibody-ligand complexes or intrinsic receptor-regulatory properties of the antibodies (Figure 43). Despite these observations, the underlying mechanisms of this phenomenon remain unclear. To date, this type of assay - designed for the *in vitro* investigation of anti-FEN antibodies by indirectly measuring the inhibition of opioid-induced cAMP attenuation through enhanced tracer displacement - has not been previously applied in this context. As a result, it cannot be ruled out that the observed effects, particularly the apparent receptor activation at low antibody concentrations, may be influenced by methodological factors. For instance, low antibody concentrations might, for unknown reasons, interfere with tracer displacement itself, thereby mimicking an enhanced opioid effect. Further studies are necessary to determine whether this phenomenon reflects a biological mechanism or an assay-specific artifact.

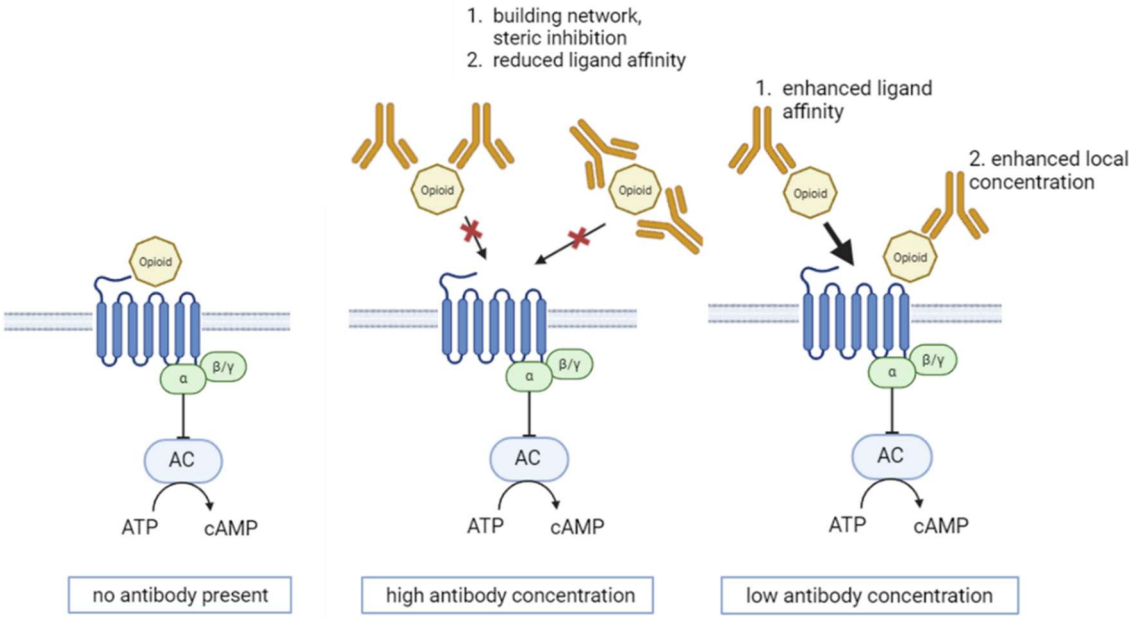

Figure 43: Potential mechanisms underlying the enhancement of FEN-induced receptor activation at low antibody concentrations

Without antibody, FEN binds to and activates the receptor, reducing cellular cAMP levels. At high antibody concentrations, FEN is neutralized through masking of functional groups, steric inhibition, or reduced receptor binding affinity, thereby preventing cAMP inhibition. At low antibody concentrations, distinct FEN-antibody complexes may form, potentially enhancing receptor binding and activation. Alternatively, low antibody concentrations could increase local FEN concentration near the receptor, promoting its binding and activity.

This study demonstrated that opioid antagonists like NLX and NLM show significantly reduced efficacy against CAR compared to other opioids. This is likely due to CAR stabilizing a unique, ultra-active receptor conformation that makes it less accessible to antagonists. Given this resistance, an alternative strategy - preventing CAR from binding to the receptor in the first place - appears particularly promising.

However, directly comparing antagonists and antibodies within the scope of this study presents challenges. Differences in their mechanisms of action and uncertainties regarding how *in vitro* concentrations translate to therapeutic plasma levels make a direct comparison difficult. For instance, Hicks et al. administered antibodies at a dose of 40 mg/kg in mice [546]. Assuming an average mouse body weight of 20 g, a blood volume of 1.4 mL, and an antibody molecular weight of 150 kDa, the theoretical plasma concentration would be approximately 4 µM. In contrast, the highest antibody concentration used in this

study's *in vitro* assays was 1 µM. This discrepancy suggests that the effects observed *in vitro* may underestimate the potential efficacy of antibodies at therapeutic concentrations, which could theoretically be higher.

Despite these challenges, the antibodies tested in this study appeared to be more selective than antagonists. While antagonists broadly affected all tested opioids, particularly MOR and ENDO, the antibodies showed no cross-reactivity with these compounds or with REMI. This suggests that, in a clinical setting, patients treated with anti-FEN or anti-CAR antibodies might still be able to receive MOR for pain management.

Overall, the tested antibodies demonstrated high potency and efficacy against FEN, reinforcing the potential of antibody-based strategies. This highlights the need to develop CAR-specific antibodies, which could achieve similar performance against CAR as anti-FEN antibodies do against FEN. Additionally, both the ligand binding and AlphaScreen assays proved to be reliable platforms for *in vitro* antibody testing.

7.3.3. Potential limitations of antibody-based opioid neutralization

Specific antibodies offer a broad therapeutic potential for treating opioid intoxications, with the advantage of tailoring their specificity to individual opioid derivatives. Their longer half-life, especially compared to clinically approved receptor antagonists, reduces the risk of post-treatment renarcotization. However, considering antibodies as a viable antidote for opioid intoxication involves several significant challenges.

Opioids, particularly FEN-like analogs, present challenges due to their low molecular weight and high lipophilicity. These properties enable rapid absorption and distribution into the bloodstream and CNS following invasive (e.g. intravenous) and non-invasive application routes (e.g. oral, transdermal, inhalational or transmucosal) [547,548]. Synthetic opioids can cross into the brain within seconds, producing physiological effects. This rapid onset requires antibodies to bind the drug immediately to prevent its entry into the brain. Interestingly, studies in model systems have shown that antibodies can bind small molecules within seconds, supporting their potential effectiveness *in vivo* [549]. However, for this, the antibody must already be present at the site of action - in

the bloodstream - at sufficient concentrations. The immunogenicity of these antibodies pose another challenge. Non-human-derived antibodies frequently trigger adverse immune reactions *in vivo*, necessitating humanization before clinical application [550].

Moreover, despite endeavors to enable antibody delivery to the CNS, due to their large molecule size, antibodies generally cannot pass the BBB [551,552]. Instead, their action depends on opioids dissociating from the receptors and returning to the bloodstream, where the antibodies can neutralize them. Whether this approach can sufficiently and quickly lower opioid plasma concentrations to sub-effective or non-pathological levels remains uncertain. A promising strategy to overcome this limitation could involve the combined use of fast-acting receptor antagonists, such as NLX or NLM, which rapidly penetrate the brain, alongside antibodies either prophylactically or post-exposure [367,553-555]. While the antagonists have relatively short half-lives compared to potent opioids like CAR, their shortcoming could be offset by the prolonged action of antibodies. Based on data from other exogenous antibodies, anti-drug antibodies might exhibit durations of action ranging from hours to weeks, reducing the risk of renarcotization [527]. Research supports this potential. Eubanks et al. observed reversal of CAR-induced respiratory depression 20 minutes after administering a monoclonal antibody, which showed prolonged efficacy compared to NLX [369]. Similarly, Triller et al. demonstrated protection against FEN effects when monoclonal antibodies were administered 24 hours prior to FEN exposure. Furthermore, they reported reversal of FEN-induced effects within 15 minutes after antibody injection [365].

In this study, several anti-FEN antibodies - tested for the first time *in vitro* on receptor-level interactions - showed significant inhibition of FEN- and CAR-induced μOR binding and activation in HEK293-μOR cells. While these findings are promising, further research is essential to evaluate their effectiveness *in vivo*.

7.4. Suitability of HEK293-μOR cell line in this work

HEK293 cells are commonly utilized in receptor expression studies due to their high transfection efficiency, rapid proliferation and ability to maintain stable expression of introduced proteins [381,383,384]. While HEK293 cells lack

endogenous μOR expression [435], their favorable characteristics make them an ideal platform for developing recombinant cell lines in OR pharmacology. [436,437]. In this study, the HEK293-μOR cell line was successfully established, expressing the rμOR, although efforts to stably express the hμOR were unsuccessful. Interestingly, most published studies in the field of OR pharmacology have utilized HEK293 cells stably transfected with rodent μOR [302,436,437], while examples involving stable transfection with hμOR are relatively rare [556]. This shortness suggests that stable integration of hμOR into HEK293 cells might be particularly challenging or that the transfection protocol used in this study was not optimized for hμOR cDNA. Given that rat and human μOR share 95% sequence homology and exhibit nearly identical ligand affinity and selectivity [72,438,439], the rat receptor is a highly suitable alternative for the human version. The strong similarity suggests that any species-specific differences are unlikely to affect the overall validity of this works results.

The established HEK293-μOR cells displayed high μOR expression and strong affinity for the radioactive tracer [^{3}H]-NLX, reflected in low K_d and high B_{max} values (Figure 15). The values determined in this work were notably higher than those reported in studies using cells that endogenously express μOR, such as F11 or amphibian brain homogenates [125, 164]. Overexpressing cell lines, like the HEK293-μOR used here - genetically modified to include the μOR gene under a viral promoter - can lead to significantly higher receptor quantities, which can be both an advantage and a limitation. In present study, this approach produced precise affinity measurements with high reproducibility. Moreover, the reliable detection of the inhibitory effects of antibodies on OR binding further underscores the cell line's suitability for analyses of receptor-ligand interactions. However, the overexpression can introduce complexities when examining signaling pathways, e.g. due to the occurance of receptor reserve, which typically affects all ligands equally.

In this study, all opioid agonists exhibited lower EC_{50} values for cAMP inhibition compared to their K_i values, confirming the presence of receptor reserve. The APR, also referred to as pharmacological shift ratio (PSR) in the literature [557], is a measure for receptor reserve and ranged from 5 to 44 in TRIS-buffer and 58-444 in DMEM in this work (Figure 19 and Figure 20). While this indicates a

substantial receptor reserve in the system, the strikingly high APR of CAR suggests an effect beyond receptor reserve alone. Thus, although receptor overexpression may influence absolute APR values, the relative differences in efficacy observed in this study remain valid and support the described conclusions. The fact that CAR deviates so markedly from the other opioids indicates that its receptor efficacy is intrinsically higher.

Given that receptor overexpression should affect all opioids similarly, one would expect comparable results in an endogenous cell line. Indeed, a study examining the affinity and potency for cAMP inhibition in SH-SY5Y cells - an endogenous human neuronal cell line naturally expressing OR [558] - found similar affinities for FEN and CAR. However, as in present study, CAR exhibited a significantly higher potency. The APRs were nearly 1 for FEN and 15 for CAR. Therefore, it is likely that the same phenomenon can be observed, regardless of the overexpression system.

While overexpressing cell lines may not fully replicate physiological conditions - particularly regarding the induction of signaling pathways influenced by receptor reserve - present study still provides crucial insights into the receptor-level mechanisms underlying CAR's extreme potency and toxicity. Even though direct translation to *in vivo* conditions should be approached with caution, the findings emphasize the importance of further research using more physiologically relevant models to fully elucidate CAR's *in vivo* pharmacological profile.

8. References

1. Nadeau SE, Wu JK, Lawhern RA. Opioids and Chronic Pain: An Analytic Review of the Clinical Evidence. Front Pain Res (Lausanne). 2021;2:721357. Epub 2022/03/18.
2. Teoh PJ, Camm CF. NICE Opioids in Palliative Care (Clinical Guideline 140) - A Guideline Summary. Ann Med Surg (Lond). 2012;1:44-8. Epub 2012/01/01.
3. Hug CC, Jr. Opioids: clinical use as anesthetic agents. J Pain Symptom Manage. 1992;7:350-5. Epub 1992/08/11.
4. Dowell D, Haegerich TM, Chou R. CDC Guideline for Prescribing Opioids for Chronic Pain--United States, 2016. Jama. 2016;315:1624-45. Epub 2016/03/16.
5. Amaechi O, Huffman MM, Featherstone K. Pharmacologic Therapy for Acute Pain. Am Fam Physician. 2021;104:63-72. Epub 2021/07/16.
6. Benyamin R, Trescot AM, Datta S, Buenaventura R, Adlaka R, Sehgal N, Glaser SE, Vallejo R. Opioid complications and side effects. Pain Physician. 2008;11:S105-20. Epub 2008/06/17.
7. Hemmings HCE, Talmage D. Pharmacology and Physiology for Anesthesia: Foundations and Clinical Application: Expert Consult – Online and Print: Elsevier Health Sciences; 2013.
8. Ogura T, Egan TD. Chapter 15 - Opioid Agonists and Antagonists. In: Hemmings HC, Egan TD, editors. Pharmacology and Physiology for Anesthesia. Philadelphia: W.B. Saunders; 2013. p. 253-71.
9. Pathan H, Williams J. Basic opioid pharmacology: an update. Br J Pain. 2012;6:11-6. Epub 2012/02/01.
10. Cruz SL. Opioids : pharmacology, abuse, and addiction: Springer International Publishing; 2022.
11. Corder G, Castro DC, Bruchas MR, Scherrer G. Endogenous and Exogenous Opioids in Pain. Annu Rev Neurosci. 2018;41:453-73. Epub 2018/06/01.
12. Herman TF, Cascella M, Muzio MR. Mu Receptors. StatPearls: StatPearls Publishing, Copyright © 2025, StatPearls Publishing LLC.; 2025.
13. Schulz R, Ehrenreich H. [Endogenous opioids]. Tierarztl Prax. 1985;13:11-27. Epub 1985/01/01.
14. Encyclopaedia TEo. opium. Encyclopaedia Britannica. 2023, December 29.
15. Beckett GH, Wright CRA. IV.—Action of the organic acids and their anhydrides on the natural alkaloids. Part II. Butyryl and benzoyl derivatives of morphine and codeine. Journal of the Chemical Society. 1875;28:15-26.
16. Zöllner C, Stein C. Opioids. In: Stein C, editor. Analgesia. Berlin, Heidelberg: Springer Berlin Heidelberg; 2007. p. 31-63.
17. Armenian P, Vo KT, Barr-Walker J, Lynch KL. Fentanyl, fentanyl analogs and novel synthetic opioids: A comprehensive review. Neuropharmacology. 2018;134:121-32. Epub 2017/10/19.
18. Leen JLS, Juurlink DN. Carfentanil: a narrative review of its pharmacology and public health concerns. Can J Anaesth. 2019;66:414-21. Epub 2019/01/23.

19. Jesus A, Bonhomme V, Evin A, Ivorra S, Soteras R, Salavert A, Antolín F, Bouby L. A morphometric approach to track opium poppy domestication. Scientific Reports. 2021;11:9778.

20. Brook K, Bennett J, Desai SP. The Chemical History of Morphine: An 8000-year Journey, from Resin to de-novo Synthesis. Journal of Anesthesia History. 2017;3:50-5.

21. Brownstein MJ. A brief history of opiates, opioid peptides, and opioid receptors. Proc Natl Acad Sci U S A. 1993;90:5391-3. Epub 1993/06/15.

22. Schmitz R. Friedrich Wilhelm Sertürner and the discovery of morphine. Pharm Hist. 1985;27:61-74. Epub 1985/01/01.

23. Krishnamurti C, Rao SC. The isolation of morphine by Serturner. Indian J Anaesth. 2016;60:861-2. Epub 2016/12/13.

24. Jurna I. [Sertürner and morphine--a historical vignette]. Schmerz. 2003;17:280-3. Epub 2003/08/19.

25. WHO. WHO Guidelines for the Pharmacological and Radiotherapeutic Management of Cancer Pain in Adults and Adolescents. National Library of Medicine2018.

26. Booth M. Opium: A history: St. Martin's Griffin; 2013.

27. Society GP. Long-term use of opioids in chronic non-cancer pain (LONTS), 2nd Update. Berlin, Germany: 2020.

28. Sandkühler J, Gebhart GF. Relative contributions of the nucleus raphe magnus and adjacent medullary reticular formation to the inhibition by stimulation in the periaqueductal gray of a spinal nociceptive reflex in the pentobarbital-anesthetized rat. Brain Res. 1984;305:77-87. Epub 1984/07/02.

29. Tortorici V, Morgan MM. Comparison of morphine and kainic acid microinjections into identical PAG sites on the activity of RVM neurons. J Neurophysiol. 2002;88:1707-15. Epub 2002/10/05.

30. Meyer PJ, Morgan MM, Kozell LB, Ingram SL. Contribution of dopamine receptors to periaqueductal gray-mediated antinociception. Psychopharmacology (Berl). 2009;204:531-40. Epub 2009/02/20.

31. Hosobuchi Y. The current status of analgesic brain stimulation. Acta Neurochir Suppl (Wien). 1980;30:219-27. Epub 1980/01/01.

32. Valentino RJ, Volkow ND. Untangling the complexity of opioid receptor function. Neuropsychopharmacology. 2018;43:2514-20.

33. Reeves KC, Shah N, Muñoz B, Atwood BK. Opioid Receptor-Mediated Regulation of Neurotransmission in the Brain. Front Mol Neurosci. 2022;15:919773. Epub 2022/07/06.

34. Al-Hasani R, Bruchas MR. Molecular mechanisms of opioid receptor-dependent signaling and behavior. Anesthesiology. 2011;115:1363-81. Epub 2011/10/25.

35. Organization WH. WHO model list of essential medicines, 20th list (March 2017, amended August 2017). 2017.

36. Stanley TH, Egan TD, Van Aken H. A tribute to Dr. Paul A. J. Janssen: entrepreneur extraordinaire, innovative scientist, and significant contributor to anesthesiology. Anesth Analg. 2008;106:451-62, table of contents. Epub 2008/01/30.

37. Vucković S, Prostran M, Ivanović M, Dosen-Mićović L, Todorović Z, Nesić Z, Stojanović R, Divac N, Miković Z. Fentanyl analogs: structure-activity-relationship study. Curr Med Chem. 2009;16:2468-74. Epub 2009/07/16.

38. Stanley TH. The History of Opioid Use in Anesthetic Delivery. In: Eger Ii EI, Saidman LJ, Westhorpe RN, editors. The Wondrous Story of Anesthesia. New York, NY: Springer New York; 2014. p. 641-59.

39. Ramos-Matos CF BK, Lopez-Ojeda W. Fentanyl 2023.

40. Manuals M. Opioidanalgetika – Tabelle: Merck & Co, Inc., Rahway, NJ, USA; 2025 [March 06, 2025]. Available from: https://www.msdmanuals.com/de/profi/multimedia/table/opioidanalgetika.

41. Stanley TH. The fentanyl story. J Pain. 2014;15:1215-26. Epub 2014/12/03.

42. Organization WH. WHO Guidelines for the Pharmacological and Radiotherapeutic Management of Cancer Pain in Adults and Adolescents. Table A6.2, Approximate potency of opioids relative to morphine; PO and immediate-release formulations unless stated otherwisea. Geneva: World Health Organization; 2018 [January 17, 2025]. Available from: https://www.ncbi.nlm.nih.gov/books/NBK537482/table/appannex6.tab2/.

43. WHO. Model List of Essential Medicines - 23rd list. Geneva: 2023.

44. Information NCfB. PubChem Compound Summary for CID 126961754, Opioid 2025 [January 22, 2025]. Available from: https://pubchem.ncbi.nlm.nih.gov/compound/Opioid.

45. Vardanyan RS, Hruby VJ. Fentanyl-related compounds and derivatives: current status and future prospects for pharmaceutical applications. Future Med Chem. 2014;6:385-412. Epub 2014/03/19.

46. Maucher IV. Gelbe Liste, Sufentanil – Drug Information 2024 [January 22, 2025]. Available from: https://www.gelbe-liste.de/wirkstoffe/Sufentanil_27385?utm_source.

47. Abbate V, Moreno AS, Wiegand TJ. Chapter16 - Novel synthetic opioids. In: Dargan P, Wood D, editors. Novel Psychoactive Substances (Second Edition). Boston: Academic Press; 2022. p. 447-74.

48. Wilhelm W. Praxis der Anästhesiologie: Springer Berlin, Heidelberg; 2018.

49. Glass PSA, Gan TJ, Howell S. A review of the pharmacokinetics and pharmacodynamics of remifentanil. Anesth Analg. 1999;89:7. Epub 1999/10/08.

50. Cohen J, Royston D. Remifentanil. Curr Opin Crit Care. 2001;7:227-31. Epub 2001/09/26.

51. Bushuven S, Kreuer S, Kranke P. [Remifentanil up2date - Part 2]. Anasthesiol Intensivmed Notfallmed Schmerzther. 2017;52:630-9. Epub 2017/09/09.

52. Information NCfB. PubChem Compound Summary for CID 62156, Carfentanil 2025. Available from: https://pubchem.ncbi.nlm.nih.gov/compound/Carfentanil.

53. Pharmacology IBGt. Carfentanil Summary 2024. Available from: https://www.guidetopharmacology.org/GRAC/LigandDisplayForward?tab=summary&ligandId=10040.

54. Cole A, Mutlow A, Isaza R, Carpenter JW, Koch DE, Hunter RP, Dresser BL. Pharmacokinetics and pharmacodynamics of carfentanil and naltrexone in female common eland (Taurotragus oryx). J Zoo Wildl Med. 2006;37:318-26. Epub 2007/02/27.

55. Kreeger TJ. Handbook of Wildlife Chemical Immobilization (6th edition) 2023.

56. Subramanian G, Paterlini MG, Portoghese PS, Ferguson DM. Molecular docking reveals a novel binding site model for fentanyl at the mu-opioid receptor. J Med Chem. 2000;43:381-91. Epub 2000/02/12.

57. Van Bever WF, Niemegeers CJ, Schellekens KH, Janssen PA. N-4-Substituted 1-(2-arylethyl)-4-piperidinyl-N-phenylpropanamides, a novel series of extremely potent analgesics with unusually high safety margin. Arzneimittelforschung. 1976;26:1548-51. Epub 1976/01/01.

58. Janssen PAVD, Georges H, inventorN-(4-Piperidinyl)-N-phenylamides patent US4179569A. 1979.

59. Feasel M. The Use of In Vitro and In Silico Technologies for Predicting Human Pharmacology and Toxicology of Carfentanil. 2017.

60. Prekupec MP, Mansky PA, Baumann MH. Misuse of Novel Synthetic Opioids: A Deadly New Trend. J Addict Med. 2017;11:256-65. Epub 2017/06/08.

61. Chatterton CN, Handy RP, Shoemaker GK, Scott-Ham M. The distribution and redistribution of carfentanil in post mortem samples. Forensic Sci Int. 2020;309:110215. Epub 2020/03/01.

62. Burt MJ, Kloss J, Apple FS. Postmortem blood free and total morphine concentrations in medical examiner cases. J Forensic Sci. 2001;46:1138-42. Epub 2001/09/25.

63. Administration USFaD. Duramorph: Labeling Information (NDA 018565/S014). 2005.

64. Lötsch J, Walter C, Parnham MJ, Oertel BG, Geisslinger G. Pharmacokinetics of Non-Intravenous Formulations of Fentanyl. Clinical Pharmacokinetics. 2013;52:23-36.

65. Uddayasankar U, Lee C, Oleschuk C, Eschun G, Ariano RE. The Pharmacokinetics and Pharmacodynamics of Carfentanil After Recreational Exposure: A Case Report. Pharmacotherapy. 2018;38:e41-e5. Epub 2018/04/22.

66. Shaw ML, Carpenter JW, Leith DE. Complications with the use of carfentanil citrate and xylazine hydrochloride to immobilize domestic horses. J Am Vet Med Assoc. 1995;206:833-6. Epub 1995/03/15.

67. DrugBank. Carfentanil - DrugBank Entry DB01535 2025 [January 22, 2025]. Available from: https://go.drugbank.com/drugs/DB01535.

68. Feasel MG, Wohlfarth A, Nilles JM, Pang S, Kristovich RL, Huestis MA. Metabolism of Carfentanil, an Ultra-Potent Opioid, in Human Liver Microsomes and Human Hepatocytes by High-Resolution Mass Spectrometry. Aaps j. 2016;18:1489-99. Epub 2016/11/05.

69. Caspi J, Klausner JM, Safadi T, Amar R, Rozin RR, Merin G. Delayed respiratory depression following fentanyl anesthesia for cardiac surgery. Crit Care Med. 1988;16:238-40. Epub 1988/03/01.

70. Lista AD, Sirimaturos M. Pharmacokinetic and Pharmacodynamic Principles for Toxicology. Crit Care Clin. 2021;37:475-86. Epub 2021/06/01.

71. Eshleman AJ, Nagarajan S, Wolfrum KM, Reed JF, Nilsen A, Torralva R, Janowsky A. Affinity, potency, efficacy, selectivity, and molecular modeling of substituted fentanyls at opioid receptors. Biochem Pharmacol. 2020;182:114293. Epub 2020/10/23.

72. Rothman RB, Xu H, Wang JB, Partilla JS, Kayakiri H, Rice KC, Uhl GR. Ligand selectivity of cloned human and rat opioid mu receptors. Synapse. 1995;21:60-4. Epub 1995/09/01.

73. Titeler M, Lyon RA, Kuhar MJ, Frost JF, Dannals RF, Leonhardt S, Bullock A, Rydelek LT, Price DL, Struble RG. Mu opiate receptors are selectively labelled by [3H]carfentanil in human and rat brain. Eur J Pharmacol. 1989;167:221-8. Epub 1989/08/22.

74. Cassel JA, Daubert JD, DeHaven RN. [3H]Alvimopan binding to the μ opioid receptor: Comparative binding kinetics of opioid antagonists. European Journal of Pharmacology. 2005;520:29-36.

75. Costa EM, Hoffmann BB, Loew GH. Opioid agonists binding and responses in SH-SY5Y cells. Life Sci. 1992;50:73-81. Epub 1992/01/01.

76. Volpe DA, McMahon Tobin GA, Mellon RD, Katki AG, Parker RJ, Colatsky T, Kropp TJ, Verbois SL. Uniform assessment and ranking of opioid μ receptor binding constants for selected opioid drugs. Regul Toxicol Pharmacol. 2011;59:385-90. Epub 2011/01/11.

77. Spetea M, Monory K, Tömböly C, Tóth G, Tzavara E, Benyhe S, Hanoune J, Borsodi A. In vitro binding and signaling profile of the novel mu opioid receptor agonist endomorphin 2 in rat brain membranes. Biochem Biophys Res Commun. 1998;250:720-5. Epub 1998/10/24.

78. Liu X, Zhao L, Wang Y, Zhou J, Wang D, Zhang Y, Zhang X, Wang Z, Yang D, Mou L, Wang R. MEL-N16: A Series of Novel Endomorphin Analogs with Good Analgesic Activity and a Favorable Side Effect Profile. ACS Chem Neurosci. 2017;8:2180-93. Epub 2017/07/22.

79. Lipiński PFJ, Kosson P, Matalińska J, Roszkowski P, Czarnocki Z, Jarończyk M, Misicka A, Dobrowolski JC, Sadlej J. Fentanyl Family at the Mu-Opioid Receptor: Uniform Assessment of Binding and Computational Analysis. Molecules. 2019;24. Epub 2019/02/23.

80. Yeadon M, Kitchen I. Differences in the characteristics of opioid receptor binding in the rat and marmoset. J Pharm Pharmacol. 1988;40:736-9. Epub 1988/10/01.

81. Maguire P, Tsai N, Kamal J, Cometta-Morini C, Upton C, Loew G. Pharmacological profiles of fentanyl analogs at mu, delta and kappa opiate receptors. Eur J Pharmacol. 1992;213:219-25. Epub 1992/03/24.

82. Newman LC, Wallace DR, Stevens CW. Selective opioid receptor agonist and antagonist displacement of [3H]naloxone binding in amphibian brain. Eur J Pharmacol. 2000;397:255-62. Epub 2000/06/14.

83. Lambert DG, Atcheson R, Hirst RA, Rowbotham DJ. Effects of morphine and its metabolites on opiate receptor binding, cAMP formation and [3H]noradrenaline release from SH-SY5Y cells. Biochem Pharmacol. 1993;46:1145-50. Epub 1993/10/05.

84. Chen ZR, Irvine RJ, Somogyi AA, Bochner F. Mu receptor binding of some commonly used opioids and their metabolites. Life Sci. 1991;48:2165-71. Epub 1991/01/01.

85. Maryanoff BE, Simon EJ, Gioannini T, Gorissen H. Potential affinity labels for the opiate receptor based on fentanyl and related compounds. J Med Chem. 1982;25:913-9. Epub 1982/08/01.

86. Miyazaki T, Choi IY, Rubas W, Anand NK, Ali C, Evans J, Gursahani H, Hennessy M, Kim G, McWeeney D, Pfeiffer J, Quach P, Gauvin D, Riley TA, Riggs JA,

Gogas K, Zalevsky J, Doberstein SK. NKTR-181: A Novel Mu-Opioid Analgesic with Inherently Low Abuse Potential. J Pharmacol Exp Ther. 2017;363:104-13. Epub 2017/08/06.

87. Hassanien SH, Bassman JR, Perrien Naccarato CM, Twarozynski JJ, Traynor JR, Iula DM, Anand JP. In vitro pharmacology of fentanyl analogs at the human mu opioid receptor and their spectroscopic analysis. Drug Test Anal. 2020;12:1212-21. Epub 2020/05/18.

88. Comer SD, Cahill CM. Fentanyl: Receptor pharmacology, abuse potential, and implications for treatment. Neurosci Biobehav Rev. 2019;106:49-57. Epub 2018/12/12.

89. Hill R, Santhakumar R, Dewey W, Kelly E, Henderson G. Fentanyl depression of respiration: comparison with heroin and morphine. bioRxiv. 2019:662627.

90. Abdulrahim D, Bowden-Jones O, The misuse of synthetic opioids: harms and clinical management of fentanyl, fentanyl analogues and other novel synthetic opioids. Information for clinicians. 2018: Publisher.

91. Schueler HE. Emerging Synthetic Fentanyl Analogs. Acad Forensic Pathol. 2017;7:36-40. Epub 2017/03/01.

92. Baumann MH, Kopajtic TA, Madras BK. Pharmacological Research as a Key Component in Mitigating the Opioid Overdose Crisis. Trends Pharmacol Sci. 2018;39:995-8. Epub 2018/11/21.

93. Schiller EY, Goyal A, Mechanic OJ. Opioid Overdose. StatPearls. Treasure Island (FL) ineligible companies. Disclosure: Amandeep Goyal declares no relevant financial relationships with ineligible companies. Disclosure: Oren Mechanic declares no relevant financial relationships with ineligible companies.: StatPearls Publishing, Copyright © 2025, StatPearls Publishing LLC.; 2025.

94. Ciottone GR, Longo D, Taichman D. Toxidrome Recognition and Response. New England Journal of Medicine. 2023;388:e58.

95. Kiyatkin EA. Respiratory depression and brain hypoxia induced by opioid drugs: Morphine, oxycodone, heroin, and fentanyl. Neuropharmacology. 2019;151:219-26. Epub 2019/02/09.

96. Banzett RB, Mulnier HE, Murphy K, Rosen SD, Wise RJ, Adams L. Breathlessness in humans activates insular cortex. Neuroreport. 2000;11:2117-20. Epub 2000/08/03.

97. McKay LC, Evans KC, Frackowiak RS, Corfield DR. Neural correlates of voluntary breathing in humans. J Appl Physiol (1985). 2003;95:1170-8. Epub 2003/05/20.

98. Smith JC, Ellenberger HH, Ballanyi K, Richter DW, Feldman JL. Pre-Bötzinger complex: a brainstem region that may generate respiratory rhythm in mammals. Science. 1991;254:726-9. Epub 1991/11/01.

99. Dahan A, Sarton E, Teppema L, Olievier C, Nieuwenhuijs D, Matthes HW, Kieffer BL. Anesthetic potency and influence of morphine and sevoflurane on respiration in mu-opioid receptor knockout mice. Anesthesiology. 2001;94:824-32. Epub 2001/06/05.

100. Romberg R, Sarton E, Teppema L, Matthes HW, Kieffer BL, Dahan A. Comparison of morphine-6-glucuronide and morphine on respiratory depressant and antinociceptive responses in wild type and mu-opioid receptor deficient mice. Br J Anaesth. 2003;91:862-70. Epub 2003/11/25.

101. Leino K, Mildh L, Lertola K, Seppälä T, Kirvelä O. Time course of changes in breathing pattern in morphine- and oxycodone-induced respiratory depression. Anaesthesia. 1999;54:835-40. Epub 1999/08/25.

102. Dahan A, Aarts L, Smith TW. Incidence, Reversal, and Prevention of Opioid-induced Respiratory Depression. Anesthesiology. 2010;112:226-38. Epub 2009/12/17.

103. White JM, Irvine RJ. Mechanisms of fatal opioid overdose. Addiction. 1999;94:961-72. Epub 2000/03/09.

104. Herlinger K, Lingford-Hughes A. Opioid use disorder and the brain: a clinical perspective. Addiction. 2022;117:495-505. Epub 2021/07/07.

105. McQuay H. Opioids in pain management. Lancet. 1999;353:2229-32. Epub 1999/07/07.

106. Zhou J, Ma R, Jin Y, Fang J, Du J, Shao X, Liang Y, Fang J. Molecular mechanisms of opioid tolerance: From opioid receptors to inflammatory mediators (Review). Exp Ther Med. 2021;22:1004. Epub 2021/08/05.

107. Hancocks S. The opioid crisis in the USA. Br Dent J. 2019;226:815. Epub 2019/06/17.

108. The Lancet Regional Health – A. Opioid crisis: addiction, overprescription, and insufficient primary prevention. The Lancet Regional Health – Americas. 2023;23.

109. Gale A. Sacklers Sacked But Purdue Still Caused Opioid Epidemic. Mo Med. 2022;119:109. Epub 2022/08/30.

110. Degenhardt L, Charlson F, Mathers B, Hall WD, Flaxman AD, Johns N, Vos T. The global epidemiology and burden of opioid dependence: results from the global burden of disease 2010 study. Addiction. 2014;109:1320-33. Epub 2014/03/26.

111. Prevention CfDCa. Annual Surveillance Report of Drug-Related Risks and Outcomes | United States. U.S. Department of Health and Human Services, 2018.

112. Service CR. The Opioid Crisis in the United States: A Brief History. Washington, D.C.: 2022.

113. Administration USDE. National Drug Threat Assessment. In: Justice UDo, editor. 2024.

114. Pardo B, Taylor J, Caulkins JP, Kilmer B, Reuter P, Stein BD. The future of fentanyl and other synthetic opioids. Santa Monica, CA: RAND Corporation; 2019.

115. Tanz LJ SA, Gladden RM, Ko JY, Owens L, O'Donnell J. Detection of Illegally Manufactured Fentanyls and Carfentanil in Drug Overdose Deaths — United States, 2021–2024. U.S. Department of Health and Human Services, 2024.

116. WHO. Critical Review Carfentanil, Agenda Item 4.8. 2017.

117. Administration DE. Carfentanil: A Dangerous New Factor in the U.S. Opioid Crisis. In: Justice USDo, editor. 2016.

118. McLaughlin K. Deadly chemistry. Science. 2017;355:1364-6.

119. O'Donnell JK, Halpin J, Mattson CL, Goldberger BA, Gladden RM. Deaths Involving Fentanyl, Fentanyl Analogs, and U-47700 - 10 States, July-December 2016. MMWR Morb Mortal Wkly Rep. 2017;66:1197-202. Epub 2017/11/03.

120. O'Donnell J, Gladden RM, Mattson CL, Kariisa M. Notes from the Field: Overdose Deaths with Carfentanil and Other Fentanyl Analogs Detected - 10 States, July 2016-June 2017. MMWR Morb Mortal Wkly Rep. 2018;67:767-8. Epub 2018/07/13.

121. Office BSCP. Sicherstellung der extrem gefährlichen Droge Carfentanyl in München. 2024.

122. Davison N. Marketing new chemical weapons. Bulletin of the Atomic Scientists. 2009.

123. Pitschmann V, Hon Z. Drugs as Chemical Weapons: Past and Perspectives. Toxics. 2023;11. Epub 2023/01/21.

124. Shafer SL. Carfentanil: a weapon of mass destruction. Can J Anaesth. 2019;66:351-5. Epub 2019/01/16.

125. Riches JR, Read RW, Black RM, Cooper NJ, Timperley CM. Analysis of clothing and urine from Moscow theatre siege casualties reveals carfentanil and remifentanil use. J Anal Toxicol. 2012;36:647-56. Epub 2012/09/25.

126. Ciottone GR. Toxidrome Recognition in Chemical-Weapons Attacks. N Engl J Med. 2018;378:1611-20. Epub 2018/04/26.

127. John P. Caves J. Fentanyl as a Chemical Weapon: Center for the Study of Weapons of Mass Destruction, National Defense University; 2019 [January 23, 2025]. Available from: https://wmdcenter.ndu.edu/Publications/Publication-View/Article/2031503/fentanyl-as-a-chemical-weapon/.

128. Organization WH. WHO recommends the most stringent level of international control for synthetic opioid carfentanil 2017 [January 23, 2025]. Available from: https://www.who.int/news/item/13-12-2017-who-recommends-the-most-stringent-level-of-international-control-for-synthetic-opioid-carfentanil.

129. (OPCW) OftPoCW. Chemical Weapons Convention. The Hague, Netherlands: Organisation for the Prohibition of Chemical Weapons; 1993.

130. Wille T, Steinritz D, Worek F, Thiermann H. [Chemical warfare agent poisoning]. Bundesgesundheitsblatt Gesundheitsforschung Gesundheitsschutz. 2019;62:1370-7. Epub 2019/10/12.

131. Bagley EE, Ingram SL. Endogenous opioid peptides in the descending pain modulatory circuit. Neuropharmacology. 2020;173:108131. Epub 2020/05/19.

132. Loizzo A, Spampinato SM, Campana G, Vella S, Fortuna A, Costa L, Capasso A, Monteleone P, Renzi P, Loizzo S. Enhanced brain performance in mice following postnatal stress. J Endocrinol. 2012;215:413-24. Epub 2012/10/10.

133. Faden AI. Role of Endogenous Opioids in Central Cardiovascular Regulation and Dysregulation. In: Herz A, Akil H, Simon EJ, editors. Opioids II. Berlin, Heidelberg: Springer Berlin Heidelberg; 1993. p. 191-204.

134. Grunstein MM, Grunstein JS. Maturational effect of enkephalin on respiratory control in newborn rabbits. J Appl Physiol Respir Environ Exerc Physiol. 1982;53:1063-70. Epub 1982/11/01.

135. Grunstein MM, Hazinski TA, Schlueter MA. Respiratory control during hypoxia in newborn rabbits: implied action of endorphins. J Appl Physiol Respir Environ Exerc Physiol. 1981;51:122-30. Epub 1981/07/01.

136. Kumazawa T, Tadaki E, Kim K. A possible participation of endogenous opiates in respiratory reflexes induced by thin-fiber muscular afferents. Brain Res. 1980;199:244-8. Epub 1980/10/13.

137. Tallett AJ, Blundell JE, Rodgers RJ. Endogenous opioids and cannabinoids: system interactions in the regulation of appetite, grooming and scratching. Physiol Behav. 2008;94:422-31. Epub 2008/04/09.

138. Bodnar RJ. Endogenous opioids and feeding behavior: a 30-year historical perspective. Peptides. 2004;25:697-725. Epub 2004/05/29.

139. Cooper SJ, Jackson A, Kirkham TC. Endorphins and food intake: kappa opioid receptor agonists and hyperphagia. Pharmacol Biochem Behav. 1985;23:889-901. Epub 1985/11/01.

140. Yeomans MR, Gray RW. Opioid peptides and the control of human ingestive behaviour. Neuroscience & Biobehavioral Reviews. 2002;26:713-28.

141. DeFeudis FV. The link between analgesia and cardiovascular function: roles for GABA and endogenous opioids. Prog Neurobiol. 1982;19:1-17. Epub 1982/01/01.

142. Flórez J, Mediavilla A. Respiratory and cardiovascular effects of met-enkephalin applied to the ventral surface of the brain stem. Brain Res. 1977;138:585-900. Epub 1977/12/23.

143. Lemaire I, Tseng R, Lemaire S. Systemic administration of beta-endorphin: potent hypotensive effect involving a serotonergic pathway. Proc Natl Acad Sci U S A. 1978;75:6240-2. Epub 1978/12/01.

144. Moore RH, 3rd, Dowling DA. Effects of intravenously administered Leu- or Met-enkephalin on arterial blood pressure. Regul Pept. 1980;1:77-87. Epub 1980/10/01.

145. Kunos G, Farsang C, Ramirez-Gonzales MD. β-Endorphin: Possible Involvement in the Antihypertensive Effect of Central α-Receptor Activation. Science. 1981;211:82-4.

146. Farsang C, Kunos G. Naloxone reverses the antihypertensive effect of clonidine. Br J Pharmacol. 1979;67:161-4. Epub 1979/10/01.

147. Kromer W, Pretzlaff W, Scheiblhuber E. IN VITRO EVIDENCE FOR AN INVOLVEMENT OF INTESTINAL ENDORPHINS IN THE CONTROL OF PERISTALSIS IN THE GUINEA PIG ILEUM. COMPARISON TO RABBIT, RAT, CAT AND DOG SMALL INTESTINE. In: Way EL, editor. Endogenous and Exogenous Opiate Agonists and Antagonists: Pergamon; 1980. p. 337-40.

148. Kromer W, Pretzlaff W. In vitro evidence for the participation of intestinal opioids in the control of peristalsis in the guinea pig small intestine. Naunyn-Schmiedeberg's Archives of Pharmacology. 1979;309:153-7.

149. Górski K, Misztal T, Dobek E, Molik E, Romanowicz K. Regulation of growth hormone secretion in nursing ewes: an involvement of μ-receptor subtype. Reprod Domest Anim. 2012;47:746-51. Epub 2012/01/04.

150. Tuominen L, Salo J, Hirvonen J, Någren K, Laine P, Melartin T, Isometsä E, Viikari J, Raitakari O, Keltikangas-Järvinen L, Hietala J. Temperament trait Harm Avoidance associates with μ-opioid receptor availability in frontal cortex: a PET study using [(11)C]carfentanil. Neuroimage. 2012;61:670-6. Epub 2012/04/10.

151. Bertoletti E, Zanoni A, Giorda R, Battaglia M. Influence of the OPRM1 gene polymorphism upon children's degree of withdrawal and brain activation in response to facial expressions. Dev Cogn Neurosci. 2012;2:103-9. Epub 2012/06/12.

152. Berezniuk I, Fricker L. Endogenous Opioids The Opiate Receptors. Gavril W. 2011.

153. Nieber K, Oehme P. [Stress and the endogenous opioid system. I. Physiology and pharmacology of opioid peptides]. Z Gesamte Inn Med. 1985;40:1-7. Epub 1985/01/01.

154. Shenoy SS, Lui F. Biochemistry, Endogenous Opioids. StatPearls. Treasure Island (FL) relationships with ineligible companies. Disclosure: Forshing Lui declares no relevant financial relationships with ineligible companies.: StatPearls Publishing, Copyright © 2024, StatPearls Publishing LLC.; 2024.

155. Meunier J-C. The opioid peptides and their receptors. Biochimie. 1986;68:1153-8.

156. Abrimian A, Kraft T, Pan YX. Endogenous Opioid Peptides and Alternatively Spliced Mu Opioid Receptor Seven Transmembrane Carboxyl-Terminal Variants. Int J Mol Sci. 2021;22. Epub 2021/05/01.

157. Stein C. Opioid Receptors. Annu Rev Med. 2016;67:433-51. Epub 2015/09/04.

158. Hackler L, Zadina JE, Ge LJ, Kastin AJ. Isolation of relatively large amounts of endomorphin-1 and endomorphin-2 from human brain cortex. Peptides. 1997;18:1635-9. Epub 1997/01/01.

159. Fichna J, Janecka A, Costentin J, Do Rego JC. The endomorphin system and its evolving neurophysiological role. Pharmacol Rev. 2007;59:88-123. Epub 2007/03/03.

160. Zadina JE, Hackler L, Ge LJ, Kastin AJ. A potent and selective endogenous agonist for the mu-opiate receptor. Nature. 1997;386:499-502. Epub 1997/04/03.

161. Horvath G. Endomorphin-1 and endomorphin-2: pharmacology of the selective endogenous mu-opioid receptor agonists. Pharmacol Ther. 2000;88:437-63. Epub 2001/05/05.

162. Kosterlitz HW, Hughes J. Peptides with morphine-like action in the brain. Br J Psychiatry. 1977;130:298-304. Epub 1977/03/01.

163. Rhodes DL, Liebeskind JC. Analgesia from rostral brain stem stimulation in the rat. Brain Res. 1978;143:521-32. Epub 1978/03/31.

164. Shang Y, Filizola M. Opioid receptors: Structural and mechanistic insights into pharmacology and signaling. European Journal of Pharmacology. 2015;763:206-13.

165. Park PSH. GPCRs: Structure, Function, and Drug Discovery: Academic Press; 2019.

166. Rask-Andersen M, Almén MS, Schiöth HB. Trends in the exploitation of novel drug targets. Nat Rev Drug Discov. 2011;10:579-90. Epub 2011/08/02.

167. Hauser AS, Attwood MM, Rask-Andersen M, Schiöth HB, Gloriam DE. Trends in GPCR drug discovery: new agents, targets and indications. Nat Rev Drug Discov. 2017;16:829-42. Epub 2017/10/28.

168. Santos R, Ursu O, Gaulton A, Bento AP, Donadi RS, Bologa CG, Karlsson A, Al-Lazikani B, Hersey A, Oprea TI, Overington JP. A comprehensive map of molecular drug targets. Nat Rev Drug Discov. 2017;16:19-34. Epub 2016/12/03.

169. Waldhoer M, Bartlett SE, Whistler JL. Opioid receptors. Annu Rev Biochem. 2004;73:953-90. Epub 2004/06/11.

170. Paterson SJ, Robson LE, Kosterlitz HW. Classification of opioid receptors. Br Med Bull. 1983;39:31-6. Epub 1983/01/01.

171. Martin WR, Eades CG, Thompson JA, Huppler RE, Gilbert PE. The effects of morphine- and nalorphine- like drugs in the nondependent and morphine-dependent chronic spinal dog. J Pharmacol Exp Ther. 1976;197:517-32. Epub 1976/06/01.

172. Henderson G, McKnight AT. The orphan opioid receptor and its endogenous ligand--nociceptin/orphanin FQ. Trends Pharmacol Sci. 1997;18:293-300. Epub 1997/08/01.

173. Meunier JC, Mollereau C, Toll L, Suaudeau C, Moisand C, Alvinerie P, Butour JL, Guillemot JC, Ferrara P, Monsarrat B, et al. Isolation and structure of the endogenous agonist of opioid receptor-like ORL1 receptor. Nature. 1995;377:532-5. Epub 1995/10/12.

174. Reinscheid RK, Nothacker HP, Bourson A, Ardati A, Henningsen RA, Bunzow JR, Grandy DK, Langen H, Monsma FJ, Jr., Civelli O. Orphanin FQ: a neuropeptide that activates an opioidlike G protein-coupled receptor. Science. 1995;270:792-4. Epub 1995/11/03.

175. Mollereau C, Parmentier M, Mailleux P, Butour JL, Moisand C, Chalon P, Caput D, Vassart G, Meunier JC. ORL1, a novel member of the opioid receptor family. Cloning, functional expression and localization. FEBS Lett. 1994;341:33-8. Epub 1994/03/14.

176. Shang Y, Filizola M. Opioid receptors: Structural and mechanistic insights into pharmacology and signaling. Eur J Pharmacol. 2015;763:206-13. Epub 2015/05/20.

177. Zaveri NT. Nociceptin Opioid Receptor (NOP) as a Therapeutic Target: Progress in Translation from Preclinical Research to Clinical Utility. J Med Chem. 2016;59:7011-28. Epub 2016/02/16.

178. Butour JL, Moisand C, Mazarguil H, Mollereau C, Meunier JC. Recognition and activation of the opioid receptor-like ORL 1 receptor by nociceptin, nociceptin analogs and opioids. Eur J Pharmacol. 1997;321:97-103. Epub 1997/02/19.

179. Toll L, Bruchas MR, Calo G, Cox BM, Zaveri NT. Nociceptin/Orphanin FQ Receptor Structure, Signaling, Ligands, Functions, and Interactions with Opioid Systems. Pharmacol Rev. 2016;68:419-57. Epub 2016/03/10.

180. Baertsch NA, Bush NE, Burgraff NJ, Ramirez J-M. Dual mechanisms of opioid-induced respiratory depression in the inspiratory rhythm-generating network. eLife. 2021;10:e67523.

181. Lynch N, Lima JD, Spinieli RL, Kaur S. Opioids, sleep, analgesia and respiratory depression: Their convergence on Mu (μ)-opioid receptors in the parabrachial area. Front Neurosci. 2023;17:1134842. Epub 2023/04/24.

182. Matthes HW, Maldonado R, Simonin F, Valverde O, Slowe S, Kitchen I, Befort K, Dierich A, Le Meur M, Dollé P, Tzavara E, Hanoune J, Roques BP, Kieffer BL. Loss of morphine-induced analgesia, reward effect and withdrawal symptoms in mice lacking the mu-opioid-receptor gene. Nature. 1996;383:819-23. Epub 1996/10/31.

183. Levran O, Yuferov V, Kreek MJ. The genetics of the opioid system and specific drug addictions. Hum Genet. 2012;131:823-42. Epub 2012/05/02.

184. Armaan Dhaliwal MG. Physiology, Opioid Receptor 2023.

185. Wacker D, Stevens RC, Roth BL. How Ligands Illuminate GPCR Molecular Pharmacology. Cell. 2017;170:414-27. Epub 2017/07/29.

186. Huang H, Tao Y-X. Functions of the DRY motif and intracellular loop 2 of human melanocortin 3 receptor. Journal of Molecular Endocrinology. 2014;53:319-30.

187. Gilman AG. Nobel Lecture. G proteins and regulation of adenylyl cyclase. Biosci Rep. 1995;15:65-97. Epub 1995/04/01.

188. Odoemelam CS, Percival B, Wallis H, Chang MW, Ahmad Z, Scholey D, Burton E, Williams IH, Kamerlin CL, Wilson PB. G-Protein coupled receptors: structure and function in drug discovery. RSC Adv. 2020;10:36337-48. Epub 2020/10/01.

189. Ippolito DL, Temkin PA, Rogalski SL, Chavkin C. N-terminal tyrosine residues within the potassium channel Kir3 modulate GTPase activity of Galphai. J Biol Chem. 2002;277:32692-6. Epub 2002/06/26.

190. Syrovatkina V, Alegre KO, Dey R, Huang XY. Regulation, Signaling, and Physiological Functions of G-Proteins. J Mol Biol. 2016;428:3850-68. Epub 2016/08/16.

191. Oldham WM, Hamm HE. Heterotrimeric G protein activation by G-protein-coupled receptors. Nat Rev Mol Cell Biol. 2008;9:60-71. Epub 2007/11/29.

192. Koehl A, Hu H, Maeda S, Zhang Y, Qu Q, Paggi JM, Latorraca NR, Hilger D, Dawson R, Matile H, Schertler GFX, Granier S, Weis WI, Dror RO, Manglik A, Skiniotis G, Kobilka BK. Structure of the μ-opioid receptor–Gi protein complex. Nature. 2018;558:547-52.

193. Hsia JA, Moss J, Hewlett EL, Vaughan M. ADP-ribosylation of adenylate cyclase by pertussis toxin. Effects on inhibitory agonist binding. J Biol Chem. 1984;259:1086-90. Epub 1984/01/25.

194. Taussig R, Iñiguez-Lluhi JA, Gilman AG. Inhibition of adenylyl cyclase by Gi alpha. Science. 1993;261:218-21. Epub 1993/07/09.

195. Bender AT, Beavo JA. Cyclic nucleotide phosphodiesterases: molecular regulation to clinical use. Pharmacol Rev. 2006;58:488-520. Epub 2006/09/14.

196. Kim KS, Lee KW, Lee KW, Im JY, Yoo JY, Kim SW, Lee JK, Nestler EJ, Han PL. Adenylyl cyclase type 5 (AC5) is an essential mediator of morphine action. Proc Natl Acad Sci U S A. 2006;103:3908-13. Epub 2006/03/16.

197. Yoshimura M, Wu PH, Hoffman PL, Tabakoff B. Overexpression of type 7 adenylyl cyclase in the mouse brain enhances acute and chronic actions of morphine. Mol Pharmacol. 2000;58:1011-6. Epub 2000/10/20.

198. Suh H-W, Sim Y-B, Choi Y-S, Song D-K, Kim Y-H. Multiplicative interaction between intrathecally and intracerebroventricularly administered morphine for antinociception in the mouse: Effects of spinally and supraspinally injected 3-isobutyl-l-methylxanthine, cholera toxin, and pertussis toxin. General Pharmacology: The Vascular System. 1995;26:1597-602.

199. Wang JF, Ren MF, Xue JC, Han JS. Cyclic AMP mediates mu and delta, but not kappa opioid analgesia in the spinal cord of the rat. Life Sciences. 1993;52:1955-60.

200. Vetter I, Wyse BD, Monteith GR, Roberts-Thomson SJ, Cabot PJ. The mu opioid agonist morphine modulates potentiation of capsaicin-evoked TRPV1 responses through a cyclic AMP-dependent protein kinase A pathway. Mol Pain. 2006;2:22. Epub 2006/07/18.

201. Endres-Becker J, Heppenstall PA, Mousa SA, Labuz D, Oksche A, Schäfer M, Stein C, Zöllner C. Mu-opioid receptor activation modulates transient receptor potential vanilloid 1 (TRPV1) currents in sensory neurons in a model of inflammatory pain. Mol Pharmacol. 2007;71:12-8. Epub 2006/09/29.

202. Shen J, Benedict Gomes A, Gallagher A, Stafford K, Yoburn BC. Role of cAMP-dependent protein kinase (PKA) in opioid agonist-induced mu-opioid receptor downregulation and tolerance in mice. Synapse. 2000;38:322-7. Epub 2000/10/06.

203. Yang H-Y, Nagpure BV, Bian J-S. Chapter 44 - Opioid Dependence and the Adenylyl Cyclase/cAMP Signaling. In: Preedy VR, editor. Neuropathology of Drug Addictions and Substance Misuse. San Diego: Academic Press; 2016. p. 449-56.

204. Pattinson KTS. Opioids and the control of respiration. BJA: British Journal of Anaesthesia. 2008;100:747-58.

205. Dahan A, van der Schrier R, Smith T, Aarts L, van Velzen M, Niesters M. Averting Opioid-induced Respiratory Depression without Affecting Analgesia. Anesthesiology. 2018;128:1027-37.

206. Arata A, Onimaru H, Homma I. Effects of cAMP on respiratory rhythm generation in brainstem-spinal cord preparation from newborn rat. Brain Research. 1993;605:193-9.

207. Ramirez JM, Burgraff NJ, Wei AD, Baertsch NA, Varga AG, Baghdoyan HA, Lydic R, Morris KF, Bolser DC, Levitt ES. Neuronal mechanisms underlying opioid-induced respiratory depression: our current understanding. J Neurophysiol. 2021;125:1899-919. Epub 2021/04/08.

208. Ballanyi K, Lalley PM, Hoch B, Richter DW. cAMP-dependent reversal of opioid- and prostaglandin-mediated depression of the isolated respiratory network in newborn rats. J Physiol. 1997;504 (Pt 1):127-34. Epub 1997/11/14.

209. Lalley PM. D1-dopamine receptor agonists prevent and reverse opiate depression of breathing but not antinociception in the cat. Am J Physiol Regul Integr Comp Physiol. 2005;289:R45-51. Epub 2005/02/12.

210. Feasel MG, Moran TS, Cheng BC, Averick S. Are carfentanil and acrylfentanyl naloxone resistant? Front Psychiatry. 2024;15:1359851. Epub 2024/03/06.

211. Ramos-Gonzalez N, Groom S, Sutcliffe KJ, Bancroft S, Bailey CP, Sessions RB, Henderson G, Kelly E. Carfentanil is a β-arrestin-biased agonist at the μ opioid receptor. Br J Pharmacol. 2023;180:2341-60. Epub 2023/04/04.

212. Dascal N. Ion-channel regulation by G proteins. Trends Endocrinol Metab. 2001;12:391-8. Epub 2001/10/12.

213. Kim D, Lewis DL, Graziadei L, Neer EJ, Bar-Sagi D, Clapham DE. G-protein βγ-subunits activate the cardiac muscarinic K+-channel via phospholipase A2. Nature. 1989;337:557-60.

214. McCormick DA. CHAPTER 5 - Membrane Potential and Action Potential. In: Byrne JH, Roberts JL, editors. From Molecules to Networks. Burlington: Academic Press; 2004. p. 115-40.

215. Zamponi GW, Snutch TP. Modulation of voltage-dependent calcium channels by G proteins. Curr Opin Neurobiol. 1998;8:351-6. Epub 1998/08/04.

216. Blackmer T, Larsen EC, Bartleson C, Kowalchyk JA, Yoon E-J, Preininger AM, Alford S, Hamm HE, Martin TFJ. G protein βγ directly regulates SNARE protein fusion machinery for secretory granule exocytosis. Nature Neuroscience. 2005;8:421-5.

217. Gerachshenko T, Blackmer T, Yoon EJ, Bartleson C, Hamm HE, Alford S. Gbetagamma acts at the C terminus of SNAP-25 to mediate presynaptic inhibition. Nat Neurosci. 2005;8:597-605. Epub 2005/04/19.

218. Roth BL. Molecular pharmacology of metabotropic receptors targeted by neuropsychiatric drugs. Nat Struct Mol Biol. 2019;26:535-44. Epub 2019/07/05.

219. Che T, Roth BL. Molecular basis of opioid receptor signaling. Cell. 2023;186:5203-19.

220. Torrecilla M, Marker CL, Cintora SC, Stoffel M, Williams JT, Wickman K. G-protein-gated potassium channels containing Kir3.2 and Kir3.3 subunits mediate the acute inhibitory effects of opioids on locus ceruleus neurons. J Neurosci. 2002;22:4328-34. Epub 2002/06/01.

221. Martin-Vega A, Cobb MH. Navigating the ERK1/2 MAPK Cascade. Biomolecules. 2023;13:1555.

222. Ünal EB, Uhlitz F, Blüthgen N. A compendium of ERK targets. FEBS Lett. 2017;591:2607-15. Epub 2017/07/05.

223. Mebratu Y, Tesfaigzi Y. How ERK1/2 activation controls cell proliferation and cell death: Is subcellular localization the answer? Cell Cycle. 2009;8:1168-75. Epub 2009/03/14.

224. Xing J, Ginty DD, Greenberg ME. Coupling of the RAS-MAPK pathway to gene activation by RSK2, a growth factor-regulated CREB kinase. Science. 1996;273:959-63. Epub 1996/08/16.

225. Shaywitz AJ, Greenberg ME. CREB: a stimulus-induced transcription factor activated by a diverse array of extracellular signals. Annu Rev Biochem. 1999;68:821-61. Epub 2000/06/29.

226. Miyatake M, Rubinstein TJ, McLennan GP, Belcheva MM, Coscia CJ. Inhibition of EGF-induced ERK/MAP kinase-mediated astrocyte proliferation by mu opioids: integration of G protein and beta-arrestin 2-dependent pathways. J Neurochem. 2009;110:662-74. Epub 2009/05/22.

227. Belcheva MM, Vogel Z, Ignatova E, Avidor-Reiss T, Zippel R, Levy R, Young EC, Barg J, Coscia CJ. Opioid modulation of extracellular signal-regulated protein kinase activity is ras-dependent and involves Gbetagamma subunits. J Neurochem. 1998;70:635-45. Epub 1998/02/07.

228. Rozenfeld R, Devi LA. Receptor heterodimerization leads to a switch in signaling: beta-arrestin2-mediated ERK activation by mu-delta opioid receptor heterodimers. Faseb j. 2007;21:2455-65. Epub 2007/03/27.

229. Sanchez GA, Jutkiewicz EM, Ingram S, Smrcka AV. Coincident Regulation of PLCβ Signaling by Gq-Coupled and μ-Opioid Receptors Opposes Opioid-Mediated Antinociception. Mol Pharmacol. 2022;102:269-79. Epub 2022/09/19.

230. Bonacci TM, Mathews JL, Yuan C, Lehmann DM, Malik S, Wu D, Font JL, Bidlack JM, Smrcka AV. Differential targeting of Gbetagamma-subunit signaling with small molecules. Science. 2006;312:443-6. Epub 2006/04/22.

231. Smrcka AV, Sternweis PC. Regulation of purified subtypes of phosphatidylinositol-specific phospholipase C beta by G protein alpha and beta gamma subunits. J Biol Chem. 1993;268:9667-74. Epub 1993/05/05.

232. Halls ML, Yeatman HR, Nowell CJ, Thompson GL, Gondin AB, Civciristov S, Bunnett NW, Lambert NA, Poole DP, Canals M. Plasma membrane localization of the μ-opioid receptor controls spatiotemporal signaling. Sci Signal. 2016;9:ra16. Epub 2016/02/11.

233. Belcheva MM, Clark AL, Haas PD, Serna JS, Hahn JW, Kiss A, Coscia CJ. Mu and kappa opioid receptors activate ERK/MAPK via different protein kinase C

isoforms and secondary messengers in astrocytes. J Biol Chem. 2005;280:27662-9. Epub 2005/06/10.

234. Belcheva MM, Szùcs M, Wang D, Sadee W, Coscia CJ. mu-Opioid receptor-mediated ERK activation involves calmodulin-dependent epidermal growth factor receptor transactivation. J Biol Chem. 2001;276:33847-53. Epub 2001/07/18.

235. Zheng H, Loh HH, Law PY. Beta-arrestin-dependent mu-opioid receptor-activated extracellular signal-regulated kinases (ERKs) Translocate to Nucleus in Contrast to G protein-dependent ERK activation. Mol Pharmacol. 2008;73:178-90. Epub 2007/10/20.

236. Blesen Tv, Hawes BE, Luttrell DK, Krueger KM, Touhara K, Porfflri E, Sakaue M, Luttrell LM, Lefkowitz RJ. Receptor-tyrosine-kinase- and Gβγ-mediated MAP kinase activation by a common signalling pathway. Nature. 1995;376:781-4.

237. Koch WJ, Hawes BE, Allen LF, Lefkowitz RJ. Direct evidence that Gi-coupled receptor stimulation of mitogen-activated protein kinase is mediated by G beta gamma activation of p21ras. Proc Natl Acad Sci U S A. 1994;91:12706-10. Epub 1994/12/20.

238. Crespo P, Xu N, Simonds WF, Gutkind JS. Ras-dependent activation of MAP kinase pathway mediated by G-protein βγ subunits. Nature. 1994;369:418-20.

239. Daub H, Weiss FU, Wallasch C, Ullrich A. Role of transactivation of the EGF receptor in signalling by G-protein-coupled receptors. Nature. 1996;379:557-60. Epub 1996/02/08.

240. Mochizuki N, Ohba Y, Kiyokawa E, Kurata T, Murakami T, Ozaki T, Kitabatake A, Nagashima K, Matsuda M. Activation of the ERK/MAPK pathway by an isoform of rap1GAP associated with Gαi. Nature. 1999;400:891-4.

241. Asensio VJ, Miralles A, García-Sevilla JA. Stimulation of mitogen-activated protein kinase kinases (MEK1/2) by mu-, delta- and kappa-opioid receptor agonists in the rat brain: regulation by chronic morphine and opioid withdrawal. Eur J Pharmacol. 2006;539:49-56. Epub 2006/05/09.

242. Macey TA, Bobeck EN, Hegarty DM, Aicher SA, Ingram SL, Morgan MM. Extracellular signal-regulated kinase 1/2 activation counteracts morphine tolerance in the periaqueductal gray of the rat. J Pharmacol Exp Ther. 2009;331:412-8. Epub 2009/08/18.

243. Gabra BH, Bailey CP, Kelly E, Smith FL, Henderson G, Dewey WL. Pre-treatment with a PKC or PKA inhibitor prevents the development of morphine tolerance but not physical dependence in mice. Brain Res. 2008;1217:70-7. Epub 2008/05/27.

244. Bailey CP, Llorente J, Gabra BH, Smith FL, Dewey WL, Kelly E, Henderson G. Role of protein kinase C and mu-opioid receptor (MOPr) desensitization in tolerance to morphine in rat locus coeruleus neurons. Eur J Neurosci. 2009;29:307-18. Epub 2009/02/10.

245. Smrcka AV, Lehmann DM, Dessal AL. G protein betagamma subunits as targets for small molecule therapeutic development. Comb Chem High Throughput Screen. 2008;11:382-95. Epub 2008/06/10.

246. Xie W, Samoriski GM, McLaughlin JP, Romoser VA, Smrcka A, Hinkle PM, Bidlack JM, Gross RA, Jiang H, Wu D. Genetic alteration of phospholipase C beta3 expression modulates behavioral and cellular responses to mu opioids. Proc Natl Acad Sci U S A. 1999;96:10385-90. Epub 1999/09/01.

247. Darcq E, Befort K, Koebel P, Pannetier S, Mahoney MK, Gaveriaux-Ruff C, Hanauer A, Kieffer BL. RSK2 Signaling in Medial Habenula Contributes to Acute Morphine Analgesia. Neuropsychopharmacology. 2012;37:1288-96.

248. Williams JT, Ingram SL, Henderson G, Chavkin C, von Zastrow M, Schulz S, Koch T, Evans CJ, Christie MJ. Regulation of μ-opioid receptors: desensitization, phosphorylation, internalization, and tolerance. Pharmacol Rev. 2013;65:223-54. Epub 2013/01/17.

249. Zhang L, Yu Y, Mackin S, Weight FF, Uhl GR, Wang JB. Differential mu opiate receptor phosphorylation and desensitization induced by agonists and phorbol esters. J Biol Chem. 1996;271:11449-54. Epub 1996/05/10.

250. Chakrabarti S, Law PY, Loh HH. Distinct differences between morphine- and [D-Ala2,N-MePhe4,Gly-ol5]-enkephalin-mu-opioid receptor complexes demonstrated by cyclic AMP-dependent protein kinase phosphorylation. J Neurochem. 1998;71:231-9. Epub 1998/07/02.

251. Sibley DR, Lefkowitz RJ. Molecular mechanisms of receptor desensitization using the beta-adrenergic receptor-coupled adenylate cyclase system as a model. Nature. 1985;317:124-9. Epub 1985/09/12.

252. Gurevich VV, Gurevich EV. GPCR Signaling Regulation: The Role of GRKs and Arrestins. Front Pharmacol. 2019;10:125. Epub 2019/03/07.

253. Sulon SM, Benovic JL. Targeting G protein-coupled receptor kinases (GRKs) to G protein-coupled receptors. Curr Opin Endocr Metab Res. 2021;16:56-65. Epub 2021/03/16.

254. Kelly E, Bailey CP, Henderson G. Agonist-selective mechanisms of GPCR desensitization. Br J Pharmacol. 2008;153 Suppl 1:S379-88. Epub 2007/12/07.

255. Zidar DA, Violin JD, Whalen EJ, Lefkowitz RJ. Selective engagement of G protein coupled receptor kinases (GRKs) encodes distinct functions of biased ligands. Proc Natl Acad Sci U S A. 2009;106:9649-54. Epub 2009/06/06.

256. Illing S, Mann A, Schulz S. Heterologous regulation of agonist-independent μ-opioid receptor phosphorylation by protein kinase C. Br J Pharmacol. 2014;171:1330-40. Epub 2013/12/07.

257. El Kouhen R, Burd AL, Erickson-Herbrandson LJ, Chang CY, Law PY, Loh HH. Phosphorylation of Ser363, Thr370, and Ser375 residues within the carboxyl tail differentially regulates mu-opioid receptor internalization. J Biol Chem. 2001;276:12774-80. Epub 2001/03/30.

258. Schulz S, Mayer D, Pfeiffer M, Stumm R, Koch T, Höllt V. Morphine induces terminal micro-opioid receptor desensitization by sustained phosphorylation of serine-375. Embo j. 2004;23:3282-9. Epub 2004/07/24.

259. Chen YJ, Oldfield S, Butcher AJ, Tobin AB, Saxena K, Gurevich VV, Benovic JL, Henderson G, Kelly E. Identification of phosphorylation sites in the COOH-terminal tail of the μ-opioid receptor. J Neurochem. 2013;124:189-99. Epub 2012/10/31.

260. Lau EK, Trester-Zedlitz M, Trinidad JC, Kotowski SJ, Krutchinsky AN, Burlingame AL, von Zastrow M. Quantitative encoding of the effect of a partial agonist on individual opioid receptors by multisite phosphorylation and threshold detection. Sci Signal. 2011;4:ra52. Epub 2011/08/27.

261. Doll C, Konietzko J, Pöll F, Koch T, Höllt V, Schulz S. Agonist-selective patterns of μ-opioid receptor phosphorylation revealed by phosphosite-specific antibodies. Br J Pharmacol. 2011;164:298-307. Epub 2011/04/01.

262. Just S, Illing S, Trester-Zedlitz M, Lau EK, Kotowski SJ, Miess E, Mann A, Doll C, Trinidad JC, Burlingame AL, von Zastrow M, Schulz S. Differentiation of opioid drug effects by hierarchical multi-site phosphorylation. Mol Pharmacol. 2013;83:633-9. Epub 2012/12/15.

263. Mann A, Illing S, Miess E, Schulz S. Different mechanisms of homologous and heterologous μ-opioid receptor phosphorylation. Br J Pharmacol. 2015;172:311-6. Epub 2014/02/13.

264. McPherson J, Rivero G, Baptist M, Llorente J, Al-Sabah S, Krasel C, Dewey WL, Bailey CP, Rosethorne EM, Charlton SJ, Henderson G, Kelly E. μ-opioid receptors: correlation of agonist efficacy for signalling with ability to activate internalization. Mol Pharmacol. 2010;78:756-66. Epub 2010/07/22.

265. Doll C, Pöll F, Peuker K, Loktev A, Glück L, Schulz S. Deciphering μ-opioid receptor phosphorylation and dephosphorylation in HEK293 cells. Br J Pharmacol. 2012;167:1259-70. Epub 2012/06/26.

266. Isberg V, Mordalski S, Munk C, Rataj K, Harpsøe K, Hauser AS, Vroling B, Bojarski AJ, Vriend G, Gloriam DE. GPCRdb: an information system for G protein-coupled receptors. Nucleic Acids Research. 2015;44:D356-D64.

267. Kooistra AJ, Mordalski S, Pándy-Szekeres G, Esguerra M, Mamyrbekov A, Munk C, Keserű GM, Gloriam David E. GPCRdb in 2021: integrating GPCR sequence, structure and function. Nucleic Acids Research. 2020;49:D335-D43.

268. Ferguson SSG. Evolving Concepts in G Protein-Coupled Receptor Endocytosis: The Role in Receptor Desensitization and Signaling. Pharmacological Reviews. 2001;53:1-24.

269. Ferguson SS. Evolving concepts in G protein-coupled receptor endocytosis: the role in receptor desensitization and signaling. Pharmacol Rev. 2001;53:1-24. Epub 2001/02/15.

270. Yousuf A, Miess E, Sianati S, Du Y-p, Schulz S, Christie MJ. Role of Phosphorylation Sites in Desensitization of μ-Opioid Receptor. Molecular Pharmacology. 2015;88:825 - 35.

271. DeWire SM, Ahn S, Lefkowitz RJ, Shenoy SK. Beta-arrestins and cell signaling. Annu Rev Physiol. 2007;69:483-510. Epub 2007/02/20.

272. Srivastava A, Gupta B, Gupta C, Shukla AK. Emerging Functional Divergence of β-Arrestin Isoforms in GPCR Function. Trends Endocrinol Metab. 2015;26:628-42. Epub 2015/10/17.

273. Raehal KM, Bohn LM. β-arrestins: regulatory role and therapeutic potential in opioid and cannabinoid receptor-mediated analgesia. Handb Exp Pharmacol. 2014;219:427-43. Epub 2013/12/03.

274. Lefkowitz RJ. G protein-coupled receptors. III. New roles for receptor kinases and beta-arrestins in receptor signaling and desensitization. J Biol Chem. 1998;273:18677-80. Epub 1998/07/21.

275. Lohse MJ, Benovic JL, Codina J, Caron MG, Lefkowitz RJ. beta-Arrestin: a protein that regulates beta-adrenergic receptor function. Science. 1990;248:1547-50. Epub 1990/06/22.

276. Attramadal H, Arriza JL, Aoki C, Dawson TM, Codina J, Kwatra MM, Snyder SH, Caron MG, Lefkowitz RJ. Beta-arrestin2, a novel member of the arrestin/beta-arrestin gene family. J Biol Chem. 1992;267:17882-90. Epub 1992/09/05.

277. Mafi A, Kim S-K, Goddard WA. Mechanism of β-arrestin recruitment by the μ-opioid G protein-coupled receptor. Proceedings of the National Academy of Sciences. 2020;117:16346-55.

278. Kohout TA, Lin FS, Perry SJ, Conner DA, Lefkowitz RJ. beta-Arrestin 1 and 2 differentially regulate heptahelical receptor signaling and trafficking. Proc Natl Acad Sci U S A. 2001;98:1601-6. Epub 2001/02/15.

279. Shenoy SK, Lefkowitz RJ. β-Arrestin-mediated receptor trafficking and signal transduction. Trends Pharmacol Sci. 2011;32:521-33. Epub 2011/06/18.

280. Ferguson SS, Downey WE, 3rd, Colapietro AM, Barak LS, Ménard L, Caron MG. Role of beta-arrestin in mediating agonist-promoted G protein-coupled receptor internalization. Science. 1996;271:363-6. Epub 1996/01/19.

281. Oakley RH, Laporte SA, Holt JA, Barak LS, Caron MG. Association of beta-arrestin with G protein-coupled receptors during clathrin-mediated endocytosis dictates the profile of receptor resensitization. J Biol Chem. 1999;274:32248-57. Epub 1999/11/05.

282. Laporte SA, Oakley RH, Zhang J, Holt JA, Ferguson SS, Caron MG, Barak LS. The beta2-adrenergic receptor/betaarrestin complex recruits the clathrin adaptor AP-2 during endocytosis. Proc Natl Acad Sci U S A. 1999;96:3712-7. Epub 1999/03/31.

283. Goodman OB, Jr., Krupnick JG, Santini F, Gurevich VV, Penn RB, Gagnon AW, Keen JH, Benovic JL. Beta-arrestin acts as a clathrin adaptor in endocytosis of the beta2-adrenergic receptor. Nature. 1996;383:447-50. Epub 1996/10/03.

284. Tian X, Kang DS, Benovic JL. β-arrestins and G protein-coupled receptor trafficking. Handb Exp Pharmacol. 2014;219:173-86. Epub 2013/12/03.

285. Kaksonen M, Roux A. Mechanisms of clathrin-mediated endocytosis. Nature Reviews Molecular Cell Biology. 2018;19:313-26.

286. Chu P, Murray S, Lissin D, von Zastrow M. Delta and kappa opioid receptors are differentially regulated by dynamin-dependent endocytosis when activated by the same alkaloid agonist. J Biol Chem. 1997;272:27124-30. Epub 1997/10/27.

287. Zastrow Mv, Svingos A, Haberstock-Debic H, Evans C. Regulated endocytosis of opioid receptors: cellular mechanisms and proposed roles in physiological adaptation to opiate drugs. Current Opinion in Neurobiology. 2003;13:348-53.

288. DeFea KA, Zalevsky J, Thoma MS, Déry O, Mullins RD, Bunnett NW. beta-arrestin-dependent endocytosis of proteinase-activated receptor 2 is required for intracellular targeting of activated ERK1/2. J Cell Biol. 2000;148:1267-81. Epub 2000/03/22.

289. Luttrell LM, Roudabush FL, Choy EW, Miller WE, Field ME, Pierce KL, Lefkowitz RJ. Activation and targeting of extracellular signal-regulated kinases by beta-arrestin scaffolds. Proc Natl Acad Sci U S A. 2001;98:2449-54. Epub 2001/02/28.

290. Miller WE, Lefkowitz RJ. Expanding roles for beta-arrestins as scaffolds and adapters in GPCR signaling and trafficking. Curr Opin Cell Biol. 2001;13:139-45. Epub 2001/03/15.

291. Luttrell LM, Miller WE. Arrestins as regulators of kinases and phosphatases. Prog Mol Biol Transl Sci. 2013;118:115-47. Epub 2013/06/15.

292. Shenoy SK, Drake MT, Nelson CD, Houtz DA, Xiao K, Madabushi S, Reiter E, Premont RT, Lichtarge O, Lefkowitz RJ. beta-arrestin-dependent, G protein-independent ERK1/2 activation by the beta2 adrenergic receptor. J Biol Chem. 2006;281:1261-73. Epub 2005/11/11.

293. Macey TA, Lowe JD, Chavkin C. Mu opioid receptor activation of ERK1/2 is GRK3 and arrestin dependent in striatal neurons. J Biol Chem. 2006;281:34515-24. Epub 2006/09/20.

294. Gurevich VV, Gurevich EV. Overview of different mechanisms of arrestin-mediated signaling. Curr Protoc Pharmacol. 2014;67:2.10.1-2..9. Epub 2014/12/03.

295. Qu C, Park JY, Yun MW, He QT, Yang F, Kim K, Ham D, Li RR, Iverson TM, Gurevich VV, Sun JP, Chung KY. Scaffolding mechanism of arrestin-2 in the cRaf/MEK1/ERK signaling cascade. Proc Natl Acad Sci U S A. 2021;118. Epub 2021/09/12.

296. Bohn LM, Lefkowitz RJ, Gainetdinov RR, Peppel K, Caron MG, Lin FT. Enhanced morphine analgesia in mice lacking beta-arrestin 2. Science. 1999;286:2495-8. Epub 2000/01/05.

297. Bohn LM, Lefkowitz RJ, Caron MG. Differential mechanisms of morphine antinociceptive tolerance revealed in (beta)arrestin-2 knock-out mice. J Neurosci. 2002;22:10494-500. Epub 2002/11/27.

298. Li Y, Liu X, Liu C, Kang J, Yang J, Pei G, Wu C. Improvement of morphine-mediated analgesia by inhibition of β-arrestin2 expression in mice periaqueductal gray matter. Int J Mol Sci. 2009;10:954-63. Epub 2009/04/29.

299. Raehal KM, Bohn LM. The role of beta-arrestin2 in the severity of antinociceptive tolerance and physical dependence induced by different opioid pain therapeutics. Neuropharmacology. 2011;60:58-65. Epub 2010/08/18.

300. Miess E, Gondin AB, Yousuf A, Steinborn R, Mösslein N, Yang Y, Göldner M, Ruland JG, Bünemann M, Krasel C, Christie MJ, Halls ML, Schulz S, Canals M. Multisite phosphorylation is required for sustained interaction with GRKs and arrestins during rapid μ-opioid receptor desensitization. Sci Signal. 2018;11. Epub 2018/07/19.

301. Bohn LM, Gainetdinov RR, Lin FT, Lefkowitz RJ, Caron MG. Mu-opioid receptor desensitization by beta-arrestin-2 determines morphine tolerance but not dependence. Nature. 2000;408:720-3. Epub 2000/12/29.

302. Keith DE, Murray SR, Zaki PA, Chu PC, Lissin DV, Kang L, Evans CJ, von Zastrow M. Morphine activates opioid receptors without causing their rapid internalization. J Biol Chem. 1996;271:19021-4. Epub 1996/08/09.

303. Zhang J, Ferguson SS, Barak LS, Bodduluri SR, Laporte SA, Law PY, Caron MG. Role for G protein-coupled receptor kinase in agonist-specific regulation of mu-opioid receptor responsiveness. Proc Natl Acad Sci U S A. 1998;95:7157-62. Epub 1998/06/17.

304. Whistler JL, von Zastrow M. Morphine-activated opioid receptors elude desensitization by beta-arrestin. Proc Natl Acad Sci U S A. 1998;95:9914-9. Epub 1998/08/26.

305. Morgan MM, Christie MJ. Analysis of opioid efficacy, tolerance, addiction and dependence from cell culture to human. Br J Pharmacol. 2011;164:1322-34. Epub 2011/03/26.

306. Raehal KM, Walker JK, Bohn LM. Morphine side effects in beta-arrestin 2 knockout mice. J Pharmacol Exp Ther. 2005;314:1195-201. Epub 2005/05/27.

307. Koch T, Widera A, Bartzsch K, Schulz S, Brandenburg L-O, Wundrack N, Beyer A, Grecksch G, Höllt V. Receptor Endocytosis Counteracts the Development of Opioid Tolerance. Molecular Pharmacology. 2005;67:280-7.

308. Wootten D, Christopoulos A, Marti-Solano M, Babu MM, Sexton PM. Mechanisms of signalling and biased agonism in G protein-coupled receptors. Nat Rev Mol Cell Biol. 2018;19:638-53. Epub 2018/08/15.

309. Jean-Charles PY, Kaur S, Shenoy SK. G Protein-Coupled Receptor Signaling Through β-Arrestin-Dependent Mechanisms. J Cardiovasc Pharmacol. 2017;70:142-58. Epub 2017/03/23.

310. Che T, Dwivedi-Agnihotri H, Shukla AK, Roth BL. Biased ligands at opioid receptors: Current status and future directions. Sci Signal. 2021;14. Epub 2021/04/08.

311. de Waal PW, Shi J, You E, Wang X, Melcher K, Jiang Y, Xu HE, Dickson BM. Molecular mechanisms of fentanyl mediated β-arrestin biased signaling. PLoS Comput Biol. 2020;16:e1007394. Epub 2020/04/11.

312. Groer CE, Tidgewell K, Moyer RA, Harding WW, Rothman RB, Prisinzano TE, Bohn LM. An opioid agonist that does not induce mu-opioid receptor--arrestin interactions or receptor internalization. Mol Pharmacol. 2007;71:549-57. Epub 2006/11/09.

313. Manglik A, Lin H, Aryal DK, McCorvy JD, Dengler D, Corder G, Levit A, Kling RC, Bernat V, Hübner H, Huang X-P, Sassano MF, Giguère PM, Löber S, Da D, Scherrer G, Kobilka BK, Gmeiner P, Roth BL, Shoichet BK. Structure-based discovery of opioid analgesics with reduced side effects. Nature. 2016;537:185-90.

314. Singla N, Minkowitz HS, Soergel DG, Burt DA, Subach RA, Salamea MY, Fossler MJ, Skobieranda F. A randomized, Phase IIb study investigating oliceridine (TRV130), a novel μ-receptor G-protein pathway selective (μ-GPS) modulator, for the management of moderate to severe acute pain following abdominoplasty. J Pain Res. 2017;10:2413-24. Epub 2017/10/25.

315. Xia J, Li X, Zhu H, Zhou X, Chen J, Li Q, Li S, Chu H, Dong M. The μ-opioid receptor-mediated Gi/o protein and β-arrestin2 signaling pathways both contribute to morphine-induced side effects. European Journal of Pharmacology. 2024;966:176333.

316. Kliewer A, Schmiedel F, Sianati S, Bailey A, Bateman JT, Levitt ES, Williams JT, Christie MJ, Schulz S. Phosphorylation-deficient G-protein-biased μ-opioid receptors improve analgesia and diminish tolerance but worsen opioid side effects. Nat Commun. 2019;10:367. Epub 2019/01/22.

317. Bachmutsky I, Wei XP, Durand A, Yackle K. ß-arrestin 2 germline knockout does not attenuate opioid respiratory depression. Elife. 2021;10. Epub 2021/05/19.

318. Kelly E, Conibear A, Henderson G. Biased Agonism: Lessons from Studies of Opioid Receptor Agonists. Annual Review of Pharmacology and Toxicology. 2023;63:491-515.

319. Gillis A, Christie MJ. Opioid overdose and tolerance: is the recruitment of β-arrestin to the μ-receptor involved? Neuropsychopharmacology. 2021;46:2226-7. Epub 2021/08/18.

320. Mullard A. FDA approves first GPCR biased agonist. Nat Rev Drug Discov. 2020;19:659. Epub 2020/09/05.

321. Altarifi AA, David B, Muchhala KH, Blough BE, Akbarali H, Negus SS. Effects of acute and repeated treatment with the biased mu opioid receptor agonist TRV130 (oliceridine) on measures of antinociception, gastrointestinal function, and abuse liability in rodents. J Psychopharmacol. 2017;31:730-9. Epub 2017/02/02.

322. Goodman AJ, Le Bourdonnec B, Dolle RE. Mu Opioid Receptor Antagonists: Recent Developments. ChemMedChem. 2007;2:1552-70.

323. Manglik A, Kruse AC, Kobilka TS, Thian FS, Mathiesen JM, Sunahara RK, Pardo L, Weis WI, Kobilka BK, Granier S. Crystal structure of the μ-opioid receptor bound to a morphinan antagonist. Nature. 2012;485:321-6.

324. Theriot J SS, Azadfard M. Opioid Antagonists: StatPearls Publishing; 2023.

325. Minozzi S, Amato L, Vecchi S, Davoli M, Kirchmayer U, Verster A. Oral naltrexone maintenance treatment for opioid dependence. Cochrane Database Syst Rev. 2011;2011:Cd001333. Epub 2011/04/15.

326. Kirchmayer U, Davoli M, Verster A. Naltrexone maintenance treatment for opioid dependence. Cochrane Database Syst Rev. 2002:Cd001333. Epub 2002/06/22.

327. Fujimoto JM. Isolation of Naloxone-3-glucuronide from Human Urine. Proceedings of the Society for Experimental Biology and Medicine. 1970;133:317-9.

328. Tylleskar I, Skarra S, Skulberg AK, Dale O. The pharmacokinetic interaction between nasally administered naloxone and the opioid remifentanil in human volunteers. Eur J Clin Pharmacol. 2021;77:1901-8. Epub 2021/07/31.

329. Saari TI, Strang J, Dale O. Clinical Pharmacokinetics and Pharmacodynamics of Naloxone. Clin Pharmacokinet. 2024;63:397-422. Epub 2024/03/15.

330. Schiller EY GA, Mechanic OJ. Opioid Overdose. : StatPearls Publishing; 2023.

331. Longnecker DE, Grazis PA, Eggers GW, Jr. Naloxone for antagonism of morphine-induced respiratory depression. Anesth Analg. 1973;52:447-53. Epub 1973/05/01.

332. Johnstone RE, Jobes DR, Kennell EM, Behar MG, Smith TC. Reversal of morphine anesthesia with naloxone. Anesthesiology. 1974;41:361-7. Epub 1974/10/01.

333. Lavonas EJ, Drennan IR, Gabrielli A, Heffner AC, Hoyte CO, Orkin AM, Sawyer KN, Donnino MW. Part 10: Special Circumstances of Resuscitation. Circulation. 2015;132:S501-S18.

334. (FDA) USFaDA. FDA Approves First Over-the-Counter Naloxone Nasal Spray. 2023.

335. Commission EMAEE. Nyxoid – European Commission Authorization Document. n.d.

336. Torralva R, Janowsky A. Noradrenergic Mechanisms in Fentanyl-Mediated Rapid Death Explain Failure of Naloxone in the Opioid Crisis. J Pharmacol Exp Ther. 2019;371:453-75. Epub 2019/09/08.

337. Moss RB, Carlo DJ. Higher doses of naloxone are needed in the synthetic opiod era. Subst Abuse Treat Prev Policy. 2019;14:6. Epub 2019/02/20.

338. Somerville NJ, O'Donnell J, Gladden RM, Zibbell JE, Green TC, Younkin M, Ruiz S, Babakhanlou-Chase H, Chan M, Callis BP, Kuramoto-Crawford J, Nields HM, Walley AY. Characteristics of Fentanyl Overdose - Massachusetts, 2014-2016. MMWR Morb Mortal Wkly Rep. 2017;66:382-6. Epub 2017/04/14.

339. Sutter ME, Gerona RR, Davis MT, Roche BM, Colby DK, Chenoweth JA, Adams AJ, Owen KP, Ford JB, Black HB, Albertson TE. Fatal Fentanyl: One Pill Can Kill. Academic Emergency Medicine. 2017;24:106-13.

340. Kuip EJ, Zandvliet ML, Koolen SL, Mathijssen RH, van der Rijt CC. A review of factors explaining variability in fentanyl pharmacokinetics; focus on implications for cancer patients. Br J Clin Pharmacol. 2017;83:294-313. Epub 2016/10/30.

341. Rzasa Lynn R, Galinkin J. Naloxone dosage for opioid reversal: current evidence and clinical implications. Therapeutic Advances in Drug Safety. 2018;9:63-88.

342. Moss RB, Pryor MM, Baillie R, Kudrycki K, Friedrich C, Reed M, Carlo DJ. Higher naloxone dosing in a quantitative systems pharmacology model that predicts naloxone-fentanyl competition at the opioid mu receptor level. PLoS One. 2020;15:e0234683. Epub 2020/06/17.

343. Tanz LJ SA, Gladden RM, Ko JY, Owens L, O'Donnell J. Detection of Illegally Manufactured Fentanyls and Carfentanil in Drug Overdose Deaths — United States, 2021–2024. . 2024.

344. Lemen PM, Garrett DP, Thompson E, Aho M, Vasquez C, Park JN. High-Dose Naloxone Formulations Are Not as Essential as We Thought. medRxiv. 2023. Epub 2023/08/30.

345. Wong B, Perkins MW, Tressler J, Rodriguez A, Devorak J, Sciuto AM. Effects of inhaled aerosolized carfentanil on real-time physiological responses in mice: a preliminary evaluation of naloxone. Inhal Toxicol. 2017;29:65-74. Epub 2017/03/24.

346. Fairbairn N, Coffin PO, Walley AY. Naloxone for heroin, prescription opioid, and illicitly made fentanyl overdoses: Challenges and innovations responding to a dynamic epidemic. Int J Drug Policy. 2017;46:172-9. Epub 2017/07/09.

347. Zuckerman M, Weisberg SN, Boyer EW. Pitfalls of intranasal naloxone. Prehosp Emerg Care. 2014;18:550-4. Epub 2014/05/17.

348. Infante AF, Elmes AT, Gimbar RP, Messmer SE, Neeb C, Jarrett JB. Stronger, longer, better opioid antagonists? Nalmefene is NOT a naloxone replacement. International Journal of Drug Policy. 2024;124:104323.

349. Harris E. FDA Approves Nalmefene, a Longer-Lasting Opioid Reversal Nasal Spray. Jama. 2023;329:2012. Epub 2023/05/31.

350. Osborn MD, Lowery JJ, Skorput AG, Giuvelis D, Bilsky EJ. In vivo characterization of the opioid antagonist nalmefene in mice. Life Sci. 2010;86:624-30. Epub 2010/02/18.

351. Hill LG, Zagorski CM, Loera LJ. Increasingly powerful opioid antagonists are not necessary. Int J Drug Policy. 2022;99:103457. Epub 2021/09/25.

352. Edinoff AN, Nix CA, Reed TD, Bozner EM, Alvarez MR, Fuller MC, Anwar F, Cornett EM, Kaye AM, Kaye AD. Pharmacologic and Clinical Considerations of Nalmefene, a Long Duration Opioid Antagonist, in Opioid Overdose. Psychiatry International. 2021;2:365-78.

353. Morell A, Terry WD, Waldmann TA. Metabolic properties of IgG subclasses in man. J Clin Invest. 1970;49:673-80. Epub 1970/04/01.

354. Mould DR, Sweeney KR. The pharmacokinetics and pharmacodynamics of monoclonal antibodies--mechanistic modeling applied to drug development. Curr Opin Drug Discov Devel. 2007;10:84-96. Epub 2007/02/03.

355. Robinson C, Gradinati V, Hamid F, Baehr C, Crouse B, Averick S, Kovaliov M, Harris D, Runyon S, Baruffaldi F, LeSage M, Comer S, Pravetoni M. Therapeutic and Prophylactic Vaccines to Counteract Fentanyl Use Disorders and Toxicity. J Med Chem. 2020;63:14647-67. Epub 2020/11/21.

356. Raleigh MD, King SJ, Baruffaldi F, Saykao A, Hamid FA, Winston S, LeSage MG, Pentel PR, Pravetoni M. Pharmacological mechanisms underlying the efficacy of antibodies generated by a vaccine to treat oxycodone use disorder. Neuropharmacology. 2021;195:108653. Epub 2021/06/15.

357. Clementi ME, Marini S, Condò SG, Giardina B. Antibodies against small molecules. Ann Ist Super Sanita. 1991;27:139-43. Epub 1991/01/01.

358. Britannica E. Hapten n.d. [10.01.2025]. Available from: https://www.britannica.com/science/hapten.

359. Smith LC, Bremer PT, Hwang CS, Zhou B, Ellis B, Hixon MS, Janda KD. Monoclonal Antibodies for Combating Synthetic Opioid Intoxication. J Am Chem Soc. 2019;141:10489-503. Epub 2019/06/13.

360. Vergara U, Tam JP. A novel design of peptide immunogens: synthetic peptide with a reversible handle for the attachment to protein carriers. Pept Res. 1989;2:134-9. Epub 1989/01/01.

361. Briand JP, Muller S, Van Regenmortel MH. Synthetic peptides as antigens: pitfalls of conjugation methods. J Immunol Methods. 1985;78:59-69. Epub 1985/04/08.

362. Deng K, Xu Z, Chen M, Liu X. Keyhole Limpet Hemocyanin-Conjugated Peptides from Hepatitis C Virus Glycoproteins Elicit Neutralizing Antibodies in BALB/c Mice. J Immunol Res. 2021;2021:3108157. Epub 2021/02/04.

363. Zhang Y, Cao P, Lu F, Yan X, Jiang B, Cheng J, Qu H. Generation of Monoclonal Antibodies Against Natural Products: 1940-087X; 2019.

364. Murphy K, Weaver C. Janeway's immunobiology: Garland science; 2016.

365. Triller G, Vlachou EP, Hashemi H, van Straaten M, Zeelen JP, Kelemen Y, Baehr C, Marker CL, Ruf S, Svirina A, Chandra M, Urban K, Gkeka A, Kruse S, Baumann A, Miller AK, Bartel M, Pravetoni M, Stebbins CE, Papavasiliou FN, Verdi JP. A trypanosome-derived immunotherapeutics platform elicits potent high-affinity antibodies, negating the effects of the synthetic opioid fentanyl. Cell Rep. 2023;42:112049. Epub 2023/02/01.

366. Torten M, Miller CH, Eisele JH, Henderson GL, Benjamini E. Prevention of the effects of fentanyl by immunological means. Nature. 1975;253:565-6.

367. Baehr C, Kelcher AH, Khaimraj A, Reed DE, Pandit SG, AuCoin D, Averick S, Pravetoni M. Monoclonal Antibodies Counteract Opioid-Induced Behavioral and Toxic Effects in Mice and Rats. J Pharmacol Exp Ther. 2020;375:469-77. Epub 2020/09/28.

368. Ban B, Barrientos RC, Oertel T, Komla E, Whalen C, Sopko M, You Y, Banerjee P, Sulima A, Jacobson AE, Rice KC, Matyas GR, Yusibov V. Novel chimeric monoclonal antibodies that block fentanyl effects and alter fentanyl biodistribution in mice. MAbs. 2021;13:1991552. Epub 2021/10/26.

369. Eubanks LM, Pholcharee T, Oyen D, Natori Y, Zhou B, Wilson IA, Janda KD. An Engineered Human-Antibody Fragment with Fentanyl Pan-Specificity That Reverses Carfentanil-Induced Respiratory Depression. ACS Chem Neurosci. 2023;14:2849-56. Epub 2023/08/03.

370. Bremer PT, Burke EL, Barrett AC, Desai RI. Investigation of monoclonal antibody CSX-1004 for fentanyl overdose. Nature Communications. 2023;14:7700.

371. Phase 1A/1B Clinical Trials of Multivalent Opioid Vaccine Components [Published2020. Available from: https://clinicaltrials.gov/study/NCT04458545.

372. Therapeutics I. A Phase 2 Study Evaluating IXT-m200 in Methamphetamine Use Disorder. ClinicalTrials.gov, 2021.

373. Wetzel HN, Webster RP, Saeed FO, Kirley TL, Ball WJ, Norman AB. Characterization of a recombinant humanized anti-cocaine monoclonal antibody produced from multiple clones for the selection of a master cell bank candidate. Biochem Biophys Res Commun. 2017;487:690-4. Epub 2017/04/27.

374. Koch T, Seifert A, Wu DF, Rankovic M, Kraus J, Börner C, Brandenburg LO, Schröder H, Höllt V. mu-opioid receptor-stimulated synthesis of reactive oxygen species is mediated via phospholipase D2. J Neurochem. 2009;110:1288-96. Epub 2009/06/13.

375. Hotchkiss RD. Bacterial transformation. J Cell Physiol Suppl. 1955;45:1-22. Epub 1955/05/01.

376. Bertani G. Studies on lysogenesis. I. The mode of phage liberation by lysogenic Escherichia coli. J Bacteriol. 1951;62:293-300. Epub 1951/09/01.

377. Graham FL, Smiley J, Russell WC, Nairn R. Characteristics of a human cell line transformed by DNA from human adenovirus type 5. J Gen Virol. 1977;36:59-74. Epub 1977/07/01.

378. Louis N, Evelegh C, Graham FL. Cloning and sequencing of the cellular-viral junctions from the human adenovirus type 5 transformed 293 cell line. Virology. 1997;233:423-9. Epub 1997/07/07.

379. Olsen PA, Krauss S. The Adenoviral E1B-55k Protein Present in HEK293 Cells Mediates Abnormal Accumulation of Key WNT Signaling Proteins in Large Cytoplasmic Aggregates. Genes (Basel). 2021;12. Epub 2021/12/25.

380. Blackford AN, Grand RJ. Adenovirus E1B 55-kilodalton protein: multiple roles in viral infection and cell transformation. J Virol. 2009;83:4000-12. Epub 2009/02/13.

381. Thomas P, Smart TG. HEK293 cell line: a vehicle for the expression of recombinant proteins. J Pharmacol Toxicol Methods. 2005;51:187-200. Epub 2005/05/03.

382. Yokoyama WM, Thompson ML, Ehrhardt RO. Cryopreservation and thawing of cells. Curr Protoc Immunol. 2012;Appendix 3:A.3g.1-a.3g.5. Epub 2012/11/07.

383. Casademunt E, Martinelle K, Jernberg M, Winge S, Tiemeyer M, Biesert L, Knaub S, Walter O, Schröder C. The first recombinant human coagulation factor VIII of human origin: human cell line and manufacturing characteristics. Eur J Haematol. 2012;89:165-76. Epub 2012/06/14.

384. Stauderman KA, Mahaffy LS, Akong M, Veliçelebi G, Chavez-Noriega LE, Crona JH, Johnson EC, Elliott KJ, Gillespie A, Reid RT, Adams P, Harpold MM, Corey-Naeve J. Characterization of human recombinant neuronal nicotinic acetylcholine receptor subunit combinations alpha2beta4, alpha3beta4 and alpha4beta4 stably expressed in HEK293 cells. J Pharmacol Exp Ther. 1998;284:777-89. Epub 1998/03/07.

385. Invitrogen. User manual pcDNA ™ 4/myc-His A, B, and C (Catalog no. V863-20). 2010.

386. Drocourt D, Calmels T, Reynes JP, Baron M, Tiraby G. Cassettes of the Streptoalloteichus hindustanus ble gene for transformation of lower and higher eukaryotes to phleomycin resistance. Nucleic Acids Res. 1990;18:4009. Epub 1990/07/11.

387. Schmid CL, Kennedy NM, Ross NC, Lovell KM, Yue Z, Morgenweck J, Cameron MD, Bannister TD, Bohn LM. Bias Factor and Therapeutic Window Correlate to Predict Safer Opioid Analgesics. Cell. 2017;171:1165-75.e13. Epub 2017/11/18.

388. Eppendorf. Stable vs. transient protein expression systems n.d. [cited 2024 20.11.2024]. Available from: https://online-shop.eppendorf.com.

389. Scientific TF. Transient transfection n.d. [20.11.2024]. Available from: https://www.thermofisher.com.

390. Breit A, Lagacé M, Bouvier M. Hetero-oligomerization between β2- and β3-Adrenergic Receptors Generates a β-Adrenergic Signaling Unit with Distinct Functional Properties*. Journal of Biological Chemistry. 2004;279:28756-65.

391. Barrera V, Rathbone S, Joseph A, Rooney P. 26 Development of human amniotic membrane products for regenerative medicine applications. BMJ Open Ophthalmol. 2022;7:A11. Epub 2023/06/07.

392. Kielkopf CL, Bauer W, Urbatsch IL. Bradford Assay for Determining Protein Concentration. Cold Spring Harb Protoc. 2020;2020:102269. Epub 2020/04/03.

393. Bradford MM. A rapid and sensitive method for the quantitation of microgram quantities of protein utilizing the principle of protein-dye binding. Anal Biochem. 1976;72:248-54. Epub 1976/05/07.

394. Kruger NJ. The Bradford Method For Protein Quantitation. In: Walker JM, editor. The Protein Protocols Handbook. Totowa, NJ: Humana Press; 2009. p. 17-24.

395. Compton SJ, Jones CG. Mechanism of dye response and interference in the Bradford protein assay. Anal Biochem. 1985;151:369-74. Epub 1985/12/01.

396. Ernst O, Zor T. Linearization of the bradford protein assay. J Vis Exp. 2010. Epub 2010/04/14.

397. Kenakin TP. Pharmacologic analysis of drug-receptor interaction. (No Title). 1993.

398. Paton WDM, Rang HP. The Uptake of Atropine and Related Drugs by Intestinal Smooth Muscle of the Guinea-Pig in Relation to Acetylcholine Receptors. Proceedings of the Royal Society of London Series B, Biological Sciences. 1965;163:1-44.

399. Flanagan CA. GPCR-radioligand binding assays. Methods Cell Biol. 2016;132:191-215. Epub 2016/03/02.

400. Maguire JJ, Kuc RE, Davenport AP. Radioligand binding assays and their analysis. Methods Mol Biol. 2012;897:31-77. Epub 2012/06/08.

401. Mendel CM, Mendel DB. 'Non-specific' binding. The problem, and a solution. Biochemical Journal. 1985;228:269-72.

402. Klotz IM. Ligand--receptor interactions: facts and fantasies. Q Rev Biophys. 1985;18:227-59. Epub 1985/08/01.

403. Wilkinson KD. Quantitative Analysis of Protein-Protein Interactions. In: Fu H, editor. Protein-Protein Interactions: Methods and Applications. Totowa, NJ: Humana Press; 2004. p. 15-31.

404. Mpye K, Gildenhuys S, Mosebi S. The effects of temperature on streptavidin-biotin binding using affinity isothermal titration calorimetry. AIMS Biophysics. 2020;7:236-47.

405. Encarnação JC, Barta P, Fornstedt T, Andersson K. Impact of assay temperature on antibody binding characteristics in living cells: A case study. Biomed Rep. 2017;7:400-6. Epub 2017/11/29.

406. Matricon P, Suresh RR, Gao Z-G, Panel N, Jacobson KA, Carlsson J. Ligand design by targeting a binding site water. Chemical Science. 2021;12:960-8.

407. Rovati GE. Ligand-binding studies: old beliefs and new strategies. Trends Pharmacol Sci. 1998;19:365-9. Epub 1998/10/24.

408. Rothe K, Solinski HJ, Boekhoff I, Gudermann T, Breit A. Morphine activates the E twenty six-like transcription factor-1/serum response factor pathway via extracellular signal-regulated kinases 1/2 in F11 cells derived from dorsal root ganglia neurons. J Pharmacol Exp Ther. 2012;342:41-52. Epub 2012/03/29.

409. Neubig RR, Spedding M, Kenakin T, Christopoulos A. International Union of Pharmacology Committee on Receptor Nomenclature and Drug Classification. XXXVIII. Update on terms and symbols in quantitative pharmacology. Pharmacol Rev. 2003;55:597-606. Epub 2003/12/06.

410. Cheng Y, Prusoff WH. Relationship between the inhibition constant (K1) and the concentration of inhibitor which causes 50 per cent inhibition (I50) of an enzymatic reaction. Biochem Pharmacol. 1973;22:3099-108. Epub 1973/12/01.

411. Wang T, Li Z, Cvijic ME, Zhang L, Sum CS. Measurement of cAMP for G(αs)- and G(αi) Protein-Coupled Receptors (GPCRs). In: Markossian S, Grossman A, Brimacombe K, Arkin M, Auld D, Austin C, Baell J, Chung TDY, Coussens NP, Dahlin JL, Devanarayan V, Foley TL, Glicksman M, Gorshkov K, Haas JV, Hall MD, Hoare S, Inglese J, Iversen PW, Kales SC, Lal-Nag M, Li Z, McGee J, McManus O, Riss T, Saradjian P, Sittampalam GS, Tarselli M, Trask OJ, Jr., Wang Y, Weidner JR, Wildey MJ, Wilson K, Xia M, Xu X, editors. Assay Guidance Manual. Bethesda (MD): Eli Lilly & Company and the National Center for Advancing Translational Sciences; 2004.

412. Hill SJ, Williams C, May LT. Insights into GPCR pharmacology from the measurement of changes in intracellular cyclic AMP; advantages and pitfalls of differing methodologies. Br J Pharmacol. 2010;161:1266-75. Epub 2010/11/05.

413. Baker JG, Hall IP, Hill SJ. Pharmacological characterization of CGP 12177 at the human beta(2)-adrenoceptor. Br J Pharmacol. 2002;137:400-8. Epub 2002/09/19.

414. Donaldson J, Brown AM, Hill SJ. Influence of rolipram on the cyclic 3',5'-adenosine monophosphate response to histamine and adenosine in slices of guinea-pig cerebral cortex. Biochem Pharmacol. 1988;37:715-23. Epub 1988/02/15.

415. Salomon Y, Londos C, Rodbell M. A highly sensitive adenylate cyclase assay. Anal Biochem. 1974;58:541-8. Epub 1974/04/01.

416. Baker JG, Hall IP, Hill SJ. Agonist and inverse agonist actions of beta-blockers at the human beta 2-adrenoceptor provide evidence for agonist-directed signaling. Mol Pharmacol. 2003;64:1357-69. Epub 2003/12/03.

417. Du J, Wang Z. Regulation of RIPK1 Phosphorylation: Implications for Inflammation, Cell Death, and Therapeutic Interventions. Biomedicines. 2024;12:1525.

418. Nuñez de Villavicencio-Diaz T, Rabalski AJ, Litchfield DW. Protein Kinase CK2: Intricate Relationships within Regulatory Cellular Networks. Pharmaceuticals. 2017;10:27.

419. Montenarh M. Protein kinase CK2 and angiogenesis. Adv Clin Exp Med. 2014;23:153-8. Epub 2014/06/11.

420. Ochoa D, Jonikas M, Lawrence RT, El Debs B, Selkrig J, Typas A, Villén J, Santos SD, Beltrao P. An atlas of human kinase regulation. Mol Syst Biol. 2016;12:888. Epub 2016/12/03.

421. Reinhardt R, Leonard TA. A critical evaluation of protein kinase regulation by activation loop autophosphorylation. eLife. 2023;12:e88210.

422. Bass JJ, Wilkinson DJ, Rankin D, Phillips BE, Szewczyk NJ, Smith K, Atherton PJ. An overview of technical considerations for Western blotting applications to physiological research. Scand J Med Sci Sports. 2017;27:4-25. Epub 2016/06/07.

423. Towbin H, Staehelin T, Gordon J. Electrophoretic transfer of proteins from polyacrylamide gels to nitrocellulose sheets: procedure and some applications. Proc Natl Acad Sci U S A. 1979;76:4350-4. Epub 1979/09/01.

424. Laemmli UK. Cleavage of structural proteins during the assembly of the head of bacteriophage T4. Nature. 1970;227:680-5. Epub 1970/08/15.

425. Smith BJ. SDS polyacrylamide gel electrophoresis of proteins. Methods Mol Biol. 1994;32:23-34. Epub 1994/01/01.

426. Ornstein L. DISC ELECTROPHORESIS. I. BACKGROUND AND THEORY. Ann N Y Acad Sci. 1964;121:321-49. Epub 1964/12/28.

427. Davis BJ. DISC ELECTROPHORESIS. II. METHOD AND APPLICATION TO HUMAN SERUM PROTEINS. Ann N Y Acad Sci. 1964;121:404-27. Epub 1964/12/28.

428. Ahn T, Yim SK, Choi HI, Yun CH. Polyacrylamide gel electrophoresis without a stacking gel: use of amino acids as electrolytes. Anal Biochem. 2001;291:300-3. Epub 2001/06/13.

429. Jimenez-Soto LF. Single Gel system based in Ahn T et al (2001) v1 2016.

430. Jimenez-Soto LF. Trans-Blot® Turbo™ Transfer with Home-made buffers v1 2016.

431. Clayton CC, Bruchas MR, Lee ML, Chavkin C. Phosphorylation of the mu-opioid receptor at tyrosine 166 (Tyr3.51) in the DRY motif reduces agonist efficacy. Mol Pharmacol. 2010;77:339-47. Epub 2009/12/05.

432. Kenakin T. A pharmacology primer: theory, applications, and methods. 2006:299.

433. Kise R, Inoue A. GPCR signaling bias: an emerging framework for opioid drug development. The Journal of Biochemistry. 2024;175:367-76.

434. Milić D, Veprintsev DB. Large-scale production and protein engineering of G protein-coupled receptors for structural studies. Front Pharmacol. 2015;6:66. Epub 2015/04/16.

435. Atwood BK, Lopez J, Wager-Miller J, Mackie K, Straiker A. Expression of G protein-coupled receptors and related proteins in HEK293, AtT20, BV2, and N18 cell lines as revealed by microarray analysis. BMC Genomics. 2011;12:14.

436. Arden JR, Segredo V, Wang Z, Lameh J, Sadée W. Phosphorylation and agonist-specific intracellular trafficking of an epitope-tagged mu-opioid receptor expressed in HEK 293 cells. J Neurochem. 1995;65:1636-45. Epub 1995/10/01.

437. Koch T, Kroslak T, Mayer P, Raulf E, Höllt V. Site mutation in the rat mu-opioid receptor demonstrates the involvement of calcium/calmodulin-dependent protein

kinase II in agonist-mediated desensitization. J Neurochem. 1997;69:1767-70. Epub 1997/11/05.

438. Wang JB, Johnson PS, Persico AM, Hawkins AL, Griffin CA, Uhl GR. Human mu opiate receptor. cDNA and genomic clones, pharmacologic characterization and chromosomal assignment. FEBS Lett. 1994;338:217-22. Epub 1994/01/31.

439. Li X, Keith DE, Evans CJ. Mu opioid receptor-like sequences are present throughout vertebrate evolution. Journal of Molecular Evolution. 1996;43:179-84.

440. Simantov R, Childers SR, Snyder SH. The opiate receptor binding interactions of 3H-methionine enkephalin, an opioid peptide. European Journal of Pharmacology. 1978;47:319-31.

441. Good NE, Winget GD, Winter W, Connolly TN, Izawa S, Singh RMM. Hydrogen Ion Buffers for Biological Research*. Biochemistry. 1966;5:467-77.

442. Bylund DB, Toews ML. Radioligand binding methods for membrane preparations and intact cells. Methods Mol Biol. 2011;746:135-64. Epub 2011/05/25.

443. Hulme EC, Trevethick MA. Ligand binding assays at equilibrium: validation and interpretation. Br J Pharmacol. 2010;161:1219-37. Epub 2010/02/06.

444. Bylund DB, Toews ML. Radioligand binding methods: practical guide and tips. Am J Physiol. 1993;265:L421-9. Epub 1993/11/01.

445. Thomson NJ, Zachariae U. Mechanism of negative μ-opioid receptor modulation by sodium ions. Structure. 2025;33:196-205.e2.

446. Wernersson S, Birgersson S, Akke M. Cosolvent Dimethyl Sulfoxide Influences Protein-Ligand Binding Kinetics via Solvent Viscosity Effects: Revealing the Success Rate of Complex Formation Following Diffusive Protein-Ligand Encounter. Biochemistry. 2023;62:44-52. Epub 2022/12/22.

447. Simon EJ, Hiller JM, Edelman I. Stereospecific binding of the potent narcotic analgesic (3H) Etorphine to rat-brain homogenate. Proc Natl Acad Sci U S A. 1973;70:1947-9. Epub 1973/07/01.

448. Pollack AE, Wooten GF. Effects of sodium on cell surface and intracellular 3H-naloxone binding sites. Life Sci. 1987;41:385-90. Epub 1987/07/27.

449. Pert CB, Pasternak G, Snyder SH. Opiate agonists and antagonists discriminated by receptor binding in brain. Science. 1973;182:1359-61. Epub 1973/12/28.

450. Brase DA, Han Y-H, Dewey WL. Effects of Glucose and Diabetes on Binding of Naloxone and Dihydromorphine to Opiate Receptors in Mouse Brain. Diabetes. 1987;36:1173-7.

451. Kuo A, Magiera J, Rethwan N, Andersson Å, Leen Lam A, Wyse B, Meutermans W, Lewis R, Smith M. In vitro profiling of opioid ligands using the cAMP formation inhibition assay and the β-arrestin2 recruitment assay: No two ligands have the same profile. Eur J Pharmacol. 2020;872:172947. Epub 2020/01/29.

452. Bart G, Schluger JH, Borg L, Ho A, Bidlack JM, Kreek MJ. Nalmefene Induced Elevation in Serum Prolactin in Normal Human Volunteers: Partial Kappa Opioid Agonist Activity? Neuropsychopharmacology. 2005;30:2254-62.

453. Toll L, Berzetei-Gurske IP, Polgar WE, Brandt SR, Adapa ID, Rodriguez L, Schwartz RW, Haggart D, O'Brien A, White A, Kennedy JM, Craymer K, Farrington L, Auh JS. Standard binding and functional assays related to medications development division testing for potential cocaine and opiate narcotic treatment medications. NIDA Res Monogr. 1998;178:440-66. Epub 1998/08/01.

454. Buchwald P. A Receptor Model With Binding Affinity, Activation Efficacy, and Signal Amplification Parameters for Complex Fractional Response Versus Occupancy Data. Front Pharmacol. 2019;10:605. Epub 2019/06/28.

455. Ahn S, Shenoy SK, Wei H, Lefkowitz RJ. Differential kinetic and spatial patterns of beta-arrestin and G protein-mediated ERK activation by the angiotensin II receptor. J Biol Chem. 2004;279:35518-25. Epub 2004/06/19.

456. Du K, Wang Z, Zhang H, Zhang Y, Su H, Wei Z, Zhang C, Yun K, Cong B. Levo-tetrahydropalmatine attenuates the acquisition of fentanyl-induced conditioned place preference and the changes in ERK and CREB phosphorylation expression in mice. Neurosci Lett. 2021;756:135984. Epub 2021/05/25.

457. Wang Z, Ma W, Chabot JG, Quirion R. Calcitonin gene-related peptide as a regulator of neuronal CaMKII-CREB, microglial p38-NFκB and astroglial ERK-Stat1/3 cascades mediating the development of tolerance to morphine-induced analgesia. Pain. 2010;151:194-205. Epub 2010/08/10.

458. Xu C, Zheng H, Loh HH, Law PY. Morphine Promotes Astrocyte-Preferential Differentiation of Mouse Hippocampal Progenitor Cells via PKCε-Dependent ERK Activation and TRBP Phosphorylation. Stem Cells. 2015;33:2762-72. Epub 2015/05/28.

459. Börner C, Warnick B, Smida M, Hartig R, Lindquist JA, Schraven B, Höllt V, Kraus Jr. Mechanisms of Opioid-Mediated Inhibition of Human T Cell Receptor Signaling1. The Journal of Immunology. 2009;183:882-9.

460. Gross ER, Hsu AK, Gross GJ. Diabetes abolishes morphine-induced cardioprotection via multiple pathways upstream of glycogen synthase kinase-3beta. Diabetes. 2007;56:127-36. Epub 2006/12/29.

461. Polakiewicz RD, Schieferl SM, Gingras A-C, Sonenberg N, Comb MJ. μ-Opioid Receptor Activates Signaling Pathways Implicated in Cell Survival and Translational Control *. Journal of Biological Chemistry. 1998;273:23534-41.

462. Fogaça MV, Fukumoto K, Franklin T, Liu RJ, Duman CH, Vitolo OV, Duman RS. N-Methyl-D-aspartate receptor antagonist d-methadone produces rapid, mTORC1-dependent antidepressant effects. Neuropsychopharmacology. 2019;44:2230-8. Epub 2019/08/28.

463. Allouche S, Noble F, Marie N. Opioid receptor desensitization: mechanisms and its link to tolerance. Front Pharmacol. 2014;5:280. Epub 2015/01/08.

464. Chu J, Zheng H, Loh HH, Law PY. Morphine-induced mu-opioid receptor rapid desensitization is independent of receptor phosphorylation and beta-arrestins. Cell Signal. 2008;20:1616-24. Epub 2008/06/19.

465. Zawilska JB, Kuczyńska K, Kosmal W, Markiewicz K, Adamowicz P. Carfentanil – from an animal anesthetic to a deadly illicit drug. Forensic Science International. 2021;320:110715.

466. Revvity. AlphaScreen Assay Method for Pharmacological Characterization of cAMP Accumulation 2024 [28.11.2024]. Available from: https://resources.revvity.com/pdfs/app-camp-alphascreen-assay-method-for-pharmacological-characterization.pdf.

467. Hill AV, Hill AV, Paganini-Hill A. The possible effects of the aggregation of the molecules of haemoglobin on its dissociation curves. The Journal of Physiology.40:4-7.

468. Kenakin TP. Chapter 1 - What Is Pharmacology? In: Kenakin TP, editor. A Pharmacology Primer (Third Edition). New York: Academic Press; 2009. p. 1-19.

469. Söldner CA, Horn AHC, Sticht H. A Metadynamics-Based Protocol for the Determination of GPCR-Ligand Binding Modes. Int J Mol Sci. 2019;20. Epub 2019/04/25.

470. Zhang M, Chen T, Lu X, Lan X, Chen Z, Lu S. G protein-coupled receptors (GPCRs): advances in structures, mechanisms, and drug discovery. Signal Transduct Target Ther. 2024;9:88. Epub 2024/04/10.

471. Xie B, Goldberg A, Shi L. A comprehensive evaluation of the potential binding poses of fentanyl and its analogs at the μ-opioid receptor. Comput Struct Biotechnol J. 2022;20:2309-21. Epub 2022/05/27.

472. Rattan AK, Tejwani GA. Sodium ions modulate differentially the effect of a benzodiazepine agonist on rat spinal mu-, delta- and kappa-opioid receptors. Pharmacology. 1994;48:30-40. Epub 1994/01/01.

473. Shang Y, LeRouzic V, Schneider S, Bisignano P, Pasternak GW, Filizola M. Mechanistic Insights into the Allosteric Modulation of Opioid Receptors by Sodium Ions. Biochemistry. 2014;53:5140-9.

474. Blume AJ. Interaction of ligands with the opiate receptors of brain membranes: regulation by ions and nucleotides. Proc Natl Acad Sci U S A. 1978;75:1713-7. Epub 1978/04/01.

475. Werling LL, Brown SR, Puttfarcken P, Cox BM. Sodium regulation of agonist binding at opioid receptors. II. Effects of sodium replacement on opioid binding in guinea pig cortical membranes. Molecular pharmacology. 1986;30:90-5.

476. Lee CY, Akera T, Brody TM. Effects of Na+, k+, mg++ and Ca++ on the saturable binding of [3H]dihydromorphine and [3H]naloxone in vitro. J Pharmacol Exp Ther. 1977;202:166-73. Epub 1977/07/01.

477. Pasternak GW, Snyder SH. Identification of novel high affinity opiate receptor binding in rat brain. Nature. 1975;253:563-5.

478. Puttfarcken P, Werling LL, Brown SR, Cote TE, Cox BM. Sodium regulation of agonist binding at opioid receptors. I. Effects of sodium replacement on binding at mu- and delta-type receptors in 7315c and NG108-15 cells and cell membranes. Molecular pharmacology. 1986;30:81-9.

479. Katritch V, Fenalti G, Abola EE, Roth BL, Cherezov V, Stevens RC. Allosteric sodium in class A GPCR signaling. Trends Biochem Sci. 2014;39:233-44. Epub 2014/04/29.

480. Fenalti G, Giguere PM, Katritch V, Huang X-P, Thompson AA, Cherezov V, Roth BL, Stevens RC. Molecular control of δ-opioid receptor signalling. Nature. 2014;506:191-6.

481. Strazzullo P, Leclercq C. Sodium. Advances in Nutrition. 2014;5:188-90.

482. Glatfelter GC, Vandeputte MM, Chen L, Walther D, Tsai MM, Shi L, Stove CP, Baumann MH. Alkoxy chain length governs the potency of 2-benzylbenzimidazole 'nitazene' opioids associated with human overdose. Psychopharmacology (Berl). 2023;240:2573-84. Epub 2023/09/04.

483. Vandeputte MM, Krotulski AJ, Walther D, Glatfelter GC, Papsun D, Walton SE, Logan BK, Baumann MH, Stove CP. Pharmacological evaluation and forensic case series of N-pyrrolidino etonitazene (etonitazepyne), a newly emerging 2-benzylbenzimidazole 'nitazene' synthetic opioid. Arch Toxicol. 2022;96:1845-63. Epub 2022/04/29.

484. Vandeputte MM, Tsai MM, Chen L, Glatfelter GC, Walther D, Stove CP, Shi L, Baumann MH. Comparative neuropharmacology of structurally distinct non-

fentanyl opioids that are appearing on recreational drug markets worldwide. Drug Alcohol Depend. 2023;249:109939. Epub 2023/06/05.

485. Gharagozlou P, Demirci H, David Clark J, Lameh J. Activity of opioid ligands in cells expressing cloned mu opioid receptors. BMC Pharmacol. 2003;3:1. Epub 2003/01/07.

486. Freire E. Statistical thermodynamic linkage between conformational and binding equilibria. Adv Protein Chem. 1998;51:255-79. Epub 1998/06/06.

487. Leff P. The two-state model of receptor activation. Trends Pharmacol Sci. 1995;16:89-97. Epub 1995/03/01.

488. Swaminath G, Xiang Y, Lee TW, Steenhuis J, Parnot C, Kobilka BK. Sequential binding of agonists to the beta2 adrenoceptor. Kinetic evidence for intermediate conformational states. J Biol Chem. 2004;279:686-91. Epub 2003/10/16.

489. Swaminath G, Deupi X, Lee TW, Zhu W, Thian FS, Kobilka TS, Kobilka B. Probing the beta2 adrenoceptor binding site with catechol reveals differences in binding and activation by agonists and partial agonists. J Biol Chem. 2005;280:22165-71. Epub 2005/04/09.

490. Park PS, Lodowski DT, Palczewski K. Activation of G protein-coupled receptors: beyond two-state models and tertiary conformational changes. Annu Rev Pharmacol Toxicol. 2008;48:107-41. Epub 2007/09/13.

491. Park PS. Ensemble of G protein-coupled receptor active states. Curr Med Chem. 2012;19:1146-54. Epub 2012/02/04.

492. Samama P, Cotecchia S, Costa T, Lefkowitz RJ. A mutation-induced activated state of the beta 2-adrenergic receptor. Extending the ternary complex model. J Biol Chem. 1993;268:4625-36. Epub 1993/03/05.

493. Smith JS, Lefkowitz RJ, Rajagopal S. Biased signalling: from simple switches to allosteric microprocessors. Nature Reviews Drug Discovery. 2018;17:243-60.

494. Gillis A, Kliewer A, Kelly E, Henderson G, Christie MJ, Schulz S, Canals M. Critical Assessment of G Protein-Biased Agonism at the μ-Opioid Receptor. Trends Pharmacol Sci. 2020;41:947-59. Epub 2020/10/25.

495. Manzke T, Guenther U, Ponimaskin EG, Haller M, Dutschmann M, Schwarzacher S, Richter DW. 5-HT4(a) receptors avert opioid-induced breathing depression without loss of analgesia. Science. 2003;301:226-9. Epub 2003/07/12.

496. Lalley PM. Dopamine1 receptor agonists reverse opioid respiratory network depression, increase CO2 reactivity. Respir Physiol Neurobiol. 2004;139:247-62. Epub 2004/05/05.

497. Ruangkittisakul A, Ballanyi K. Methylxanthine reversal of opioid-evoked inspiratory depression via phosphodiesterase-4 blockade. Respiratory Physiology & Neurobiology. 2010;172:94-105.

498. Montandon G, Ren J, Victoria NC, Liu H, Wickman K, Greer JJ, Horner RL. G-protein-gated Inwardly Rectifying Potassium Channels Modulate Respiratory Depression by Opioids. Anesthesiology. 2016;124:641-50. Epub 2015/12/18.

499. Miess E, Gondin AB, Yousuf A, Steinborn R, Mösslein N, Yunshi, Yang, Göldner M, Ruland JG, Bünemann M, Krasel C, MacDonald JIS, Christie, Halls ML, Schulz S, Canals M, Multisite phosphorylation is required for sustained interaction with GRKs and arrestins in mediating rapid mu-opioid receptor desensitization. 2019: Publisher.

500. Grecksch G, Just S, Pierstorff C, Imhof AK, Glück L, Doll C, Lupp A, Becker A, Koch T, Stumm R, Höllt V, Schulz S. Analgesic tolerance to high-efficacy agonists but not to morphine is diminished in phosphorylation-deficient S375A μ-opioid receptor knock-in mice. J Neurosci. 2011;31:13890-6. Epub 2011/10/01.

501. Duraffourd C, Kumala E, Anselmi L, Brecha NC, Sternini C. Opioid-Induced Mitogen-Activated Protein Kinase Signaling in Rat Enteric Neurons following Chronic Morphine Treatment. PLOS ONE. 2014;9:e110230.

502. Zhou LF, Zhu YP. Changes of CREB in rat hippocampus, prefrontal cortex and nucleus accumbens during three phases of morphine induced conditioned place preference in rats. J Zhejiang Univ Sci B. 2006;7:107-13. Epub 2006/01/20.

503. Khezri A, Mohsenzadeh MS, Mirzayan E, Bagherpasand N, Fathi M, Abnous K, Imenshahidi M, Mehri S, Hosseinzadeh H. Quetiapine attenuates the acquisition of morphine-induced conditioned place preference and reduces ERK phosphorylation in the hippocampus and cerebral cortex. Am J Drug Alcohol Abuse. 2022;48:422-32. Epub 2022/06/07.

504. Ram A, Edwards TM, McCarty A, McDermott MV, Bobeck EN. Morphine-induced kinase activation and localization in the periaqueductal gray of male and female mice. J Neurochem. 2021;159:590-602. Epub 2021/09/10.

505. Shi C, Liu Y, Zhang W, Lei Y, Lu C, Sun R, Sun Y, Jiang M, Gu X, Ma Z. Intraoperative electroacupuncture relieves remifentanil-induced postoperative hyperalgesia via inhibiting spinal glial activation in rats. Mol Pain. 2017;13:1744806917725636. Epub 2017/08/22.

506. Nowoczyn M, Marie N, Coulbault L, Hervault M, Davis A, Hanouz JL, Allouche S. Remifentanil produces cross-desensitization and tolerance with morphine on the mu-opioid receptor. Neuropharmacology. 2013;73:368-79. Epub 2013/06/25.

507. Sakamoto K, Karelina K, Obrietan K. CREB: a multifaceted regulator of neuronal plasticity and protection. J Neurochem. 2011;116:1-9. Epub 2010/11/04.

508. Otani T, Matsuda M, Mizokami A, Kitagawa N, Takeuchi H, Jimi E, Inai T, Hirata M. Osteocalcin triggers Fas/FasL-mediated necroptosis in adipocytes via activation of p300. Cell Death Dis. 2018;9:1194. Epub 2018/12/14.

509. Kornhauser JM, Cowan CW, Shaywitz AJ, Dolmetsch RE, Griffith EC, Hu LS, Haddad C, Xia Z, Greenberg ME. CREB Transcriptional Activity in Neurons Is Regulated by Multiple, Calcium-Specific Phosphorylation Events. Neuron. 2002;34:221-33.

510. Belcheva MM, Tan Y, Heaton VM, Clark AL, Coscia CJ. Mu opioid transactivation and down-regulation of the epidermal growth factor receptor in astrocytes: implications for mitogen-activated protein kinase signaling. Mol Pharmacol. 2003;64:1391-401. Epub 2003/12/03.

511. Belcheva MM, Szùcs M, Wang D, Sadee W, Coscia CJ. μ-Opioid Receptor-mediated ERK Activation Involves Calmodulin-dependent Epidermal Growth Factor Receptor Transactivation *. Journal of Biological Chemistry. 2001;276:33847-53.

512. Gross ER, Hsu AK, Gross GJ. The JAK/STAT pathway is essential for opioid-induced cardioprotection: JAK2 as a mediator of STAT3, Akt, and GSK-3 beta. Am J Physiol Heart Circ Physiol. 2006;291:H827-34. Epub 2006/03/07.

513. Sanna MD, Ghelardini C, Galeotti N. Activation of JNK pathway in spinal astrocytes contributes to acute ultra-low-dose morphine thermal hyperalgesia. Pain. 2015;156:1265-75. Epub 2015/03/26.

514. Liu X, Yang H, Liu Y, Jiao Y, Yang L, Wang X, Yu W, Su D, Tian J. Remifentanil upregulates hepatic IL-18 binding protein (IL-18BP) expression through transcriptional control. Lab Invest. 2018;98:1588-99. Epub 2018/08/10.

515. Madishetti S, Schneble N, König C, Hirsch E, Schulz S, Müller JP, Wetzker R. PI3Kγ integrates cAMP and Akt signalling of the μ-opioid receptor. Br J Pharmacol. 2014;171:3328-37. Epub 2014/03/25.

516. Xu J, Tian W, Ma X, Guo J, Shi Q, Jin Y, Xi J, Xu Z. The molecular mechanism underlying morphine-induced Akt activation: roles of protein phosphatases and reactive oxygen species. Cell Biochem Biophys. 2011;61:303-11. Epub 2011/06/01.

517. Yu Z, Jin S, Tian S, Wang Z. Morphine stimulates cervical cancer cells and alleviates cytotoxicity of chemotherapeutic drugs via opioid receptor-dependent and -independent mechanisms. Pharmacol Res Perspect. 2022;10:e01016. Epub 2022/10/07.

518. Wang Z, Jiang L, Wang J, Chai Z, Xiong W. Morphine promotes angiogenesis by activating PI3K/Akt/HIF-1α pathway and upregulating VEGF in hepatocellular carcinoma. J Gastrointest Oncol. 2021;12:1761-72. Epub 2021/09/18.

519. Liu W, Chen Y, Xu W, Wang W, Tang L, Xia R, Zhu Q. Fentanyl stimulates tumor angiogenesis via activating multiple pro-angiogenic signaling pathways. Biochem Biophys Res Commun. 2020;532:225-30. Epub 2020/08/31.

520. Basu A, Lambring CB. Akt Isoforms: A Family Affair in Breast Cancer. Cancers (Basel). 2021;13. Epub 2021/07/25.

521. Duron DI, Lei W, Barker NK, Stine C, Mishra S, Blagg BSJ, Langlais PR, Streicher JM. Inhibition of Hsp90 in the spinal cord enhances the antinociceptive effects of morphine by activating an ERK-RSK pathway. Sci Signal. 2020;13. Epub 2020/05/07.

522. Roux PP, Shahbazian D, Vu H, Holz MK, Cohen MS, Taunton J, Sonenberg N, Blenis J. RAS/ERK Signaling Promotes Site-specific Ribosomal Protein S6 Phosphorylation via RSK and Stimulates Cap-dependent Translation*. Journal of Biological Chemistry. 2007;282:14056-64.

523. Anjum R, Blenis J. The RSK family of kinases: emerging roles in cellular signalling. Nat Rev Mol Cell Biol. 2008;9:747-58. Epub 2008/09/25.

524. Polakiewicz RD, Schieferl SM, Gingras AC, Sonenberg N, Comb MJ. mu-Opioid receptor activates signaling pathways implicated in cell survival and translational control. J Biol Chem. 1998;273:23534-41. Epub 1998/08/29.

525. Flynn SM, France CP. Discriminative stimulus effects of carfentanil in rats discriminating fentanyl: Differential antagonism by naltrexone. Drug Alcohol Depend. 2021;221:108599. Epub 2021/02/26.

526. Rodarte J, Baehr C, Hicks D, McGovern M, Zhang Y, Silva-Ortiz P, Hannon B, Duddu S, Pancera M, Pravetoni M. Structure-Based Engineering of Monoclonal Antibodies for Improved Binding to Counteract the Effects of Fentanyl and Carfentanil. ACS Omega. 2024;9:42506-19. Epub 2024/10/21.

527. Gorelick DA. Pharmacokinetic strategies for treatment of drug overdose and addiction. Future Med Chem. 2012;4:227-43. Epub 2012/02/04.

528. Almeida MB, Costa-Malaquias A, Nascimento JL, Oliveira KR, Herculano AM, Crespo-López ME. Therapeutic concentration of morphine reduces oxidative stress in glioma cell line. Braz J Med Biol Res. 2014;47:398-402. Epub 2014/04/15.

529. Shanks KG, Behonick GS. Detection of Carfentanil by LC–MS-MS and Reports of Associated Fatalities in the USA. Journal of Analytical Toxicology. 2017;41:466-72.

530. Fomin D, Baranauskaite V, Usaviciene E, Sumkovskaja A, Laima S, Jasulaitis A, Minkuviene ZN, Chmieliauskas S, Stasiuniene J. Human deaths from drug overdoses with carfentanyl involvement-new rising problem in forensic medicine: A STROBE-compliant retrospective study. Medicine (Baltimore). 2018;97:e13449. Epub 2018/12/05.

531. Noble C, Papsun DM, Diaz S, Logan BK. Detection of two potent synthetic opioids carfentanil and 3-methylfentanyl in forensic investigations during a four-year period 2017–2020. Emerging Trends in Drugs, Addictions, and Health. 2021;1:100022.

532. SpringerMedizin. Opioide in der Anästhesiologie [cited 2025 09.01.2025]. Available from: https://www.springermedizin.de/emedpedia/detail/die-anaesthesiologie/opioide-in-der-anaesthesiologie?epediaDoi=10.1007%2F978-3-662-45539-5_20.

533. Gill JR, Lin PT, Nelson L. Reliability of postmortem fentanyl concentrations in determining the cause of death. J Med Toxicol. 2013;9:34-41. Epub 2012/08/15.

534. Edinboro LE, Poklis A, Trautman D, Lowry S, Backer R, Harvey CM. Fatal fentanyl intoxication following excessive transdermal application. J Forensic Sci. 1997;42:741-3. Epub 1997/07/01.

535. Olson KN, Luckenbill K, Thompson J, Middleton O, Geiselhart R, Mills KM, Kloss J, Apple FS. Postmortem Redistribution of Fentanyl in Blood. American Journal of Clinical Pathology. 2010;133:447-53.

536. Rochholz GR, Lars; Bormann, Katharina. Analyse von Remifentanil in einem Fall einer letalen Intoxikation. Toxichem Krimtech 81(1):27. 2014.

537. Eleveld DJ, Colin P, Absalom AR, Struys MMRF. Target-controlled-infusion models for remifentanil dosing consistent with approved recommendations. British Journal of Anaesthesia. 2020;125:483-91.

538. Nagatomo S, Nagai M, Kitagawa T. Structural origin of cooperativity in human hemoglobin: a view from different roles of α and β subunits in the α(2)β(2) tetramer. Biophys Rev. 2022;14:483-98. Epub 2022/05/10.

539. Bartels HJ, Hesch RD. [Homotropic cooperative effects and rising B-F-curves in hormone-antibody reactions (author's transl)]. Z Klin Chem Klin Biochem. 1973;11:311-8. Epub 1973/07/01.

540. Metzger H. Effect of antigen binding on the properties of antibody. Adv Immunol. 1974;18:169-207. Epub 1974/01/01.

541. Yang D, Kroe-Barrett R, Singh S, Roberts CJ, Laue TM. IgG cooperativity - Is there allostery? Implications for antibody functions and therapeutic antibody development. MAbs. 2017;9:1231-52. Epub 2017/08/17.

542. Bowen A, Casadevall A. Revisiting the Immunoglobulin Intramolecular Signaling Hypothesis. Trends Immunol. 2016;37:721-3. Epub 2016/09/19.

543. Ceglia V, Zurawski S, Montes M, Bouteau A, Wang Z, Ellis J, Igyártó BZ, Lévy Y, Zurawski G. Anti-CD40 Antibodies Fused to CD40 Ligand Have Superagonist Properties. J Immunol. 2021;207:2060-76. Epub 2021/09/24.

544. Mosch A, Ettl T, Mamilos A, Schreml S, Spörl S, Spanier G, Klingelhöffer C. Physiological concentrations of denosumab enhance osteogenic differentiation in

human mesenchymal stem cells of the jaw bone. Archives of Oral Biology. 2019;101:23-9.

545. Li Y, Liu J, Chen W, Wang W, Yang F, Liu X, Sheng Y, Du K, He M, Lyu X, Li H, Zhao L, Wei Z, Wang F, Zheng S, Sui J. A pH-dependent anti-CD47 antibody that selectively targets solid tumors and improves therapeutic efficacy and safety. J Hematol Oncol. 2023;16:2. Epub 2023/01/18.

546. Hicks D, Baehr C, Silva-Ortiz P, Khaimraj A, Luengas D, Hamid FA, Pravetoni M. Advancing humanized monoclonal antibody for counteracting fentanyl toxicity towards clinical development. Hum Vaccin Immunother. 2022;18:2122507. Epub 2022/10/05.

547. Bird HE, Huhn AS, Dunn KE. Fentanyl Absorption, Distribution, Metabolism, and Excretion: Narrative Review and Clinical Significance Related to Illicitly Manufactured Fentanyl. J Addict Med. 2023;17:503-8. Epub 2023/10/04.

548. Burns SM, Cunningham CW, Mercer SL. DARK Classics in Chemical Neuroscience: Fentanyl. ACS Chem Neurosci. 2018;9:2428-37. Epub 2018/06/13.

549. Orson FM, Kinsey BM, Singh RA, Wu Y, Gardner T, Kosten TR. The future of vaccines in the management of addictive disorders. Curr Psychiatry Rep. 2007;9:381-7. Epub 2007/10/05.

550. Presta LG. Engineering of therapeutic antibodies to minimize immunogenicity and optimize function. Advanced Drug Delivery Reviews. 2006;58:640-56.

551. Kouhi A, Pachipulusu V, Kapenstein T, Hu P, Epstein AL, Khawli LA. Brain Disposition of Antibody-Based Therapeutics: Dogma, Approaches and Perspectives. Int J Mol Sci. 2021;22. Epub 2021/07/03.

552. Zhao P, Zhang N, An Z. Engineering antibody and protein therapeutics to cross the blood-brain barrier. Antib Ther. 2022;5:311-31. Epub 2022/12/22.

553. Information NCfB. PubChem Compound Summary for CID 5284596, Naloxone 2025 [January 14, 2025]. Available from: https://pubchem.ncbi.nlm.nih.gov/compound/Naloxone.

554. Ellison M, Hutton E, Webster L, Skolnick P. Reversal of Opioid-Induced Respiratory Depression in Healthy Volunteers: Comparison of Intranasal Nalmefene and Intranasal Naloxone. J Clin Pharmacol. 2024;64:828-39. Epub 2024/03/04.

555. Berkowitz BA. The relationship of pharmacokinetics to pharmacological activity: morphine, methadone and naloxone. Clin Pharmacokinet. 1976;1:219-30. Epub 1976/01/01.

556. Melkes B, Hejnova L, Novotny J. Biased μ-opioid receptor agonists diversely regulate lateral mobility and functional coupling of the receptor to its cognate G proteins. Naunyn-Schmiedeberg's Archives of Pharmacology. 2016;389:1289-300.

557. Zsuga J, Erdei T, Szabó K, Lampe N, Papp C, Pinter A, Szentmiklosi AJ, Juhasz B, Szilvássy Z, Gesztelyi R. Methodical Challenges and a Possible Resolution in the Assessment of Receptor Reserve for Adenosine, an Agonist with Short Half-Life. Molecules. 2017;22. Epub 2017/05/24.

558. Kazmi SM, Mishra RK. Opioid receptors in human neuroblastoma SH-SY5Y cells: evidence for distinct morphine (mu) and enkephalin (delta) binding sites. Biochem Biophys Res Commun. 1986;137:813-20. Epub 1986/06/13.

9. Appendix

List of abbreviations

μOR	Mu opioid receptor
AC	Adenylate cyclase
AKT 1/2/3	Protein kinase B 1, 2, and 3
AMP	Adenosine monophosphate
ANOVA	Analysis of variance
AP2	Adapter protein 2
ATP	Adenosine triphosphate
AUC	Area under the curve
BBB	Blood brain barrier
Bgg	Bovine gamma globuline
B_{max}	Maximum binding
BRET	Bioluminescence Resonance Energy Transfer
BSA	Bovine serum albumin
cAMP	Cyclic adenosine monophosphate
CAR	Carfentanil
cDNA	Complementary desoxyribonucleic acid
Chk-2	Checkpoint kinase 2
CHO	Chinese Hamster Ovary Cells
c-Jun	Jun proto-oncogene
CNS	Central nervous system
COS	CV-1 in origin with SV40

CRE	cAMP response element
CREB	cAMP response element binding protein
DAG	Diacylglycerol
DAMGO	[D-Ala2, N-MePhe4, Gly-ol]-enkephalin
DMSO	Dimethylsulfoxide
DNA	Desoxyribonucleic acid
DPDPE	[D-Pen2,D-Pen5]enkephalin
EC_{50}	Halfmaximal effective concentration
EGFR	Epidermal growth factor receptor
ENDO	Endomorphin-1
eNOS	Endothelial nitric oxide synthase
ERK1/2	Extracellular signal regulated kinases 1 and 2
FDA	US Food and Drug Administration
FEN	Fentanyl
Fgr	Feline Gardner-Rasheed sarcoma viral oncogene homolog
FSK	Forskolin
GDP	Guanosine diphosphate
GIRK	G protein gated inwardly rectifying potassium channel
GPCR	G protein coupled receptor
GRK	G protein coupled receptor kinase
GSK	Glycogen synthase kinase
GTP	Guanosine triphosphate
hμOR	Human mu opioid receptor

HEK293	Human embryonic kidney 293 cells
HEPES	4-(2-hydroxyethyl)-1-piperazineethanesulfonic acid
HRP	Horseradish peroxidase
HSP	Heat shock protein
IBMX	3-isobutyl-1-methylxanthine
IC_{50}	Halfmaximal inhibitory concentration
IP3	Inositol-1,4,5-triphosphate
JNK 1/2/3	c-Jun N-terminal kinase 1/2/3
K_d	Dissociation constant
K_i	Inhibition constant
KLH	Keyhole limpet hemocyanine
LB	Luria-Bertani or lysogenic broth
Lck	Lymphocyte-specific protein tyrosine kinase
Lyn	Lyn proto-oncogene, Src family tyrosine kinase
MAPK	Mitogen activated protein kinase
MEK1	Mitogen activated protein kinase kinase 1
MOR	Morphine
MSK1/2	Mitogen- and stress-activated protein kinase 1/2
NaCl	Natrium chloride
NaOH	Natrium hydroxide
NLM	Nalmefene
NLX	Naloxone
NOR	Nociceptin/Orphanin NQ receptor
NPF	Nonpharmaceutical fentanyls

ORL-1	opioid receptor-like 1
p38α	p38 alpha mitogen-activated protein kinase
p53	Tumor protein p53
p70 S6 kinase	Ribosomal protein S6 kinase beta-1
PBS	Phosphate-buffered saline
PDE	Phosphodiesterase
PDGF Rβ	Platelet-derived growth factor receptor beta
pERK1/2	Phosphorylated extracellular signal regulated kinases 1 and 2
PIP2	Phosphatidylinositol 4,5-bisphosphate
PKA	Proteinkinase A
PKC	Proteinkinase C
PLC	Phospholipase C
PRAS40	Proline-rich AKT substrate 40 kDa
PYK2	Protein tyrosine kinase 2 beta or proline-rich tyrosine kinase 2
Raf	Rapidly Accelerated Fibrosarcoma
rμOR	Rat mu opioid receptor
REMI	Remifentanil
RSK1/2	Ribosomal S6 kinase 1/2
RT	Room temperature
SDS	Sodium dodecyl sulfate
SEM	Standard error of the mean
SNARE	Soluble N-Ethylmaleimide-Sensitive Factor Attachment Protein Receptors

Src	Proto-oncogene tyrosine-protein kinase Src
STAT	Signal transducer and activator of transcription
TEMD	Buffer containing TRIS, EDTA, $MgCl_2$ and dithiothreitol
VSG	variant surface glycoprotein
WNK1	WNK lysine-deficient protein kinase 1
Yes	Proto-oncogene tyrosine-protein kinase Yes
δOR	Delta opioid receptor
κOR	Kappa opioid receptor

List of figures

List of tables

List of publications

Endt F, Guo T, Steinritz D, Amend N, Gudermann T, Breit A, *Carfentanil stabilizes μ opioid receptor conformations that are ultra-efficient in inhibiting cAMP, resistant to naloxone or nalmefene but sensitive to naltrexon*e, Arch Toxicol, DOI 10.1007/s00204-025-04048-6, accepted for publication, in press (2025)

The following figures contain already published results in the above-mentioned article in Archives of Toxicology and were reproduced with permission from Springer Nature:

Figures 15, 16, 18, 19, 21, 22, 26, 29

Conference contributions

F. Endt, N. Amend, D. Steinritz, T. Gudermann, A. Breit, *Pharmacodynamic assessment of carfentanil actions at mu opioid receptor (μOR) in HEK293 cells,* 9th German Pharm-Tox Summit 2024

F. Endt, N. Amend, D. Steinritz, T. Gudermann, A. Breit, *Carfentanil stabilizes ultra-active, antagonist-resistant μ opioid receptor conformations – introducing antibodies as an alternative carfentanil countermeasure,* Advances in Developing Medical Countermeasures Against Opioids and Drug-Induced Respiratory Depression 2024

F. Endt, N. Amend, D. Steinritz, T. Gudermann, A. Breit, *Addressing Carfentanil's stabilization of ultra-active, antagonist-resistant μ opioid receptors: Antibodies as potential countermeasures*, 10th German Pharm-Tox Summit 2025

Affidavit

LMU LUDWIG-MAXIMILIANS-UNIVERSITÄT MÜNCHEN

Dean's Office Medical Faculty
Faculty of Medicine

Affidavit

Endt, Franziska Clara

Surname, first name

I hereby declare, that the submitted thesis entitled

Pharmacodynamics of carfentanil and its neutralization by antagonists and antibodies in HEK293-μOR cells

is my own work. I have only used the sources indicated and have not made unauthorised use of services of a third party. Where the work of others has been quoted or reproduced, the source is always given.

I further declare that the dissertation presented here has not been submitted in the same or similar form to any other institution for the purpose of obtaining an academic degree.

12.11.2025

Place, Date

Franziska Clara Endt

Signature doctoral candidate

Confirmation of congruency

LMU LUDWIG-MAXIMILIANS-UNIVERSITÄT MÜNCHEN

Dean's Office Medical Faculty
Doctoral Office

Confirmation of congruency between printed and electronic version of the doctoral thesis

Endt, Franziska Clara

Surname, first name

I hereby declare that the electronic version of the submitted thesis, entitled:

Pharmacodynamics of carfentanil and its neutralization by antagonists and antibodies in HEK293-μOR cells

is congruent with the printed version both in content and format.

12.11.2025

Place, Date

Franziska Clara Endt

Signature doctoral candidate

Congruency of submitted versions Human Biology

Date: 14.03.2025

Danksagung

An erster Stelle möchte ich Prof. Dr. Gudermann meinen tiefen Dank aussprechen, für die Möglichkeit, meine Arbeit am Walther-Straub-Institut anzufertigen. Ohne diese Chance wäre dieser Weg nicht möglich gewesen. Ich danke auch den Gutachterinnen und Gutachtern meiner Dissertation herzlich für ihre wertvolle Zeit und die sorgfältige Begutachtung meiner Arbeit.

Mein besonderer Dank gilt Dr. Andreas Breit. Du warst mir in jeder Phase der Doktorarbeit die allergrößte Unterstützung. Deine engmaschige Betreuung, deine stets offene Tür, deine Gelassenheit und unermüdliche Einsatzbereitschaft für die Studierenden sind außergewöhnlich. Danke für jede Hilfe und die neuen Ideen - sei es bei Präsentationen oder bei wissenschaftlichen Fragestellungen - und auch für die vielen nicht wissenschaftlichen Diskussionen während der Mittagspausen. Die Weihnachtsfeiern, Sommerfeste und Faschingsweißwurstessen wären ohne Dich garnicht möglich und nur halb so schön gewesen.

Prof. Dr. med. Dirk Steinritz und Dr. med. Niko Amend, euch - vom Institut für Pharmakologie und Toxikologie der Bundeswehr - danke ich herzlich für die Zusammenarbeit und vor allem für die finanzielle Unterstützung, die mir durch die Bundeswehr für mein Projekt zuteilwurde. Mit dem spannenden Projekt hätte ich nicht glücklicher sein können. Mit euch in die USA zu reisen und an der Konferenz dort teilzunehmen, war eine wertvolle Erfahrung. Dirk, als mein zweiter Doktorvater danke ich dir besonders für deine pragmatische Herangehensweise und auch für die Sightseeing-Tipps für New York.

Dr. rer. biol. hum. Luisa Jiménez-Soto, liebe Luisa - ich danke dir für dein stets offenes Ohr, deine wertvollen Ratschläge beim Schreiben und für die geballte Girl Power, die du ins Institut bringst. Deine Obstversorgung und dein Engagement, das Institut zu einem angenehmen Ort zu machen, werde ich nicht vergessen - ebenso wie den legendären Burrito-Donnerstag, den ich leider viel zu selten genutzt habe.

Ein besonderer Dank gilt auch Frau Schreier und Frau Lakatos im Sekretariat. Danke, dass Sie immer Zeit gefunden haben zu helfen, bei allen

organisatorischen Fragen mit Rat und Tat zur Seite standen und für die netten Pläuschchen zwischendurch.

Liebe Sarah, danke dir für einen so warmen und leichten Start am Institut. Deine Gesellschaft beim Feierabendbier, unsere dm-Ausflüge und die gemeinsamen Stunden im Labor - so viel Spaß, der leider viel zu schnell verging. Steffi, du warst mein Lichtblick an jedem Dienstag und Donnerstag! Danke für die Verschnaufpausen an der frischen Luft, deine Empathie und Hilfsbereitschaft bei jedem noch so kleinen Problem. Danke euch beiden für die Freundschaft, die ich nicht mehr missen möchte.

Liebe Tanja, danke, dass du meine Büro-Einsamkeit beendet hast - für jede Zeichnung, die den Tag versüßte, für deine Herzlichkeit und für das gemeinsame Durchstehen schwieriger Phasen. Liebe Anna, danke für deine großartigen Western Blots! Und ein herzliches Dankeschön an euch alle - Alex, Ahmed, Tao, Ziska, Lea und alle KollegInnen, die ich hier nicht namentlich erwähnt habe. Ihr habt den Arbeitsalltag am Institut einzigartig gemacht.

Mama und Papa, mein tiefster Dank geht an euch. Danke für eure Unterstützung in jeglicher Hinsicht, euer ehrliches Interesse an meiner Arbeit und den Wissensdurst, den ihr mir mitgegeben habt. An meine Geschwister, meine Schwiegerfamilie und meine Freunde: Ihr seid mein wertvolles soziales Netz, das ich unendlich schätze und ihr habt oft mehr an mich geglaubt, als ich selbst.

Mein liebster Vincent - es gibt keine Worte, die ausdrücken können, wie dankbar ich dir bin. Für deine bedingungslose Liebe, deine unerschütterliche Motivation, deinen Optimismus, deine unendliche Unterstützung und dafür, dass du immer mein sicherer Hafen bist. Ohne dich hätte ich das alles nicht geschafft.

Und zu guter Letzt: Danke an dich, kleines Würmchen in meinem Bauch. Du warst meine größte Motivation, diese Arbeit schneller abzuschließen, als ich es mir selbst zugetraut hätte. Du warst beim Schreiben immer da, ganz still und doch so präsent. Danke, dass du mich auf diesem Weg begleitet hast - ich freue mich auf das neue Kapitel, das wir bald gemeinsam zu dritt beginnen.